Arthritis & Rheumatology

An Official Journal of the American College of Rheumatology
www.arthritisrheum.org and wileyonlinelibrary.com

Cover design: Todd Machen

♾This journal is printed on acid-free paper.

Arthritis & Rheumatology

An Official Journal of the American College of Rheumatology
www.arthritisrheum.org and wileyonlinelibrary.com

VOLUME 77 • November 2025 • NO. 11

Cover image: The image on the cover (Coveney et al; pages 1488–1502) features a coronal section of the medial compartment of a mouse knee joint, using SafO to highlight proteoglycan staining in the articular cartilage. This section is representative of OARSI scoring of homozygous animals harbouring a deletion within the upstream regulatory region (R2) of GDF5. This region is responsible for driving expression within the major forelimb and hind limb joints, its loss resulting in a ~40% reduction in GDF5 expression and shape changes localized to the femoral head, femoral condyle and tibial plateau. Despite this, these shape changes did not lead to an increased predisposition of developing OA at 1.5 yrs of age.

Clinical Connections

Dietary Polyunsaturated Fatty Acid and the Risk of RA

Chen et al. *Arthritis Rheumatol.* 2025;77:1475–1487.

CORRESPONDENCE
Qianchun Deng, PhD: dengqianchun@caas.cn

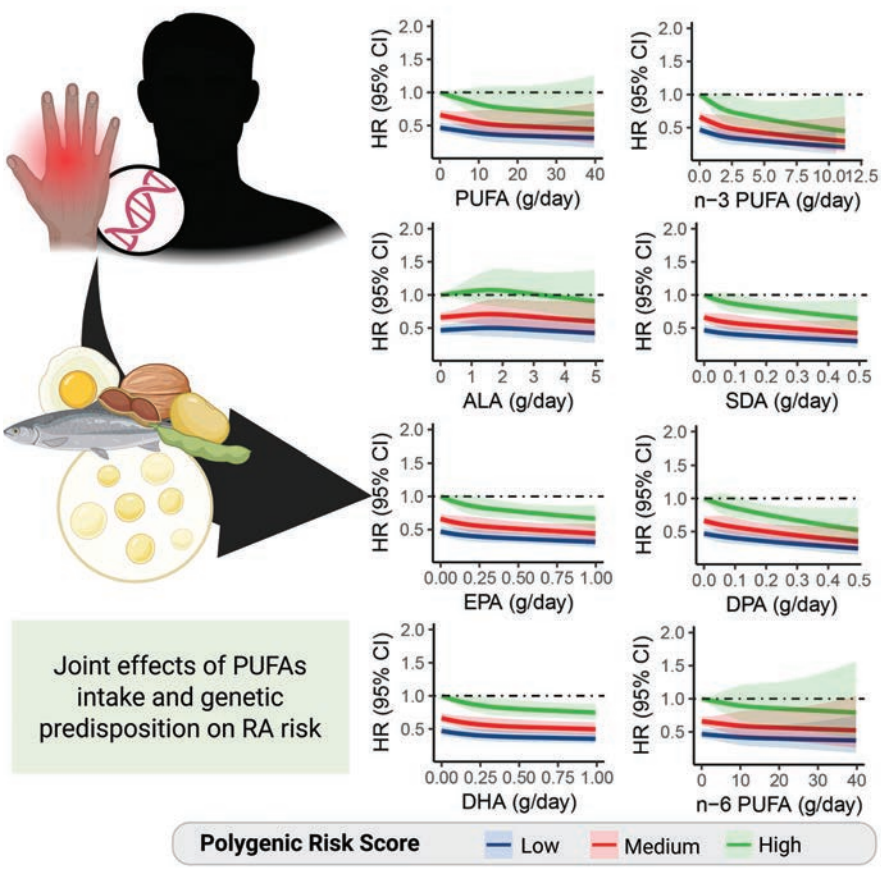

KEY POINTS

- Each standard deviation increase in the intake of specific marine omega-3 PUFAs was associated with a 9–10% reduction in the risk of incident RA.
- The inverse association was strongest in individuals with a high genetic risk for RA, with significant antagonistic interactions observed, indicating that high intake of these PUFAs may offset genetic susceptibility.
- Proteomic analyses revealed that the protective effects are mediated through specific proteins (e.g., CD80, TNFRSF4) involved in critical immune and inflammatory pathways.

SUMMARY

Dietary intake of polyunsaturated fatty acids (PUFAs) is a controllable factor for the prevention of numerous diseases, and intake of long-chain omega-3 fatty acids (n-3 PUFAs) has been shown to alleviate clinical symptoms in patients with rheumatoid arthritis (RA). However, the evidence linking dietary PUFAs to the incident risk of RA is scarce. Chen et al. conducted a large-scale prospective cohort study using data from the UK Biobank to explore the association between dietary intake of total and specific PUFAs and incident RA.

The results provide robust evidence that dietary intake of marine omega-3 PUFAs is associated with a significantly reduced risk of developing RA. The protective effect was particularly evident among individuals with a high genetic predisposition to RA, suggesting diet may help mitigate inherited risk. Integrated proteomic and mediation analyses further uncovered the biological mechanisms, identifying key circulating proteins involved in immune regulation and inflammation as mediators of this protective association. These findings offer valuable avenues for future research on therapeutic targets and RA prevention.

Precision Medicine in Pediatric Autoimmunity: Leniolisib Treatment of Childhood-Onset LN Due to Activated PI3Kδ

Lim et al. *Arthritis Rheumatol.* 2025;77:1596–1604.

CORRESPONDENCE
Elena W.Y. Hsieh, MD: elena.hsieh@cuanschutz.edu

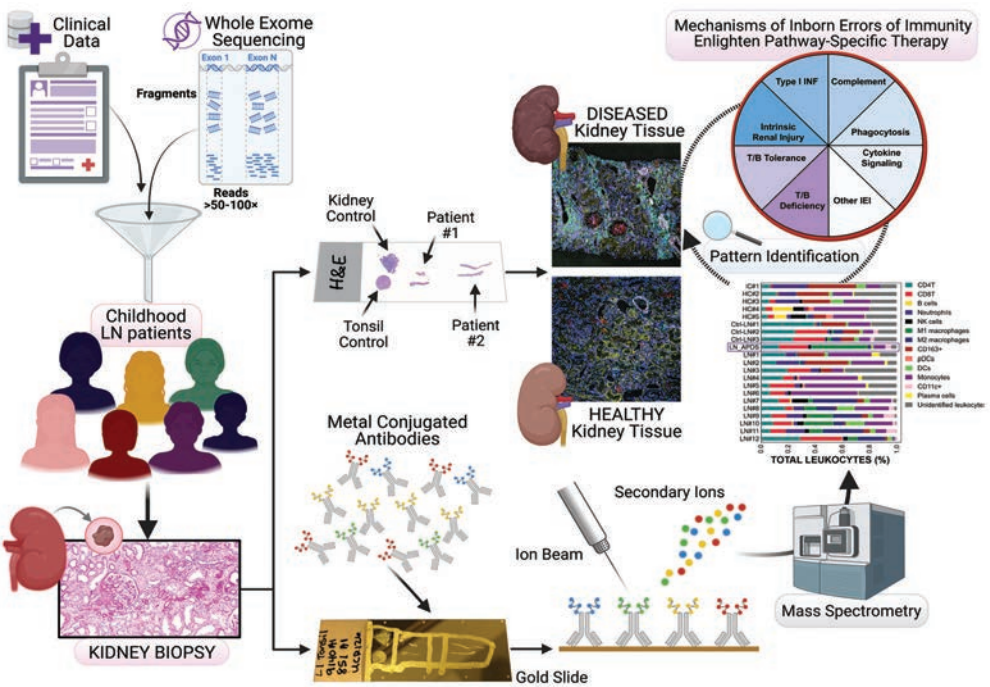

KEY POINTS

- Genetic testing for primary immunodeficiencies should be considered when pediatric LN fails to respond to standard immunosuppressive therapies.
- Children with genetic disorders, such as APDS, display unique molecular and cellular immune signatures in their kidneys, explaining their resistance to conventional treatments.
- Targeted therapy achieved superior disease control and improved kidney function, while eliminating the need for broad immunosuppression, reducing infection risk in vulnerable pediatric patients.

SUMMARY

Identifying the underlying genetic defect behind treatment-resistant autoimmune kidney disease enables precision therapy—targeting a specific molecular pathway rather than broadly suppressing the immune system—to great effect.

Lim et al. studied an 18-year-old girl who presented at 14 years old with severe lupus nephritis (LN). She did not respond to standard LN treatments, including glucocorticoids and other cytotoxic immunosuppressive drugs. After years of broad immunosuppressive therapy that failed to improve her renal function, genetic testing revealed the patient to have a rare inherited condition, activated phosphoinositide-3-kinase δ syndrome type 1 (APDS1). APDSI is characterized by mutation of a single gene that causes immune cell hyperactivity via a specific molecular pathway. Identification of this pathway enabled targeted treatment with leniolisib, a drug recently approved by the FDA for treatment of APDS. Unlike the previous broad-spectrum, symptom-based treatments, leniolisib treatment improved her renal function and allowed for gradual weaning of other immunosuppression. Importantly, advanced tissue imaging revealed that kidney biopsies from children with immune-mediated kidney disease exhibit distinct immune cell patterns that reflect their underlying disease mechanisms (genetic etiology).

In the future, these unique tissue signatures may be used to diagnose specific disease subtypes and guide precision treatment decisions.

Hand Swelling: A Common Initial Presentation of Systemic Sclerosis

Previous studies have found that some patients with systemic sclerosis (SSc), primarily those with diffuse cutaneous involvement, manifest puffy fingers/hands before the onset of Raynaud phenomenon (RP). p. 1585 **In this issue, Hanif et al. (p. 1585)** report the initial clinical manifestations and anti-nuclear antibody (ANA) profiles of patients in two early SSc cohorts. They found that although RP is the most common initial symptom of SSc, it is not uncommon for other symptoms to precede the onset of RP by several months.

The two independent cohorts, the Genetics vs. Environment in Scleroderma Outcomes Study (GENISOS) and the Collaborative National Quality and Efficacy Registry (CONQUER), had enrollment spanning from the late 1990s to the present, and both yielded similar findings. The authors note the data on SSc manifestation preceding study enrollment relied on patient report, thereby possibly introducing risks of recall bias and imprecision. Nevertheless, more than 30% of patients in the cohorts began to manifest SSc with puffy fingers/hands or other symptoms.

The patients who presented with hand swelling did not have the warning sign of RP as their initial symptom. They displayed more severe skin and musculoskeletal disease on average than did those who presented first with RP. The most common autoantibody associated with an initial symptom of hand swelling was RNA polymerase III. The investigators also reported that tendon friction rubs were more prevalent among patients with non-RP presentations than those with RP presentations. Moreover, >75% of those patients who had developed classifiable SSc in the absence of RP had abnormal nailfold capillaries.

The observations regarding initial SSc symptoms reinforce the concept of heterogeneity in the clinical presentation of SSc. The authors underscore the importance of recognition of hand swelling as a presentation of SSc. They write that puffy fingers/hands, even in the absence of RP, should prompt consideration of early SSc and testing for ANA and SSc-associated autoantibodies, including RNA polymerase III.

Journal Club

A monthly feature designed to facilitate discussion on research methods in rheumatology.

Differences in Dynamics of Specific ANAs and Their Susceptibility to B Cell–Targeting Treatment in SLE

van Dooren et al. *Arthritis Rheumatol.* 2025;77:1560–1572.

This study reported on the dynamics of anti-nuclear antibodies (ANAs) in patients with systemic lupus erythematosus (SLE) and their response to B cell–targeting treatment. Using three different datasets, the authors showed that anti-dsDNA and anti-Sm/RNP levels fluctuate considerably, whereas anti–SSA and SSB levels are much more stable, similar to long-lived vaccination-induced responses.

Three types of data were used in this study. 1) Electronic health record data on clinical laboratory measurements of specific ANAs were used to get a comprehensive overview of seroconversion. Due to the low frequency of some autoantibodies in SLE, this large cohort (n=836) provided sufficient power to compare each ANA specificity. 2) Serum from a longitudinal SLE biobank cohort was analyzed to determine antibody titers by serial dilution. Two timepoints from each patient (n=61) were included, approximately one year apart. This provided exact estimates of antibody titers not restricted by assay detection limits. 3) Serum samples from two clinical trials of SLE were analyzed to determine response of antibody titers to B cell–targeting treatments. The Calibrate trial compared rituximab (R) + cyclophosphamide (C) with R+C+belimumab (B), while the Synbiose trial studied the effects of R+B. Titers of anti-varicella zoster virus served as positive control for titer stability.

Analysis of ANA dynamics revealed differences between specific ANAs and their changes with treatment. These findings suggest different contributions of short- and long-lived plasma cells to each specific ANA response, with a strong contribution of short-lived plasma cells to anti-dsDNA and anti-Sm/RNP production. The different dynamics of specific ANAs have important implications for diagnosis and therapeutic targeting. Because anti-dsDNA and anti-Sm/RNP can seroconvert to become either positive or negative, disease classification can change over time. Further, new therapies targeting stable versus fluctuating autoantibodies may differentially impact specific ANAs and may be utilized to more specifically target pathogenic populations of B cells/plasma cells.

Questions

1. **What were the pre-existing paradigms on autoantibody stability? How do these findings change these concepts?**
2. **How do these methods to determine antibody levels compare with clinical diagnostic assays? What are advantages and limitations of each method?**
3. **What is the expected response of each ANA specificity to new B cell/plasma cell–targeting treatments?**
4. **How do the dynamics of ANAs in SLE compare with autoantibodies in other rheumatic autoimmune diseases?**

In this Issue

Highlights from this issue of *A&R* | By Lara C. Pullen, PhD

Complex Regulatory Interactions Shape OA Disease Risk

GDF5, a gene expressed during joint formation, is critical in determining joint shape, and is the best studied osteoarthritis (OA) locus to date. Although previous studies have evaluated the regulatory activity of *GDF5* and identified broad patterns across the locus or specific regulatory sequences, researchers have not been able to locate a regulatory region that can fully recapitulate endogenous *GDF5* expression. **In this issue, Coveney et al. (p. 1488)** report the results of their analysis of *GDF5* and reveal the contribution of gene regulatory interactions and local epistasis (i.e., when one gene's expression modifies the effect of another gene) to OA disease risk. Their findings suggest that the presence of individual genetic variants implicated in genome-wide association studies (GWAS) does not equate to causality; GWAS-identified risk variants could reside in enhancers, repressors, or sequences that behave as both.

p. 1488

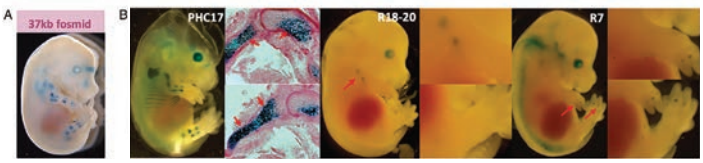

Figure 1. Restriction of *GROW1* to the perichondrium exerted by downstream regulatory regions. Transgenic embryos driving *lacZ* were collected at E14.5 of (A) 37-kb human fosmid driving growth plate expression and (B) regulatory region *PHC17* (*GROW1*, *R18–R20*, and *R7*) with two histologic panels of the hind limb showing *PHC17*-driven *lacZ* expression throughout the entire growth plate.

The investigators conducted *in vivo* and *in vitro* studies, as well as modeling of OA variants. They found evidence of activation and repression for all regulatory regions between or within regions that affected patterns of joint-specific expression. This suggests that location-specific decreases in *GDF5* expression are far more important mediators of complex disease risk (e.g., OA, dysplasia of the hip) than reduced expression observed across different joint sites and tissues.

One example of this regulation of joint-specific expression is the *R4* enhancer. It is considered to be activating, but has dual roles—not only enhancing but also repressing expression in adjacent tissues and sites. Another example is that adjacent sequences confine the growth plate–specific expression patterns by the *GROW1* regulatory region to restrict expression to the perichondrium.

Novel Candidate Genes Identified in Patients With Childhood-Onset Lupus

Genome-wide association studies (GWAS) can identify common variants, but they tend to be unsuccessful in identifying rare variants. Rare variants often have a larger effect size and are frequently found within protein-coding regions. Identification of rare variants can thus offer insights into disease mechanisms missed by traditional GWAS. **In this issue, Ma et al. (p. 1548)** highlight the abundance of lupus-relevant rare gene variants that can be found in Chinese patients with childhood-onset systemic lupus erythematosus (cSLE). Their findings indicate that *de novo* variants frequently contribute to disease, and they were able to identify genes that may constitute novel therapeutic targets of relevance to patients of Chinese descent.

p. 1548

The investigators performed whole-exome sequencing in 50 Chinese trios with cSLE and employed a minor allele frequency threshold of <0.005 for variant filtration. They found that at least two children had monogenic disease, and one-third carried novel genes or rare variants accepted to cause monogenic SLE. The researchers found a median of six novel or rare variants in a known SLE gene per child, with each child carrying at least one rare variant in an SLE risk gene; some carry as many as 10 rare variants. They identified *TYK2* among the top five genes in both Chinese and White cohorts.

The researchers prioritized analysis of the *de novo* variants by first determining if they were found among the top 20 SLE gene ontology (GO) pathways and then if they were expressed in plasma B cells and age-associated B cells (ABCs: a B cell subpopulation thought to be pathogenic in SLE). Although only two *de novo* variants occurred in genes previously associated with SLE, 12 of the 50 genes were enriched in the top 20 SLE-related pathways and were highly expressed in ABCs and plasma B cells. The investigators also found that more than half of the *de novo* variants occurred in genes that were not previously associated with SLE or autoimmunity but were highly expressed in ABCs. The authors conclude by highlighting two *de novo* variants occurring in genes not previously linked to SLE or autoimmunity that enhanced type I interferon signaling.

Hand Swelling: A Common Initial Presentation of Systemic Sclerosis

Previous studies have found that some patients with systemic sclerosis (SSc), primarily those with diffuse cutaneous involvement, manifest puffy fingers/hands before the onset of Raynaud phenomenon (RP). p. 1585 **In this issue, Hanif et al. (p. 1585)** report the initial clinical manifestations and anti-nuclear antibody (ANA) profiles of patients in two early SSc cohorts. They found that although RP is the most common initial symptom of SSc, it is not uncommon for other symptoms to precede the onset of RP by several months.

The two independent cohorts, the Genetics vs. Environment in Scleroderma Outcomes Study (GENISOS) and the Collaborative National Quality and Efficacy Registry (CONQUER), had enrollment spanning from the late 1990s to the present, and both yielded similar findings. The authors note the data on SSc manifestation preceding study enrollment relied on patient report, thereby possibly introducing risks of recall bias and imprecision. Nevertheless, more than 30% of patients in the cohorts began to manifest SSc with puffy fingers/hands or other symptoms.

The patients who presented with hand swelling did not have the warning sign of RP as their initial symptom. They displayed more severe skin and musculoskeletal disease on average than did those who presented first with RP. The most common autoantibody associated with an initial symptom of hand swelling was RNA polymerase III. The investigators also reported that tendon friction rubs were more prevalent among patients with non-RP presentations than those with RP presentations. Moreover, >75% of those patients who had developed classifiable SSc in the absence of RP had abnormal nailfold capillaries.

The observations regarding initial SSc symptoms reinforce the concept of heterogeneity in the clinical presentation of SSc. The authors underscore the importance of recognition of hand swelling as a presentation of SSc. They write that puffy fingers/hands, even in the absence of RP, should prompt consideration of early SSc and testing for ANA and SSc-associated autoantibodies, including RNA polymerase III.

Journal Club

A monthly feature designed to facilitate discussion on research methods in rheumatology.

Differences in Dynamics of Specific ANAs and Their Susceptibility to B Cell–Targeting Treatment in SLE

van Dooren et al. *Arthritis Rheumatol.* 2025;77:1560–1572.

This study reported on the dynamics of anti-nuclear antibodies (ANAs) in patients with systemic lupus erythematosus (SLE) and their response to B cell–targeting treatment. Using three different datasets, the authors showed that anti-dsDNA and anti-Sm/RNP levels fluctuate considerably, whereas anti–SSA and SSB levels are much more stable, similar to long-lived vaccination-induced responses.

Three types of data were used in this study. 1) Electronic health record data on clinical laboratory measurements of specific ANAs were used to get a comprehensive overview of seroconversion. Due to the low frequency of some autoantibodies in SLE, this large cohort (n=836) provided sufficient power to compare each ANA specificity. 2) Serum from a longitudinal SLE biobank cohort was analyzed to determine antibody titers by serial dilution. Two timepoints from each patient (n=61) were included, approximately one year apart. This provided exact estimates of antibody titers not restricted by assay detection limits. 3) Serum samples from two clinical trials of SLE were analyzed to determine response of antibody titers to B cell–targeting treatments. The Calibrate trial compared rituximab (R) + cyclophosphamide (C) with R+C+belimumab (B), while the Synbiose trial studied the effects of R+B. Titers of anti-varicella zoster virus served as positive control for titer stability.

Analysis of ANA dynamics revealed differences between specific ANAs and their changes with treatment. These findings suggest different contributions of short- and long-lived plasma cells to each specific ANA response, with a strong contribution of short-lived plasma cells to anti-dsDNA and anti-Sm/RNP production. The different dynamics of specific ANAs have important implications for diagnosis and therapeutic targeting. Because anti-dsDNA and anti-Sm/RNP can seroconvert to become either positive or negative, disease classification can change over time. Further, new therapies targeting stable versus fluctuating autoantibodies may differentially impact specific ANAs and may be utilized to more specifically target pathogenic populations of B cells/plasma cells.

Questions

1. **What were the pre-existing paradigms on autoantibody stability? How do these findings change these concepts?**
2. **How do these methods to determine antibody levels compare with clinical diagnostic assays? What are advantages and limitations of each method?**
3. **What is the expected response of each ANA specificity to new B cell/plasma cell–targeting treatments?**
4. **How do the dynamics of ANAs in SLE compare with autoantibodies in other rheumatic autoimmune diseases?**

Arthritis & Rheumatology
Vol. 77, No. 11, November 2025, pp 1461–1464
DOI 10.1002/art.43220

American College of Rheumatology
Empowering Rheumatology Professionals

EDITORIAL

The Dynamics of Antinuclear Antibody Production in Systemic Lupus Erythematosus: New Insights for New Therapies

Martin Aringer[1] and David S. Pisetsky[2]

The study by van Dooren et al[1] in this issue of *Arthritis & Rheumatology* provides an intriguing perspective on antinuclear antibody (ANA) expression in systemic lupus erythematosus (SLE) and the implications for new therapies. By quantitatively assessing the expression of a broad range of ANAs during the course of disease, the investigators construct a more complete picture of these responses and reveal dynamic variations previously not appreciated. Although the central role of ANAs in tissue inflammation and injury in SLE is well established, the advent of novel therapies to target B cells (cellular, biologic, and small molecule) requires more precise understanding of the induction and regulation of autoantibody producing cells and strategies for their elimination. Indeed, serologic assays will represent critical biomarkers to elucidate the effects of the next generation of immunomodulatory and immunosuppressive therapies as exemplified by studies on chimeric antigen receptor (CAR) T cells.[2]

Even though immune disturbances are rampant in SLE, ANA responses are neither random nor indiscriminate but rather display two distinctive features: patterning and clustering.[3] The patterning relates to the targeting of discrete sets of nuclear molecules. Inside the cell, these molecules exist as multicomponent complexes that can translocate to the extracellular space during cell death, in which they display immune activity. These complexes contain either DNA or RNA and be sorted into two broad categories: antibodies to nucleosomes and antibodies to RNA protein complexes. Nucleosomal antigens include DNA and histones; DNA and histones can interact to form nucleosomes, also known as chromatin. Of this group, antibodies to double-stranded DNA (dsDNA) are the serologic hallmark of SLE, present in approximately three in four patients[4] and in all animal models.[5]

In contrast to antibodies to nucleosomal antigens, antibodies to RNA-to-protein complexes (also called small nuclear ribonucleoproteins or spliceosomes) bind primarily to the protein components known as RNA-binding proteins (RBPs).[6] Reflecting the classical preparation of these antigens from tissue extracts, these antibodies have also been called antibodies to extractable nuclear antigen (ENA). ENA antigens relevant for the immunopathogenesis and clinical phenotyping include Smith (Sm), U1RNP, Ro (SSA), and La (SSB). In patients with SLE, anti-ENA responses can come in pairs; anti-Sm and anti-U1RNP often occur together, as do anti-Ro and anti-La. Pairing can extend to other diseases such as Sjögren disease, in which anti-Ro and anti-La are prominent biomarkers.[3]

In individual patients, different ANAs show clustering as exemplified by their pattern of coexpression. These clusters, which number from three to five depending on the study, are defined by the array of ANAs expressed and have clinical significance in terms of their association with disease manifestations (eg, nephritis, rash, thrombosis), genetic determinants, and ancestry.[7] Of ANAs, only anti-DNA and anti-Sm serve as classification criteria[8] and can be coexpressed as part of a cluster that is associated with nephritis. Although clustering is an important clue to the mechanisms of autoantibody induction, it can hinder the identification of the role of different ANAs in disease manifestations (eg, levels of C3 and C4).

Clinical experience has indicated that antibodies to DNA can vary with measures of disease activity, especially nephritis, although detecting these changes may depend on the sensitivity of the assay used; the extent of the change of anti-dsDNA levels that is considered clinically significant can also affect this assessment. In line with the role of DNA–anti-dsDNA immune complexes (ICs) in promoting inflammation and disease activity, decreases in levels of C3 and C4 commonly accompany increases of anti-dsDNA levels.[5]

[1]Martin Aringer, MD: Division of Rheumatology, Department of Medicine III and University Center for Autoimmune and Rheumatic Entities, University Medical Center and Faculty of Medicine, Technische Universität Dresden, Dresden, Germany; [2]David S. Pisetsky, MD, PhD: Durham VA Medical Center and Duke University Medical Center, Durham, North Carolina.

Author disclosures are available at https://onlinelibrary.wiley.com/doi/10.1002/art.43220.

Address correspondence via email to Martin Aringer, MD, at martin.aringer@uniklinikum-dresden.de.

Submitted for publication April 15, 2025; accepted April 21, 2025.

In view of these findings, anti-dsDNA is extensively used as a biomarker to monitor disease activity and treatment response. In contrast, anti-RBP levels are generally thought to show little variation in levels and lack a clear relationship to disease activity.[9] Assay of anti-RBP levels has therefore not been part of routine laboratory assessment. This knowledge gap on actual antibody levels now needs to be filled to advance targeting of B cells in new therapy.

To explore more comprehensively the dynamics of ANA responses, van Dooren et al[1] have constructed a detailed picture of the serology of SLE based on data on standard-of-care therapies as well as clinical trials involving anti–B cell agents. In a clever approach, the authors combined the analysis of routine data from a Dutch cohort of 836 patients with SLE with antibody measurements in 72 serum samples from a longitudinal US medical center SLE cohort and 61 serum samples from two small clinical trials assessing the effects of rituximab with either cyclophosphamide or belimumab or the combination of both,[10,11] including a total of 103 patients with at least one of the specific antibodies.

The results from the different patient populations were reassuringly concordant. As expected, the study demonstrated changes over time in levels of both anti-dsDNA antibodies and antibodies to histones and chromatin. Perhaps surprisingly, levels of antibodies to Sm and U1RNP also showed fluctuations resembling of those of anti-DNA. This finding contrasts with the traditional view that anti-dsDNA antibodies and anti-RBPs differ in their dynamics. On the other hand, antibodies to the Ro antigen showed stability over time; as in the case of CAR T cell therapy, anti-Ro antibodies showed impressive resistance to immunosuppression.[2]

In the study of van Dooren et al,[1] anti-dsDNA antibodies remained stable in half of the patients, suggesting that antibodies to the same nuclear antigen may be produced by different cell populations. These findings suggest caution in the use of anti-DNA antibodies as an invariable marker of disease; they also suggest that different treatment approaches may be needed to eliminate pathogenic antibodies. Figure 1 illustrates the traditional and current model for ANA dynamics.

van Dooren et al[1] also explored the association of fluctuations in ANA levels with measures of clinical and serological improvement. As results of these studies indicated, a fall in anti-dsDNA antibodies correlated with decreases in measures of complement activation (ie, C3 and C4) and improvement in proteinuria. These findings are consistent with the postulated role of anti-dsDNA antibodies in forming ICs that deposit in the kidney and induce complement activation. In contrast, the study did not find a similar negative association of C3 and C4 with antibodies

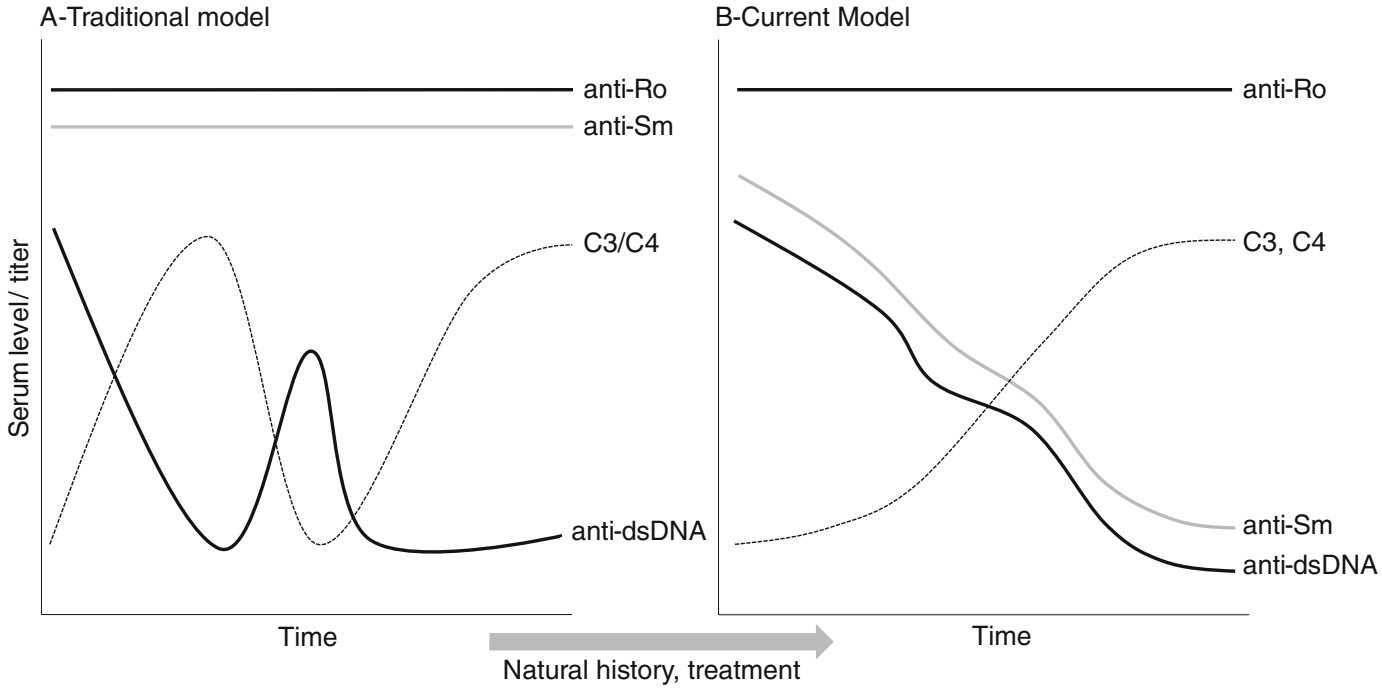

Figure 1. Antinuclear antibody (ANA) trajectories during SLE. The figure illustrates hypothetical trajectories of ANA responses during the course of SLE. Panel A depicts the traditional model in which anti-dsDNA levels vary with disease activity in association with reciprocal changes in levels of C3 and C4; in this model, levels of anti-Sm and anti-Ro remain stable. Panel B depicts the current model in which both anti-dsDNA and anti-Sm decline while levels of C3 and C4 rise; levels of anti-Ro nevertheless remain stable. The reasons for the change in the model are not clear but could relate to either the natural history of disease or the effects of treatments especially those that affect the generation or maintenance of plasma cells. The period of autoimmunity after diagnosis and initiation of treatment has been termed postclinical autoimmunity by analogy with preclinical autoimmunity, which is the period before diagnosis. In the future, new therapies directed at B cells may lead to even further changes in the model as even greater shifts in B cell populations occur. Anti-dsDNA, anti–double-stranded DNA; anti-Sm, anti-Smith; SLE, systemic lupus erythematosus.

to Sm, suggesting that although anti-Sm antibodies may form ICs, these structures may fail to activate complement. Because levels of anti-Ro did not change in the majority of patients, an association with complement activation cannot be established. This finding, however, is nevertheless of interest because of the association of anti-Ro antibodies with subacute cutaneous lupus erythematosus skin lesions.[12] The reason that these lesions can appear and disappear despite the persistence of the antibodies remains an important question.

Although the study of van Dooren et al[1] did not address mechanisms, it seems likely the differences in the dynamics of ANA production reflect the role of different B cell populations in antibody production and, most pertinently, the roles of memory cells, double-negative cells, short lived plasmablasts, plasma cells, and long-lived plasma cells. With advances in treatment, new strategies may allow more effective or selective elimination of various B cell populations by novel agents such as CAR T cells directed to different surface molecules (eg, CD19, CD20, or BCMA).[13] In this regard, eliminating plasma cells comes with distinct risks because these cells are the source of protective antibody responses whose lifespan can be years and decades. Whether autoantibodies and protective antibodies are produced by the same or different subpopulations of plasmablasts or plasma cells remains to be resolved.

An interesting question concerns the apparent change in the commonly held idea that antibodies to dsDNA and RBP follow different trajectories (Figure 1). One explanation is quite simple and technical. Because anti-RBP responses have long been considered unrelated to disease activity (or complement activation), clinicians have had little reason to assay anti-RBP responses over time, especially as many of the assay platforms available provide only qualitative information. Current technology, however, can provide quantitative ANA assessments to fill in the knowledge gap. Furthermore, nuclear antigens are complicated, multicomponent structures; as such, assays measuring antibodies to only one nucleic acid or protein in the complex (as done in this study) may produce an incomplete picture of the overall response. It will be important to determine whether the apparent differences in the response to the various nuclear antigens relate to assay as opposed to biologic factors.

Another influence on ANA dynamics relates to previous and concomitant therapy, with agents such as mycophenolate that impact B cell function and generation of plasma cells.[14,15] As discussed elsewhere, changes in autoantibody dynamics can occur after diagnosis and initiation of treatment during a period that can be considered postclinical autoimmunity (ie, after diagnosis). During this period, ANA responses can be gained or lost perhaps because of therapy or the natural history of disease, although different therapies may vary in their impact on ANA responses.[16] In the study by van Dooren et al,[1] the average disease duration of patients was approximately 10 years, providing ample time for fluxes in B cell populations to occur.

Finally, fluctuations in the levels of anti-DNA and anti-Sm could impact SLE classification if ANA responses come and go, even though the criterion is fulfilled if ever positive.[8] On the other hand, if proposed new therapies are more effective than current agents in ablating ANA responses by deeper killings of B cells or by targeting specific B cell populations more precisely,[17] for example, then changes in classification may signal an important therapeutic effect. With the insights gained from the study by van Dooren et al,[1] future research will determine whether new therapies on the horizon can induce an immune reset and permanently alter the dynamics of ANA production.

ACKNOWLEDGMENT

The authors would like to thank Dr Peter Lipsky for his input.

AUTHOR CONTRIBUTIONS

Both authors contributed to at least one of the following manuscript preparation roles: conceptualization AND/OR methodology, software, investigation, formal analysis, data curation, visualization, and validation AND drafting or reviewing/editing the final draft. As corresponding author, Dr Aringer confirms that all authors have provided the final approval of the version to be published and takes responsibility for the affirmations regarding article submission (eg, not under consideration by another journal), the integrity of the data presented, and the statements regarding compliance with institutional review board/Declaration of Helsinki requirements.

REFERENCES

1. van Dooren HJ, van Schaik M, Dorjée A, et al. Differences in dynamics of specific antinuclear antibodies and their susceptibility to B cell targeting treatment in patients with systemic lupus erythematosus. Arthritis Rheumatol 2025;77(11):1560–1572.
2. Müller F, Taubmann J, Bucci L, et al. CD19 CAR T-cell therapy in autoimmune disease - a case series with follow-up. N Engl J Med 2024;390(8):687–700.
3. Pisetsky DS, Lipsky PE. New insights into the role of antinuclear antibodies in systemic lupus erythematosus. Nat Rev Rheumatol 2020; 16(10):565–579.
4. Aringer M, Brinks R, Dörner T, et al. European League Against Rheumatism (EULAR)/American College of Rheumatology (ACR) SLE classification criteria item performance. Ann Rheum Dis 2021;80(6):775–781.
5. Pisetsky DS. Anti-DNA antibodies–quintessential biomarkers of SLE. Nat Rev Rheumatol 2016;12(2):102–110.
6. Bossuyt X, De Langhe E, Borghi MO, et al. Understanding and interpreting antinuclear antibody tests in systemic rheumatic diseases. Nat Rev Rheumatol 2020;16(12):715–726.
7. Diaz-Gallo LM, Oke V, Lundström E, et al. Four systemic lupus erythematosus subgroups, defined by autoantibodies status, differ regarding HLA-DRB1 genotype associations and immunological and clinical manifestations. ACR Open Rheumatol 2022;4(1):27–39.
8. Aringer M, Costenbader K, Daikh D, et al. 2019 European League Against Rheumatism/American College of Rheumatology Classification Criteria for Systemic Lupus Erythematosus. Arthritis Rheumatol 2019;71(9):1400–1412.
9. McCarty GA, Rice JR, Bembe ML, et al. Independent expression of autoantibodies in systemic lupus erythematosus. J Rheumatol 1982; 9(5):691–695.

10. Atisha-Fregoso Y, Malkiel S, Harris KM, et al. Phase II randomized trial of rituximab plus cyclophosphamide followed by belimumab for the treatment of lupus nephritis. Arthritis Rheumatol 2021; 73(1):121–131.
11. Kraaij T, Arends EJ, van Dam LS, et al. Long-term effects of combined B-cell immunomodulation with rituximab and belimumab in severe, refractory systemic lupus erythematosus: 2-year results. Nephrol Dial Transplant 2021;36(8):1474–1483.
12. Stull C, Sprow G, Werth VP. Cutaneous involvement in systemic lupus erythematosus: a review for the rheumatologist. J Rheumatol 2023; 50(1):27–35.
13. Robinson WH, Fiorentino D, Chung L, et al. Cutting-edge approaches to B-cell depletion in autoimmune diseases. Front Immunol 2024;15: 1454747.
14. Karnell JL, Karnell FG III, Stephens GL, et al. Mycophenolic acid differentially impacts B cell function depending on the stage of differentiation. J Immunol 2011;187(7):3603–3612.
15. Eickenberg S, Mickholz E, Jung E, et al. Mycophenolic acid counteracts B cell proliferation and plasmablast formation in patients with systemic lupus erythematosus. Arthritis Res Ther 2012; 14(3): R110.
16. Fassbinder T, Saunders U, Mickholz E, et al. Differential effects of cyclophosphamide and mycophenolate mofetil on cellular and serological parameters in patients with systemic lupus erythematosus. Arthritis Res Ther 2015;17(1):92.
17. Dörner T, Lipsky PE. The essential roles of memory B cells in the pathogenesis of systemic lupus erythematosus. Nat Rev Rheumatol 2024; 20(12):770–782.

Arthritis & Rheumatology
Vol. 77, No. 11, November 2025, pp 1465–1467
DOI 10.1002/art.43247

American College of Rheumatology
Empowering Rheumatology Professionals

EDITORIAL

A Historical Perspective on Approaches to Understanding the Genetics of Systemic Lupus Erythematosus

S. Louis Bridges Jr,[1,2] Betty P. Tsao,[3] and Peter K. Gregersen[4]

Genetic factors contribute to the susceptibility and onset of most autoimmune and inflammatory multisystem rheumatic diseases, with variable evidence of heritability. Systemic lupus erythematosus (SLE) has strong evidence of heritability, and it is associated with many relatively common genetic variants in multiple different genes. In general, genetic polymorphisms associated with rheumatic disease have modest effect sizes, and their pathophysiologic consequences remain poorly characterized. A more precise understanding of their function is likely to aid in diagnosis or treatment of multiple rheumatic diseases, including SLE.[1] Recent studies have also identified monogenic or oligogenic forms of SLE due to the presence of novel or rare pathogenic variants[2,3] such as those in *TLR7* and *UNC93B1*. The subset of patients with SLE with these novel and rare variants often manifest clinically as severe childhood-onset SLE (cSLE), such as that seen with variants[4] in *DNAse1L3*.

In this issue of *Arthritis & Rheumatology*, Ma et al[5] report analyses of trios (probands and their parents) to identify rare gene variants in Chinese patients with cSLE. The trio approach came about because of years of work on inheritance of human disease, family studies, and molecular genetic tools. Historically, the trio study design was used as an alternative approach to genetic association studies of common variants. Nontransmitted alleles (parental alleles that are not inherited by the offspring) are considered as a "pseudocontrol" group and are used to investigate possible indirect genetic effects of parents on their child's phenotype. The trio approach has many strengths including its ability to distinguish de novo mutations, which occur spontaneously in the child, and inherited mutations, in which the child receives the altered gene from one of their parents.

The article by Ma et al[5] led us to reflect on the amazing progress in understanding lupus genetics and to highlight the many technical, genetic, analytic, and data science resources that have emerged over many decades. We thus considered their findings in the context of what research approaches were available for genetic studies of SLE around 1990, a time when the three authors of this editorial were deeply engaged in genetic studies of human autoimmune rheumatic diseases.

The present era of research is blessed by the availability of a large array of research tools, many of which were catalyzed by the massive leap forward marked by the sequencing the human genome[6] in 2001. These advances include (1) the increasing feasibility of genotyping very large numbers of participants, thus providing statistical power to detect genetic associations with small effect size; (2) technologies to rapidly and inexpensively analyze millions of genetic variants in hundreds of thousands of research participants; (3) better understanding of the human genome and its population structure, allowing consideration of race and ethnicity in human genetic studies; (4) availability of large genetic reference panels of unaffected controls of different ethnic backgrounds; and (5) sophisticated tools to predicting protein structure and deleterious changes in genetic variants. Each of these will be briefly discussed to demonstrate the remarkable advances that have occurred over the research careers of investigators studying genetics of rheumatic diseases.

Before the availability of technologies to study huge numbers of genetic variants in large cohorts of unrelated patients, family-based approaches were used to provide evidence of genetic linkage. Multiplex families with SLE and other autoimmune diseases have been recognized for many years. For example, in 1901, Rona[7] reported SLE in siblings; Leonhardt[8] reported familial SLE in 1957. The heritability of SLE is in the range of 40% to 50%, based on previous twin and family studies.[9,10] In the 1990s, analysis of affected sibling pairs in families with multiple individuals affected by rheumatic diseases helped to identify genetic regions that cosegregate with SLE.[11–13] Other studies of the genetics of lupus focused on C4A null alleles[14] and other complement components[15,16] such as CR1 and complement protein C2.

[1]S. Louis Bridges, Jr, MD, PhD: Hospital for Special Surgery, New York, New York; [2]Weill Cornell Medicine, New York, New York; [3]Betty P. Tsao, PhD: Medical University of South Carolina, Charleston; [4]Peter K. Gregersen, MD: Feinstein Institutes for Medical Research, Manhasset, New York.

Author disclosures are available at https://onlinelibrary.wiley.com/doi/10.1002/art.43247.

Address correspondence via email to S. Louis Bridges, Jr, MD, PhD, at bridgesl@hss.edu.

Submitted for publication April 21, 2025; accepted in revised form April 30, 2025.

Many studies used a tedious indirect approach, Restriction Fragment Length Polymorphism, to identify genetic associations.

Genotyping technologies began to advance exponentially, as did our understanding of the structure of the human genome. In 1989, *Science* magazine named the polymerase chain reaction (PCR) the Major Scientific Development and DNA polymerase as Molecule of the Year due to an explosion in the use of PCR in biomedical science.[17] A ground-breaking genome-wide association study (GWAS) in age-related macular degeneration was published[18] in 2005, establishing the feasibility of actually identifying a gene associated with an important disorder. GWAS subsequently became a commonly used approach to analyze thousands of unrelated individuals, and this study design overshadowed family-based studies.[19] Continuous advancements leading to high throughput genotyping at significantly lower costs made wide-scale genotyping useful for identification of genetic variants associated with rheumatic diseases. Next-generation sequencing technologies led to the availability of whole-genome sequencing, now rapidly declining in cost; a focus on variants encoding changes in protein structure has also benefited from the whole-exome sequencing approach, defined as sequencing protein-coding regions (exons) of a person's genome, which accounts for ~1% of the total DNA.

One of the more vexing problems in previous genetics studies of lupus was the lack of availability of reference panels for genetic findings. Because of efforts such as the International HapMap Project[20] and the 1000 Genomes Project,[21] there are now reference panels of ancestry-informative markers (single-nucleotide polymorphisms that exhibit significantly different allele frequencies across different populations) to help characterize genetically determined ethnicity by estimating admixture.[22] These panels can help provide context for genetic association studies and are crucial for studying and understanding human ancestry and its relationship to health and disease. In the current study, the majority of the probands were of Eastern Chinese, Dai of South China, and Yi of Southwest China ancestry. Although many studies have investigated the burden of rare gene and de novo variants in cSLE, this is the first study to analyze a Chinese cohort. In the study by Ma et al,[5] the Gene4denovo whole-exome sequencing database was used to compare de novo rare variants in cSLE to those in 2,049 healthy control individuals.

Among 33 probands, Ma et al[5] identified 125 de novo variants in 93 genes, approximately half of which were not previously known to be associated with SLE. They also found 269 rare variants known to be associated with SLE (45 with monogenic SLE and 224 with SLE through GWA studies). Thus, approximately one-third of variants were de novo mutations. Although they are somatic (rather than germline), de novo mutations are associated with VEXAS syndrome[23] and clonal hematopoiesis.[24] Thus, the findings in the article by Ma et al[5] underscore the growing appreciation of the contributions of de novo genetic variants to rheumatic diseases.

Resources for pathway enrichment analysis, such as Gene Ontology pathways and Kyoto Encyclopedia of Genes and Genomes pathways have been commonly used for many years. Additional open science platform resources are now available, including the Reactome pathway browser (started in 2003), Wiki pathways, and Metascape, a gene annotation and analysis resource that provides tools to understand common or unique pathways and protein networks. The most statistically significant pathways associated with de novo rare variants found in cSLE in the study by Ma et al[5] confirm the relevance of positive regulation of immune response, the innate immune response, immune cell activation, cytokine signaling, cellular responses to virus, nucleic acid metabolism, inflammatory response, regulation of immune effector process, and regulation of phosphorylation.

Algorithms to predict the functional impact of amino acid substitutions and deleteriousness of single nucleotide variants and insertion or deletion variants in the human genome are now publicly available. These include the Polymorphism Phenotyping version 2, Sorting Intolerant from Tolerant, and Combined Annotation Dependent Depletion programs. Pathogenicity assessments using these programs estimated that 22% of de novo rare variants and 42% of rare variants in SLE-associated genes found by Ma et al[5] were likely to be deleterious. Approximately two-thirds of the probands in this study had rare variants of unknown significance in genes with the potential to cause SLE due to their putative involvement in pathways of type I interferon regulation, disruption of B cell and T cell tolerance, and metabolic disorders.

In summary, the study by Ma et al[5] is reminiscent of older, family-based approaches to identify genes associated with SLE. Trio-based genetic analysis has returned to frequent use to provide valuable information on identification of rare and de novo variants. Deep diving into rare variants, especially childhood-onset disorders, is likely to be a fruitful way to continue to gain valuable insights into rheumatic diseases such as SLE.

AUTHOR CONTRIBUTIONS

All authors contributed to at least one of the following manuscript preparation roles: conceptualization AND/OR methodology, software, investigation, formal analysis, data curation, visualization, and validation AND drafting or reviewing/editing the final draft. As corresponding author, Dr Bridges confirms that all authors have provided the final approval of the version to be published and takes responsibility for the affirmations regarding article submission (eg, not under consideration by another journal), the integrity of the data presented, and the statements regarding compliance with institutional review board/Declaration of Helsinki requirements.

REFERENCES

1. Bridges SL Jr, Shapira R, Aksentijevich I, et al; ClinGen Rheumatologic Autoimmune Disease Clinical Domain Working Group. Curating genetic associations with rheumatologic autoimmune diseases to improve patient outcomes. Arthritis Rheumatol 2024;76(11):1577–1581.

2. Brown GJ, Cañete PF, Wang H, et al. TLR7 gain-of-function genetic variation causes human lupus. Nature 2022;605(7909):349–356.
3. David C, Arango-Franco CA, Badonyi M, et al. Gain-of-function human UNC93B1 variants cause systemic lupus erythematosus and chilblain lupus. J Exp Med 2024;221(8):e20232066.
4. Coke LN, Wen H, Comeau M, et al. Arg206Cys substitution in DNASE1L3 causes a defect in DNASE1L3 protein secretion that confers risk of systemic lupus erythematosus. Ann Rheum Dis 2021; 80(6):782–787.
5. Ma J, Qin Y, Hong S, et al. Trio whole exome sequencing in Chinese childhood-onset lupus reveals novel candidate genes. Arthritis Rheumatol 2025;77(11):1548–1559.
6. Lander ES, Linton LM, Birren B, et al; International Human Genome Sequencing Consortium. Initial sequencing and analysis of the human genome. Nature 2001;409(6822):860–921.
7. Rona S. Lupus erythematosus bei geschwistern. Arch Derm u Syph 1901;56:381.
8. Leonhardt T. Familial hypergammaglobulinemia and systemic lupus erythematosus. Lancet 1957;273(7007):1200–1203.
9. Kuo C, Grainge MJ, Valdes AM, et al. Familial aggregation of systemic lupus erythematosus and coaggregation of autoimmune diseases in affected families. JAMA Intern Med 2015;175(9):1518–1526.
10. Lawrence JS, Martins CL, Drake GL. A family survey of lupus erythematosus. 1. Heritability. J Rheumatol 1987;14(5):913–921.
11. Gaffney PM, Kearns GM, Shark KB, et al. A genome-wide search for susceptibility genes in human systemic lupus erythematosus sib-pair families. Proc Natl Acad Sci USA 1998;95(25):14875–14879.
12. Tsao BP, Cantor RM, Kalunian KC, et al. Evidence for linkage of a candidate chromosome 1 region to human systemic lupus erythematosus. J Clin Invest 1997;99(4):725–731.
13. Jawaheer D, Seldin MF, Amos CI, et al. A genomewide screen in multiplex rheumatoid arthritis families suggests genetic overlap with other autoimmune diseases. Am J Hum Genet 2001;68(4):927–936.
14. Sturfelt G, Truedsson L, Johansen P, et al. Homozygous C4A deficiency in systemic lupus erythematosus: analysis of patients from a defined population. Clin Genet 1990;38(6):427–433.
15. Tebib JG, Martinez C, Granados J, et al. The frequency of complement receptor type 1 (CR1) gene polymorphisms in nine families with multiple cases of systemic lupus erythematosus. Arthritis Rheum 1989;32(11):1465–1469.
16. Zhu ZB, Volanakis JE. Allelic associations of multiple RFLPs of the gene encoding complement protein C2. Am J Hum Genet 1990; 46(5):956–962.
17. Guyer RL, Koshland DEJ Jr. The Molecule of the Year. Science 1989; 246(4937):1543–1546.
18. Klein RJ, Zeiss C, Chew EY, et al. Complement factor H polymorphism in age-related macular degeneration. Science 2005;308(5720): 385–389.
19. Ott J, Wang J, Leal SM. Genetic linkage analysis in the age of whole-genome sequencing. Nat Rev Genet 2015;16(5):275–284.
20. Sudmant PH, Rausch T, Gardner EJ, et al; 1000 Genomes Project Consortium. An integrated map of structural variation in 2,504 human genomes. Nature 2015;526(7571):75–81.
21. 1000 Genomes Project Consortium; Auton A, Brooks LD, Durbin RM, et al. A global reference for human genetic variation. Nature 2015; 526(7571):68–74.
22. Hughes LB, Morrison D, Kelley JM, et al. The HLA-DRB1 shared epitope is associated with susceptibility to rheumatoid arthritis in African Americans through European genetic admixture. Arthritis Rheum 2008;58(2):349–358.
23. Beck DB, Ferrada MA, Sikora KA, et al. Somatic mutations in UBA1 and severe adult-onset autoinflammatory disease. N Engl J Med 2020;383(27):2628–2638.
24. Bucala R, Tsao BP. The emerging spectrum of somatic mutation in rheumatic disease: clonal hematopoiesis connects aging with giant cell arteritis. Arthritis Rheumatol 2024;76(3):351–353.

American College of Rheumatology
Empowering Rheumatology Professionals

Arthritis & Rheumatology
Vol. 77, No. 11, November 2025, pp 1468–1470
DOI 10.1002/art.43234

NOTES FROM THE FIELD

National Academies' Committee Review of Women's Health Research at the NIH and Recommendations

Jane E. Salmon[1] and Nancy E. Lane[2]

Introduction

The United States is a leader in research innovation and health discoveries, but more than half of the US population, composed of women and girls, has not seen the expected breakthroughs to improve health and well-being. Attention and support for research into conditions specific to, more common among, or that affect women and girls differently is inadequate and chronically underfunded. Girls, women, families, society, employers, and the economy all pay a high price for these inequities.

The long-standing focus on male physiology and anatomy in animal and human health research has contributed to the gaps in what is known about diseases in women. The historical exclusion or underrepresentation of women in clinical research is a major reason for the extensive gaps in the evidence base on women's health. Traditionally, it was felt that research conducted in men was generalizable to women, and women were viewed as a vulnerable population; systematically excluding them from biomedical research was seen as protective and assumed not to create significant barriers to their health or health care. Although inclusion of women in clinical trials has improved in recent years, biomedical research that involves both men and women still often misses the opportunities to analyze sex differences because of, for example, inadequate sample sizes. A true scientific understanding of basic sex-based differences in physiology is needed. The intentional investigation of underlying sex differences would lead to stronger science and to interventions that will benefit the health of the whole population.

Why is this relevant to rheumatology?

Prevalence, presentation, and the severity of rheumatic diseases differs between women and men, and, in many cases, it is striking. Understanding the basis of the differential disease expression and incidence between men and women might lead to deeper understanding of disease pathogenesis and uncover new targets for therapy. In addition, responses to therapy also vary between women and men, and this is a neglected area of study. There are other areas where research on sex differences is deficient. What protects women from gout? Why are women more vulnerable to systemic lupus erythematosus (SLE), scleroderma, and Sjögren disease? And what genes and environmental factors contribute to their susceptibility? How do hormones influence disease pathogenesis and disease activity? What is the basis for these effects? A better understanding of the basis for these differences is likely to accelerate the diagnoses of rheumatic diseases and improve outcomes.

Why focus on sex and gender in rheumatic disease research?

The following discoveries in rheumatic and musculoskeletal diseases underscore the importance of considering sex as a biologic variable for clinical studies as well as more basic science studies. They emphasize the value of comparing women and men in research and how knowledge of the differences can advance our understanding of mechanisms of disease and improve outcomes.

Pharmacologic responses to medications represent an example of how research conducted in male participants may not generalize to female patients. Because many drugs were originally tested solely on male participants, dosing recommendations did not account for sex differences in drug metabolism.[1] It has been more than 35 years since the US Food and Drug Administration approved "statins," and adverse events associated with the XX chromosomes have not been carefully examined. Epidemiologic studies find that after age, female sex is the second most significant risk factor for statin intolerance(age [odds ratio (OR) 1.33, $P = 0.04$], female sex [OR 1.47, $P = 0.007$]).[2] Statin-induced myositis and dysglycemia, two common adverse events,

[1]Jane E. Salmon, MD: Hospital for Special Surgery, New York City, New York; [2]Nancy E. Lane, MD: Department of Internal Medicine, U.C. Davis Health, Sacramento, California.

Author disclosures are available at https://onlinelibrary.wiley.com/doi/10.1002/art.43234.

Address correspondence via email to Jane E. Salmon, MD, at salmonj@hss.edu; or to Nancy E. Lane, MD, at nelane@ucdavis.edu.

Submitted for publication January 16, 2025; accepted in revised form April 30, 2025.

have recently been evaluated in a preclinical model, and the reported X chromosome dosage drives statin-induced dysglycemia and mitochondrial dysfunction. Recently, a treatment with omega-3-fatty acids reduced the adverse effects in female mice.[3]

Ankylosing spondylitis (AS) is more common in men, but there are notable sex differences in symptom presentation.[4] Women tend to have more pronounced symptoms at the time of diagnosis, whereas men often show more radiographic changes and higher markers of inflammation. These differences can contribute to a delayed diagnosis of AS in women. The assumption that research conducted in men will be generalizable to women has turned out to be incorrect.[4] This mirrors studies in cardiovascular disease. Early research on heart attack symptoms was based on male participants, which led to a focus on chest pain as the cardinal symptom. Women, however, are less likely than men to experience chest pain and more likely to have other symptoms, including shortness of breath, nausea, and pain between the shoulder blades, during a myocardial infarction.[5] Differences in symptom presentation have led to misdiagnosis and delayed diagnosis of heart attacks in women, delayed treatment, and worse outcomes.

Eighty percent of people with autoimmune diseases are women, yet diagnosis is often delayed because of a limited understanding of the fundamental mechanisms for most of these conditions. Recently, investigators have begun to elucidate what triggers the disease in women, a discovery that lays the foundation for why women are more susceptible to autoimmune diseases, most dramatically evident in SLE. Xist long noncoding RNA is expressed only in women to randomly inactivate one of the two X chromosomes. Xist also encourages the formation of complexes of RNA, DNA, and proteins, and these RNP complexes, containing autoantigens, are drivers of sex-biased autoimmunity. Male mice require expression of transgenic Xist to develop the autoantibodies and multiorgan autoimmune disease after exposure to a chemical inducer of SLE, and severity mimics that in female mice with the same susceptible genetic background.[6]

The state of women's health research in the United States

Congress commissioned a study as part of the Consolidated Appropriations Act of 2023 to assess the state of women's health research at the National Institutes of Health (NIH). Women's health research was defined as the scientific study of the range of and variability in women's health and the mechanisms and outcomes in disease across the life course. It considers how sex and gender affect women's health, disease risk, pathophysiology, symptoms, diagnosis, and treatment, as well as interactions related to social and structural determinants. The study was sponsored by the Office of Research in Women's Health at the NIH and was implemented by an ad hoc committee assembled by the National Academies of Sciences, Engineering, and Medicine (National Academies).[7] The committee was asked to (1) analyze the proportion of research that the NIH funds on conditions that are female specific, that are more common among women, or that differently impact women and how these conditions are defined across different stages of life, as well as assess sex differences and racial health disparities and (2) provide recommendations on NIH research priorities; NIH training and education efforts needed to build, support, and maintain a robust women's health research workforce; NIH structure, systems, and review processes to optimize women's health research; and the allocation of funding needed to address gaps in women's health research at the NIH.

The committee, composed of 17 members and 2 National Academy of Medicine fellows with diverse expertise and life experiences, met over 11 months, received input from a broad range of stakeholders, and prepared a 9-chapter report with 15 conclusions and 8 recommendations, which were subject to external peer review by 17 experts. To inform its work, the committee conducted a literature review and held information-gathering meetings, where it heard from a range of speakers, including NIH current and former staff, medical subspecialty organizations, women's health organizations, and women's health researchers, as well as perspectives from clinicians and patients. The committee's report, *A New Vision for Women's Health Research: Transformative Change at the National Institutes of Health*, contains its analysis, conclusions, and recommendations.[7]

Conclusions of the National Academies Committee

The committee found in its analysis that on average, just 8.8% of NIH spending from fiscal year (FY) 2013 to FY 2023 across all institutes, centers, and offices focused on women's health research. During the 11-year analysis period, funding on women's health research had been flat, despite steady increases in the NIH budget and total projects. Increased funding for women's health research is essential, but this must be part of a comprehensive and robust women's health research agenda, with a strong infrastructure at the NIH. This includes seamless integration of women's health research across NIH institutes, centers, and offices.

The committee identified several significant gaps in women's health research at the NIH that could be addressed. These include the absence of a comprehensive strategy to develop a robust women's health research agenda, a lack of a clear vision for women's health in the strategic plans of many individual institutes and centers, insufficient tracking of funding for diseases related to women's health research, inadequate attention to developing the research workforce, and limited support for mentors training the next generation of women's health researchers. Additionally, there appears to be a lack of institute and center program officers and extramural investigators with expertise in women's health research to advocate for these issues within the

NIH institutes and centers, including on study sections. These shortcomings, the committee believes, can be remedied.[8]

Recommendations of the National Academies Committee

The 2025 National Academies report provides recommendations on NIH structure, policies, and programs to optimize women's health research, as well as recommendations to build, support, and maintain a robust NIH workforce for women's health research.[8] The committee identified five steps Congress and the NIH should take to advance women's health research:

1. Create pathways to facilitate and support innovative and transformative research for women's health
2. Strengthen oversight, prioritization, and coordination for women's health research across the NIH
3. Expand, train, support, and retain the women's health research workforce
4. Optimize NIH programs and policies to support women's health research
5. Increase NIH investment in women's health research

Conclusions

We hope American College of Rheumatology members will review the recommendations in this report and engage with their congressional representatives to support the NIH to continue funding sex differences in all aspects of health, with a special emphasis on rheumatic and immunologic diseases and the training and support of an expanded rheumatology research workforce. Increased NIH investment in women's health research could allow for the establishment of rheumatic disease population cohorts in female-predominant diseases that extend from the period before disease manifestation to the development of symptoms and disease, as well as patient cohorts to examine progression, coexisting morbidities, and long-term outcomes of autoimmune diseases, as recommended by the National Academies report "Enhancing NIH Research on Autoimmune Disease."[8] We believe that implementation of the recommendations of the Committee on Assessment of NIH Research on Women's Health will improve the health of both our female and male patients with rheumatic diseases.

ACKNOWLEDGMENTS

We sincerely thank and recognize the staff and members of the National Academies Assessment of NIH Research on Women's Health Committee for their invaluable expertise, unwavering commitment, and tireless contributions.

AUTHOR CONTRIBUTIONS

Both authors contributed to at least one of the following manuscript preparation roles: conceptualization AND/OR methodology, software, investigation, formal analysis, data curation, visualization, and validation AND drafting or reviewing/editing the final draft. As corresponding authors, Drs Salmon and Lane confirm that all authors have provided the final approval of the version to be published and take responsibility for the affirmations regarding article submission (eg, not under consideration by another journal), the integrity of the data presented, and the statements regarding compliance with institutional review board/Declaration of Helsinki requirements.

REFERENCES

1. Soldin OP, Mattison DR. Sex differences in pharmacokinetics and pharmacodynamics. Clin Pharmacokinet 2009;48(3):143–157.
2. Bytyçi I, Penson PE, Mikhailidis DP, et al. Prevalence of statin intolerance: a meta-analysis. Eur Heart J 2022;43(34):3213–3223.
3. Zhang P, Munier JJ, Wiese CB, et al. X chromosome dosage drives statin-induced dysglycemia and mitochondrial dysfunction. Nat Commun 2024;15(1):5571.
4. Rusman T, van Vollenhoven RF, van der Horst-Bruinsma IE. Gender differences in axial spondyloarthritis: women are not so lucky. Curr Rheumatol Rep 2018;20(6):35.
5. van Oosterhout REM, de Boer AR, Maas AHEM, et al. Sex differences in symptom presentation in acute coronary syndromes: a systematic review and meta-analysis. J Am Heart Assoc 2020;9(9):e014733.
6. Dou DR, Zhao Y, Belk JA, et al. Xist ribonucleoproteins promote female sex-biased autoimmunity. Cell 2024;187(3):733–749.e16.
7. National Academies of Sciences, Engineering, and Medicine; Health and Medicine Division; Board on Population Health and Public Health Practice; Committee on the Assessment of NIH Research on Women's Health. Geller A, Salganicoff A, Burke SP, eds. A New Vision for Women's Health Research: Transformative Change at the National Institutes of Health. The National Academies Press; 2025.
8. National Academies of Sciences, Engineering, and Medicine; Health and Medicine Division; Board on Population Health and Public Health Practice; Committee for the Assessment of NIH Research on Autoimmune Diseases. Enhancing NIH Research on Autoimmune Disease. The National Academies Press; 2022.

Arthritis & Rheumatology
Vol. 77, No. 11, November 2025, pp 1471–1474
DOI 10.1002/art.43233

Importance of Considering the Gout Flare: Let's Learn to Walk and Chew Gum at the Same Time in Gout Clinical Trial Design

Lisa K. Stamp,[1] Martin A. Kennedy,[2] and Nicola Dalbeth[3]

Introduction

For people with gout, the most important aspect of the disease is the gout flare.[1,2] Thus, a key focus in the management of gout should be the prevention of gout flares. Clinical trial design and researcher focus on serum urate (SU) level reduction to a predefined target has been driven by the scientific understanding that reducing the SU level below the point of saturation will lead to dissolution of monosodium urate crystals and thus remove the trigger for the flare; in other words, SU has been used as a surrogate marker for gout flares. For this reason, SU has been the primary end point for clinical trials of urate-lowering therapy (ULT) in the modern era. The focus on SU in clinical trials without sufficient consideration of gout flares and their impact leaves clinicians with many unanswered questions about management of gout. Herein we discuss the importance of the gout flare and the rationale for changing our thinking to include a greater focus on the gout flare as a clinical trial outcome and what this might mean for gout management and research.

The experience and impact of the gout flare

The gout flare is experienced as an unpredictable episode of intense joint inflammation, with the pain described as "extreme," "excruciating," "horrendous," and "one of the worst pains I've ever had."[3] The gout flare typically lasts 5 to 14 days and can impact all aspects of life.[4] In qualitative research, participants described experiences of a severe gout flare: "It was difficult to even just get out of bed…shower, toilet. All those daily things, it was just, pretty much, very difficult"; and "I felt horrible…when I got the gout it played around with my mind."[3] In addition, gout flares are temporarily associated with other serious health conditions, including deep venous thrombosis, pulmonary embolus,[5] acute myocardial infarction, and stroke.[6]

Challenges of gout flares as a primary or secondary end point in clinical trials of ULT

The Veterans Affairs STOP Gout trial is the first (and to date, only) randomized clinical trial of ULT to report gout flares as the primary end point.[7] All other clinical trials of ULT, including trials for regulatory approval of new ULTs, have reported the SU level as the primary end point. The SU level as the primary end point has significant advantages when it comes to clinical trial design; it is not subject to recall error, it is an inexpensive standard validated laboratory measure that is widely available, and it allows for short, smaller, and less expensive clinical trials. The acceptance of the SU level by regulatory bodies as the primary end point has assumed SU is a biomarker or surrogate for patient important outcomes. Showing SU is a surrogate for gout flares has been complex because flares paradoxically increase in the initial period after commencing ULT and take an extended period after achieving the target SU level to cease.[8]

Conversely, there are challenges when considering using gout flares as the primary end point in clinical trials. Trial design needs to allow for the paradoxical increase in flares when starting ULT as well as the delay after achieving the target SU level for the reduction and/or cessation of flares. Trials of oral ULTs require two years to show that a reduction in SU levels results in a corresponding future reduction in gout flares,[8,9] and such lengthy trials incur significant cost. The increase in cost is also due to the need for a larger sample size to show a change in flares between randomized groups than a change in SU levels. There are currently trials underway, including the Treat-to-Target Serum Urate Versus Treat-to-Avoid Symptoms in Gout (TRUST) trial (ClinicalTrials.gov identifier NCT04875702) and the GO TEST final

[1]Lisa K. Stamp, PhD: University of Otago, Christchurch and Health New Zealand, Christchurch, New Zealand; [2]Martin A. Kennedy, PhD: University of Otago, Christchurch, Christchurch, New Zealand; [3]Nicola Dalbeth, MD: University of Auckland and Health New Zealand, Auckland, New Zealand.
Author disclosures are available at https://onlinelibrary.wiley.com/doi/10.1002/art.43233.

Address correspondence via email to Lisa K. Stamp, PhD, at lisa.stamp@cdhb.health.nz
Submitted for publication February 3, 2025; accepted in revised form May 6, 2025.

trial,[10] that may help provide further evidence about the relationship between SU and gout flares.

Definition of the gout flare

The Gout and Crystal Arthritis Network defines a gout flare as "a clinically evident episode of acute inflammation induced by monosodium urate crystals."[11] The most common definition in the research setting is "self-reported gout flare requiring treatment."[12] A formal gout flare definition has been developed and validated for use in research in people with known gout. In this definition, a flare requires fulfillment of at least three of the following: patient-defined flare, pain at rest score of >3 on a 0 to 10 numerical scale, presence of at least one swollen joint, and presence of at least one warm joint.[13]

Serum urate	Flares	Patient response	Healthcare provider response	Research focus/questions
SU ≥6mg/dL (0.36 mmol/L)	YES			Target population for clinical trials of new urate-lowering and anti-inflammatory therapies What is the best way to prevent gout flares in this group when starting urate lowering therapy? What are the best strategies to improve uptake of urate lowering therapy?
	NO		 ?????	Is there a serum urate above which people should receive urate lowering therapy despite the absence of gout flares? What are the risks versus benefits of starting or intensifying urate-lowering therapy in this group? What strategies enabled gout flare prevention?
SU<6mg/dL (0.36 mmol/L)	YES			Target population for clinical trials of new anti-inflammatory therapies What is the best way to prevent gout flares in this group? Are there some individuals who require a lower target serum urate to prevent gout flares?
	NO			What strategies enabled successful urate-lowering and gout flare prevention?

Figure 1. Integrating SU and gout flares to ensure the best outcomes in gout management. SU, serum urate.

Capture and reporting of gout flares

Capturing flare data in clinical trials is complex. Typically, clinical trials have focused on the proportion of participants experiencing a gout flare as a binary yes or no outcome within a predefined period. However, flares occur sporadically, and research visits are not typically timed to coincide with gout flares, resulting in retrospective data capture during protocol scheduled visits. Flare measurement in trials needs to balance asking frequently about the occurrence of flares, which can result in participant fatigue, and the risk of recall errors if participants are questioned too infrequently. Strategies such as participant diaries have been tried, but in our experience, these are frequently incomplete and/or not returned by participants. A variety of technology-based methods for gout flare capture have been trialed with varying success. Smartphone apps have shown high adherence, good acceptability, and clinical feasibility for people with gout,[14] and the use of wearable activity trackers shows a reduction in activity during the time of a gout flare.[15] Such strategies may be alternatives in the future to alleviate the necessity for repeated questioning and diaries.

There is also significant variation in the way in which gout flare data are reported,[12,16] which gives rise to challenges in undertaking meta-analyses and comparing between different studies. Simply capturing the occurrence of a gout flare, or not, during a predefined period neglects important aspects of gout flares, such as variation in pain intensity, flare duration, when a flare resolves, and whether flares occurring in rapid succession are separate flares or part of the same flare, not only between patients but also between flares experienced by the same patient. It also fails to recognize the impact that the gout flare has on other aspects of the individual's life.

Impact of focusing on the SU level as the key clinical trial end point

SU level reduction is essential for long-term gout management and dealing with the underlying basis of gout. For example, a recent population-based study[17] documented that higher baseline SU levels were associated with increased risk of recurrent gout, with 95% of flares occurring in individuals with SU levels ≥6 mg/dL and 98% in those with SU levels ≥5 mg/dL. However, there is a paradoxical rise in gout flares on commencing ULT, which contributes to many people stopping ULT.[18] Current guidelines recommend use of anti-inflammatory prophylaxis to prevent gout flares during the first three to six months of ULT.[19,20] Even when anti-inflammatory prophylaxis is used during the initial phase of ULT, around 15% of people will have at least one gout flare, and this doubles to ~30% having at least one gout flare in the three-month period after ceasing anti-inflammatory prophylaxis.[21]

In the long-term, ULT using the treat-to-target SU strategy will result in reduction and ultimately cessation in gout flares, but short-term impacts on flare rates can complicate interpretation of trials. For example, in clinical trials of pegloticase, which induces profound reductions in SU levels and improvements in flare outcomes after six months of treatment, there is a substantial flare burden in the first three-month period compared with placebo, which cannot be ignored.[22] Therefore, it is critical for prescribers and people with gout to understand the delay between achieving target SU levels and the cessation of gout flares and for prescribers to ensure access to effective anti-inflammatory prophylaxis during the initial phase of ULT.

Furthermore, new trials need to address areas of clinical uncertainty. In clinical interactions, assessing both gout flares and SU levels results in four possible scenarios (Figure 1). Both patient and health care provider agree treatment should be improved when gout flares continue to occur and the SU level is above target, and, conversely, both agree that no change is needed in the absence of flares and when the SU level is at target. Challenges occur when the health care provider is focused on the SU level and the patient is focused on flares as the outcome and these views do not align.[17,23]

How to balance the flare and SU level together rather than as disparate outcomes

As clinicians and researchers, we need to be able to "walk and chew gum at the same time" in long-term gout trials and clinical management. In other words, we need to manage the SU level and focus more on gout flare prevention and treatment when flares occur. In the clinical setting, we need to ensure that people with gout understand about the time course of gout flare cessation when using the treat-to-target strategy, ensure effective anti-inflammatory prophylaxis, and provide a gout flare action plan with a ready supply of the medication on hand. From a clinical trial perspective, we need to ensure that we capture all aspects of gout flares, including severity and impact on life, rather than just whether they occur.

ACKNOWLEDGMENT

Open access publishing facilitated by University of Otago, as part of the Wiley - University of Otago agreement via the Council of Australian University Librarians.

AUTHOR CONTRIBUTIONS

All authors contributed to at least one of the following manuscript preparation roles: conceptualization AND/OR methodology, software, investigation, formal analysis, data curation, visualization, and validation AND drafting or reviewing/editing the final draft. As corresponding author, Dr Stamp confirms that all authors have provided the final approval of the version to be published and takes responsibility for the affirmations regarding article submission (eg, not under consideration by another journal), the integrity of the data presented, and the statements regarding compliance with institutional review board/Declaration of Helsinki requirements.

REFERENCES

1. Tabi-Amponsah AD, Stewart S, Hosie G, et al. The patient experience of gout remission: a qualitative study. ACR Open Rheumatol 2023; 5(8):399–406.
2. Coulshed A, Nguyen AD, Stocker SL, et al. Australian patient perspectives on the impact of gout. Int J Rheum Dis 2020;23(10):1372–1378.
3. Garcia-Guillen A, Stewart S, Su I, et al. Gout flare severity from the patient perspective: a qualitative interview study. Arthritis Care Res (Hoboken) 2022;74(2):317–323.
4. Stewart S, Guillen AG, Taylor WJ, et al. The experience of a gout flare: a meta-synthesis of qualitative studies. Semin Arthritis Rheum 2020; 50(4):805–811.
5. Cipolletta E, Tata LJ, Nakafero G, et al. Risk of venous thromboembolism with gout flares. Arthritis Rheumatol 2023;75(9):1638–1647.
6. Cipolletta E, Tata LJ, Nakafero G, et al. Association between gout flare and subsequent cardiovascular events among patients with gout. JAMA 2022;328(5):440–450.
7. O'Dell JR, Brophy MT, Pillinger MH, et al. Comparative effectiveness of allopurinol and febuxostat in gout management. NEJM Evid 2022; 1(3):EVIDoa2100028.
8. Stamp L, Morillon MB, Taylor WJ, et al. Serum urate as surrogate endpoint for flares in people with gout: a systematic review and meta-regression analysis. Semin Arthritis Rheum 2018;48(2):293–301.
9. Stamp LK, Frampton C, Morillon MB, et al. Association between serum urate and flares in people with gout and evidence for surrogate status: a secondary analysis of two randomised controlled trials. Lancet Rheumatol 2022;4(1):e53–e60.
10. Peeters IR, den Broeder AA, Taylor WJ, et al. Urate-lowering therapy following a treat-to-target continuation strategy compared to a treat-to-avoid-symptoms discontinuation strategy in gout patients in remission (GO TEST Finale): study protocol of a multicentre pragmatic randomized superiority trial. Trials 2023;24(1):282.
11. Bursill D, Taylor WJ, Terkeltaub R, et al. Gout, hyperuricemia, and crystal-associated disease network consensus statement regarding labels and definitions for disease elements in gout. Arthritis Care Res (Hoboken) 2019;71(3):427–434.
12. Stewart S, Tallon A, Taylor WJ, et al. How flare prevention outcomes are reported in gout studies: a systematic review and content analysis of randomized controlled trials. Semin Arthritis Rheum 2020;50(2): 303–313.
13. Gaffo AL, Schumacher HR, Saag KG, et al. Developing a provisional definition of flare in patients with established gout. Arthritis Rheum 2012;64(5):1508–1517.
14. Elmagboul N, Coburn BW, Foster J, et al. Comparison of an interactive voice response system and smartphone application in the identification of gout flares. Arthritis Res Ther 2019;21(1):160.
15. Elmagboul N, Coburn BW, Foster J, et al. Physical activity measured using wearable activity tracking devices associated with gout flares. Arthritis Res Ther 2020;22(1):181.
16. Morillon MB, Nørup A, Singh JA, et al; OMERACT Gout Working Group. Outcome reporting in randomized trials in gout: a systematic scoping review from the OMERACT gout working group assessing the uptake of the core outcome set. Semin Arthritis Rheum 2023;60: 152191.
17. McCormick N, Yokose C, Challener GJ, et al. Serum urate and recurrent gout. JAMA 2024;331(5):417–424.
18. Harrold LR, Mazor KM, Velten S, et al. Patients and providers view gout differently: a qualitative study. Chronic Illn 2010;6(4):263–271.
19. FitzGerald JD, Dalbeth N, Mikuls T, et al. 2020 American College of Rheumatology guideline for the management of gout. Arthritis Care Res (Hoboken) 2020;72(6):744–760.
20. Richette P, Doherty M, Pascual E, et al. 2016 updated EULAR evidence-based recommendations for the management of gout. Ann Rheum Dis 2017;76(1):29–42.
21. Stamp LK, Frampton C, Newcomb JA, et al. Gout flares after stopping anti-inflammatory prophylaxis: a rapid literature review and meta-analysis. Arthritis Care Res (Hoboken) 2025;77(6):720–726.
22. Sundy JS, Baraf HS, Yood RA, et al. Efficacy and tolerability of pegloticase for the treatment of chronic gout in patients refractory to conventional treatment: two randomized controlled trials. JAMA 2011;306(7): 711–720.
23. Dalbeth N, Saag KG, Palmer WE, et al. Effects of febuxostat in early gout: a randomized, double-blind, placebo-controlled study. Arthritis Rheumatol 2017;69(12):2386–2395.

Arthritis & Rheumatology
Vol. 77, No. 11, November 2025, pp 1475–1487
DOI 10.1002/art.43229

American College of Rheumatology
Empowering Rheumatology Professionals

Dietary Polyunsaturated Fatty Acid and the Risk of Rheumatoid Arthritis: Insights From Genetic Predisposition and Proteomics

Li Chen,[1] Tianqi Tan,[2] Yashu Chen,[1] Feipeng Cui,[3] Huimin Chen,[3] Ying Zhao,[4] Yuhan Tang,[3] Xia Xiang,[1] and Qianchun Deng[1]

Objective. Our objective was to investigate the associations of polyunsaturated fatty acids (PUFAs) intake with rheumatoid arthritis (RA) risk, alongside the role of genetic predisposition and the potential mediating effects of circulating proteins.

Methods. Using data from 188,597 RA-free participants in the UK Biobank, Cox proportional hazard models assessed the association of PUFAs intake with RA risk. The polygenic risk score for RA further allowed evaluation of genetic predisposition's modifying effects. Olink proteomics identified protein signatures associated with PUFAs intake and RA risk, with mediation analyses highlighting specific proteins as potential mediators.

Results. Over a median follow-up of 9.1 years, 1,640 RA cases were documented. Each one-SD deviation increase in the intakes of stearidonic acid (SDA), eicosapentaenoic acid (EPA), docosapentaenoic acid (DPA), and docosahexaenoic acid (DHA) reduced RA risk by 9% to 10%. Among individuals with high genetic risk, omega-3 fatty acids (n-3 PUFAs) intake (including SDA, EPA, DPA, and DHA) significantly decreased RA risk, with antagonistic additive interactions against genetic predisposition. Olink-based proteomic analysis displayed that RA risk and specific n-3 PUFAs intake (DHA, DPA, and SDA) were primarily associated with immune response and inflammation, cytokine interactions, signal transduction, cell adhesion and migration, and metabolic pathways. Mediation analyses identified 55 mediating proteins involved in immune regulation, inflammation, and cell homeostasis. Notably, CD80 and tumor necrosis factor receptor superfamily 4 emerged as vital mediators in the relationship between specific n-3 PUFAs intake and RA risk.

Conclusion. These findings indicated the potential benefits of n-3 PUFAs intake in reducing RA risk and provided new insights into the mechanisms by which n-3 PUFAs influence RA risk.

INTRODUCTION

Rheumatoid arthritis (RA) is a chronic and incurable autoimmune disorder characterized by persistent inflammation.[1] RA affects up to 1% of the adult population, causing progressive joint damage and functional disability.[2] The reductions in life expectancy ascribed to RA range from 1 to 10 years.[3] Despite advancements in therapeutic strategies, the etiology and prevention of RA remain areas of active research.[4] Genetic predisposition plays a significant role in RA risk, but lifestyle and environmental factors, such as diet, have also been implicated in modulating disease onset and progression.

Dietary intakes of polyunsaturated fatty acids (PUFAs) are pivotal controllable factors for the prevention of numerous diseases.[5–7] Long-chain omega-3 fatty acids (n-3 PUFAs) intake has been shown to alleviate clinical symptoms in patients with

Supported by the Earmarked Fund for China Agriculture Research System (CARS-14) and Innovation Group Project of Hubei Province (2023AFA042).

[1]Li Chen, PhD, Yashu Chen, PhD, Xia Xiang, PhD, Qianchun Deng, PhD: Oil Crops Research Institute of the Chinese Academy of Agricultural Sciences, Hubei Key Laboratory of Lipid Chemistry and Nutrition and Key Laboratory of Oilseeds Processing, Ministry of Agriculture, Oil Crops and Lipids Process Technology National and Local Joint Engineering Laboratory, Wuhan, China; [2]Tianqi Tan, PhD: Institute of Maternal and Child Health, Wuhan Children's Hospital (Wuhan Maternal and Child Healthcare Hospital), Tongji Medical College, Huazhong University of Science and Technology, Wuhan, China; [3]Feipeng Cui, PhD, Huimin Chen, PhD, Yuhan Tang, PhD: Department of Nutrition and Food Hygiene, Hubei Key Laboratory of Food Nutrition and Safety, Ministry of Education Key Laboratory of Environment and Health and MOE Key Lab of Environment and Health, Key Laboratory of Environment and Health (Wuhan), Ministry of Environmental Protection, State Key Laboratory of Environment Health (Incubation), School of Public Health, Tongji Medical College, Huazhong University of Science and Technology, Wuhan, China; [4]Ying Zhao, PhD: School of Public Health, Kunming Medical University, Kunming, China.

Drs Xiang and Deng contributed equally to this work.

Additional supplementary information cited in this article can be found online in the Supporting Information section (https://acrjournals.onlinelibrary.wiley.com/doi/10.1002/art.43229).

Author disclosures and a graphical abstract are available at https://onlinelibrary.wiley.com/doi/10.1002/art.43229.

Address correspondence via email to Qianchun Deng, PhD, at dengqianchun@caas.cn.

Submitted for publication November 20, 2024; accepted in revised form April 14, 2025.

RA.[8] However, the evidence linking dietary PUFAs to the incident risk of RA is both scarce and fraught with limitations.[9] The few available observational studies have primarily focused on women, lacked detailed evaluation of specific PUFAs, or had relatively small sample sizes.[10–12] Consequently, it is difficult to draw broadly applicable conclusions on the association between PUFAs and RA risk. Besides, the underlying mechanisms by which PUFAs affect RA risk are poorly understood.

The proteomic analysis offers a promising approach to evaluating health status, forecasting disease risk, exploring underlying mechanisms, and uncovering therapeutic targets.[13,14] Integrating dietary and proteomic data can provide an understanding of biologic mechanisms connecting PUFAs intake with RA risk. Additionally, genetic susceptibility is a key risk factor in RA, and polygenic risk scores (PRSs) offer a tool to assess the cumulative effects of multiple genetic variants associated with the disease.[15] It is well accepted that both genetic and behavioral factors contribute to the development of diseases. However, the interaction between dietary PUFAs intake and genetic predisposition remains unknown. Investigating how genetic risk modifies the effect of PUFAs intakes could yield new insights into RA risk prediction.

Therefore, we conducted a large-scale prospective cohort study using data from the UK Biobank to explore the association between dietary intake of total and specific PUFAs and incident RA. We also evaluated the potential modification effect of genetic susceptibility. Moreover, proteomic signatures both related to RA and PUFAs were identified, with further exploration of the mediating role of proteins in linking PUFAs intake to RA risk.

MATERIALS AND METHODS

Study design and population. The UK Biobank is a large prospective cohort study involving more than half a million participants recruited between 2006 and 2010 from England, Scotland, and Wales. Detailed descriptions of the study design and methods have been published previously.[16] Ethical approval for the UK Biobank was granted by the North West Multi-Centre Research Ethics Committee, and informed consent was obtained from all participants. As illustrated in Figure S1, this study included 210,954 participants who had completed at least one online 24-hour dietary questionnaire. After excluding participants with a history of RA, use of antirheumatic medications, implausible energy intake (<800 or >4,200 kcal/day for men; <500 or >3,500 kcal/day for women), or extreme body mass index (BMI) values (<15 or >50), a total of 188,597 participants were retained for the main analysis. Additionally, 19,672 participants were included in the proteomic analysis, following the exclusion of individuals without proteomic data (UK Biobank Application Number: 88159).

Assessment of dietary PUFA intakes. Participants with valid email addresses were invited to complete the Oxford WebQ questionnaire on five occasions between April 2009 and June 2012. The Oxford WebQ is a 24-hour dietary assessment tool that captures data on 206 foods and 32 beverages consumed during the previous day. The quantity of each food or beverage consumed was calculated by multiplying the standard portion size of each food or beverage by the amount consumed. The calculation of dietary PUFAs intake has been described in previous publications.[17,18] Briefly, the food code for each food and beverage was matched using the McCance and Widdowson (MCW) food database. When food codes were unavailable in the MCW database, similar food codes from the US Department of Agriculture database were used as substitutes. Using these food codes, the UK Nutrient Databank food composition table was applied to estimate individual PUFA intake from all consumed food or drink for each participant. Individual PUFA intake was averaged for participants who had more than one occasion of 24-hour dietary recall. In this study, the dietary exposure included total PUFAs, n-3 PUFAs, and omega-6 fatty acids (n-6 PUFAs). Total n-6 PUFAs included linoleic acid (LA) and arachidonic acid (AA), whereas total n-3 PUFAs included alpha-LA (ALA), stearidonic acid (SDA), eicosapentaenoic acid (EPA), docosapentaenoic acid (DPA), and docosahexaenoic acid (DHA).

Assessment of circulating PUFA levels. Circulating concentrations of PUFAs were measured from a randomly selected subset of EDTA plasma samples collected at baseline in the UK Biobank. The measurements were performed by using a high-throughput nuclear magnetic resonance (NMR)–based metabolic biomarker profiling platform developed by Nightingale Health Ltd. Detailed information has been described previously[19] and is available at https://biobank.ctsu.ox.ac.uk/crystal/label.cgi?id=220. Plasma samples were analyzed using six 500-MHz NMR spectrometers (Bruker AVANCE III HD). Two NMR spectra were recorded for each sample to detect proteins, lipids, and low MW metabolites. The biomarkers were quantified using Nightingale Health's proprietary software (Quantification Library 2020). In this study, the circulating PUFAs included total PUFAs, total n-3 PUFAs, total n-6 PUFAs, DHA, and LA.

Outcome ascertainment. Incident RA diagnoses were primarily obtained from inpatient hospital records using the *International Classification of Diseases, Tenth Revision* (ICD-10) (M05, M06; ICD-9: 71400-71406, 71409). Additional diagnostic information was derived from UK Biobank's self-reports, primary care data, and death registrations (Field IDs: 20002, 131848-131850). Censoring was defined by the earliest occurrence of death, study withdrawal, or the end of follow-up.

Covariates. The analyses were adjusted for the following covariates: age (continuous), sex (male or female), race and

ethnicity (White or not White), BMI (continuous), smoking status (never, former, or current), alcohol consumption (never, former, or current), metabolic equivalent task (MET) (continuous), Townsend deprivation index (continuous), total energy intake (continuous), vitamin A intake (continuous), and vitamin E intake (continuous). Age was calculated based on birth dates, whereas sex, race and ethnicity, smoking, and alcohol intake were self-reported at baseline. BMI was measured at baseline, and physical activity (MET) was assessed using the International Physical Activity Questionnaire. Socioeconomic status was determined by calculating the Townsend deprivation index, which incorporated factors such as unemployment, overcrowding, and home and car ownership. Dietary intake variables were derived from the online 24-hour dietary questionnaire.

PRS calculation. Genotyping in the UK Biobank was performed using a custom Axiom array with 825,927 genetic variants, followed by genome-wide imputation.[20] The Standard PRS for RA was developed in a previous project using trait-specific meta-analyses and Bayesian algorithms. Individual PRS values were calculated as the genome-wide sum of posterior effect sizes per variant, multiplied by allele dosage, based on meta-analyzed summary statistics from genome-wide association studies (UK Biobank Field ID: 26273). In this study, PRS was categorized into low (lowest quintile), medium (quintiles 2–4), and high (highest quintile) risk.[21]

Proteomics. The blood samples used for the proteomics analysis were randomly collected at baseline during the recruitment phase of the UK Biobank (2006–2010). Blood samples were sent to the Olink Analysis Service in Sweden for proteomic analysis (https://biobank.ndph.ox.ac.uk/). Proteins were measured across four panels focusing on cardiometabolic, inflammatory, neurologic, and oncologic pathways. Protein levels were assessed using Olink's proximity extension assay technology, which provided normalized protein expression values. Detailed methodologic descriptions have been reported in previous studies.[22] After excluding proteins with more than 20% missingness, 2,915 proteins were included, and protein levels were $\log_2$-transformed and standardized in the final analyses (Table S1).[23]

Statistical analysis. Baseline characteristics by RA status were compared using chi-square tests and Student's *t*-tests. Continuous variables were presented as medians with interquartile ranges (IQRs) or means ± SDs, and categorical variables were presented as numbers with percentages. All analyses were adjusted for covariates. Missing data for the covariates were coded as a missing indicator category for categorical variables and were imputed with the medians for continuous variables.

The relationships among all PUFA intakes were assessed using Spearman's rank correlation coefficient. Cox proportional hazard models were used to estimate hazard ratios (HRs) and 95% confidence intervals (CIs) for the associations between PUFAs intake (per SD increment) and incident RA. When specific PUFAs were mixed exposed, the contribution weight of specific PUFAs to RA risk was estimated using quantitative g-computation (qgcomp) models (R package "qgcomp").[24] Restricted cubic spline regression was applied to analyze the dose-response relationships between PUFAs intake and RA risk with three knots positioned at the 25th, 50th, and 75th percentiles.

Stratified analyses were conducted by age (<60 or ≥60 years), sex (female or male), and BMI (<25 or ≥25). Sensitivity analyses were performed by using a propensity score–based inverse probability of treatment weighting method to mimic a matched cohort design, excluding participants whose outcomes occurred within two years of follow-up, excluding those with fewer than two dietary assessments, and adjusting for additional factors, including major chronic diseases (cancer, diabetes, and cardiovascular disease), routine clinical indicators (glycosylated hemoglobin, triglyceride levels, and systolic blood pressure), immune-related markers (lymphocyte percentage, white blood cell count, and C-reactive protein), circulating vitamin D levels, and lifestyle factors. Healthy lifestyle scores were constructed based on smoking status, physical activity, diet, and alcohol consumption, and participants were categorized into poor (0–1 points), medium (2 points), or healthy (3–4 points) lifestyle groups.

Cox proportional hazards regression models also examined how the interactions between genetic predisposition and PUFAs intake were associated with RA risk with further adjustment of the genotyping batch and genetic principal components. The multiplicative interaction was tested using adding product terms in the Cox models. Additive interactions were evaluated using relative excess risk due to interaction and attributable proportion due to interaction.[25]

For proteomic analysis, we applied Cox models to examine the association between 2,915 proteins and RA risk. After the false discovery rate (FDR) adjustment, the least absolute shrinkage and selection operator (LASSO) regression (R package "glmnet") was used to identify representative proteomic biomarkers for RA risk. The proteomic signature score was then calculated using a weighted sum of proteins identified by LASSO. Receiver operating characteristic (ROC) curve analysis was conducted to assess the predictive performance of the proteomic signature score for RA risk. Additionally, multivariable-adjusted linear regressions were employed to assess the association of DHA, DPA, and SDA intakes with protein levels. Subsequently, Kyoto Encyclopedia of Genes and Genomes (KEGG) and Gene Ontology (GO) analyses were used to identify related pathways or biologic processes.

Mediation analyses were performed using the %mediate SAS macro (SAS Institute, Inc) to investigate whether specific proteins mediated the association between PUFAs intake and RA risk.[26] The %mediate SAS macro partitions the total effect

Table 1. Baseline characteristics of participants by RA status*

Variables	Total (N = 188,597)	Non-RA (n = 186,957)	Incident RA (n = 1,640)	*P* value
Age, y (SD)	55.8 (8.0)	55.8 (8.0)	58.7 (7.3)	<0.0001
Sex, n (%)				<0.0001
Female	102,279 (54.2)	101,196 (54.1)	1,083 (66.0)	
Male	86,318 (45.8)	85,761 (45.9)	557 (34.0)	
Race and ethnicity, n (%)				0.2907
White	179,881 (95.4)	178,328 (95.4)	1,553 (94.7)	
Not White	8,015 (4.2)	7,933 (4.2)	82 (5.0)	
Missing (%)	701 (0.4)	696 (0.4)	5 (0.3)	
BMI (SD)				<0.0001
Mean (SD)	26.9 (4.5)	26.9 (4.5)	28.2 (5.3)	
Missing (%)	534 (0.3)	524 (0.3)	10 (0.6)	
Alcohol intake, n (%)				<0.0001
Never	6,020 (3.2)	5,941 (3.2)	79 (4.8)	
Previous	5,592 (3.0)	5,522 (3.0)	70 (4.3)	
Current	176,792 (93.7)	175,304 (93.7)	1,488 (90.7)	
Missing (%)	193 (0.1)	190 (0.1)	3 (0.2)	
Smoking status, n (%)				<0.0001
Never	106,984 (56.7)	106,213 (56.7)	771 (47.0)	
Previous	66,050 (35.0)	65,366 (35.0)	684 (41.7)	
Current	15,066 (8.0)	14,886 (8.0)	180 (11.0)	
Missing (%)	497 (0.3)	492 (0.3)	5 (0.3)	
Metabolic equivalent task, min/wk				0.3160
Median (IQR)	1,710.0 (813.0 to 3,295.0)	1,710.0 (813.0 to 3,293.0)	1,695.0 (730.0 to 3,492.0)	
Missing (%)	28,354 (15.0)	28,021 (15.0)	333 (20.3)	
Townsend deprivation index				0.0678
Median (IQR)	−2.3 (−3.7 to 0.1)	−2.3 (−3.7 to 0.1)	−2.2 (−3.7 to 0.3)	
Missing (%)	234 (0.1)	230 (0.1)	4 (0.2)	
Energy intake, median (IQR), kj	8,373.1 (6,993.3 to 9,944.2)	8,375.4 (6,996.6 to 9,946.2)	8,105.7 (6,699.0 to 9,794.9)	<0.0001
Vitamin A intake, median (IQR), μg	731.0 (477.5 to 1,119.9)	731.0 (477.7 to 1,119.2)	731.9 (457.4 to 1,186.6)	0.1078
Vitamin E intake, median (IQR), mg	10.3 (7.8 to 13.3)	10.3 (7.8 to 13.3)	9.9 (7.5 to 13.2)	0.0014

* BMI, body mass index; IQR, interquartile range; RA, rheumatoid arthritis.

(TE) of an exposure (PUFAs intake) on an outcome (RA risk) into two components: the direct effect, which represents the portion of the effect not mediated by the protein, and the indirect effect (IE), which captures the portion of the effect mediated by the protein. The proportion of mediation was calculated as the ratio of the IE to the TE, expressed as a percentage.

The general data analyses and manipulation were performed using SAS (version 9.4) and R (version 4.2.3). Bioinformatics tools used included https://www.omicstudio.cn, https://www.cnsknowall.com, and https://hiplot.com.cn/.

Data availability statement. The UK Biobank resource can be accessed by researchers on application. Data are available from the UK Biobank (https://www.ukbiobank.ac.uk/).

RESULTS

Baseline characteristics. Over a median follow-up for 9.1 years (IQR 9.0–9.9 years), 1,640 incident cases of RA were documented among a total of 188,597 participants. The mean ± SD age of study participants was 55.8 ± 8.0 years, and 54.2% of participants (n = 102,279) were female. Participants who developed RA tended to be older and were predominantly female, smokers, nondrinkers, and overweight. They also had a lower total energy intake and vitamin E intake (Table 1).

The median of estimated total dietary PUFA intake was 12.16 (IQR 9.01–16.04) g/day, including 1.83 (IQR 1.32–2.51) g/day for n-3 PUFAs and 10.21 (IQR 7.47–13.63) g/day for n-6 PUFAs (Table S2). There were relatively strong correlations among total PUFA, n-3 PUFA, n-6 PUFAs, LA, and ALA ($r > 0.5$), whereas SDA, AA, EPA, DPA, and DHA showed weaker correlations with total and n-6 PUFAs ($r < 0.5$) but higher correlations with n-3 PUFAs ($r > 0.5$). Additionally, marine PUFAs (EPA, DPA, and DHA) were highly correlated with each other (Figure S2).

Association between PUFA intakes and RA risk. Cox regression models revealed that total n-3 PUFA intake was inversely associated with RA risk, with an HR of 0.91 (95% CI 0.85–0.98; $P = 0.0073$). Specifically, each one-SD increment in SDA, EPA, DPA, and DHA intakes was associated with a reduction in RA risk by 9% (95% CI 0.86–0.96), 10% (95% CI 0.85–0.95), 9% (95% CI 0.86–0.96), and 10% (95% CI 0.85–0.95), respectively (Figure 1). Dose-response analyses displayed a linear relationship between the intakes of total and specific n-3 PUFAs (SDA, EPA, DPA, and DHA) and RA risk (nonlinearity $P > 0.05$) (Figure 1). Furthermore, qgcomp models showed that DHA

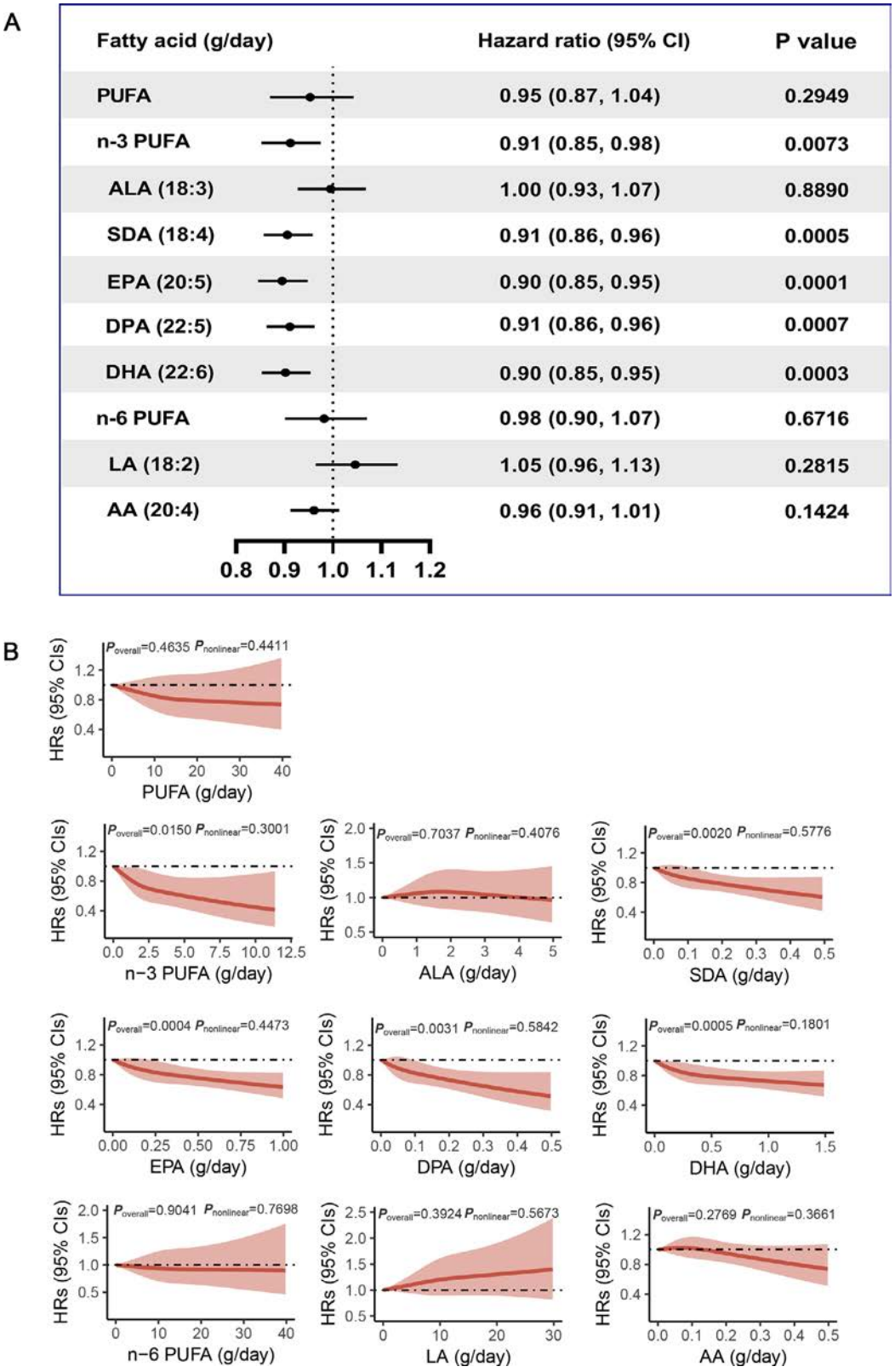

Figure 1. Association between PUFA intake and rheumatoid arthritis risk. (A) The forest plot displays the HRs and 95% CIs. (B) Dose-response relationship. Models were adjusted for age, sex, race and ethnicity, body mass index, alcohol intake, smoking status, metabolic equivalent task, Townsend deprivation index, energy intake, vitamin A intake, and vitamin E intake. AA, arachidonic acid; ALA, alpha linoleic acid; CI, confidence interval; DHA, docosahexaenoic acid; DPA, docosapentaenoic acid; EPA, eicosapentaenoic acid; HR, hazard ratio; LA, linoleic acid; PUFA, polyunsaturated fatty acid; SDA, stearidonic acid.

Table 2. Association between per SD increment in PUFA intake and rheumatoid arthritis risk stratified by polygenic risk score*

	Low genetic risk (36,844/213)		Medium genetic risk (110,533/911)		High genetic risk (36,844/458)	
Fatty acids	Hazard ratio (95% CI)	*P* value	Hazard ratio (95% CI)	*P* value	Hazard ratio (95% CI)	*P* value
PUFA	0.98 (0.94–1.03)	0.3735	1.00 (0.98–1.02)	0.7820	0.98 (0.95–1.01)	0.1493
n-3 PUFA	0.85 (0.70–1.03)	0.0904	0.97 (0.89–1.06)	0.5126	0.84 (0.73–0.97)	0.0155
ALA (18:3)	0.90 (0.73–1.10)	0.2971	1.01 (0.92–1.11)	0.7631	0.96 (0.83–1.10)	0.5477
SDA (18:4)	0.89 (0.76–1.03)	0.1261	0.94 (0.87–1.01)	0.0825	0.87 (0.78–0.98)	0.0201
EPA (20:5)	0.88 (0.75–1.02)	0.0973	0.92 (0.85–0.99)	0.0212	0.89 (0.79–0.99)	0.0385
DPA (22:5)	0.90 (0.77–1.05)	0.1690	0.95 (0.89–1.02)	0.1462	0.85 (0.76–0.96)	0.0069
DHA (22:6)	0.89 (0.76–1.04)	0.1337	0.93 (0.87–1.00)	0.0535	0.87 (0.77–0.98)	0.0181
n-6 PUFA	0.99 (0.94–1.04)	0.6122	1.00 (0.98–1.02)	0.8987	0.98 (0.95–1.02)	0.3526
LA (18:2)	1.02 (0.81–1.28)	0.8679	1.06 (0.95–1.18)	0.3315	0.98 (0.84–1.15)	0.8403
AA (20:4)	1.02 (0.89–1.18)	0.7754	1.00 (0.94–1.07)	0.9406	0.87 (0.78–0.97)	0.0123

* Models were adjusted for age, sex, race and ethnicity, body mass index, alcohol intake, smoking status, metabolic equivalent task, Townsend deprivation index, energy intake, vitamin A intake, vitamin E intake, genotyping batch, and genetic principal components. AA, arachidonic acid; ALA, alpha linoleic acid; CI, confidence interval; DHA, docosahexaenoic acid; DPA, docosapentaenoic acid; EPA, eicosapentaenoic acid; LA, linoleic acid; n-3 PUFA, omega-3 fatty acid; n-6 PUFA, omega-6 fatty acid; PUFA, polyunsaturated fatty acid; SDA, stearidonic acid.

accounted for the largest proportion of weight in reducing RA risk when specific PUFAs were exposed together (weight = 0.53) (Figure S3). Consistently, circulating n-3 PUFA and DHA levels were inversely and linearly associated with RA risk, with HRs of 0.83 (95% CI 0.75–0.93) for n-3 PUFA and 0.83 (95% CI 0.74–0.93) for DHA (Tables S3 and S4 and Figure S4). A similar pattern of associations between n-3 PUFA intake and RA risk was observed across a series of sensitivity analyses (Table S5).

Significant interactions were observed between total n-3 PUFA intake and both age (interaction $P = 0.0257$) and sex (interaction $P = 0.0449$). Subgroup analyses demonstrated stronger inverse associations between total and specific n-3 PUFAs intake and RA risk in younger individuals (<60 years) and women compared to their respective counterparts (Figure S5).

PUFAs intake and genetic predisposition. We constructed an RA-related PRS and observed an increase in the RA risk across genetic risk categories (P for trend <0.0001) (Table S6). Among participants with high genetic predisposition, the intakes of n-3 PUFA (HR 0.84 [95% CI 0.73–0.97]), SDA (HR 0.87 [95% CI 0.78–0.98]), EPA (HR 0.89 [95% CI 0.79–0.99]), DPA (HR 0.85 [95% CI 0.76–0.96]), DHA (HR 0.87 [95% CI 0.77–0.98]), and AA (HR 0.87 [95% CI 0.78–0.97]) were significantly associated with RA risk. Conversely, there was no significant association among participants with a low genetic predisposition (Table 2). Notably, the intakes of DPA, DHA, and AA had antagonistic additive interactions with genetic predisposition on RA risk (P for additive interactions = 0.0341, 0.0478, and 0.0065, respectively) (Table S7). Joint effects analyses also revealed participants with low PRS and high total or specific n-3 PUFAs intake had the lowest RA risk compared to those with high PRS and low corresponding PUFAs intake (Figure S6).

Proteomic signature for RA risk. Proteins play a crucial role in mediating biologic processes and serve as functional executors within the body, making them valuable biomarkers for understanding disease mechanisms and predicting disease risk.[23] The baseline characteristics of 19,672 participants with proteomic data are shown in Table S8. Cox regression models showed that 308 proteins were significantly associated with RA risk (Figure 2A and Table S9). After adjusting by the FDR, 25 proteins were still significantly associated with RA risk (Figure S7A). The protein-protein interaction network displayed that CD80 served as a central node, interacting with several key proteins, including CCL7, CXCL10, CXCL9, lysosome-associated membrane protein 3 (LAMP-3), galectin-9, programmed cell death protein 1 (PDCD1), plasminogen activator urokinase receptor, tumor necrosis factor (TNF) receptor superfamily 4 (TNFRSF4), and TNFRSF9. This complex network was related to the pathways of immune responses, cell adhesion, and inflammation (Figure S7B). Furthermore, we constructed a proteomic signature score by LASSO regression (Figure S8A). ROC curve analyses showed that the area under the curve (AUC) for the covariate features alone was 0.67, whereas the AUC for the proteomic signature score alone was 0.69. When the proteomic signature score was combined with covariates, the AUC improved to 0.73, representing a 9% increase in predictive ability compared to using covariates alone (Figure S8B).

KEGG analysis of the 308 proteins revealed that RA-related pathways were primarily involved in immune response and inflammation (eg, interleukin-17 [IL-17] and TNF signaling pathways), cytokine interactions (eg, cytokine-cytokine receptor interaction), signal transduction pathways (eg, JAK-STAT, NF-κB, and phosphatidylinositol 3-kinase [PI3K]–protein kinase B [Akt] protein kinase B signaling pathways), cell adhesion and migration (eg, cell adhesion molecules), and metabolic pathways (eg, lipid and atherosclerosis, protein digestion, and absorption)

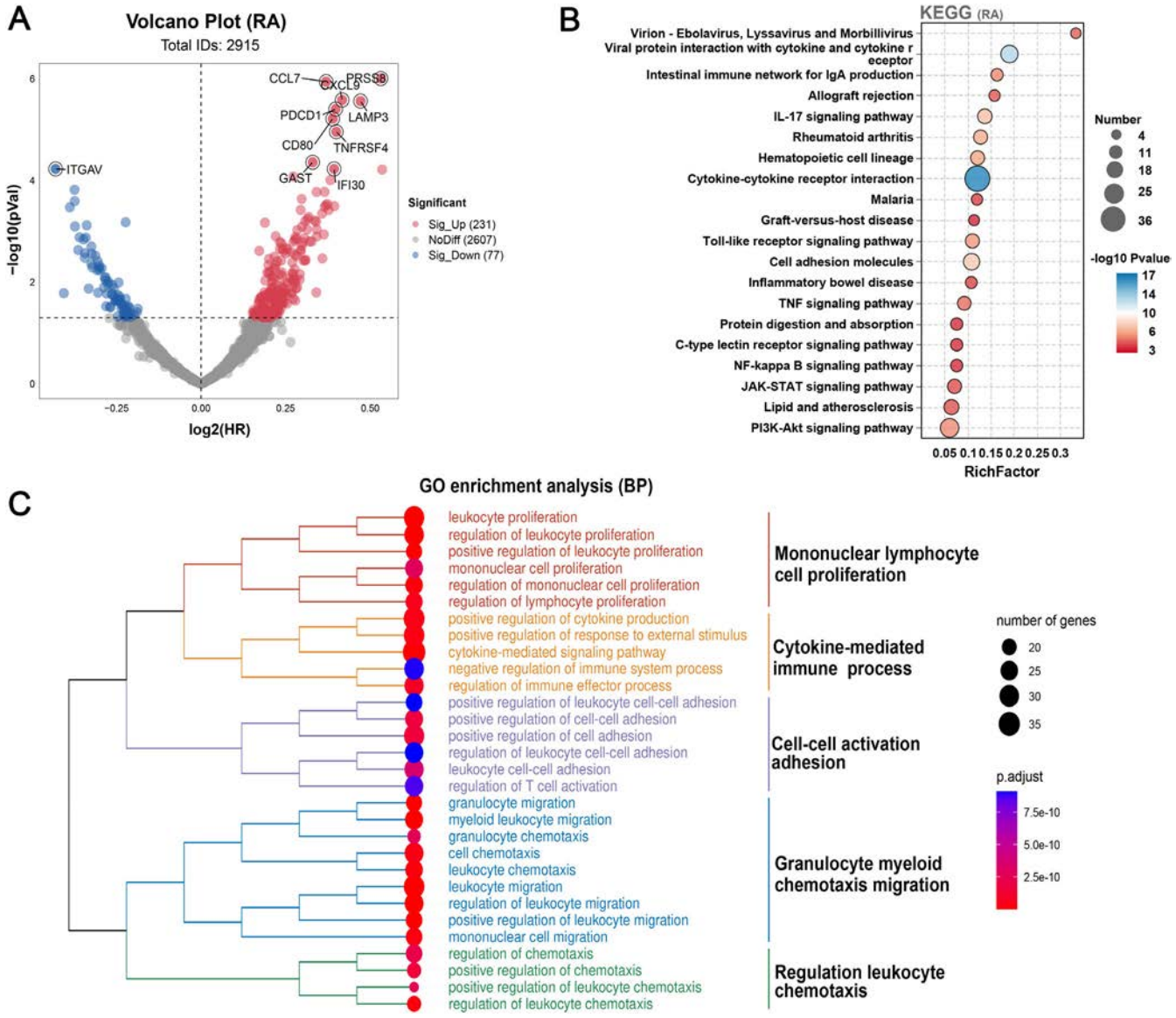

Figure 2. Bioinformatic analysis of proteins associated with RA risk. (A) Volcanic maps of the association of 2,915 proteins with RA risk. The top associated proteins were labeled. (B) Top enriched pathways from KEGG analysis of RA-associated proteins. (C) Clustering of top enriched BP from GO analysis of RA-associated proteins. Akt, protein kinase B; BP, biologic processes; GAST, glutathione S-transferase; GO, Gene Ontology; IFI30, interferon-inducible protein 30; ITGAV, integrin alpha-V; KEGG, Kyoto Encyclopedia of Genes and Genomes; HR, hazard ratio; LAMP-3, lysosome-associated membrane protein 3; NoDiff, no difference; PDCD1, programmed cell death protein 1; PI3K, phosphatidylinositol 3-kinase; PRSS8, prostasin; RA, rheumatoid arthritis; Sig_Down, significantly downregulated; Sig_Up, significantly upregulated; TNF, tumor necrosis factor; TNFSF4, tumor necrosis factor receptor superfamily 4. Color figure can be viewed in the online issue, which is available at http://onlinelibrary.wiley.com/doi/10.1002/art.43229/abstract.

(Table S10). The clustering of GO analysis found that key biologic processes associated with RA risk included mononuclear lymphocyte proliferation, cytokine-mediated immune responses, cell-cell adhesion and activation, granulocyte and myeloid chemotaxis, and leukocyte chemotaxis (Table S10).

Proteomic signature for specific n-3 PUFAs. Among participants with proteomic data (case/n = 198/19,672), the intakes of DHA, DPA, and SDA were significantly associated with RA risk (all $P < 0.05$) (Table S11). We further analyzed the protein signatures related to these specific PUFAs. Linear regression models with FDR adjustment identified 1,450, 1,238, and 1,376 proteins significantly associated with DHA, DPA, and SDA intakes, respectively (Figure 3A, C, and E; Table S12). KEGG enrichment analysis revealed common involvement of the above specific n-3 PUFAs in immune and inflammatory pathways, including apoptosis, TNF signaling, NF-κB signaling, cytokine-cytokine receptor interaction, and cell adhesion molecules (Table S13). DHA was specifically linked to pathways such as epidermal growth factor receptor tyrosine kinase inhibitor resistance,

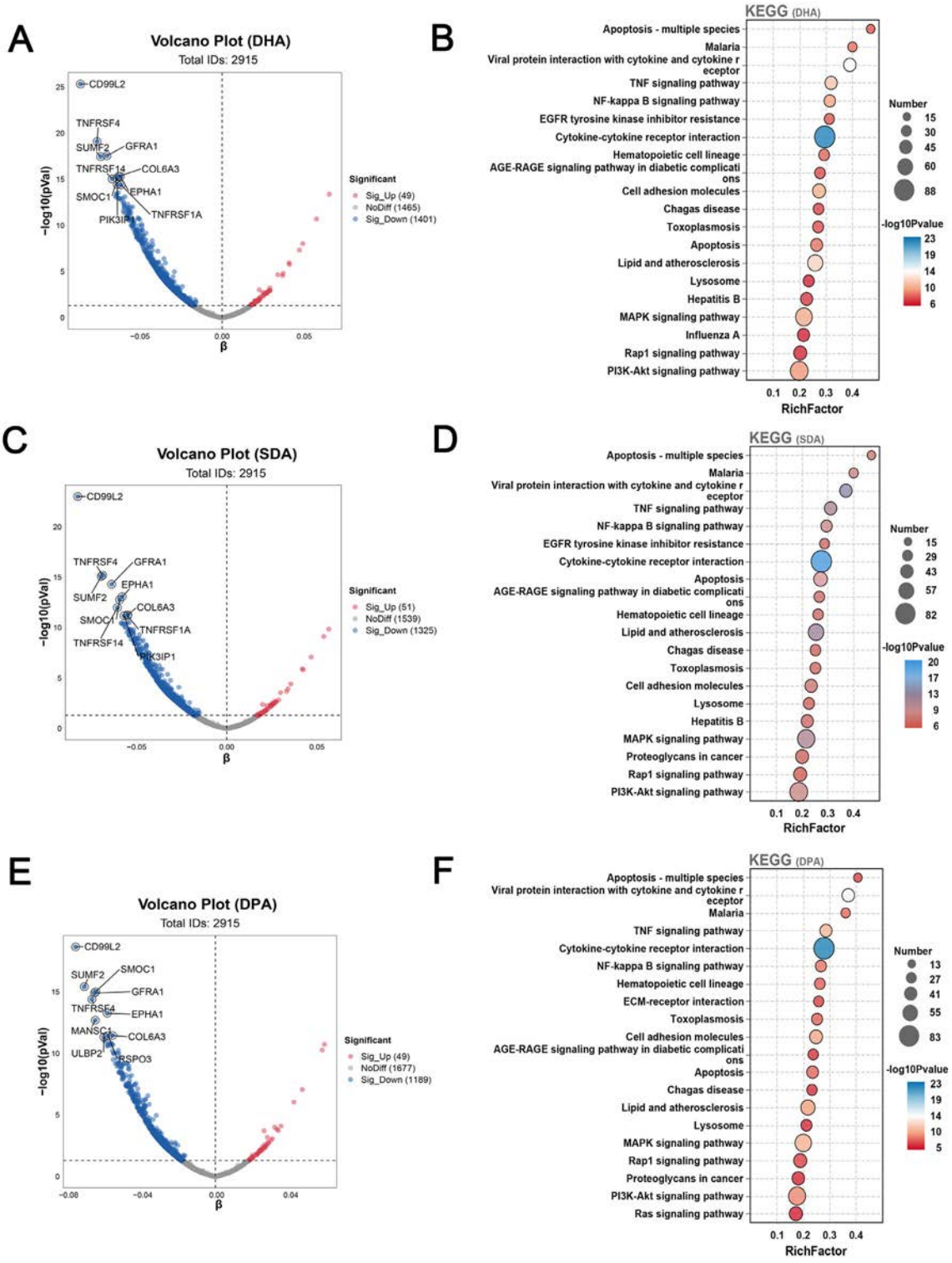

Figure 3. Bioinformatic analysis of proteins associated with fatty acids. (A, C, and E) Volcanic maps of the association of 2,915 proteins with DHA, DPA, and SDA intake. Top associated proteins were labeled. (B, D, and F) Top enriched pathways from KEGG analysis of proteins associated with DHA, DPA, and SDA intake. AGE-RAGE, advanced glycation end product–receptor for advanced glycation end products; Akt, protein kinase B; COL6A3, collagen alpha-3(VI) chain; DHA, docosahexaenoic acid; DPA, docosapentaenoic acid; ECM, extracellular matrix; EGFR, epidermal growth factor receptor; EPHA1, EPH receptor A1; GFRA1, GDNF family receptor alpha 1; KEGG, Kyoto Encyclopedia of Genes and Genomes; NoDiff, no difference; PI3K, phosphatidylinositol 3-kinase; PIK3IP1, phosphoinositide-3-kinase interacting protein 1; RA, rheumatoid arthritis; RSPO3, R-spondin 3; SDA, stearidonic acid; Sig_Down, significantly downregulated; Sig_Up, significantly upregulated; SMOC1, SPARC-related modular calcium-binding protein 1; SUMF2, sulfatase modifying factor 2; TNF, tumor necrosis factor; TNFSF4, tumor necrosis factor receptor superfamily 4; ULBP2, UL16-binding protein 2. Color figure can be viewed in the online issue, which is available at http://onlinelibrary.wiley.com/doi/10.1002/art.43229/abstract.

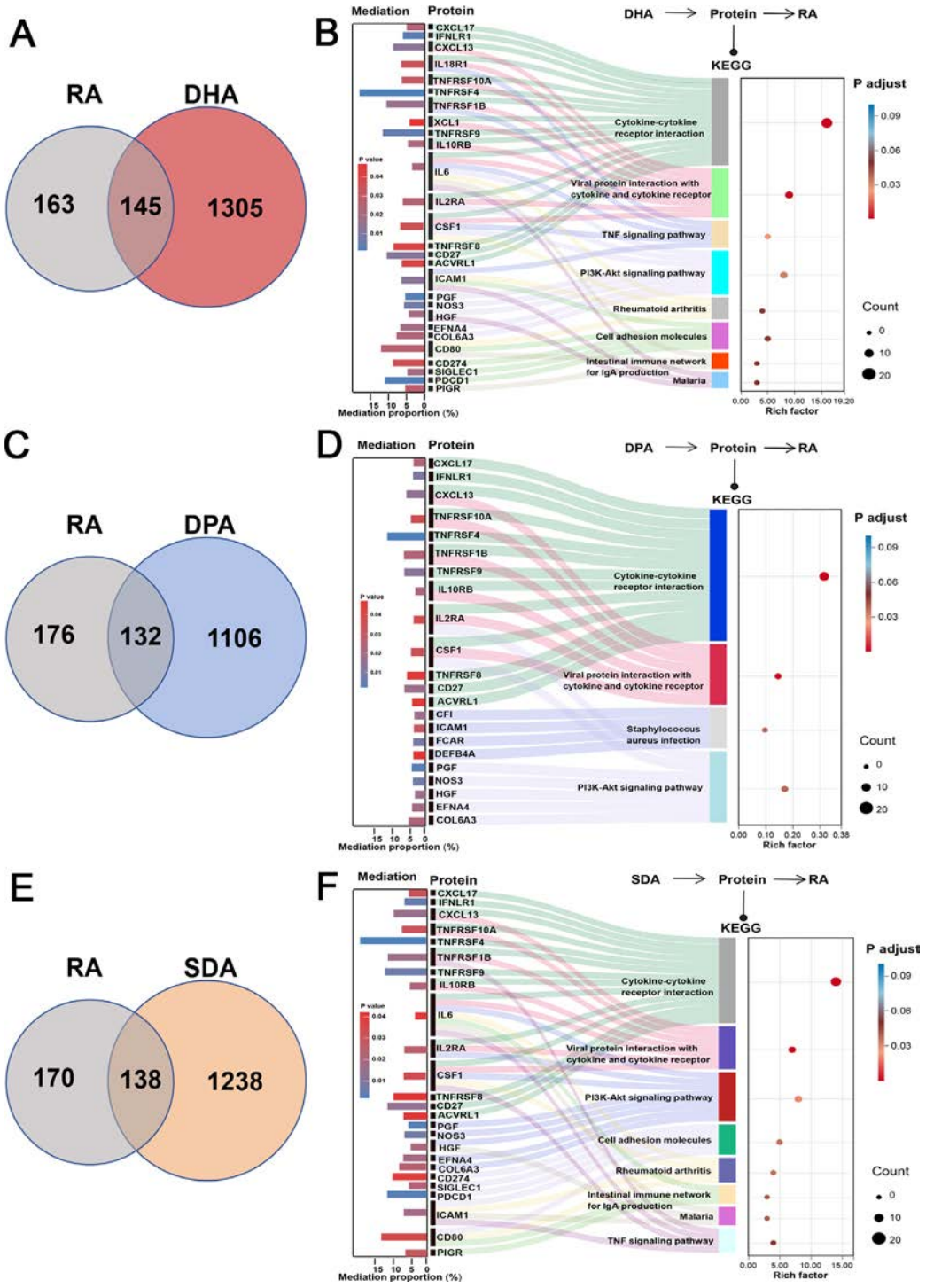

Figure 4. Mediation and bioinformatic analysis. (A, C, and E) Venn diagram of proteins significantly associated with both RA risk and DHA, DPA, or SDA intake. (B, D, and F) Left: mediating proportion of proteins on the association of per SD increment in DHA, DPA, or SDA intake with RA risk. Models were adjusted for age, sex, race and ethnicity, body mass index, alcohol intake, smoking status, metabolic equivalent task, Townsend deprivation index, energy intake, vitamin A intake, and vitamin E intake. Right: Top enriched pathways from KEGG analysis of mediating proteins. ACVRL1, activin A receptor-like kinase 1; Akt, protein kinase B; CFI, complement factor I; COL6A3, collagen alpha-3(VI) chain; CSF1, colony-stimulating factor 1; DEFB4A, defensin beta 4A; DHA, docosahexaenoic acid; DPA, docosapentaenoic acid; ECM, extracellular matrix; EFNA4, ephrin A4; EGFR, epidermal growth factor receptor; EPHA1, EPH receptor A1; FCAR, immunoglobulin alpha Fc receptor; HGF, hepatocyte growth factor; ICAM-1, intercellular adhesion molecule 1; IFNLR1, interferon λ receptor 1; IL-6, interleukin 6; KEGG, Kyoto Encyclopedia of Genes and Genomes; NOS3, nitric oxide synthase 3; PDCD1, programmed cell death protein 1; PGF, prostaglandin; PI3K, phosphatidylinositol 3-kinase; PIGR, polymeric Ig receptor; PIK3IP1, phosphoinositide-3-kinase interacting protein 1; RA, rheumatoid arthritis; SDA, stearidonic acid; SIGLEC1, sialoadhesin; TNF, tumor necrosis factor; TNFSF1B, tumor necrosis factor receptor superfamily 1B. Color figure can be viewed in the online issue, which is available at http://onlinelibrary.wiley.com/doi/10.1002/art.43229/abstract.

advanced glycation end product–receptor for advanced glycation end products signaling in diabetic complications, and PI3K-Akt signaling, which were crucial for both inflammation and metabolic regulation (Figure 3B). DPA highlighted interactions with extracellular matrix receptor interaction, proteoglycans in cancer, and Ras signaling, suggesting additional roles in extracellular matrix dynamics and cellular signaling (Figure 3D). SDA was associated with pathways such as lipid and atherosclerosis, MAPK signaling, and lysosomal activity, further indicating its function in metabolic and immune processes (Figure 3E). GO enrichment analyses emphasized the importance of these specific n-3 PUFAs in immune responses and intercellular interactions (Figure S9).

Mediation analysis of proteins on associations between specific n-3 PUFAs with RA risk. There were 145, 132, and 138 proteins that were commonly associated with both RA risk and the dietary intakes of DHA, DPA, and SDA, respectively (Figure 4A, C, and E). Mediation analysis identified key proteins with the highest mediation proportions, including TNFRSF4, LAMP-3, CD80, TNFRSF9, PDCD1, CD27, and TNFRSF1B, with proportions ranging from 6.8% to 17.6% (Table S14). These proteins linked the intakes of DHA, DPA, and SDA to RA risk through immune and inflammatory pathways (Tables S15 and S16). For DHA, critical pathways included cytokine-cytokine receptor interaction, TNF signaling, and PI3K-Akt signaling, along with roles in cell adhesion and RA (Figure 4D). For DPA, enriched pathways included cytokine-cytokine receptor interaction, *Staphylococcus aureus* infection, and PI3K-Akt signaling (Figure 4E). SDA shared similar pathways, including cytokine-cytokine receptor interaction, PI3K-Akt signaling, and TNF signaling (Figure 4F).

A total of 55 proteins commonly mediated the associations of DHA, DPA, and SDA intakes with RA risk (Figure S10A). These proteins were enriched in cytokine-cytokine receptor interaction and PI3K-Akt signaling pathways, highlighting the role of immune, inflammation, and cellular homeostasis in mediating the link between specific n-3 PUFAs and RA risk (Figure S10B and Table S16). Additionally, 18 proteins, such as CD80, TNFRSF4, and colony-stimulating factor 1, also mediated the association between circulating DHA levels and RA risk, with mediation proportions ranging from 8.7% to 55.8% (Table S17).

DISCUSSION

In the current study, we found that total and specific n-3 PUFAs (SDA, EPA, DPA, and DHA) were inversely and linearly associated with RA risk. These associations were particularly significant in individuals with high genetic predisposition. DPA, DHA, and AA exhibited antagonistic additive interactions with genetic risk. Additionally, RA-related pathways primarily involved immune response, inflammation, signal transduction, and metabolic processes. Specific n-3 PUFAs (SDA, DPA, and DHA) notably altered apoptosis pathways, TNF signaling, NF-κB signaling, cytokine receptor interactions, and cell adhesion. Mediation analyses further revealed that immune function, inflammation, and cellular homeostasis mediated the relationship between specific n-3 PUFAs and RA risk.

Previous studies have primarily focused on the relationship between PUFAs and RA prognosis, highlighting the benefits of marine n-3 PUFAs to patients with RA.[8] To date, however, the evidence from observational studies has been limited, with some cross-sectional studies finding no significant association between PUFAs and RA.[12,27,28] A prospective study involving 32,232 women reported a negative association between long-chain n-3 PUFA intake and RA risk.[11] Building on this, our study expanded the sample population and specifically evaluated the associations of individual PUFAs with RA risk. We found that total n-3 PUFA intake was significantly associated with a reduced RA risk, largely driven by marine n-3 PUFAs such as DHA, DPA, and EPA. Furthermore, qgcomp analyses identified DHA as the leading contributor to RA risk reduction when multiple PUFAs were exposed together. Consistently, circulating DHA levels were significantly associated with RA risk. These findings suggested the protective effects of marine n-3 PUFAs in RA occurrence and progression.

Extensive research has established that genetic predisposition is a major factor in the risk of RA.[29] As far as we know, this study is the first to explore the potential interactions between PUFAs consumption and genetic susceptibility to RA. Among individuals with high genetic risk, higher specific n-3 PUFAs intake, namely SDA, EPA, DPA, and DHA, were associated with a lower risk of RA, whereas a nonsignificant association was observed in those with low genetic risk. This suggested that prioritizing dietary marine n-3 PUFAs may be especially important for genetically susceptible populations. Additionally, we found antagonistic additive interactions between DHA, DPA, and AA and genetic factors, indicating that modifying dietary intakes of n-3 PUFAs may offset the genetic risk of developing RA. Interestingly, AA, an n-6 PUFA, was significantly associated with RA risk only among people with high genetic risk and women. In these high-risk RA populations, specific genetic and hormonal conditions may disrupt the immune balance, allowing AA to modulate excessive immune responses through its dual proinflammatory and anti-inflammatory properties.[30,31]

Using the Olink assay, we identified 308 proteins associated with RA risk without FDR correction. Enrichment analysis showed that these proteins were primarily involved in immune response, inflammation, signal transduction, cell adhesion, and lipid metabolism pathways. Similar studies found that 20 altered proteins in patients with RA (n = 50), including CCL18, TNFRSF10A, TNFRSF11A, and IL-6, were mainly linked to cytokine-cytokine receptor interactions.[32] Notably, our study showed CD80 emerged as a central protein interacting with multiple RA-related

proteins. CD80 is a key cell surface protein for T cell activation through costimulatory signals.[31] Its significance in RA has been demonstrated in previous studies.[33] For example, abatacept inhibited T cell activation by binding to CD86 and CD80 to block the interaction with CD28, or targeted B cells by reducing CD80/CD86 expression, serving as a treatment for RA.[34,35] Besides, classic therapeutic targets of RA for clinical application also included inhibitors of cyclooxygenase 2, aminoimidazole carboxamide ribonucleotide transformylase, dihydroorotate dehydrogenase, folate metabolizing enzymes, IL-1Ra, IL-6Ra, TNFα, CD20, and JAK.[36,37] Notably, our studies identified that the members of the TNF ligand-receptor superfamily and (CXC motif) ligand family, such as TNFRSF4, TNFRSF9, CXCL9, and CXCL10, were also significantly associated with RA risk. Collectively, analyzing these proteins enhanced our understanding of RA's molecular mechanisms, potentially leading to new therapeutic targets and biomarkers for prevention and treatment.

Moreover, we examined the association between specific n-3 PUFAs and 2,950 proteins related to cardiometabolic, inflammatory, neurologic, and oncologic processes. Enrichment analysis revealed that DHA, DPA, and SDA commonly regulated immune and inflammatory pathways, with DHA uniquely linked to metabolic regulation, DPA to extracellular matrix signaling, and SDA to metabolic and immune-specific processes. Although numerous animal studies have consistently demonstrated the anti-inflammatory effects of n-3 PUFAs,[38,39] population-based studies were relatively limited. One study involving 268 individuals exhibited associations between n-3 PUFAs and inflammatory biomarkers[40] such as vascular cell adhesion molecule 1, intercellular adhesion molecule 1, and IL-15. These findings indicated the regulation of n-3 PUFAs on immune and inflammatory pathways. Furthermore, mediation analyses identified a total of 55 proteins that commonly mediated the association between specific n-3 PUFAs and RA risk. These proteins were enriched in cytokine-cytokine receptor interaction and PI3K-Akt signaling pathways, underscoring the roles of immune regulation, inflammation, and cellular homeostasis. Notably, TNFRSF4 and CD80 were key mediators in the link between specific n-3 PUFAs and RA risk. These observations provided a relatively comprehensive population-based analysis of the mechanisms by which n-3 PUFAs influence RA risk.

Benefiting from the large sample size and long follow-up periods of the UK Biobank, this study can explore the relationship between PUFA intakes and RA risk, with adjustment for a variety of confounders and several sensitivity analyses. This study was also the first to investigate the interaction of dietary PUFAs with genetic susceptibility to RA and the mediated effects of proteins on the association between n-3 PUFAs intake and RA risk.

There were also some limitations. Firstly, the identification of incident RA cases primarily relied on hospital inpatient records from the UK Biobank, which may overlook patients with milder clinical symptoms, potentially leading to an underestimation of the total number of RA cases. Secondly, although many relevant confounders were controlled, we cannot entirely rule out the possibility of residual confounding, reverse causation, or bias from unmeasured confounders and measurement errors. Thirdly, dietary data were available only at baseline, and thus time-varying changes in PUFAs intakes were difficult to investigate.

Fourthly, previous studies have suggested moderate to substantial agreement between baseline and repeat dietary assessments,[41] and our results are still robust excluding participants with fewer than two dietary assessments. However, it is important to acknowledge that dietary intake data were self-reported, which may introduce potential measurement bias, and there were disparities in the number of 24-hour online dietary questionnaires completed by participants. Further research is warranted to validate dietary fatty acid intake and its associations with RA risk using more objective measures or repeated assessments. Fifth, although the median time gap between dietary assessment and blood collection was 1.87 years, dietary habits in middle-aged and older adult populations are generally stable over four to five years.[42,43] Sixth, the lack of significant associations in the low genetic risk group may be due to limited statistical power. Finally, the mediation analysis results should be interpreted with caution, as the assumed causal relationships and temporal order among variables cannot be confirmed in this observational study.

In conclusion, this study presented the inverse associations of total and specific n-3 PUFAs with RA risk, especially in individuals with high genetic susceptibility. Proteomic analyses highlighted the mediating effects of immune, inflammation, and cellular homeostasis on linking specific n-3 PUFAs to RA risk, with CD80 and TNFRSF4 emerging as key mediators. These findings indicated the potential benefits of n-3 PUFAs in reducing RA risk via modulating immune responses and inflammation pathways, offering valuable avenues for future research on therapeutic targets and RA prevention.

ACKNOWLEDGMENT

We are grateful to the participants of the UK Biobank Study and those who collected and managed the data.

AUTHOR CONTRIBUTIONS

All authors contributed to at least one of the following manuscript preparation roles: conceptualization AND/OR methodology, software, investigation, formal analysis, data curation, visualization, and validation AND drafting or reviewing/editing the final draft. As corresponding author, Dr Deng confirms that all authors have provided the final approval of the version to be published and takes responsibility for the affirmations regarding article submission (eg, not under consideration by another journal), the integrity of the data presented, and the statements

regarding compliance with institutional review board/Declaration of Helsinki requirements.

REFERENCES

1. Di Matteo A, Bathon JM, Emery P. Rheumatoid arthritis. Lancet 2023; 402(10416):2019–2033.
2. Finckh A, Gilbert B, Hodkinson B, et al. Global epidemiology of rheumatoid arthritis. Nat Rev Rheumatol 2022;18(10):591–602.
3. Chiu YM, Lu YP, Lan JL, et al. Lifetime risks, life expectancy, and health care expenditures for rheumatoid arthritis: a nationwide cohort followed up from 2003 to 2016. Arthritis Rheumatol 2021;73(5): 750–758.
4. Brown P, Pratt AG, Hyrich KL. Therapeutic advances in rheumatoid arthritis. BMJ 2024;384:e070856.
5. Yang B, Tseng PT, Hu X, et al. Comparative efficacy of omega-3 polyunsaturated fatty acids on major cardiovascular events: a network meta-analysis of randomized controlled trials. Prog Lipid Res 2022; 88:101196.
6. Shchepinov MS. Polyunsaturated fatty acid deuteration against neurodegeneration. *Trends Pharmacol Sci* 202;41(4):236–248.
7. Schulze MB, Minihane AM, Saleh RNM, et al. Intake and metabolism of omega-3 and omega-6 polyunsaturated fatty acids: nutritional implications for cardiometabolic diseases. Lancet Diabetes Endocrinol 2020;8(11):915–930.
8. Tański W, Świątoniowska-Lonc N, Tabin M, et al. The relationship between fatty acids and the development, course and treatment of rheumatoid arthritis. Nutrients 2022;14(5):1030.
9. Navarini L, Afeltra A, Gallo Afflitto G, et al. Polyunsaturated fatty acids: any role in rheumatoid arthritis? Lipids Health Dis 2017; 16(1):197.
10. de Pablo P, Romaguera D, Fisk HL, et al. High erythrocyte levels of the n-6 polyunsaturated fatty acid linoleic acid are associated with lower risk of subsequent rheumatoid arthritis in a southern European nested case-control study. Ann Rheum Dis 2018;77(7);981–987.
11. Di Giuseppe D, Wallin A, Bottai M, et al. Long-term intake of dietary long-chain n-3 polyunsaturated fatty acids and risk of rheumatoid arthritis: a prospective cohort study of women. Ann Rheum Dis 2014;73(11):1949–1953.
12. Pedersen M, Stripp C, Klarlund M, et al. Diet and risk of rheumatoid arthritis in a prospective cohort. J Rheumatol 2005;32(7):1249–1252.
13. Karczewski KJ, Snyder MP. Integrative omics for health and disease. Nat Rev Genet 2018;19(5):299–310.
14. Emilsson V, Gudnason V, Jennings LL. Predicting health and life span with the deep plasma proteome. Nat Med 2019;25(12): 1815–1816.
15. Zhang J, Fang XY, Wu J, et al. Association of combined exposure to ambient air pollutants, genetic risk, and incident rheumatoid arthritis: a prospective cohort study in the UK Biobank. Environ Health Perspect 2023;131(3):37008.
16. Sudlow C, Gallacher J, Allen N, et al. UK Biobank: an open access resource for identifying the causes of a wide range of complex diseases of middle and old age. PLoS Med 2015;12(3):e1001779.
17. Perez-Cornago A, Pollard Z, Young H, et al. Description of the updated nutrition calculation of the Oxford WebQ questionnaire and comparison with the previous version among 207,144 participants in UK Biobank. Eur J Nutr 2021;60(7):4019–4030.
18. Kelly RK, Pollard Z, Young H, et al. Evaluation of the new individual fatty acid dataset for UK Biobank: analysis of intakes and sources in 207,997 participants. Nutrients 2022;14(17):3606.
19. Julkunen H, Cichońska A, Tiainen M, et al. Atlas of plasma NMR biomarkers for health and disease in 118,461 individuals from the UK Biobank. Nat Commun 2023;14(1):604.
20. Chen L, Wu B, Mo L, et al. Associations between biological ageing and the risk of, genetic susceptibility to, and life expectancy associated with rheumatoid arthritis: a secondary analysis of two observational studies. Lancet Healthy Longev 2024;5(1):e45–e55.
21. Cui F, Tang L, Li D, et al. Early-life exposure to tobacco, genetic susceptibility, and accelerated biological aging in adulthood. Sci Adv 2024;10(18):eadl3747.
22. Sun BB, Chiou J, Traylor M, et al; Alnylam Human Genetics; AstraZeneca Genomics Initiative; Biogen Biobank Team; Bristol Myers Squibb; Genentech Human Genetics; GlaxoSmithKline Genomic Sciences; Pfizer Integrative Biology; Population Analytics of Janssen Data Sciences; Regeneron Genetics Center. Plasma proteomic associations with genetics and health in the UK Biobank. Nature 2023; 622(7982):329–338.
23. Zhu K, Li R, Yao P, et al. Proteomic signatures of healthy dietary patterns are associated with lower risks of major chronic diseases and mortality. Nat Food 2025;6(1):47–57.
24. Chen L, Sun Q, Peng S, et al. Associations of blood and urinary heavy metals with rheumatoid arthritis risk among adults in NHANES, 1999-2018. Chemosphere 2022;289:133147.
25. Cui F, Sun Y, Xie J, et al. Air pollutants, genetic susceptibility and risk of incident idiopathic pulmonary fibrosis. Eur Respir J 2023;61(2): 2200777.
26. Chen L, Zhao Y, Liu F, et al. Biological aging mediates the associations between urinary metals and osteoarthritis among U.S. adults. BMC Med 2022;20(1):207.
27. Shapiro JA, Koepsell TD, Voigt LF, et al. Diet and rheumatoid arthritis in women: a possible protective effect of fish consumption. Epidemiology 1996;7(3):256–263.
28. Rosell M, Wesley AM, Rydin K, et al; EIRA study group. Dietary fish and fish oil and the risk of rheumatoid arthritis. Epidemiology 2009; 20(6):896–901.
29. Kronzer VL, Sparks JA, Raychaudhuri S, et al. Low-frequency and rare genetic variants associated with rheumatoid arthritis risk. Nat Rev Rheumatol 2024;20(5):290–300.
30. Xu L, Chang C, Jiang P, et al. Metabolomics in rheumatoid arthritis: advances and review. Front Immunol 2022;13:961708.
31. Rodríguez-Carrio J, Coras R, Alperi-López M, et al. Profiling of serum oxylipins during the earliest stages of rheumatoid arthritis. Arthritis Rheumatol 2021;73(3):401–413.
32. Cuesta-López L, Escudero-Contreras A, Hanaee Y, et al. Exploring candidate biomarkers for rheumatoid arthritis through cardiovascular and cardiometabolic serum proteome profiling. Front Immunol 2024; 15:1333995.
33. Cornélis F, Fauré S, Martinez M, et al; ECRAF. New susceptibility locus for rheumatoid arthritis suggested by a genome-wide linkage study. Proc Natl Acad Sci USA 1998;95(18):10746–10750.
34. Lorenzetti R, Janowska I, Smulski CR, et al. Abatacept modulates CD80 and CD86 expression and memory formation in human B-cells. J Autoimmun 2019;101:145–152.
35. Pollard LC. Inhibiting costimulatory activation of T cells: a viable treatment option for rheumatoid arthritis? Drugs 2007;67(1):1–9.
36. Buch MH, Eyre S, McGonagle D. Persistent inflammatory and non-inflammatory mechanisms in refractory rheumatoid arthritis. Nat Rev Rheumatol 2021;17(1):17–33.
37. Ding Q, Hu W, Wang R, et al. Signaling pathways in rheumatoid arthritis: implications for targeted therapy. Signal Transduct Target Ther 2023;8(1):68.

38. Yan Y, Jiang W, Spinetti T, et al. Omega-3 fatty acids prevent inflammation and metabolic disorder through inhibition of NLRP3 inflammasome activation. Immunity 2013;38(6):1154–1163.
39. Yates CM, Calder PC, Ed Rainger G. Pharmacology and therapeutics of omega-3 polyunsaturated fatty acids in chronic inflammatory disease. Pharmacol Ther 2014;141(3):272–282.
40. Susai SR, Mongan D, Healy C, et al. The association of plasma inflammatory markers with omega-3 fatty acids and their mediating role in psychotic symptoms and functioning: an analysis of the NEURAPRO clinical trial. Brain Behav Immun 2022;99:147–156.
41. Bradbury KE, Young HJ, Guo W, et al. Dietary assessment in UK Biobank: an evaluation of the performance of the touchscreen dietary questionnaire. J Nutr Sci 2018;7:e6.
42. Nagel G, Zoller D, Ruf T, et al. Long-term reproducibility of a food-frequency questionnaire and dietary changes in the European Prospective Investigation into Cancer and Nutrition (EPIC)-Heidelberg cohort. Br J Nutr 2007;98(1):194–200.
43. Jankovic N, Steppel MT, Kampman E, et al. Stability of dietary patterns assessed with reduced rank regression; the Zutphen Elderly Study. Nutr J 2014;13(1):30.

American College of Rheumatology
Empowering Rheumatology Professionals

Arthritis & Rheumatology
Vol. 77, No. 11, November 2025, pp 1488–1502
DOI 10.1002/art.43231

Complex Regulatory Interactions at *GDF5* Shape Joint Morphology and Osteoarthritis Disease Risk

Clarissa R. Coveney,[1] David Maridas,[2] Hao Chen,[3] Pushpanathan Muthuirulan,[4] Zun Liu,[4] Evelyn Jagoda,[4] Siddharth Yarlagadda,[4] Mohammadreza Movahhedi,[5] Benedikt Proffen,[5] Babak Dashtdar,[5] Mahdi Aghaalikhani,[5] Daniel Richard,[3] Vicki Rosen,[6] Ata M. Kiapour,[5] and Terence D. Capellini[1]

Objective. The objective of this study was to reveal causal-level osteoarthritis (OA) disease biology by targeting regulatory interactions at *GDF5.*

Methods. By investigating different *GDF5* regulatory regions (*R2*, *R3–R5*, *R7–R9*, *R18–R20*, *GROW1*), we explored their functional impacts on gene expression and joint morphology in vivo and in vitro. We additionally modeled OA variants in said enhancers in in vitro and in vivo mouse models for expression and disease effects.

Results. For all regulatory regions, we found evidence of activation and repression between or within said regions that impacted patterns of joint-specific expression. Examples are as follows: (1) the *R4* enhancer, although considered to be activating, has dual roles repressing expression in adjacent tissues and sites, and (2) growth plate–specific expression patterns by the *GROW1* regulatory region are confined by adjacent sequences to restrict its expression to the perichondrium. We next targeted different regions and variants in vivo. Testing the *R2de* region resulted in ∼40% reduction in *Gdf5* expression and joint morphology changes but no increase in OA risk; likewise, modeling the most cited OA risk variant (rs143384) in mice had no impact on expression, joint morphology, or disease. However, we identified epistatic interactions between this rs143384 risk variant and downstream disease risk variants lying within regulatory regions subject to repression, which compound to impact expression.

Conclusion. These findings, at the best studied OA locus to date, serve as lessons on the nature of how gene regulatory interactions and local epistasis work in the etiology of OA disease risk, and that assessment of individual variants of high genome-wide association study significance need not alone be considered causal.

INTRODUCTION

Osteoarthritis (OA) is a serious aging disease and the leading cause of disability worldwide, affecting ∼7.6% of the global population.[1] Knee and hip OA are highly heritable (40%–60%), and for both joints, morphology and mechanical injury are additional risk factors.[2–6] Indeed, ∼50% of hip OA cases result from undiagnosed developmental dysplasia of the hip (DDH),[7,8] and recently, knee shape has been linked to osteoarthritic disease.[5,9] For both joints, developmental genetic programs underlying cartilage formation before and during endochondral ossification aid in determining joint shape.[10] The *GDF5* gene, expressed during embryonic joint formation,[11–13] is critical in this regard; its loss in the *brachypodism* mouse model (*bp/bp*) results in serious knee and hip malformations.[14] When challenged with collagenase, *bp/bp* mice go on to develop OA.[15]

Of the numerous OA genome-wide association study (GWAS) loci, *GDF5* is also the most replicable. Hip and knee OA

Dr Yarlagadda's work was supported by Harvard University PRISE. Dr Kiapour's work was supported by the Children's Orthopaedic Surgery Foundation, Institutional Centers for Clinical and Translational Research at Boston Children's Hospital, Harvard Clinical and Translational Science Center (National Center for Advancing Translational Sciences, NIH award 1UM1-TR-004408-01), and the NIH (grant P30-AR-075042). Dr Capellini's work was supported by the National Institute of Arthritis and Musculoskeletal and Skin Diseases, NIH (grant 1R01-AR-070139), Harvard University Dean's Competitive Fund, and Harvard University Milton Fund for Human Research.

[1]Clarissa R. Coveney, PhD, Terence D. Capellini, PhD: Harvard University and Broad Institute of Massachusetts Institute of Technology and Harvard, Cambridge; [2]David Maridas, PhD: Harvard School of Dental Medicine, Boston, Massachusetts; [3]Hao Chen, PhD, Daniel Richard, PhD: Stanford University, Stanford, California; [4]Pushpanathan Muthuirulan, PhD, Zun Liu, PhD, Evelyn Jagoda, PhD, Siddharth Yarlagadda, MD: Harvard University, Cambridge, Massachusetts; [5]Mohammadreza Movahhedi, PhD, Benedikt Proffen, MD, Babak Dashtdar, MD, Mahdi Aghaalikhani, MD, Ata M. Kiapour, PhD: Boston Children's Hospital and Harvard Medical School, Boston, Massachusetts; [6]Vicki Rosen, PhD: Broad Institute of Massachusetts Institute of Technology and Harvard, Cambridge.

Additional supplementary information cited in this article can be found online in the Supporting Information section (https://acrjournals.onlinelibrary.wiley.com/doi/10.1002/art.43231).

Author disclosures are available at https://onlinelibrary.wiley.com/doi/10.1002/art.43231.

Address correspondence via email to Terence D. Capellini, PhD, at tcapellini@fas.harvard.edu.

Submitted for publication November 14, 2024; accepted in revised form May 2, 2025.

and DDH GWAS consistently reveal ~100 variants on a common 130-kb risk haplotype spanning the *GDF5* regulatory locus. We previously narrowed this haplotype to two causal variants for knee OA and DDH, revealing their unique impacts on joint shape and disease. We first created a mouse model harboring a knee OA risk variant, rs6060369, in the downstream *GDF5* regulatory region, *R4*, and saw it caused statistically significant morphologic changes to femoral condyles and tibial plateaus and a 30% increase in knee OA risk.[9] This finding mirrored the morphologic changes observed in patients with OA harboring the risk allele. We then generated a mouse model, harboring a different risk variant, rs4911178, present in the *GDF5* growth plate enhancer, *GROW1*. This variant resulted in alterations to acetabular and femoral neck shape but not the knee proper, with patients with DDH stratified for this risk allele showing the same directions of effect.[9] Despite this work, the most associated risk variants,[16–21] rs143383 and rs143384, still exist on this haplotype, and are located in the 5′-untranslated region (5′-UTR) of *GDF5*. Although reporter gene studies[22] and allele-specific expression (ASE) studies on patient knee tissue[23] have functionally tested these variants, their functional interrogation in vivo is lacking, and thus it is unclear if they are relevant to joint disease.

Importantly, ours and others' research[14,18,19,21,24–26] has led to the *GDF5* regulatory locus as one of the most well-annotated loci in the genome. Besides *R4* and *GROW1*, four other identified regulatory regions (Supplementary Figure 1) reside upstream or downstream of *GDF5*. All six enhancers drive different *GDF5* expression patterns in vivo, as assessed via *lacZ* mouse transgenesis (at embryonic day [E] 14.5) and epigenomic studies on developing (E50–E60) human joints, findings that demonstrate that the mouse and human regulatory loci are functionally orthologous. Yet as extensive as this work is, a major issue is that no regulatory region alone is able to reproduce the entire endogenous expression pattern of *GDF5*, indicating that regulatory regions must work together to either enhance, repress, or restrict expression in a modular and tissue-specific manner. Elucidating this regulatory activity for *GDF5* and how locus-specific activation and repression mechanisms operate should give us insights into how disease risk variants function. Here, we set out to further explicate and characterize the interactions of *GDF5* regulatory regions, interrogate the function of the leading OA GWAS risk variants rs143383 and rs143384, and explore potential variant interactions across the *GDF5* locus.

MATERIALS AND METHODS

Ethics. All experiments performed on adult or embryonic mice, including euthanasia, were approved by Stanford University's and Harvard University's respective Institutional Animal Care and Use Committees with protocols (SU, 10665; HU, 13-04-161-2). No human participants were used.

Animal models. The 5′-UTR$^{rs143384\text{-}T/rs143384\text{-}+}$ single allelic replacement mouse line contains a single "T" basepair replacement of the orthologous human rs143384 variant in the 5′-UTR at the mm10 position (chr2:155,945,103-155,945,103). The *R2de* mouse model contains a specific 428-bp deletion of the *R2* (*d* + *e*) regulatory region plus an adjacent sequence at the mm10 position (chr2:155,945,327-155,945,755). Both were CRISPR-Cas9 generated on C57BL/6J *Mus musculus* backgrounds by Applied StemCell as previously described.[9] All animals used were generated by breeding heterozygous animals together to obtain litters of wild-type (WT), heterozygous, and homozygous animals. All animals were housed in the same location under the same conditions at a minimum of three and a maximum of five per cage. No animals were excluded.

Transgenic mice. Transgenic mice were generated as previously described.[19] Briefly, transgenic mouse embryos were generated by pronuclear injection into FVB or C57BL6/CBA F1 fertilized oocytes.[27,28] Embryos were collected at E14.5 for X-Gal staining. For each construct, multiple transgenic embryos derived from independent integration events were analyzed, and only consistent patterns are reported (Supplementary Table 1).

X-Gal staining/in situ hybridization. Whole mount β-galactosidase activity was performed as described with minor modifications.[28] Embryos were fixed in ice cold 4% paraformaldehyde (PFA) in phosphate buffered saline, hemisected, and then fixed for an additional 15 minutes at 4°C. Following three washes in wash buffer, embryos were stained for 16 to 24 hours in the dark with 1 mg/mL of X-Gal in staining buffer at room temperature. Embryos were then washed and fixed in 4% PFA for five hours. For sectioning, X-Gal-stained embryos were placed in sucrose solution before being embedded in gelatin and then cryosectioned at 25 μm. Nuclear fast red was used to counterstain sections. Antisense and sense digoxigenin-labeled probes for in situ hybridization were generated for *Gdf5*.[29]

Transcription factor binding site analysis. To find upstream transcription factors (TFs) predicted to bind to *R4* regulatory sequences, we used UNIPROBE.[30,31] At the recommended enrichment threshold (0.4), UNIPROBE identified more than 1,000 sites (ie, specific 8-mer sequences bound by a TF) in mouse and human *R4* sequences. Predicted factors were intersected with expression and phenotypic data (Eurexpress, http://www.eurexpress.org/ee/; Genepaint, http://www.genepaint.org/Frameset.html; Mouse Genome Informatics, http://www.informatics.jax.org) to narrow down to factors expressed or required in limbs and joints; indicative of homeodomain TFs, *Barx1-2* displayed overlap with known *Gdf5* expression patterns, specifically at gestational days when *R4* enhancer was active.[32–34] We next engineered *R4* sequences carrying site-specific BARX mutations, which generally removed homeodomain binding

preferences, and these were synthesized by GenScript. The Supplementary Materials shows the sequence changes per BARX site as calculated using UNIPROBE enrichment score analysis. This technique allowed us to identify those sequences where BARX (but likely any homeodomain TF) could bind strongly in the WT sequence, as described previously, versus those where BARX could no longer bind via mutated sites. Each WT or mutated *R4* element was cloned between *R3* and *R5* within the Hsp68 *lacZ* reporter. Each resulting concatenated construct was then used to generate multiple independent E14.5 transgenic mouse embryos for *lacZ* expression analysis (Supplementary Table 1). TF binding site sequence analysis was also performed using the CIS-BP online software[35] by testing the nonrisk and risk variant within an endogenous region of 15 bp (7 bp either side of variant). All TF binding sites that are gained, lost, or unchanged as a result of the risk variant are reported (Supplementary Materials).

ASE. Pyrosequencing was performed to calculate the allelic ratio of C57BL/6J *R2de (*or 5′-UTR rs143384 mouse "T" allele) in the heterozygous state to 129x1/SVJ (WT). Heterozygous ratios determined from complementary DNA (cDNA) products were then normalized by the ratio of WT C57BL/6J to 129x1/SVJ genomic products, amplified from known 1:1 mixtures of each sequence. A nonparametric permutation test was used to assess the significance of affect between the WT and heterozygous allelic expression allele in R.

Histomorphology. The left hind limbs of a minimum of four animals per genotype per sex per timepoint were obtained for histologic analysis to assess cartilage integrity. For larger cohorts, a minimum of seven joints were randomly selected for histomorphometry analysis across different cages (number of biologic replicates "n" determined based on our previous work[9,26]). Post euthanasia, skin and excess muscle were removed, and each limb was fixed in 10% neutral buffered formalin for 24 hours at room temperature before being decalcified in 14% EDTA at a pH of 7.5 for eight days. Formalin-fixed tissues were sent to the Massachusetts General Hospital Center for Skeletal Research Histology and Histomorphometry Services core facility and processed in one batch for proper sectioning and histologic staining using fast green and Safranin O staining. Embedding, sectioning, and staining were performed without knowledge of genotype. A minimum of 10 coronal sections taken throughout the joint (60–80-μm levels) were generated per knee joint. Sections were blind scored by two readers (CRC and AMK, BP, BD, or MA) using the summed Osteoarthritis Research Society International (OARSI) scoring method of OA in the mouse.[36] Briefly, per slide, each quadrant (medial and lateral tibial plateaus, medial and lateral femoral condyles) was assigned a score and summed, with 0 representing intact cartilage and 6 representing cartilage erosion down to the bone extending >75% of the articular surface. The top three summed slides per joint were added to generate one final score per joint. All scorers were blinded to sex and genotype. One-way analysis of variance (ANOVA) (*R2de*) was used to compare OARSI scores between genotypes, whereas two-way ANOVA (5′-UTR$^{rs143384/rs143384}$) was used to compare OARSI scores between the sex and genotype.

Functional analysis of *GROW1/R4* + 5′-UTR risk and nonrisk variants using luciferase reporter assays. CHON-002 cells, derived from human fetal femoral growth plate chondrocytes at 18 weeks' gestation (female) were sourced from ATCC (CRL-2847) NIH/3T3 (Hoekstra Lab, Harvard University) cells, and T/C28a2 cells were cultured at 37°C in a 5% CO_2 environment using ATCC's complete growth medium, which consists of Dulbecco's Modified Eagle's Medium (DMEM) supplemented with 10% fetal bovine serum (FBS), 50 μg/mL of penicillin-streptomycin, and 0.1 mg/mL of G-418. For transfection experiments, CHON-002 (*GROW1* constructs) cells, T/C-28a2 (*R4* constructs and *R4* single variant constructs previously described[26] and *R9* variant constructs) cells, or NIH/3T3 (*R4* single variant constructs) cells were seeded in 96-well plates at a density of 1–4 × 10^4 cells per well and cultured in DMEM supplemented with 10% FBS for 24 hours. Transient transfections were performed using Lipofectamine 3000 (Invitrogen L3000015) in serum-free DMEM, according to the manufacturer's protocol. The transfection complex was prepared by diluting Lipofectamine 3000 in Opti-MEM Medium (5 μL of Opti-MEM + 0.3 μL of Lipofectamine 3000 per well of a 96-well plate). Separately, a DNA-P3000 mix was prepared (5 μL of Opti-MEM + 100 ng [or 200 ng for NIH/3T3] of DNA + 0.2 μL of P3000 Reagent per well). The diluted DNA solution was then added to the diluted Lipofectamine 3000 in a 1:1 ratio and incubated at room temperature for 10 to 15 minutes. Cells were transfected with a firefly luciferase reporter vector containing a *GROW1* and 5′-UTR or an *R4* and 5′-UTR and fusion sequence with various combinations of either *GROW1* (rs4911178) and 5′-UTR (rs143383 and rs143384) variants or *R4* (rs6060369) and 5′-UTR (rs143383 and rs143384) variants (100 ng total). An empty pGL4.23 luciferase vector (100 ng) was used as a control.

To normalize transfection efficiency, the pRL-CMV Renilla luciferase vector (Promega; E226A) was cotransfected. The epistatic activity of the fusion variant combinations was measured 24 hours post transfection using the Dual-Luciferase Reporter Assay System (Promega, TM040) on an Agilent BioTek Synergy Neo2 Hybrid Multimode Reader (Thermo Fisher Scientific), following the manufacturer's instructions. Standard and variant synthesis of either *R4* or *GROW1* sequences concatenated to the 5′-UTR, including added 5′ KpnI and 3′ HindIII sequences with sequence verification and custom cloning into pGL4.23 custom (Ampicillin) via 5′ KpnI and 3′ HindIII (by recombination), were generated by Genewiz and delivered as a mini-scale DNA sample (see Supplementary Materials for sequences of each construct). The constructs used for the functional analysis of *GROW1* and

5′-UTR variants in the Dual-Luciferase Reporter Assay are shown in the Supplementary Materials. We were unable to generate the plasmid testing the nonrisk rs2248393 "G" and risk rs2378349 "C" variant combination using traditional cloning mechanisms or construct synthesis, and therefore this combination of alleles could not be generated and tested.

CRISPR methods: CRISPR targeting of regulatory regions *R9* and *R2de* in vitro. All single-guide RNAs (sgRNAs) flanking (1) the *R9* regulatory region and (2) the *R2de* region were designed using the Massachusetts Institute of Technology CRISPR Tools (http://genetargeter.mit.edu/), synthesized by Integrated DNA Technologies, Inc, and cloned into a PX458 vector as previously described in published protocols.[37] See the Supplementary Materials for sequences and chromosomal locations of sgRNAs. All guide RNAs were tested for deletion efficiency of respective human elements in cultured T/C-28a2 cells (n = 3 biologic replicates per assay). T/C-28a2 cells were maintained as described previously and seeded in a six-well plate 24 hours before transfection. Transfection efficiency was measured using a fluorescence microscope (>70% of cells were green fluorescent protein positive). Extraction of DNA was performed using the E.Z.N.A Tissue DNA Kit (Omega Bio-Tek), and respective regulatory elements were amplified using polymerase chain reaction (PCR) with primers flanking each sgRNA location (Supplementary Table 2), followed by purification from 1% agarose gel (E.Z.N.A Gel Extraction Kit). Sanger sequencing was used to verify each successful targeting event.

Impacts of each modification on *GDF5*, *UQCC*, and *CEP250* expression were assessed by extracting RNA from control and CRISPR-Cas9-targeted T/C-28a2 or NIH/3T3 cells (n = 3 biologic replicates, with 3 technical replicates per experiment per condition) using Trizol Reagent (Thermo Fisher Scientific) and Direct-zol RNA Miniprep kit (ZYMO). SuperScript III First-Strand Synthesis System (Thermo Fisher Scientific) was used to prepare cDNA. Quantitative reverse transcriptase–PCR analysis was then performed with gene-specific primers[9,26] and Applied Biosystems Power SYBR master mix (Thermo Fisher Scientific) with the GAPDH housekeeping gene as an internal control.

Hi-C interaction analysis. Promoter-capture (Hi-C) data were obtained from Jung et al,[38] particularly the file 'GSE86189_all_interaction.po.txt.gz' containing processed information on genomic regions with significant contacts of targeted promoters. This data set was generated from promoter-capture assays across a number of different tissues and cell types. Because developmental cartilage samples were not included, we reasoned that significant enhancer–promoter interactions detected in at least two distinct tissues are, by definition, not cell type restricted and thus may represent more pleiotropic interactions. Thus, we considered only significant interactions (reported $P < 0.01$), which were detected in at least two different tissues (excluding ovary). Subsequently, we aggregated the set of appendicular skeleton assay of transposase accessible chromatin followed by sequencing peaks from the study by Richard et al[39] and intersected these with the set of significant interactions. We used the Gviz[40] package (version 1.42.1) and the GenomicInteractions[41] package (version 1.32.0) to visualize our interaction and accessibility intersections around the *GDF5* locus.

Micro–computed tomography and anatomic measurements. The acetabular joint, femur, and tibia from right hind limbs were collected using high-resolution micro–computed tomography (micro-CT) (μCT40, SCANCO Medical AG). Scan parameters were as follows: 12 μm^3 isotropic voxel size, 70 kVp peak x-ray tube intensity, 114 mA x-ray tube current, and 200 ms integration time. Resultant Digital Imaging and Communication in Medicine (DICOM) images were exported for measurements following anatomic features in Osirix MD v7.5 (Pixemo SARL). First, using previously described methods,[9] measurements were taken of the acetabulum (depth, diameter, inclination), proximal femur (valgus cut angle, neck-shaft angle, neck length, neck diameter, head offset, head diameter), distal femur (bicondylar width, notch width, condylar width [medial and lateral], condylar curvature [medial and lateral], trochlear width [medial, central, and lateral], trochlear groove depth, trochlear angle), and proximal tibia (plateau width, posterior tibial slope [medial and lateral], tibial spine height [medial and lateral]). All measurements displayed strong interexaminer and intraexaminer reliability (intraclass correlation coefficient > 0.78). Second, micro-CT DICOM images were segmented to generate three-dimensional (3D) models of each bone using image processing software (Mimics v17.0, Materialise). 3D models were imported to 3-matic software package (v9.0, Materialise) and coregistered together using a global n = point registration method. 3D models of WT and homozygous mice were used to generate 3D heatmaps indicating the geometric differences between genotypes for each mouse line. The heatmaps were generated by calculating the distance between the corresponding points in coregistered models, where dark blue indicates the maximum deviation in the negative direction and red indicates the maximum deviation in the positive direction. All assessors were blinded to sex and genotype. Some femurs were broken on loading for micro-CT analysis and therefore had to be excluded from analysis.

Statistical analysis. Expression data for *GDF5*, *CEP250*, and *UQCC1* were normalized relative to *GAPDH* house-keeping gene expression and compared between control and *R2de* enhancer deletion. All data are presented as the mean ± SEM unless otherwise stated. Individual pairwise comparisons between control and experimental conditions were analyzed by two-sample, two-tailed Student's *t*-test, with $P < 0.05$ regarded

as significant; n = 4 technical replicates per biologic replicate (3 biologic replicates).

RESULTS

Activation and repression domains within a 37-kb sequence containing *GROW1*. We previously reported on a broad 37-kb human sequence downstream of *GDF5* (purple region, Supplementary Figure 1, Figure 1A) that drives *GDF5* expression only in the subperichondral region of long-bone growth plates, identical to that of *GROW1*, a 2.54-kb enhancer containing a key DDH risk variant (rs4911178). Interestingly, this 37-kb sequence consists of an ~12.17-kb subregion *PHC17* (Supplementary Figure 1, light gray) that drives expression in chondrocytes throughout the entire growth plate (ie, not only in the subperichondral region) and an ~10-kb subregion *PHC18* (Supplementary Figure 1, dark gray) that drives expression in the shoulder joint proper (Figure 1B and C). Because *Gdf5* is not endogenously expressed throughout the growth plate (Supplementary Figure 1), this means that built-in or adjacent to *PHC17*, there are repressors that restrict expression to the subperichondral space. We therefore first tested two conserved *PHC17* subregions, one called *R18-20* (~2.7 kb from *GROW1*) and another called *R7* (~6.9 kb from *GROW1*). We found that neither region drives growth plate expression (Figure 1B and C), observing expression only at joint and digit sites. As noted, the adjacent *PHC18* (Figure 1C) drives expression in the shoulder, which is not a pattern controlled by the larger 37-kb sequence. We next tested two conserved regions within *PHC18* termed *R8* and *R9*. Surprisingly, *R8* alone drives expression within many more hind limb and forelimb joints, indicating that it is being repressed in the *PHC18* and 37-kb constructs. Upon testing *R9*, we found no expression in limbs indicating it might act as a repressor, especially when considered in *PHC18* and 37-kb parental constructs. To test this, we deleted *R9* in human T/C-28a2 chondrocytes and observed a significant increase in *GDF5* expression, thus revealing a normal repressor role (Figure 1D). We note that in this *R9* repressor, there exists two OA GWAS risk variants (rs2378349 and rs2248393) that may modulate repressor and thus *GDF5* expression levels. We performed a luciferase reporter test of these two variants in T/C-28a2 chondrocytes and observed some impacts of the risk allele on *GDF5* expression (see Supplementary Table 1), noting considerable changes to TF binding sequences as a result of each variant (Supplementary Table). Thus, in considering both *PHC17* and *PHC18* within the 37-kb region, we note that the endogenous growth plate subperichondral expression, recapitulated by both 37-kb and *GROW1* regions (Figure 1A), results from two potential repression systems: (1) a localized system within *PHC17* via *R18-20* and/or *R7* and (2) a long-range system within *PHC18* via the actions of the *R9* repressor.

Activation and repression domains within a 41-kb sequence containing *R4*. We had characterized a human 41-kb sequence (blue region, Supplementary Figure 1,

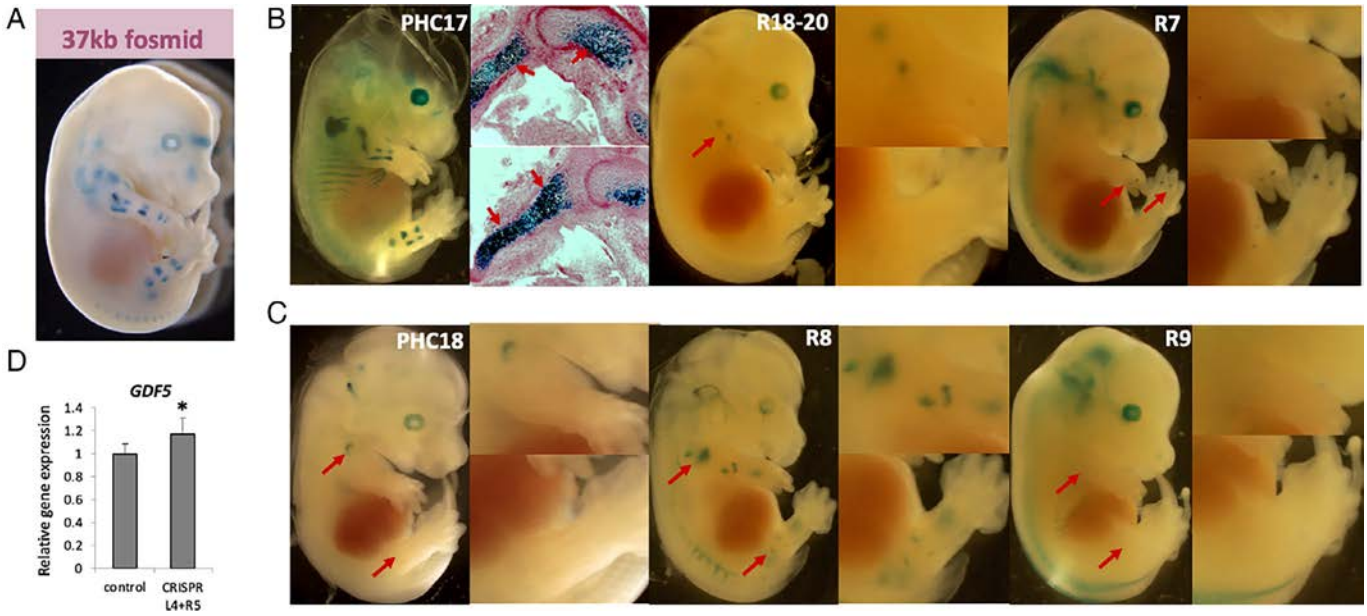

Figure 1. Restriction of *GROW1* to the perichondrium exerted by downstream regulatory regions. Transgenic embryos driving *lacZ* were collected at E14.5 of (A) 37-kb human fosmid driving growth plate expression and (B) regulatory region *PHC17* (*GROW1*, *R18–R20*, and *R7*) with two histologic panels of the hind limb showing *PHC17*-driven *lacZ* expression throughout the entire growth plate. (C) Transgenic embryos collected at E14.5 of region *PHC18* (which includes *R8* and *R9*). Red arrows indicate locations of differential expression patterns between regulatory elements. (D) Relative *Gdf5* expression following *R9* CRISPR knockout via guide RNAs (L4/R5) in T/C-28a2 cells. E, embryonic day.

Figure 2A) further downstream of *GDF5*, showing it recapitulated the classic *Gdf5* limb joint–specific expression pattern. This region's three known enhancers drive unique patterns: *R3* in the interdigital space, digital transverse stripes, and knee and elbow joints (*R3*, Figure 2C); *R4* in the elbow and knee and digit joints, with weaker expression in the hip and shoulder (R4, Figure 2C); and *R5* in the prechondrogenic phalangeal mesenchyme and weakly in the elbow and knee (*R5*, Figure 2C).[19] Alone, *R3*, *R4*, or *R5* cannot drive the broader 41-kb pattern. Moreover, the complete *R3* and *R5* patterns are not observed by the broader 41-kb sequence, nor are they known *Gdf5* expression territories. Interestingly, when concatenated (in construct *PHC19*, Figure 2B), *R3*

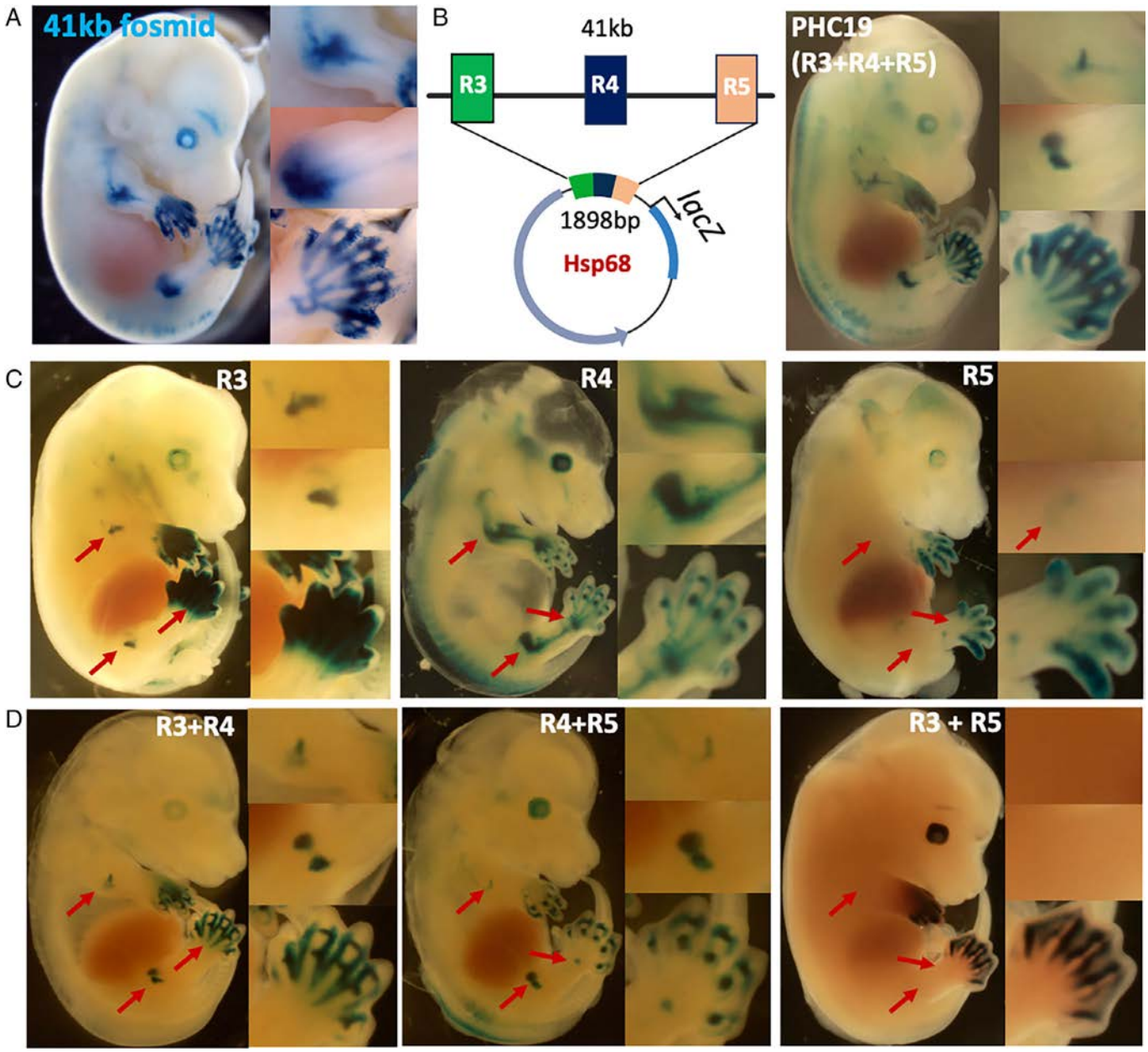

Figure 2. Repressive interactions between nearby regulatory elements affects expression patterns. (A and B) Transgenic embryos collected at E14.5 of (A) the 41-kb human construct encompassing *R3*, *R4*, and *R5* and (B) the mouse *PHC19* construct concatenating regulatory elements *R3*, *R4*, and *R5* (1,898 bp), both of which drive expression in the same limb domains. Cartoon depiction of construct containing concatenated regions. (C) Transgenic embryos collected at E14.5 of the *R3* region, driving *lacZ* expression in the autopod and forelimb and hind limb joints; the *R4* region, driving expression in the forelimb, hind limb, and digit synovial joints; and the *R5* region, driving expression predominantly in the digits. (D) Transgenic embryos collected at E14.5 showing how *R3* + *R4* drive expression in the forelimb, hind limb, and digit joints, with some expression in the digit periphery; how *R4* + *R5* drive expression in the forelimb, hind limb, and digit joints; and how *R3* + *R5* drive expression only in the webbing of the digits. Red arrows indicate areas of expression patterns that change between constructs. See text for details. E, embryonic day. Color figure can be viewed in the online issue, which is available at http://onlinelibrary.wiley.com/doi/10.1002/art.43231/abstract.

(586 bp) + *R4* (975 bp) + *R5* (337 bp) (ie,1,898 bp out of the 41 kb) strikingly generated the 41-kb pattern. To understand this complex interaction further, we first concatenated *R3* + *R4* and found that together they drive strong expression in the knee and elbow and digit joints, including transverse stripes and some interdigital webbing (Figure 2D). Here, *R3* acts to restrict knee, elbow, and shoulder expression of *R4*, whereas *R4* represses *R3* expression in the interdigital webbing. We next tested *R4* + *R5* and found that together they drive weak expression in the elbow but strong expression in the knee, transverse stripes of the digits, and weak expression of the metacarpals (Figure 2D). Here, *R4* acts to suppress *R5* digital mesenchyme expression, whereas *R5* acts to restrict (and weaken) *R4* expression in large joints. Finally, we tested *R3* + *R5* and found that together they cause the strong digital mesenchyme expression of *R5* to be lost, whereas *R3* expression becomes further restricted in the interdigital webbing (Figure 2D). These studies reveal that in addition to enhancer activities, each regulatory element can act as a repressor.

As we have shown, the ability of a regulatory region to restrict expression appears to be joint and tissue dependent, emphasizing the importance of location for gene regulatory activity to recapitulate endogenous *Gdf5* expression. To emphasize the importance of this finding to causal disease biology, we tested the previously reported *R4* "T" OA risk allele at rs6060369 in two contexts. First, by testing the risk "T" allele (compared to the nonrisk "C" allele) in human T/C-28a2 chondrocytes (a cell type in the developing knee), we find that the *R4* element acts as an enhancer, and the "T" risk allele decreases its activity (Supplementary Figure 2a). However, when the "T" risk allele is tested in a fibroblast line (NIH/3T3 cells; another cell type in the developing knee), we find it serves to derepress the activity (and thus increase expression toward baseline) (Supplementary Figure 2b). These findings reveal that as in our in vivo *lacZ* experiments, *R4* in different human cellular contexts can repress or activate and, importantly, that its risk variant effects depend on the epigenomic context.

Although variant roles in disease biology are dependent on the epigenomic *cis*-regulatory context for which they are located, the TF or *trans*-environment is also important to consider. We next deeply interrogated the *R4* regulatory element given its importance to knee OA risk. Using published methods (Materials and methods) we identified five core homeodomain TF binding sites across *R4* (Supplementary Figure 3a).[32] Although these sites may be bound by a host of different homeodomain TFs, each dependent on cellular context, we note here that of the list of predicted factors, the strongest binding preferences were for BARX factors. BARX1 and BARX2 are known to be expressed across developing joints, exhibiting strong overlap with *GDF5* expression.[32–34,42] We next sought to experimentally test each binding site using in vivo *lacZ* approaches (Materials and methods). We first tested all five homeodomain sites within *R4* by mutating each to destroy (through reshuffling) their predicted binding sequence. When all five sites were mutated (MUTB1–MUTB5), *lacZ* expression was restricted only to the digits, reducing expression in digit webbing and eliminating large limb joint expression (Supplementary Figure 3b–d). We next generated separate *lacZ* constructs with each TF binding site mutated independently and found no impact on expression patterns as a result of MUTB1, MUTB4, or MUTB5 (Supplementary Figure 3e) but strong repression of knee and shoulder expression as a result of MUTB3 (Supplementary Figure 3e). MUTB2 (Supplementary Figure 3e) also reduced expression within the limb joints but not as strongly as MUTB3. Interestingly, the OA GWAS-associated *R4* variant (rs6060369)[9] lies between MUTB2 (92 bp away) and MUTB3 (66 bp away). Overall, these data reveal the importance of TF functioning on *R4* activity and that individual TF binding sites (and variants nearby) can have sizable impacts of the regulatory activity of important enhancers.

Activation and repression domains within the upstream *R2* joint enhancer. We had reported[19] an ~1-kb enhancer, *R2* (green region, Supplementary Figure 1), that drives strong expression within limb joints and recapitulates a subset of the entire endogenous *Gdf5* expression pattern. This element resides near the *GDF5* promoter and 5′-UTR. There are five highly conserved regions[19] across the *R2* element, denoted *a*–*e* (Figure 3A). Interestingly, although *a*, *b*, and *c* do not reproduce expression either independently or together (*a* + *b* + *c*) (Figure 3B), subelements *d* and *e* can recapitulate expression in the hip and knee or shoulder and elbow, respectively,[19] We identified a shorter 112-bp sequence within *d* that suppresses elbow and metapodial joint expression (Supplementary Figure 4). Most strikingly, by concatenating *abc* with either *d* or *e* (ie, *a* + *b* + *c* + *d* or *a* + *b* + *c* + *e*), *abc* suppresses expression in both the hind limb and forelimb. This reveals built-in repression domains within individual enhancers. Strikingly, under any combination of subelement concatenation, digit expression could not be recapitulated, revealing that digit expression requires the full *R2* regulatory element to be intact for expression.

Deletion of *R2de* results in morphologic changes not associated with OA development. Enhancer *R2* is adjacent to *GDF5* 5′-UTR, in which resides the most associated OA GWAS variant, rs143384. To understand the role of *R2* in large joint (eg, knee) biology and OA risk, we generated a mouse line using CRISPR-Cas9 with a deletion of the *R2de* region that drives limb joint–specific expression. Using ASE analysis on seven separate E15.5 limb joint sites, we observe a consistent ~40% decrease in *Gdf5* expression at each site (Supplementary Figure 5a). When deleted in T/C-28a2 human chondrocytes, *GDF5* (but not nearby *UQCC1* and *CEP250*) expression is similarly reduced (Supplementary Figure 5b, c, and d, respectively). Given the expression reduction, we performed micro-CT morphologic analyses on WT, $R2de^{-/+}$ and $R2de^{-/-}$ mice at P56 and found

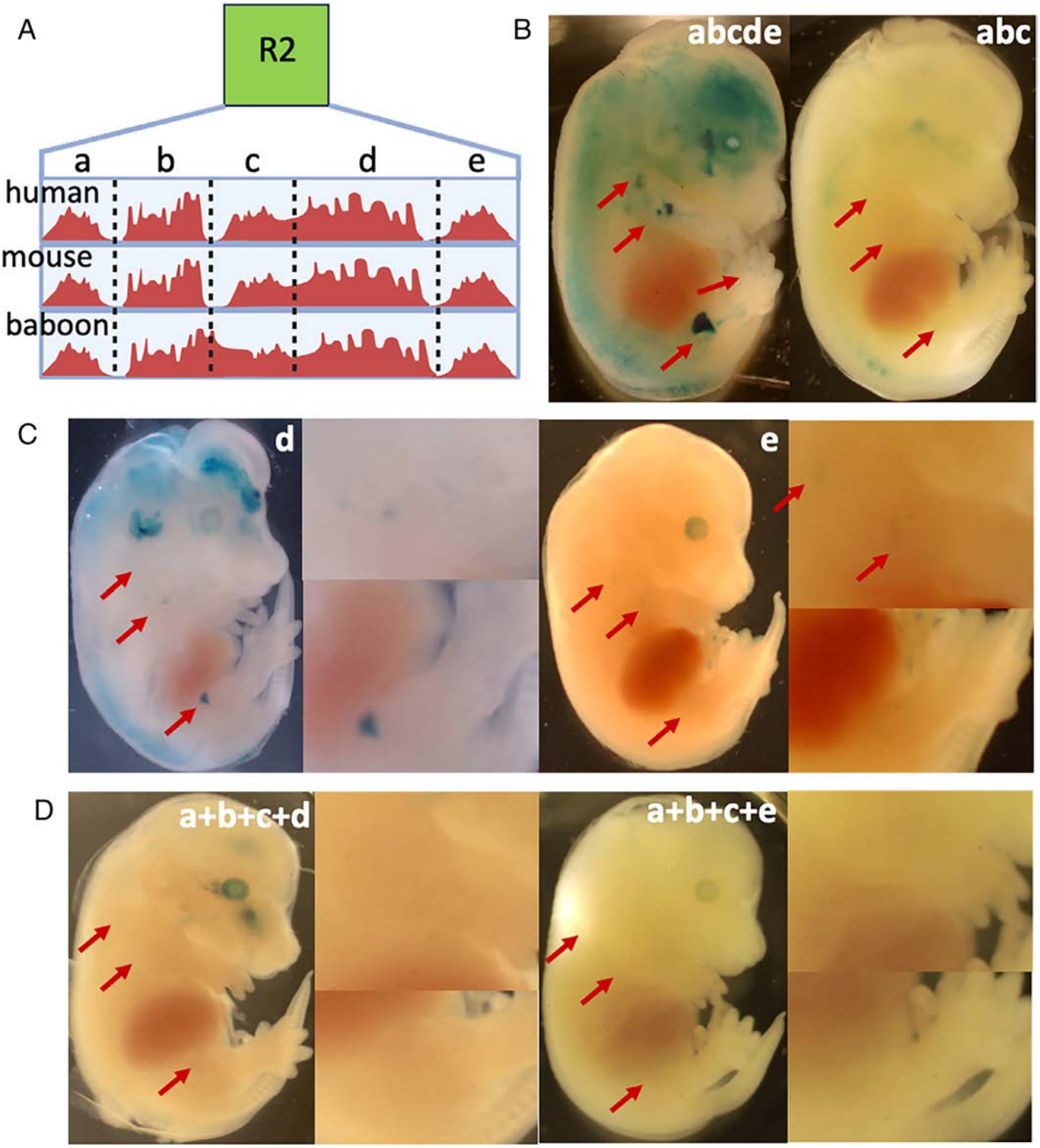

Figure 3. Subregions of *R2* repress regulatory region activity. (A) Cartoon representation of five conserved subregions (a–e) within the *R2* element across different species (19). (B) Transgenic E14.5 embryos of the entire *R2a–e* sequence, driving expression in the forelimb, hind limb, and digit joints; subregion *R2abc* is unable to drive expression in any joint, whereas subregions *d* and *e* drive expression in hind limb and forelimb joints but not in digit joints. (C) Transgenic E14.5 embryos show subregions *R2d* and *R2e* are able to drive expression in hind limb and forelimb joints, respectively. (D) Transgenic E14.5 embryos showing that subregions *abc*, when placed adjacent to subregion *d* or *e*, repress hind limb or forelimb expression, respectively. Red arrows indicate areas of expression patterns that change between constructs. E, embryonic day. Color figure can be viewed in the online issue, which is available at http://onlinelibrary.wiley.com/doi/10.1002/art.43231/abstract.

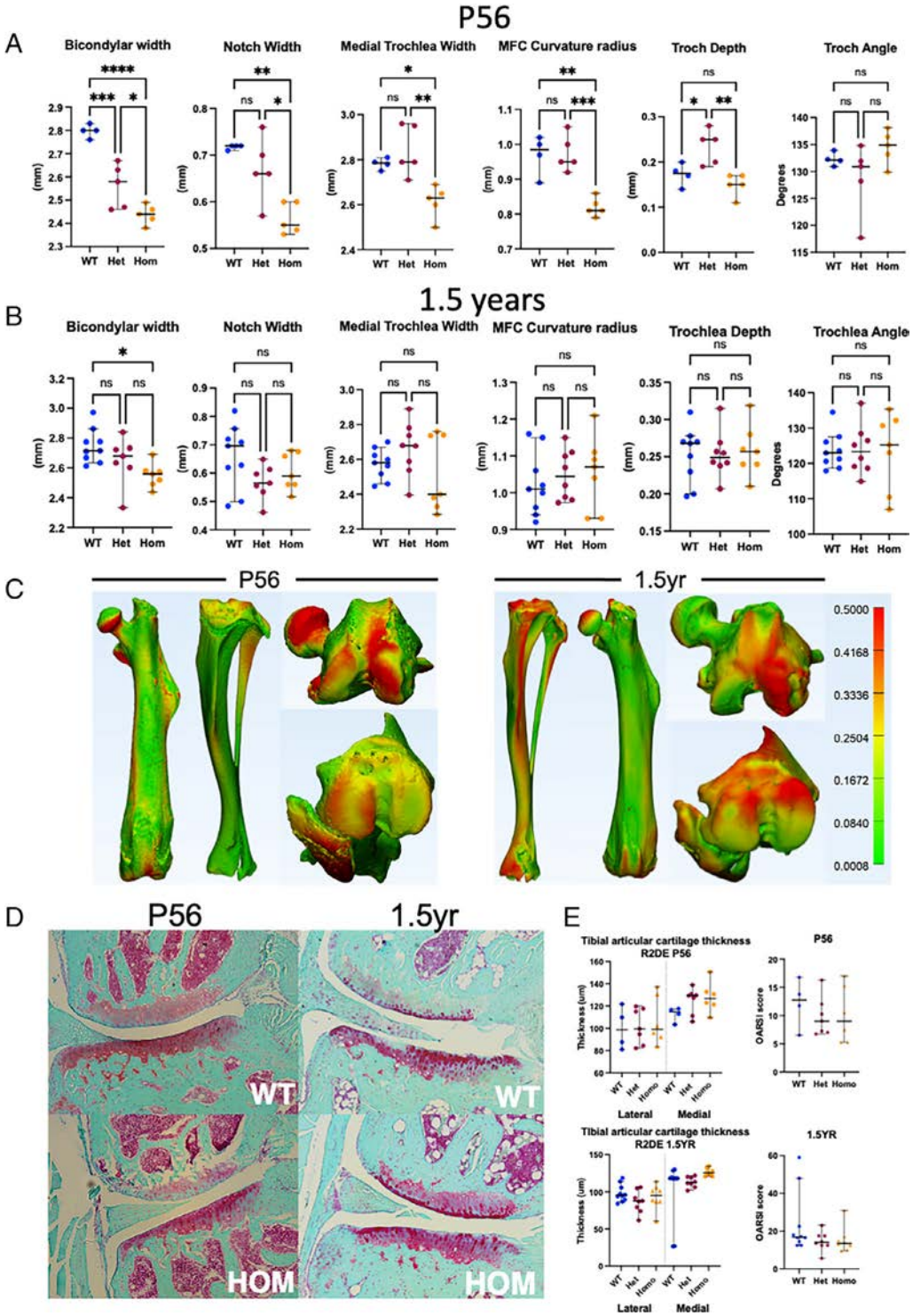

Figure 4. Morphologic characterization of the *Gdf5 R2de* enhancer mouse model. (A) Micro-CT measurements of significantly different anatomic features in *R2de* deletion mice at P56 (WT n = 4, Het n = 5, Hom n = 6) and 1.5 years (WT n= 8, Het n= 7, Hom n = 7). One-way analysis of variance with the Tukey–Kramer test was used for comparisons between all groups (*$P < 0.05$, **$P < 0.01$, ***$P < 0.001$, ****$P < 0.0001$; bars indicate medians and 95% confidence intervals) at both P56 and (B) 1.5 years of age. (C) Three-dimensional morphologic comparative analysis indicating locations of largest anatomic differences between WT and homozygous *R2de* null hind limbs at P56 and 1.5 years. (D) Coronal histologic sections of the medial compartment stained with Safranin O for representative osteoarthritis score per time point. (E) Tibial articular cartilage thickness measurements of the lateral and medial plateaus at P56 and 1.5 years alongside respective OARSI scores for each time point (P56: WT n = 4, Het n = 5, Hom n = 6; 1.5 years: WT n = 8, Het n = 7, Hom n = 7). Het, heterozygous; Hom, homozygous; MFC, medial femoral condyle; micro-CT, micro–computed tomography; ns, non significant; OARSI, Osteoarthritis Research Society International; WT, wild type. Color figure can be viewed in the online issue, which is available at http://onlinelibrary.wiley.com/doi/10.1002/art.43231/abstract.

statistically significant shape changes across the knee's femoral and tibial plateau and the hip's acetabulum (Figure 4A and Supplementary Figure 5f). Strikingly, by 1.5 years, only knee bicondylar width remained statistically impacted (Figure 4B and Supplementary Figure 5g). By 3D analysis, these changes predominantly locate to the medial femoral condyles at P56 and 1.5 years, whereas at 1.5 years, hip alterations are ameliorated, though some changes remain at the anterior tibial plateau (Figure 4C). Apart from two WT cases of spontaneous OA at 1.5 years, there are no changes to cartilage integrity measured by OARSI scoring at P56 or 1.5 years of age, and separation of scores by plateau and condyle does not reveal regionally specific effects (Figure 4D and E and Supplementary Figure 5e). Likewise, no statistically significant changes are observed in tibial or femoral articular cartilage thickness at either time point (Figure 4E and Supplementary Figure 5e). Thus, the loss of *R2de*, which has a marked effect on *Gdf5* gene expression, has no long-term observable impacts on joint morphology and no increased risk of spontaneous OA.

rs143384 risk allelic mice lack joint alterations and OA disease. Within the *GDF5* 5′-UTR is the OA GWAS risk variant, rs143384, a 'G' to 'A' risk mutation. Although others have shown that the variant impacts reporter gene expression in vitro and *GDF5* expression in patients,[23] no one has tested its role in joint development and homeostasis in vivo. We generated a humanized 5′-UTR$^{rs143384\text{-}A/rs143384\text{-}G}$ allelic replacement line. Using ASE at E15.5 on seven joint sites, we observe no impact of the risk "A" allele on *Gdf5* expression (Supplementary Figure 6a). Using micro-CT imaging on P56 WT, 5′-UTR$^{rs143384\text{-}G/rs143384\text{-}A}$, and 5′-UTR$^{rs143384\text{-}A/rs143384\text{-}A}$ mice, we find that the "A" allele causes no significant changes to the width and curvature of the knee's femoral condyles or to the size and slope of the tibial plateau at P56 (Figure 5A and B and Supplementary Figure 6c). We observe only a modest impact on notch height in female mice, albeit *GDF5* does not exhibit sex effects on OA risk in any GWAS to date. Histologically, we observe no increase in disease risk between each genotype or sex by OARSI scoring at P56 or one year (Figure 5C and Supplementary Figure 6b). We conclude that modeling the variant alone reveals little-to-no impact on knee OA biology and disease risk.

Modeling variant epistasis across the complex *GDF5* regulatory locus. The common 130-kb risk haplotype spanning *GDF5* is associated with knee OA, DDH, height, and other musculoskeletal disease traits.[18] We had revealed causal risk alleles at rs4911178 ("A") in *GROW1* and rs6060369 ("T") in *R4*, uncoupling risk for DDH and knee OA, respectively. Yet we revealed complex regulatory interactions within the vicinity of each variant and across the locus. Given that risk "A" rs143384 is in strong linkage disequilibrium with both risk "A" rs4911178 and "T" rs6060369 risk alleles, we hypothesized that there could be epistatic interactions between these variant positions (Supplementary Figure 1, variants in red). To first test for epistasis, we generated constructs containing different combinations of risk and nonrisk alleles at three variants: rs143383 (5′-UTR) (an additional associated variant), rs143384 (5′-UTR), and rs6060369 (*R4*) (Figure 6A) and transfected them into T/C-28a2 human chondrocytes (methods). We found that the *R4* risk/nonrisk alleles drive lower luciferase expression than 5′-UTR risk/nonrisk alleles. Strikingly, risk alleles at *R4* and 5′-UTR variants (Figure 6A, red values) together drive nearly half the expression on nonrisk alleles, indicating a strong epistatic interaction (Figure 6A, blue values). In the same manner, we tested for epistasis between rs4911178 (in *GROW1*) and 5′-UTR variants but transfected constructs into the human growth plate chondrocyte cell line, CHON-002. Here, we first observe much lower luciferase expression with constructs containing *GROW1* nonrisk/risk alleles in comparison with 5′-UTR nonrisk/risk alleles, yet with risk alleles driving much lower expression than the nonrisk alleles. Second, the 5′-UTR variants appear to somewhat rescue suppressed expression by the *GROW1* nonrisk/risk alleles. Third, we observe that all three risk alleles at *GROW1* and the 5′-UTR (Figure 6B, red values) result in no significant change to luciferase expression in comparison to nonrisk alleles (Figure 6B). We note that although the 5′-UTR is included in all open chromatin regions across developmental joint sites,[39] we find that the *R4* and *GROW1* regulatory regions lie in highly skeletal element–specific open chromatin regions, further emphasizing the potential modular nature of these variant interactions (Supplementary Figure 7). Together, these studies reveal complex interactions between variants that impact *GDF5* expression. We have included a diagram showing all interactions across the locus discovered to date (Figure 6C).

DISCUSSION

Before this study, what was known about *Gdf5* regulatory activity was restricted to broad patterns across the locus or specific regulatory sequences, with no large or small regulatory region able to fully recapitulate endogenous *Gdf5* expression. On interrogation of a downstream 37-kb region encompassing the reported *GROW1* subperichondral enhancer (Supplementary Figure 1, purple region), we identified an overlapping conserved subregion *PHC17* that drove *lacZ* expression throughout the growth plate, a pattern not observed for any larger or smaller construct or for endogenous *Gdf5* expression. Indeed, *PHC17* individual components *GROW1*, *R18–R20*, and *R7* were each unable to recapitulate this full growth plate signal. Interestingly, in the adjacent *PHC18* subregion, we found that the *R9* element acts to restrict *R8* expression patterns to only the shoulder joint, with its repressor activity confirmed in human chondrocytes. Therefore, *R9* is the strongest candidate to restrict *GROW1* to the

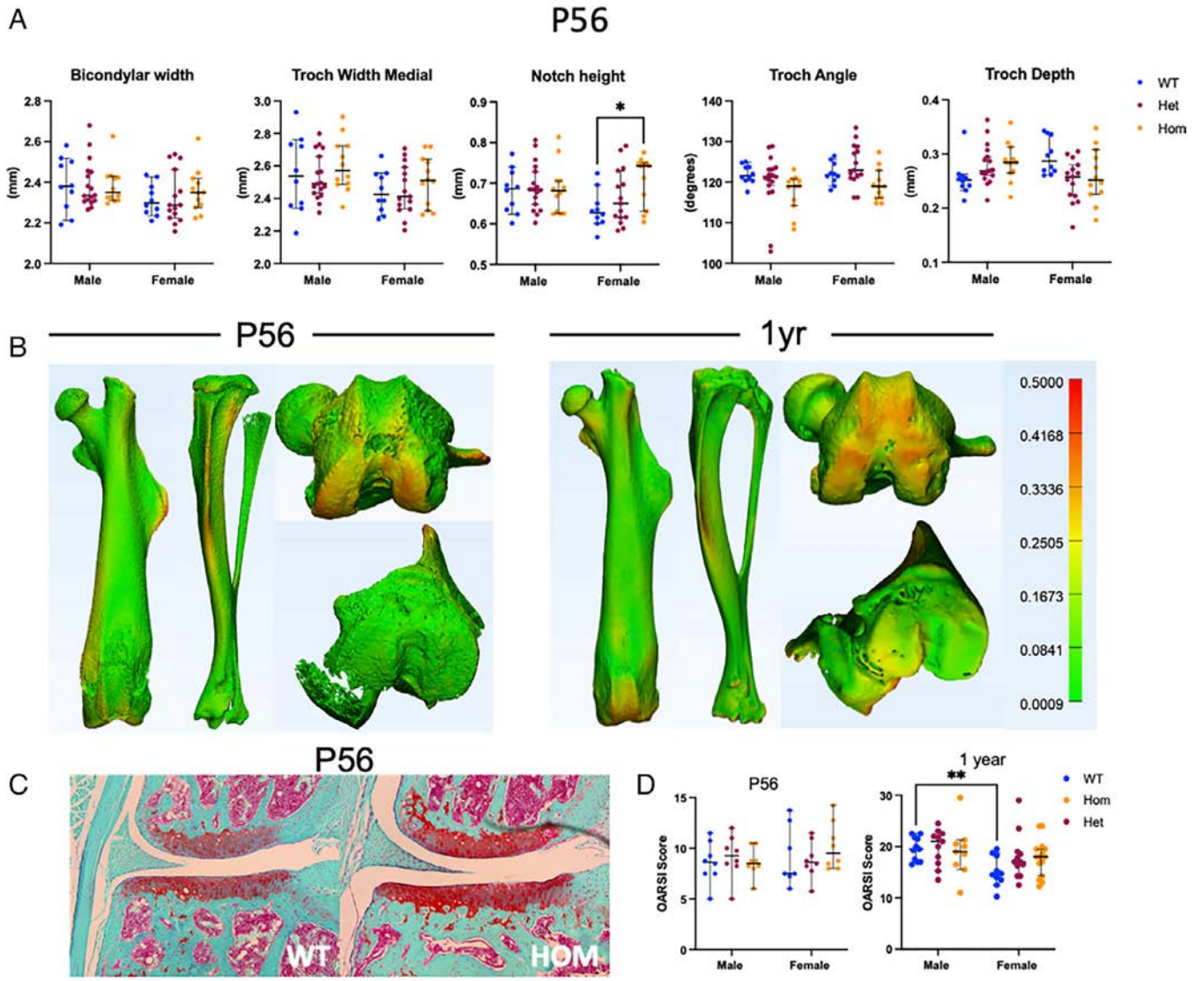

Figure 5. Morphologic characterization of the *GDF5* 5′-UTR rs143384 variant in the mouse model. (A) Micro-CT measurements of anatomic features in 5′-UTR rs143384 single basepair replacement mice at P56 (males: WT n = 10, Het n = 17, Hom n = 12; females: WT n = 10, Het n = 15, Hom n= 12). Welch's *t*-test was used for comparisons between WT and homozygous measurements (*$P < 0.05$; bars indicate medians with 95% confidence intervals). (B) Three-dimensional morphologic comparative analysis indicating locations of largest anatomic differences between WT and homozygous risk 5′-UTR rs143384 hind limbs at P56 and one year. (C) Coronal histologic sections of the medial compartment from WT and 5′-UTR rs143384 knee joints stained with Safranin O of representative OARSI scoring in panel D. (D) OARSI scoring of P56 and one-year knee joints (P56: males: WT n = 8, Het n = 8, Hom n = 8; females: WT n = 7, Het n = 8, Hom n = 8; one year: males: WT n = 11, Het n = 8, Hom n = 8; females: WT n = 10, Het n = 12, Hom n = 15). Two-Way analysis of variance performed with Šídák's multiple comparison test found no significant results between genotypes (**$P < 0.01$; bars indicate medians with 95% confidence intervals). Het, heterozygous; Hom, homozygous; micro-CT, micro–computed tomography; OARSI, Osteoarthritis Research Society International; UTR, untranslated region; WT, wild type. Color figure can be viewed in the online issue, which is available at http://onlinelibrary.wiley.com/doi/10.1002/art.43231/abstract.

subperichondral region across the entire 37-kb window. We also identified two OA risk variants within the *R9* region that, with each introduction, substantially modify the class of TF binding to each site. This indicates an additional layer of regulation at these variants that can be cell type and tissue specific, impacting *GDF5* expression. Further downstream in the 41-kb joint region, we then observed that different combinations of the *R3*, *R4*, and *R5* enhancers regions drove very distinct patterns across limb joints, with none alone able to recapitulate the complete 41-kb, *PHC19*, or *Gdf5* expression patterns. Here, we identified that these enhancers also act as repressors, with small or large impacts on expression depending on the skeletal site. Finally, for the upstream joint region *R2*, we identified subregion *abc* as a repressor sequence of the *d* and *e* subregions. Moreover, we identified a shorter 112-bp sequence within the *d* region itself that restricts *d* expression to the major hind limb joints only. From these findings, we conclude that there are complex activator and repressor sequences that operate between and within regulatory regions that

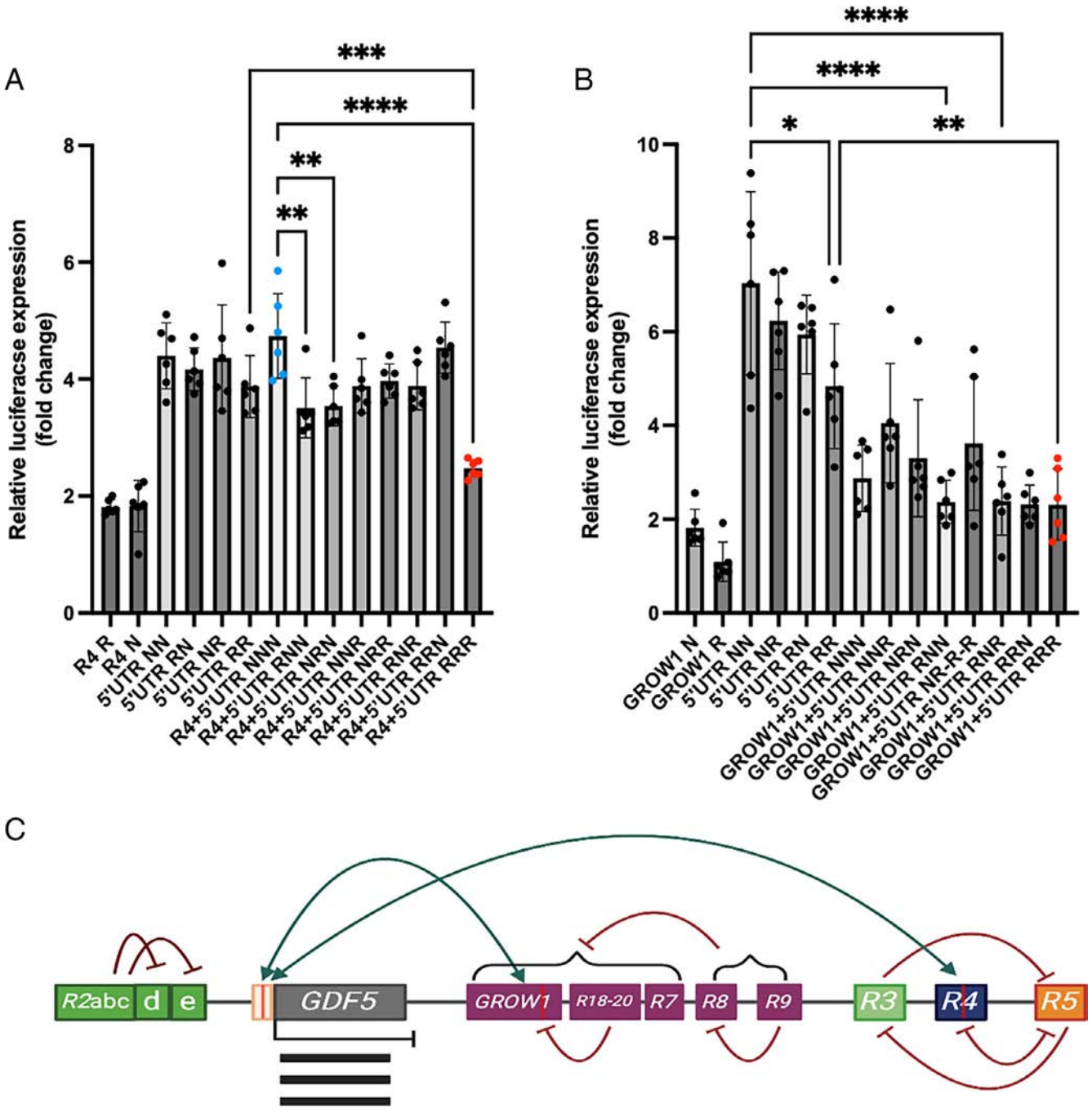

Figure 6. Disease risk variants interact to impact expression. (A) Relative normalized luciferase expression produced by plasmids containing different nonrisk (N) or risk (R) variants of either the *R4* variant rs6060369 or the 5′-UTR variants rs143383 and rs143384 in T/C-28a2 cells. (B) Relative normalized luciferase expression produced by plasmids containing different nonrisk (N) or risk (R) variants of either the *GROW1* variant rs4911178 or the 5′-UTR variants rs143383 and rs143384 in CHON-002 cells. (C) Cartoon model of identified interactions across the *GDF5* locus including risk variants marked as red lines (depictions not to scale). *$p < 0.05$; **$p < 0.01$; ***$p < 0.001$; ****$p < 0.0001$. Color figure can be viewed in the online issue, which is available at http://onlinelibrary.wiley.com/doi/10.1002/art.43231/abstract.

can be tissue and cell type dependent as well as joint specific. We argue that this complex regulatory landscape likely evolved to precisely shape joints and long bones, a point evinced by the high dysmorphic joints of *Gdf5* complete loss-of-function (*bp/bp)* mice.

By generating mice with a deletion of the *R2de* sequence adjacent to *Gdf5* 5′-UTR, we identified a 40% decrease per allele in *Gdf5* expression at all large limb joint skeletal sites. Interestingly, complete loss-of-function (*R2de*$^{-/-}$ mice) did lead to hip and knee morphologic changes early on (P56), but by 1.5 years, these differences were no longer significant and importantly did not lead to any increase in OA disease. This is in line with what is observed in mice with *Gdf5* coding mutations (ie, *bp/+* mice have a 50%

drop in expression, and *bp/bp* mice have no functional expression, and neither develop OA, even though *bp/bp* mice have massive joint disruptions throughout life). These observations are in stark contrast to our findings from functional tests of individual *Gdf5* regulatory sequences and variants therein. Mice with an *R4* enhancer deletion have decreases (of ~32% per allele) in *Gdf5* expression only in the knee but not in other joint sites. This joint-specific decrease led to morphologic changes in $R4^{-/-}$ mice only in the knee at P56 and one year, with resulting effects on OA. Humanized mice with a GWAS OA risk variant (rs6060369, C→T) in *R4* also have decreased *Gdf5* expression (~16% per allele) within knee epiphyseal and articular cartilage only, and this reduction causes significant morphologic changes in the same direction as patients with OA and a 30% increase in OA in homozygous "T/T" mice.[9] Mice with a *GROW1* enhancer deletion have decreases (16% per allele) in *Gdf5* expression only in the proximal femur and acetabulum but not at other joint sites. This leads to femoral head and neck and acetabulum alterations (but not in knees), recapitulating those observed in patients with DDH. Finally, humanized mice with a GWAS DDH risk variant (rs4911178, G→A) in *GROW1* also have decreased *Gdf5* expression (16% per allele) only within the proximal femur and acetabulum subperichondral chondrocytes, and this causes hip changes in mice in the same direction of effect as patients with DDH.[9]

Collectively, these functional studies reveal that location-specific decreases in *Gdf5* expression are far more important mediators of complex disease risk (OA, DDH, etc) than large effects of expression reduction observed across different joint sites and tissues, the latter of which are typically not observed in human patients with complex (ie, common variant mediated) joint disease (but in fact are more indicative of patients with syndromic disorders due to *GDF5* coding mutations). We argue that this is the case because such location-specific decreases alter joint shape locally, changes that are not reciprocated on the opposing joint surface, resulting in a misregistration of joint articulation, which developmentally (DDH) or over time (OA) can predispose to disease. Furthermore, these effects on complex disease risk are in turn the product of the fine sculpting of *GDF5* expression by complex interacting regulatory sequences.

We have shown that across the locus, GWAS risk variants can reside in enhancers (eg, rs4911178 in *GROW1*), repressors (rs2378349 and rs2248393 in *R9*), or sequences that behave as both (eg, rs6060369 in *R4*), which in turn markedly obscures one's ability to pinpoint causality at the individual basepair level and at cell type resolution. For example, by generating humanized mice harboring the most highly cited OA single-nucleotide polymorphism variant (rs143384, G→A) located in *GDF5* 5′-UTR, we did not observe any significant expression reductions at any joint site, nor did we find any significant morphologic changes or evidence of knee OA disease in adult mice at P56 or one year. This reveals that alone, rs143384 "A" is likely not causal for OA disease risk. Yet we would be remiss to have not considered this (or any) variant within the complex *cis*-regulatory architecture of *GDF5*, a system that has evolved built-in activation and repression mechanisms locally (ie, within a regulatory element) and further afield (across broad growth plate or joint regions) to generate endogenous *Gdf5* expression territories at each joint site and thus precisely sculpt joints. Indeed, by testing for epistasis, we did observe substantial interactions between 5′-UTR rs143384 "A" and *R4* rs6060369 "T" risk alleles and partially with *GROW1* rs4911178 "A" risk alleles. These data are further corroborated by analyses of Hi-C interaction data (Supplementary Figure 8). In each context, we argue that *cis*-regulatory variants provide locational and cell type specificity, and by doing so they (ie, *R4* and *GROW1*) both reduce and direct how reductions caused by other (5′-UTR) variants become channeled to specific tissues. This in turn results in local joint misregistration causing developmentally driven site-specific musculoskeletal disease risk at *GDF5*. We posit that disease risk at this developmental locus and most others is analogous to the risks for developing cancers due to the actions of double or triple hits, but here hits are the myriad *cis*-regulatory variants residing on risk haplotypes and within their built-in complex epigenetic interactions.[43,44] Additionally, all these studies were performed without challenge, excluding environmental factors such as injury and obesity.[26,45] These factors could modulate the epigenetic landscape impacting regulatory region and variant interactions, potentially exacerbating these interactions to initiate disease progression. Therefore, understanding the epistatic context in which a disease risk variant lies will be fundamental to disentangling and prioritizing the close to 2,000 OA-associated GWAS[46,47] variants that have been identified to date.

ACKNOWLEDGMENTS

The authors would like to thank EpigenDx for ASE; Applied StemCell for mice; Drs Li Zeng (Tufts University, Boston, Massachusetts) and Mary Goldring (The Hospital for Special Surgery, New York City, New York) for the T/C-28a2 cell line; Dr Hopi Hoekstra for the NIH3T3 cell line; Dr David Kingsley for advisement and guidance; and members of the Capellini Lab for support.

AUTHOR CONTRIBUTIONS

All authors contributed to at least one of the following manuscript preparation roles: conceptualization AND/OR methodology, software, investigation, formal analysis, data curation, visualization, and validation AND drafting or reviewing/editing the final draft. As corresponding author, Dr Capellini confirms that all authors have provided the final approval of the version to be published and takes responsibility for the affirmations regarding article submission (eg, not under consideration by another journal), the integrity of the data presented, and the statements regarding compliance with institutional review board/Declaration of Helsinki requirements.

REFERENCES

1. Steinmetz JD, Culbreth GT, Haile LM, et al; GBD 2021 Osteoarthritis Collaborators. Global, regional, and national burden of osteoarthritis, 1990-2020 and projections to 2050: a systematic analysis for the Global Burden of Disease Study 2021. Lancet Rheumatol 2023;5(9): e508–e522.
2. Guilak F. Biomechanical factors in osteoarthritis. Best Pract Res Clin Rheumatol 2011;25(6):815–823.
3. Vincent TL. Mechanoflammation in osteoarthritis pathogenesis. Semin Arthritis Rheum 2019;49(3S):S36–S38.
4. Felson DT. Osteoarthritis as a disease of mechanics. Osteoarthritis Cartilage 2013;21(1):10–15.
5. Faber BG, Frysz M, Tobias JH. Unpicking observational relationships between hip shape and osteoarthritis: hype or hope? Curr Opin Rheumatol 2020;32(1):110–118.
6. van Buuren MMA, Arden NK, Bierma-Zeinstra SMA, et al. Statistical shape modeling of the hip and the association with hip osteoarthritis: a systematic review. Osteoarthritis Cartilage 2021;29(5):607–618.
7. Cooperman D. What is the evidence to support acetabular dysplasia as a cause of osteoarthritis? J Pediatr Orthop 2013;33(suppl 1): S2–S7.
8. Baird DA, Evans DS, Kamanu FK, et al. Identification of novel loci associated with hip shape: a meta-analysis of genomewide association studies. J Bone Miner Res 2019;34(2):241–251.
9. Muthuirulan P, Zhao D, Young M, et al. Joint disease-specificity at the regulatory base-pair level. Nat Commun 2021;12(1):4161.
10. Young M, Richard D, Grabowski M, et al. The developmental impacts of natural selection on human pelvic morphology. Sci Adv 2022;8(33): eabq4884.
11. Storm EE, Kingsley DM. Joint patterning defects caused by single and double mutations in members of the bone morphogenetic protein (BMP) family. Development 1996;122(12):3969–3979.
12. Brunet LJ, McMahon JA, McMahon AP, et al. Noggin, cartilage morphogenesis, and joint formation in the mammalian skeleton. Science 1998;280(5368):1455–1457.
13. Merino R, Macias D, Gañan Y, et al. Expression and function of Gdf-5 during digit skeletogenesis in the embryonic chick leg bud. Dev Biol 1999;206(1):33–45.
14. Pregizer SK, Kiapour AM, Young M, et al. Impact of broad regulatory regions on Gdf5 expression and function in knee development and susceptibility to osteoarthritis. Ann Rheum Dis 2018;77(3):450–458.
15. Daans M, Luyten FP, Lories RJ. GDF5 deficiency in mice is associated with instability-driven joint damage, gait and subchondral bone changes. Ann Rheum Dis 2011;70(1):208–213.
16. Southam L, Rodriguez-Lopez J, Wilkins JM, et al. An SNP in the 5′-UTR of GDF5 is associated with osteoarthritis susceptibility in Europeans and with in vivo differences in allelic expression in articular cartilage. Hum Mol Genet 2007;16(18):2226–2232.
17. Egli RJ, Southam L, Wilkins JM, et al. Functional analysis of the osteoarthritis susceptibility-associated GDF5 regulatory polymorphism. Arthritis Rheum 2009;60(7):2055–2064.
18. Capellini TD, Chen H, Cao J, et al. Ancient selection for derived alleles at a GDF5 enhancer influencing human growth and osteoarthritis risk. Nat Genet 2017;49(8):1202–1210.
19. Chen H, Capellini TD, Schoor M, et al. Heads, shoulders, elbows, knees, and toes: modular Gdf5 enhancers control different joints in the vertebrate skeleton. PLoS Genet 2016;12(11):e1006454.
20. Syddall CM, Reynard LN, Young DA, et al. The identification of trans-acting factors that regulate the expression of GDF5 via the osteoarthritis susceptibility SNP rs143383. PLoS Genet 2013;9(6): e1003557.
21. Reynard LN, Bui C, Syddall CM, et al. CpG methylation regulates allelic expression of GDF5 by modulating binding of SP1 and SP3 repressor proteins to the osteoarthritis susceptibility SNP rs143383. Hum Genet 2014;133(8):1059–1073.
22. Miyamoto Y, Mabuchi A, Shi D, et al. A functional polymorphism in the 5′ UTR of GDF5 is associated with susceptibility to osteoarthritis. Nat Genet 2007;39(4):529–533.
23. Rice SJ, Brumwell A, Falk J, et al. Genetic risk of osteoarthritis operates during human skeletogenesis. Hum Mol Genet 2023;32(13): 2124–2138.
24. Kania K, Colella F, Riemen AHK, et al. Regulation of Gdf5 expression in joint remodelling, repair and osteoarthritis. Sci Rep 2020;10(1):157.
25. Kiapour AM, Cao J, Young M, et al. The role of Gdf5 regulatory regions in development of hip morphology. PLoS One 2018;13(11): e0202785.
26. Richard D, Liu Z, Cao J, et al. Evolutionary selection and constraint on human knee chondrocyte regulation impacts osteoarthritis risk. Cell 2020;181(2):362–381.e28.
27. DiLeone RJ, Marcus GA, Johnson MD, et al. Efficient studies of long-distance Bmp5 gene regulation using bacterial artificial chromosomes. Proc Natl Acad Sci USA 2000;97(4):1612–1617.
28. DiLeone RJ, Russell LB, Kingsley DM. An extensive 3′ regulatory region controls expression of Bmp5 in specific anatomical structures of the mouse embryo. Genetics 1998;148(1):401–408.
29. Storm EE, Huynh TV, Copeland NG, et al. Limb alterations in brachypodism mice due to mutations in a new member of the TGFβ-superfamily. Nature 1994;368(6472):639–643.
30. Loots GG, Ovcharenko I, Pachter L, et al. rVista for comparative sequence-based discovery of functional transcription factor binding sites. Genome Res 2002;12(5):832–839.
31. Loots GG, Ovcharenko I. rVISTA 2.0: evolutionary analysis of transcription factor binding sites. Nucleic Acids Res 2004;32(suppl 2): W217–W221.
32. Meech R, Edelman DB, Jones FS, et al. The homeobox transcription factor Barx2 regulates chondrogenesis during limb development. Development 2005;132(9):2135–2146.
33. Smith DM, Tabin CJ. Chick Barx2b, a marker for myogenic cells also expressed in branchial arches and neural structures. Mech Dev 1999;80(2):203–206.
34. Gray PA, Fu H, Luo P, et al. Mouse brain organization revealed through direct genome-scale TF expression analysis. Science 2004; 306(5705):2255–2257.
35. Weirauch MT, Yang A, Albu M, et al. Determination and inference of eukaryotic transcription factor sequence specificity. Cell 2014; 158(6):1431–1443.
36. Glasson SS, Blanchet TJ, Morris EA. The surgical destabilization of the medial meniscus (DMM) model of osteoarthritis in the 129/SvEv mouse. Osteoarthritis Cartilage 2007;15(9):1061–1069.
37. Ran FA, Hsu PD, Wright J, et al. Genome engineering using the CRISPR-Cas9 system. Nat Protoc 2013;8(11):2281–2308.
38. Jung I, Schmitt A, Diao Y, et al. A compendium of promoter-centered long-range chromatin interactions in the human genome. Nat Genet 2019;51(10):1442–1449.
39. Richard D, Muthuirulan P, Young M, et al; GIANT Consortium. Functional genomics of human skeletal development and the patterning of height heritability. Cell 2025;188(1):15–32.e24.
40. Hahne F, Ivanek R. Visualizing genomic data using Gviz and Bioconductor. In: Mathé E, Davis S, eds. Statistical Genomics: Methods and Protocols. Springer; 2016:335–351.
41. Harmston N, Ing-Simmons E, Perry M, et al. GenomicInteractions: an R/Bioconductor package for manipulating and investigating chromatin interaction data. BMC Genomics 2015;16(1):963.

42. Barlow AJ, Bogardi JP, Ladher R, et al. Expression of chick Barx-1 and its differential regulation by FGF-8 and BMP signaling in the maxillary primordia. Dev Dyn 1999;214(4):291–302.
43. Roberts JB, Rice SJ. Osteoarthritis as an enhanceropathy: gene regulation in complex musculoskeletal disease. Curr Rheumatol Rep 2024;26(6):222–234.
44. Raghavan N, Tosto G. Genetics of Alzheimer's disease: the importance of polygenic and epistatic components. Curr Neurol Neurosci Rep 2017;17(10):78.
45. Richard D, Capellini TD. Shifting epigenetic contexts influence regulatory variation and disease risk. Aging (Albany NY) 2021;13(12):15699–15749.
46. Klein JC, Keith A, Rice SJ, et al. Functional testing of thousands of osteoarthritis-associated variants for regulatory activity. Nat Commun 2019;10(1):2434.
47. Boer CG, Hatzikotoulas K, Southam L, et al; arcOGEN Consortium; HUNT All-In Pain; ARGO Consortium; Regeneron Genetics Center. Deciphering osteoarthritis genetics across 826,690 individuals from 9 populations. Cell 2021;184(18):4784–4818.e17.

Arthritis & Rheumatology
Vol. 77, No. 11, November 2025, pp 1503–1511
DOI 10.1002/art.43241

American College of Rheumatology
Empowering Rheumatology Professionals

Global Burden of Osteoarthritis Attributable to High Body Mass Index, 1990 to 2021: Insights From the Global Burden of Disease Study 2021

Yi Lu, Wenyu Xiao, and Kun Tao

Objective. This study was undertaken to quanitfy the global burden of osteoarthritis (OA) attributable to high body mass index (BMI) from 1990 to 2021 using the Global Burden of Disease (GBD) 2021 data.

Methods. Using GBD 2021 data, this research examines the OA burden related to high BMI across 204 countries and regions. Statistical analyses were performed to profile disease burdens, and joinpoint regression was used to identify temporal trends. The study also investigated the relationship between the Sociodemographic Index (SDI) and OA burden attributable to high BMI.

Results. From 1990 to 2021, years lived with disability (YLDs) owing to OA attributable to high BMI increased threefold globally, from 1,449,681 to 4,422,954. The age-standardized YLD rates of OA attributable to high BMI increased from 33.97 (95% uncertainty interval [UI] −3.14 to 102.31) to 50.59 (95% UI −4.81 to 141.35) per 100,000 population, with an average annual percentage change of 1.11 (95% confidence interval 1.07–1.14). The burden of OA YLDs attributable to high BMI was higher in women than men across all age groups. The age-standardized rates of OA YLDs attributable to high BMI were positively correlated with SDI levels, with higher burdens observed in regions with higher SDI levels.

Conclusion. Between 1990 and 2021, the global burden of OA attributable to high BMI increased markedly, with a consistent upward trend across most regions. The burden was more pronounced among women, middle-aged and older adults, and populations in high-SDI regions, reflecting a growing and uneven global health challenge.

INTRODUCTION

Osteoarthritis (OA) is a prevalent musculoskeletal disorder and ranks among the foremost causes of chronic pain and persistent disability in the adult population.[1] OA represents a significant contributor to health care expenditures. In 2016, the financial burden of OA-related health care costs in the United States was approximately $80 billion.[2] This burden continues to escalate concomitant with population growth and aging demographics. OA is acknowledged as one of the 10 most prevalent disabling conditions among older adults within developed nations.[3,4] The World Health Organization's designation of 2021–2030 as the decade of healthy aging has heightened awareness of the burden imposed by OA in the realm of adult health.[5] OA is characterized as a chronic, progressive disease marked by irreversible structural alterations. Given that OA manifestations can occur relatively early in adulthood, even in individuals younger than 50 years,[6] the implementation of early and proactive management strategies is imperative.

Modifiable risk factors for OA prominently include high body mass index (BMI) and joint trauma.[7,8] Additional risk factors include physically demanding occupations,[9] participation in high-intensity sports,[10] previous surgical interventions,[11] joint anatomic features, and muscle weakness.[12] A high BMI is linked to the onset of numerous diseases. On a global scale, the number of deaths and disability-adjusted life-years (DALYs) attributable to high BMI has surged, increasing by more than 2.5-fold from 1990 to 2021.[13] In current Global Burden of Disease (GBD) studies, high BMI is the sole risk factor identified with OA as an outcome.[5] However, the quantitative burden of OA attributable to high BMI, along with its temporal trends, remains inadequately characterized at both the regional and national levels.[14,15]

Given the substantial societal burden of OA and the necessity for targeted interventions, understanding the evolving

Yi Lu, MS, Wenyu Xiao, MS, Kun Tao, MD: Department of Orthopedics, Chongming Branch, Shanghai Tenth People's Hospital, Shanghai, China.

Additional supplementary information cited in this article can be found online in the Supporting Information section (https://acrjournals.onlinelibrary.wiley.com/doi/10.1002/art.43241).

Author disclosures are available at https://onlinelibrary.wiley.com/doi/10.1002/art.43241.

Address correspondence via email to Yi Lu, MS, at lyyi61today@163.com.

Submitted for publication November 25, 2024; accepted in revised form May 9, 2025.

relationship between BMI and OA across different geographies provides critical insights. Although previous GBD studies have quantified OA burdens attributable to high BMI,[15,16] critical uncertainties persist. Firstly, prior analyses focused on DALYs or years lived with disability (YLDs) up to 2019, leaving post-2019 trends (especially those impacted by the evolving obesity patterns) unexplored. Secondly, regional and national disparities in OA burden linked to high BMI remain uncharacterized, particularly in low- and middle-income countries where obesity rates are rising rapidly but OA surveillance is limited. Thirdly, although previous studies have highlighted sex- and age-specific disparities, there is a need for an updated assessment of the interaction between demographic shifts (eg, aging populations in high Sociodemographic Index [SDI] regions) and BMI-related OA burden. Therefore, this study aims to fill these gaps by providing a detailed analysis of the global, regional, and national burden of YLDs attributable to OA associated with high BMI using data from the latest GBD 2021 study. This analysis offers a comprehensive examination of temporal trends and regional disparities, thereby supporting the development of more effective and targeted prevention strategies.

PATIENTS AND METHODS

Overview and GBD data sources. An overview of the study design is presented in Figure S1. This study extracted OA as the combination of hip and knee OA, which are regarded as contributing to significant disability in the GBD 2021 study. The data on OA (hip and knee) attributed to high BMI used in this study were sourced from the Global Health Data Exchange GBD Results Tool, developed by the Institute for Health Metrics and Evaluation (http://ghdx.healthdata.org/gbd-results-tool). The GBD 2021 data were extracted from vital registration systems, verbal autopsies, censuses, household surveys, disease-specific registries, health service contact data, and various other sources.[17]

There is no strong evidence linking BMI to OA of the hand,[5] thus our analysis concentrates on the hip and knee, which are more directly impacted by mechanical load and weight bearing. The main sources of input data for the hip and knee OA models were cross-sectional, population-based survey data from locations worldwide and state-level US insurance claims data captured by *International Classification of Diseases, Ninth Revision* (*ICD-9*) four-digit or five-digit codes starting with 715 specific to knee or hip, and *ICD-10* codes M16 and M17. *ICD-10* used the terminology "osteoarthritis" and replaced *ICD-9*, which used osteoarthrosis to reflect the recognition that inflammatory processes are involved in the pathogenesis of OA.[5] High BMI was defined as a BMI ≥25 kg/m^2 for individuals aged over 20 years. A BMI range of 20 to 24.9 kg/m^2 is considered the theoretical minimum risk exposure level.[18] We extracted the data on OA associated with high BMI by age (≥30 years), sex, and location across 204 countries and territories from 1990 to 2021. The choice of focusing on individuals aged ≥30 years is based on established methods in OA research. Specifically, the *Lancet Rheumatology* article on the GBD study[5] states that the prevalence estimates for each OA site are produced for individuals aged ≥30 years.

Bayesian meta-regressions using DisMod-MR 2.1 set the incidence of OA to zero before age 30 years. DisMod-MR 2.1 is an age-integrating Bayesian meta-regression log-normal disease model designed to handle heterogeneous data from multiple sources and ensure consistency between different disease parameters, such as incidence and prevalence. In the GBD study, the measurement of DALYs for OA equates to YLDs, given the nonfatal nature of OA. YLDs represent the total number of healthy life-years lost because of illness, calculated by multiplying the prevalence of OA in specific age-sex cohorts by the disability weight of OA, using the DisMod-MR 2.1 program. The disability weight is an indicator ranging from 0 to 1, with the highest value signifying a state equivalent to death. The 95% uncertainty intervals (UIs) were calculated by sampling 1,000 iterations from the posterior distribution at each step of the modeling process, with the UIs reported as the 2.5th and 97.5th percentiles for each estimate. It is important to note that a negative lower limit does not suggest a protective effect but rather indicates the absence of a relationship.[5]

This study also examined the relationship between the SDI and the burden of OA attributable to high BMI. The SDI is a composite indicator reflecting the development status of a geographic location, calculated based on the total fertility rate among female individuals aged <25 years, with educational attainment for those aged ≥15 years, and lag-distributed income per capita.[19] The SDI ranges from 0 to 1, where 0 denotes the minimum level of development and 1 represents the maximum level of development. The 204 countries and territories were categorized into five groups based on SDI quintiles: low SDI, low-middle SDI, middle SDI, high-middle SDI, and high SDI.

Statistical analysis. This study first presents the number of YLDs and age-standardized rates (ASRs) of OA related to high BMI from 1990 to 2021, with visualizations illustrating the disease burden across 204 countries and territories and multiple age groups and sexes. The ASR was calculated by adjusting for the global age structure, a critical step when comparing populations across different regions or over time. We then used joinpoint regression analysis to identify localized trends in the burden of OA attributable to high BMI. This analysis segments the overall trend into subsections based on inflection points and estimates the average annual percentage change (AAPC) with 95% confidence intervals (CIs) by calculating the annual percentage change (APC) for each subsection, indicating the trend's direction and magnitude. The selection of inflection points was based on the minimization criterion using the Bayesian information criterion.

We employed Joinpoint software version 5.1.0.0, setting a maximum of six joinpoints with Monte Carlo *P* value correction. If both the APC/AAPC estimate and the lower boundary of the 95% CI were more significant than 0, an increasing trend was identified for that period. Conversely, if both the APC/AAPC estimate and the upper boundary of the 95% CI were less significant than 0, a decreasing trend was determined. Otherwise, the trend was considered stable. Finally, Spearman correlation analyses were performed to calculate r indices and *P* values for the relationship between the SDI and ASR of YLDs for OA associated with high BMI across different countries. All analyses were conducted at a significance level of 0.05. All statistical analyses and graphs were conducted using R software (version 4.4.1) and Joinpoint software (version 5.1.0.0).

RESULTS

The burden of OA attributable to high BMI at global, regional, and national levels. As shown in Table 1, from 1990 to 2021, the number of OA YLDs attributable to high BMI tripled globally, rising from 1,449,681 to 4,422,954. The YLD ASRs of OA attributable to high BMI (per 100,000 population) increased from 33.97 (95% UI –3.14 to 102.31) to 50.59 (95% UI –4.81 to 141.35). The AAPC was 1.11 (95% CI 1.07–1.14). At the regional level, both the number and ASR of OA YLDs associated with high BMI demonstrated an upward trend. East Asia had the highest AAPC at 2.14 (95% CI 2.10–2.18), followed by Southeast Asia at 2.09 (95% CI 2.06–2.12) and South Asia at 2.09 (95% CI 2.06–2.12). In 2021, high-income North America (82.03; 95% UI –9.14 to 215.01), Australasia (79.24; 95% UI –8.19 to 213.4), and southern Latin America (76.31; 95% UI –8.39 to 196.56) reported the highest YLD ASRs. In contrast, South Asia (27.81; 95% UI –2.2 to 81.78), Southeast Asia (27.87; 95% UI –2.18 to 80.99), and eastern Sub-Saharan Africa (28.76; 95% UI –2.22 to 84.57) had the lowest rates at the regional level.

Figure 1 displays the geographic distribution of the ASR for OA YLDs attributable to high BMI in 2021 across 204 countries. Figure S2 depicts the distribution of the number for these YLDs attributable to high BMI in the same year and countries. The top three countries with the highest ASR of YLDs changed from the United States, American Samoa, and Cook Islands in 1990 to the United States, Cook Islands, and Tonga in 2021, with the Cook Islands showing the largest increase of 26.98%. Similarly, the top three countries with the highest number of YLDs shifted from China, the United States, and the Russian Federation in 1990 to China, the United States, and India in 2021, with India experiencing the largest increase of 426.41%. Detailed data are available in Table S1. At the country level, the burden of OA attributable to high BMI varies significantly worldwide. Health care accessibility in each country may affect data quality, potentially leading to underestimation in those with lower health care levels. Additionally, cultural differences may influence data quality and precision.

The burden of OA attributable to high BMI by age and sex. Figure 2 and Figure S3 show the ASR and number of OA YLDs attributable to high BMI by age and sex globally in 2021. Figure 2 illustrates that the ASR of OA YLDs attributable to high BMI gradually increases from ages 30 to 74 years, stabilizes at 75 to 79 years, and declines after 80 years, with a more pronounced decrease in women. Figure S3 shows a gradual increase in the number of YLDs from ages 30 to 59 years, peaking at 55 to 59 years, followed by a decline after 70 years and a sharp drop after age 80 years. The burden of OA YLDs attributable to high BMI is higher in women than men across all ages.

Joinpoint regression analysis. Figure 3A depicts the joinpoint regression analysis of the ASR for OA YLDs attributable to high BMI globally from 1990 to 2021. The APC showed a fairly consistent upward trend globally over the study period, with some year-to-year variability. The global ASR of OA YLDs attributable to high BMI demonstrated a steady increase, with accelerated growth during 2006 to 2009 (APC = 1.53, $P < 0.05$). The upward trend is more pronounced for women than for men in all the contemporaneous years. Among the 21 global regions, all exhibited upward trends to varying degrees, except for high-income North America (Figure 3B), which experienced a significant decline from 2000 to 2005 (APC = –2.5, $P < 0.05$), and women in Andean Latin America, who experienced a slight decline from 2019 to 2021 (APC = –0.61, $P < 0.05$). For further details, see Figure S4.

Relationship between SDI and the impact of OA burden attributable to high BMI. In 1990, the number and ASR of OA YLDs attributable to high BMI were positively correlated with SDI levels. By 2021, the highest number of YLDs shifted from the high-SDI quintile to the middle-SDI quintile. However, the number of YLDs for men with middle SDI in 2021 was slightly lower than those with high SDI, ranking second. The ASR of OA YLDs attributable to high BMI remained positively unchanged. See Table S2 for details.

Between 1990 and 2021, there was an increasing trend between SDI and ASR of OA YLDs attributable to high BMI globally and across all GBD regions (Figure 4A). In regions such as western Sub-Saharan Africa, North Africa and the Middle East, southern Sub-Saharan Africa, high-income North America, the Caribbean, Andean Latin America, Central Latin America, southern Latin America, tropical Latin America, Australia, and Oceania, the OA burdens attributable to high BMI were higher than expected based on the SDI during this period. Eastern Sub-Saharan Africa and Western Europe had lower-than-expected burdens only in the early years, whereas central Sub-Saharan

Table 1. Global and regional burden of years lived with disability because of osteoarthritis attributed to high body mass index, 1990 and 2021*

Location	Number of cases (95% UI)		ASR (95% UI) per 100,000 people		AAPC (95% CI)
	1990	2021	1990	2021	1990–2021
Global	1,449,681 (−127,136 to 4,113,313)	4,422,954 (−421,237 to 12,338,125)	35.97 (−3.14 to 102.31)	50.59 (−4.81 to 141.35)	1.11 (1.07 to 1.14)
High-income Asia Pacific	82,639 (−6,623 to 243,996)	201,743 (−15,797 to 603,492)	39.93 (−3.2 to 117.82)	51.5 (−4.14 to 153.08)	0.82 (0.80 to 0.85)
Central Asia	16,488 (−1,541 to 45,709)	36,183 (−3,860 to 97,115)	34.8 (−3.21 to 97.26)	42.04 (−4.37 to 113.44)	0.61 (0.59 to 0.63)
Southeast Asia	41,753 (−3,099 to 125,493)	201,325 (−15,981 to 582,465)	14.76 (−1.09 to 44.76)	27.87 (−2.18 to 80.99)	2.09 (2.06 to 2.12)
East Asia	256,084 (−20,940 to 755,795)	1,201,664 (−108,095 to 3,403,965)	27.46 (−2.23 to 81.48)	52.85 (−4.73 to 150.44)	2.14 (2.10 to 2.18)
Central Europe	63,283 (−5,876 to 172,457)	107,282 (−11,052 to 289,261)	42.05 (−3.89 to 114.92)	51.25 (−5.32 to 138.21)	0.64 (0.63 to 0.66)
Eastern Europe	120,262 (−11,249 to 330,991)	189,332 (−19,437 to 497,720)	42.78 (−3.96 to 118.19)	54.95 (−5.69 to 144.57)	0.81 (0.80 to 0.82)
North Africa and Middle East	72,033 (−6,989 to 198,284)	296,603 (−34,260 to 774,588)	40.23 (−3.83 to 111.53)	59.76 (−6.78 to 155.92)	1.29 (1.27 to 1.31)
Australasia	13,064 (−1,251 to 35,716)	39,024 (−3,963 to 105,319)	56.54 (−5.43 to 154.09)	79.24 (−8.19 to 213.4)	1.09 (1.07 to 1.11)
Western Europe	282,128 (−25,877 to 786,738)	525,195 (−51,633 to 1,415,590)	50.71 (−4.69 to 140.96)	62.95 (−6.27 to 168.56)	0.70 (0.68 to 0.71)
Andean Latin America	9,894 (−919 to 27,078)	39,752 (−4,230 to 105,663)	46.29 (−4.26 to 127.24)	65.71 (−6.95 to 175.47)	1.13 (1.12 to 1.15)
Caribbean	11,258 (−979 to 31,879)	32,229 (−3,204 to 86,895)	42.82 (−3.72 to 121.23)	59.71 (−5.93 to 160.98)	1.08 (1.07 to 1.09)
High-income North America	223,661 (−22,013 to 599,743)	501,347 (−55,304 to 1,308,805)	67.01 (−6.64 to 178.76)	82.03 (−9.14 to 215.01)	0.69 (0.56 to 0.82)
Western Sub-Saharan Africa	25,536 (−2,047 to 75,156)	92,011 (−8,076 to 256,559)	27.47 (−2.18 to 81.74)	42.2 (−3.6 to 119.63)	1.40 (1.38 to 1.41)
South Asia	84,240 (−6,104 to 248,489)	439,406 (−35,033 to 1,289,376)	13.18 (−0.94 to 39.29)	27.81 (−2.2 to 81.78)	2.09 (2.06 to 2.12)
Oceania	1,315 (−123 to 3,652)	4,314 (−450 to 11,533)	38.94 (−3.57 to 109.06)	48.86 (−4.96 to 132.98)	0.74 (0.71 to 0.76)
Central Sub-Saharan Africa	4,802 (−338 to 14,210)	21,121 (−1,649 to 62,061)	19.6 (−1.37 to 58.77)	34.18 (−2.59 to 101.87)	1.81 (1.80 to 1.82)
Central Latin America	44,279 (−4,270 to 121,093)	174,201 (−18,966 to 458,371)	50.85 (−4.85 to 139.84)	67.69 (−7.32 to 178.75)	0.93 (0.91 to 0.95)
Southern Latin America	26,720 (−2,620 to 71,379)	64,938 (−7,109 to 167,297)	57.23 (−5.61 to 153.03)	76.31 (−8.39 to 196.56)	0.93 (0.92 to 0.95)
Tropical Latin America	43,719 (−3,905 to 120,749)	165,101 (−16,733 to 441,786)	45.65 (−4.02 to 126.66)	62.95 (−6.35 to 168.57)	1.04 (1.03 to 1.05)
Eastern Sub-Saharan Africa	14,444 (−1,066 to 43,729)	54,047 (−4,256 to 157,360)	17.9 (−1.31 to 54.97)	28.76 (−2.22 to 84.57)	1.55 (1.53 to 1.57)
Southern Sub-Saharan Africa	12,079 (−1,083 to 33,236)	36,137 (−3,684 to 95,528)	43.15 (−3.83 to 120.08)	59.34 (−5.99 to 158.72)	1.04 (1.03 to 1.06)

* AAPC, average annual percent change; ASR, age-standardized rate; CI, confidence interval; UI, uncertainty interval.

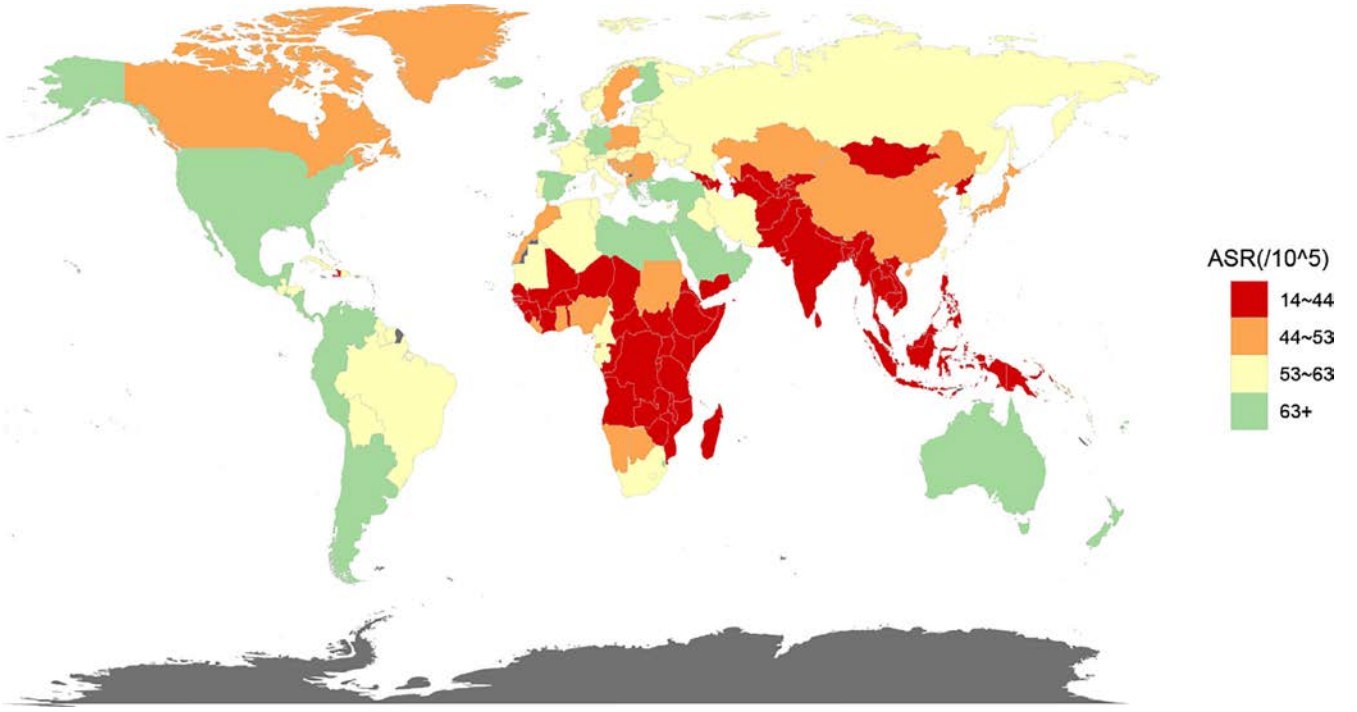

Figure 1. The geographic distribution of the ASR of osteoarthritis years lived with disability attributable to high body mass index in 2021 across 204 countries and territories. ASR, age-standardized rate.

Africa had higher-than-expected burdens only in the later years of the measurement period.

Figure 4B illustrates the relationship between the ASR of OA YLDs attributable to high BMI and the SDI for each country and territory in 2021. Across countries, the ASR of OA YLDs attributable to high BMI increases with the SDI until it levels off at an SDI of approximately 0.56 to 0.67, then rises again until the SDI exceeds 0.8, after which it begins to decrease. Based on the SDI alone, the ASR of OA YLDs attributable to high BMI was significantly higher than expected in the United States, Cook Islands, American Samoa, and Tonga.

DISCUSSION

This study provides a comprehensive analysis of the global burden and trends of OA attributable to high BMI from 1990 to 2021 using the GBD 2021 data. Our findings indicate a consistent global increase in both the ASR and the number of YLDs owing to OA linked to high BMI. The ASR rose by 48.9% over the 32-year period, with the burden peaking around age 75 years and being consistently higher in women than in men. Both the ASR and number of OA YLDs attributable to high BMI were positively correlated with SDI levels. For context, the global ASR of total OA YLDs increased by only 9.7% during the same period,[20] suggesting that high BMI is contributing disproportionately to the rising OA burden and playing an increasingly important role beyond general demographic or epidemiologic changes.

The GBD models suggest that regions such as high-income North America, Australasia, and southern Latin America had the highest ASRs in 2021, whereas South Asia, Southeast Asia, and eastern Sub-Saharan Africa had the lowest. These patterns align with global obesity prevalence data and reflect the influence of demographic and lifestyle transitions (https://data.who.int/indicators/i/C6262EC/BEFA58B). However, it is important to note that in some countries, such as the Cook Islands and Tonga, OA was not directly assessed but estimated based on population-level BMI data and modeled relationships. This highlights the need to interpret the findings in the context of data availability and modeling assumptions.

The observed increase in OA burden is likely driven by population aging and rising obesity rates, particularly in high-SDI countries.[21,22] The most significant rise in the ASR of OA YLDs attributable to high BMI occurred between 2006 and 2009, likely reflecting the global obesity epidemic. The higher burden of OA in women is consistent with previous studies[15,23,24] and may be influenced by biologic, hormonal, and biomechanical factors.[25–27] 27 Previous studies have found that the global prevalence of overweight and obesity is significantly higher in older women than in older men.[18,28] This suggests that women are a subgroup requiring more attention and treatment.

The joinpoint regression analysis revealed a notable acceleration in the ASR of OA YLDs attributable to high BMI growth between 2006 and 2009, possibly reflecting the compounding effects of these demographic and lifestyle shifts. Interestingly, a temporary decline in high-income North

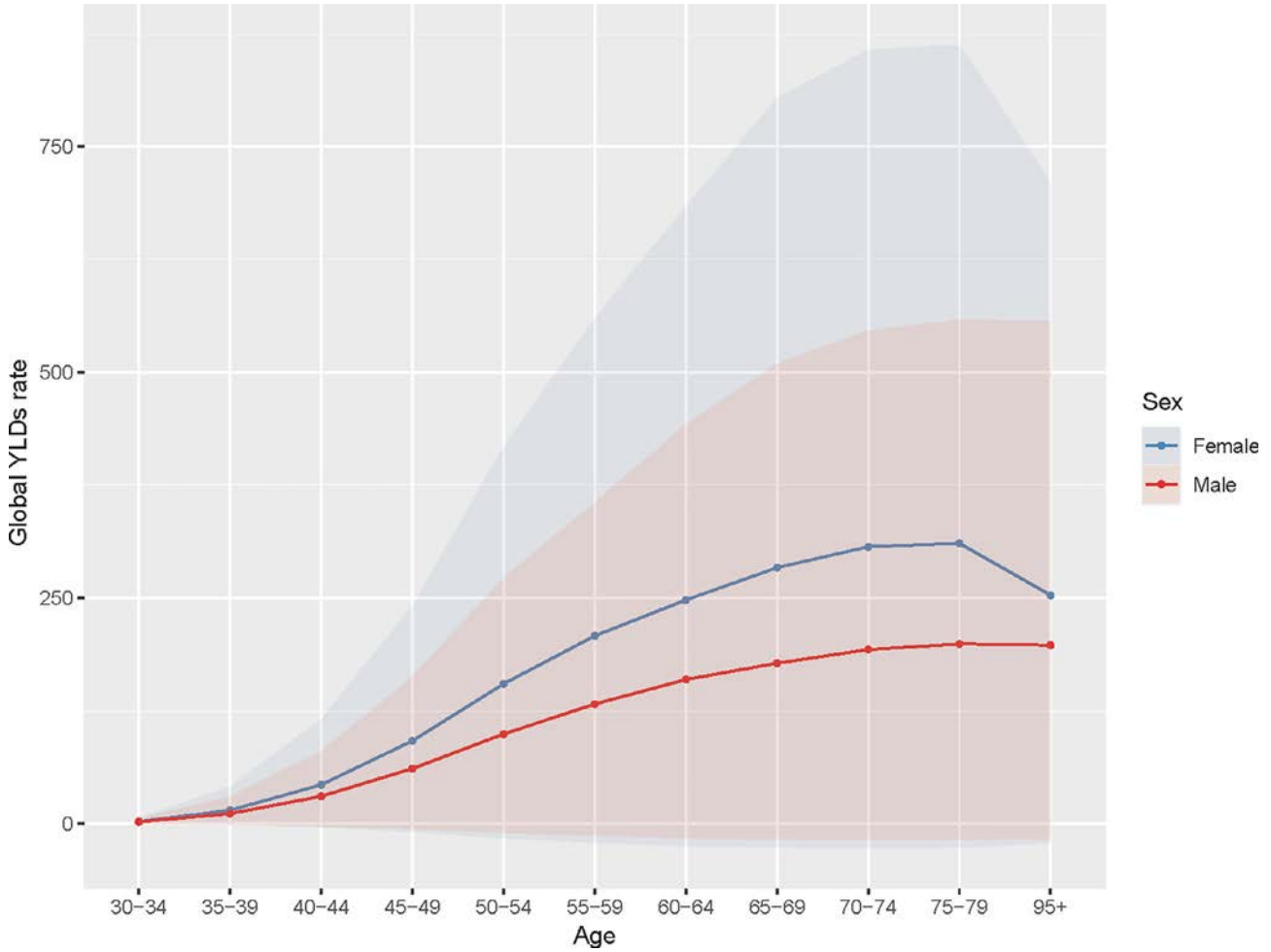

Figure 2. The age-standardized rates of osteoarthritis YLDs attributable to high body mass index by age and sex globally in 2021. YLD, year lived with disability. Color figure can be viewed in the online issue, which is available at http://onlinelibrary.wiley.com/doi/10.1002/art.43241/abstract.

America between 2000 and 2005 may reflect the impact of public health initiatives and updated clinical guidelines during that period.[29]

We found a positive correlation between the burden of OA attributable to high BMI and the level of the SDI. The disproportionate burden of OA in high-SDI countries can be attributed to

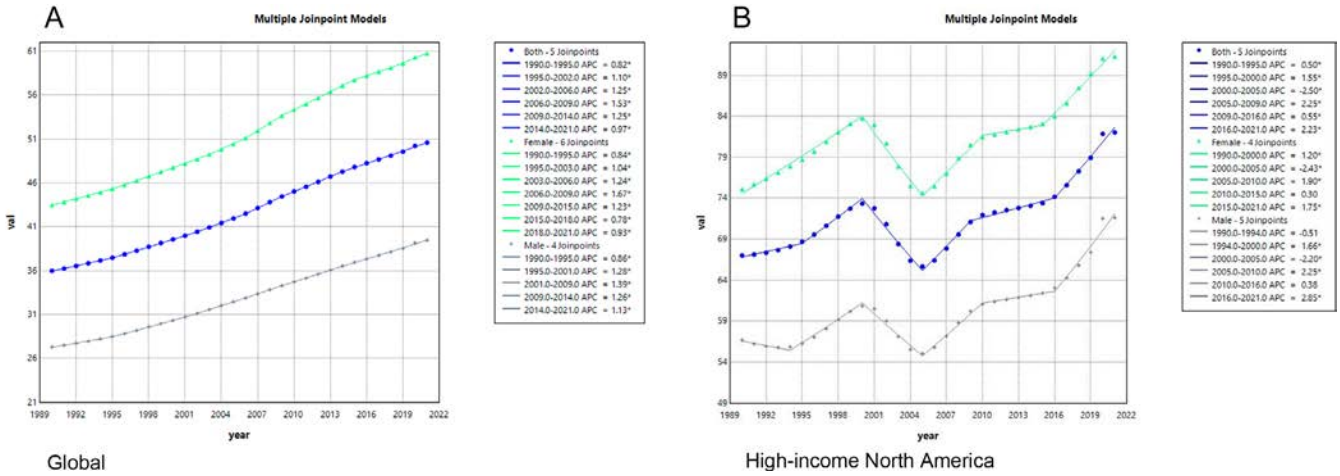

Figure 3. Joinpoint regression analysis of the age-standardized rates of osteoarthritis years live with disability attributable to high body mass index, (A) globally and in (B) high-income North America, from 1990 to 2021. Solid lines indicate model-fitted trends; joinpoints represent statistically significant changes in slope over time. *The APC is significantly different from zero at the α = 0.05 level. APC, annual percentage change. Color figure can be viewed in the online issue, which is available at http://onlinelibrary.wiley.com/doi/10.1002/art.43241/abstract.

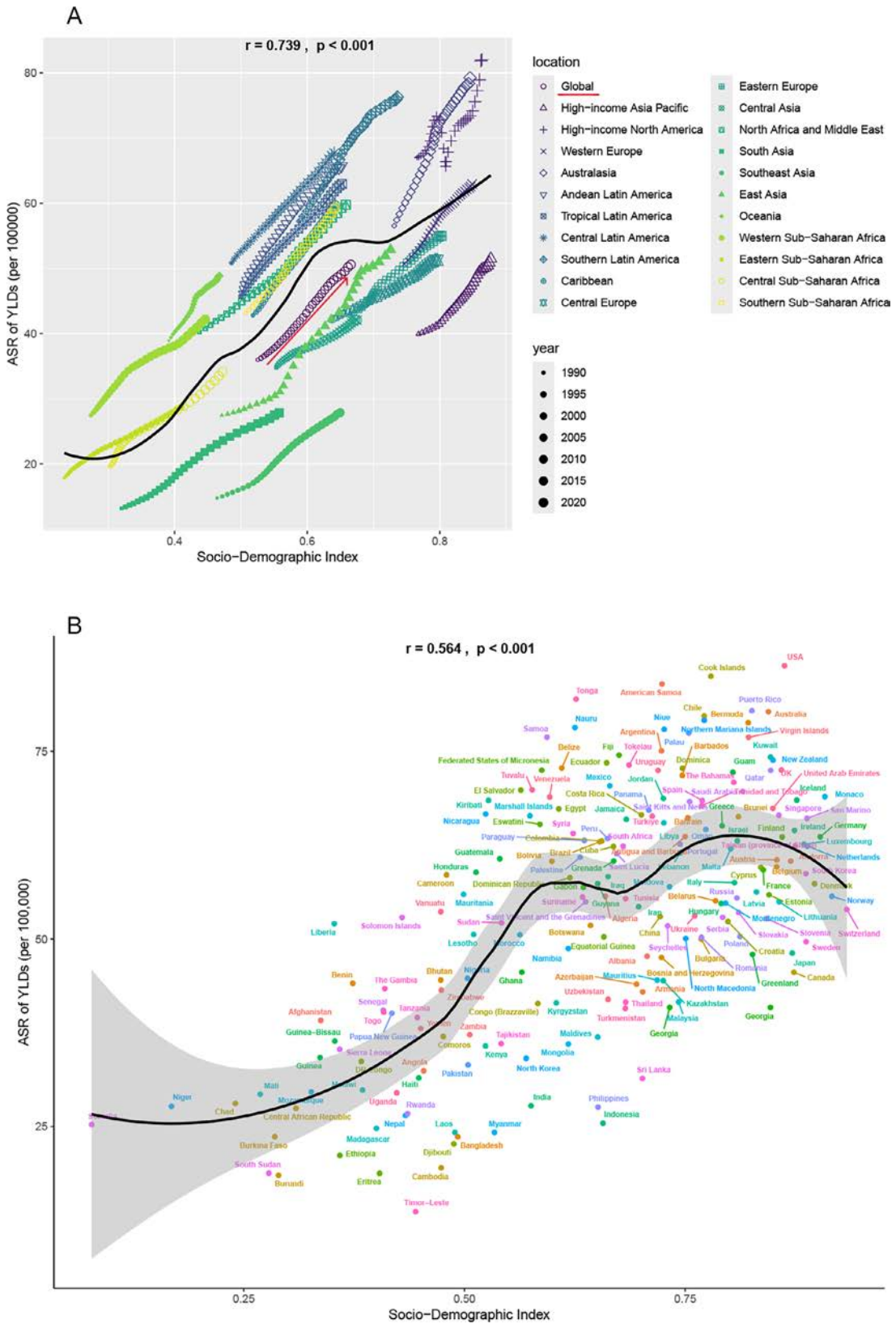

Figure 4. (A) ASR of YLDs for osteoarthritis attributable to high body mass index by the Sociodemographic Index (2021), both globally and across 21 Global Burden of Disease regions, from 1990 to 2021. For each region, 32 points are plotted, representing the observed ASR of YLDs for each year from 1990 to 2021. Points above the solid line indicate a higher-than-expected burden, and those below the line indicate a lower-than-expected burden. Global data are marked with a red line. (B) ASR of YLDs for osteoarthritis attributable to high body mass index by different Sociodemographic Index levels across 204 countries and territories in 2021. ASR, age-standardized rate; YLD, year lived with disability. Color figure can be viewed in the online issue, which is available at http://onlinelibrary.wiley.com/doi/10.1002/art.43241/abstract.

two main factors. Firstly, these countries often face population aging and obesity epidemics, which are significant risk factors for OA. Secondly, in developed countries, there is still no cure for OA, resulting in elevated prevalence among populations. However, diagnostic bias and data limitations in low-SDI countries may lead to underestimation of the true burden.

BMI is a convenient indicator of overall weight and obesity levels. Findings from 32 prospective observational studies have demonstrated an association between high BMI and 20 health outcomes, including OA.[28] In Asian populations, the health risks associated with BMI may occur at lower thresholds than in Western populations. Evidence suggests that individuals with a BMI below 25 kg/m^2 may still face elevated risks of OA, particularly when abdominal obesity is present.[30,31] This highlights the limitations of BMI as a sole indicator of obesity-related health risks and supports the use of additional measures, such as waist circumference, in future research and public health strategies.

This study has several limitations. First, the GBD database only includes high BMI as a risk factor for OA, limiting our ability to assess the relative contribution of other factors. Second, although the GBD database is continually updated and expanded, it does not encompass data from every country and region worldwide. Third, the estimates are based on modeled data, which may be affected by the quality and availability of local health information. Fourth, the GBD study did not provide data on the prevalence of high BMI, so we were unable to include this information in our analyses.

In conclusion, the GBD models suggest that OA attributable to high BMI is a growing global health concern, particularly in high-SDI countries and among women and older adults. The consistent rise in ASR of OA YLDs attributable to high BMI highlights the urgent need for effective, population-level strategies to prevent and manage obesity as a means of reducing OA-related disability worldwide.

AUTHOR CONTRIBUTIONS

All authors contributed to at least one of the following manuscript preparation roles: conceptualization AND/OR methodology, software, investigation, formal analysis, data curation, visualization, and validation AND drafting or reviewing/editing the final draft. As corresponding author, Mr Lu confirms that all authors have provided the final approval of the version to be published and takes responsibility for the affirmations regarding article submission (eg, not under consideration by another journal), the integrity of the data presented, and the statements regarding compliance with institutional review board/Declaration of Helsinki requirements.

REFERENCES

1. Katz JN, Arant KR, Loeser RF. Diagnosis and treatment of hip and knee osteoarthritis: a review. JAMA 2021;325(6):568–578.
2. Dieleman JL, Baral R, Birger M, et al. US spending on personal health care and public health, 1996-2013. JAMA 2016;316(24):2627–2646.
3. Hunter DJ, Bierma-Zeinstra S. Osteoarthritis. Lancet 2019; 393(10182):1745–1759.
4. Litwic A, Edwards MH, Dennison EM, et al. Epidemiology and burden of osteoarthritis. Br Med Bull 2013;105(1):185–199.
5. Steinmetz JD, Culbreth GT, Haile LM, et al; GBD 2021 Osteoarthritis Collaborators. Global, regional, and national burden of osteoarthritis, 1990-2020 and projections to 2050: a systematic analysis for the Global Burden of Disease Study 2021. Lancet Rheumatol 2023;5(9): e508–e522.
6. Snoeker B, Turkiewicz A, Magnusson K, et al. Risk of knee osteoarthritis after different types of knee injuries in young adults: a population-based cohort study. Br J Sports Med 2020;54(12): 725–730.
7. Zheng H, Chen C. Body mass index and risk of knee osteoarthritis: systematic review and meta-analysis of prospective studies. BMJ Open 2015;5(12):e007568.
8. Poulsen E, Goncalves GH, Bricca A, et al. Knee osteoarthritis risk is increased 4-6 fold after knee injury - a systematic review and meta-analysis. Br J Sports Med 2019;53(23):1454–1463.
9. Schram B, Orr R, Pope R, et al. Risk factors for development of lower limb osteoarthritis in physically demanding occupations: a narrative umbrella review. J Occup Health 2020;62(1):e12103.
10. Alentorn-Geli E, Samuelsson K, Musahl V, et al. The association of recreational and competitive running with hip and knee osteoarthritis: a systematic review and meta-analysis. J Orthop Sports Phys Ther 2017;47(6):373–390.
11. Roos H, Laurén M, Adalberth T, et al. Knee osteoarthritis after meniscectomy: prevalence of radiographic changes after twenty-one years, compared with matched controls. Arthritis Rheum 1998;41(4): 687–693.
12. Vina ER, Kwoh CK. Epidemiology of osteoarthritis: literature update. Curr Opin Rheumatol 2018;30(2):160–167.
13. Zhou XD, Chen QF, Yang W, et al. Burden of disease attributable to high body mass index: an analysis of data from the Global Burden of Disease Study 2021. EClinicalMedicine 2024;76:102848.
14. O'Neill TW, McCabe PS, McBeth J. Update on the epidemiology, risk factors and disease outcomes of osteoarthritis. Best Pract Res Clin Rheumatol 2018;32(2):312–326.
15. Zhao G, Zhu S, Zhang F, et al. Global burden of osteoarthritis associated with high body mass index in 204 countries and territories, 1990-2019: findings from the Global Burden of Disease Study 2019. Endocrine 2023;79(1):60–71.
16. Yang S, Zhou L, Gong W, et al. Global burden of osteoarthritis from 1990 to 2019 attributable to high body mass index. Arch Med Sci 2024;20(6):1841–1853.
17. Ferrari AJ, Santomauro DF, Aali A, et al; GBD 2021 Diseases and Injuries Collaborators. Global incidence, prevalence, years lived with disability (YLDs), disability-adjusted life-years (DALYs), and healthy life expectancy (HALE) for 371 diseases and injuries in 204 countries and territories and 811 subnational locations, 1990-2021: a systematic analysis for the Global Burden of Disease Study 2021. Lancet 2024;403(10440):2133–2161.
18. Ng M, Fleming T, Robinson M, et al. Global, regional, and national prevalence of overweight and obesity in children and adults during 1980-2013: a systematic analysis for the Global Burden of Disease Study 2013. Lancet 2014;384(9945):766–781.
19. Stanaway JD, Afshin A, Gakidou E, et al; GBD 2017 Risk Factor Collaborators. Global, regional, and national comparative risk assessment of 84 behavioural, environmental and occupational, and metabolic risks or clusters of risks for 195 countries and territories, 1990-2017: a systematic analysis for the Global Burden of Disease Study 2017. Lancet 2018;392(10159):1923–1994.

20. Wu R, Guo Y, Chen Y, et al. Osteoarthritis burden and inequality from 1990 to 2021: a systematic analysis for the Global Burden of Disease study 2021. Sci Rep 2025;15(1):8305.
21. Hoveidaei AH, Nakhostin-Ansari A, Hosseini-Asl SH, et al. Increasing burden of hip osteoarthritis in the Middle East and North Africa (MENA): an epidemiological analysis from 1990 to 2019. Arch Orthop Trauma Surg 2023;143(6):3563–3573.
22. Zhakhina G, Gusmanov A, Sakko Y, et al. The regional burden and disability-adjusted life years of knee osteoarthritis in Kazakhstan 2014-2020. Biomedicines 2023;11(1):216.
23. Cao F, Xu Z, Li XX, et al. Trends and cross-country inequalities in the global burden of osteoarthritis, 1990-2019: a population-based study. Ageing Res Rev 2024;99:102382.
24. Li H, Kong W, Liang Y, et al. Burden of osteoarthritis in China, 1990-2019: findings from the Global Burden of Disease Study 2019. Clin Rheumatol 2024;43(3):1189–1197.
25. Lovejoy JC. The influence of sex hormones on obesity across the female life span. J Womens Health 1998;7(10):1247–1256.
26. Geusens PP, van den Bergh JP. Osteoporosis and osteoarthritis: shared mechanisms and epidemiology. Curr Opin Rheumatol 2016; 28(2):97–103.
27. Hussain SM, Cicuttini FM, Alyousef B, Wang Y. Female hormonal factors and osteoarthritis of the knee, hip and hand: a narrative review. Climacteric 2018;21(2):132–139.
28. Afshin A, Forouzanfar MH, Reitsma MB, et al; GBD 2015 Obesity Collaborators. Health effects of overweight and obesity in 195 countries over 25 years. N Engl J Med 2017;377(1):13–27.
29. American College of Rheumatology Subcommittee on Osteoarthritis Guidelines. Recommendations for the medical management of osteoarthritis of the hip and knee: 2000 update. Arthritis Rheum 2000;43(9): 1905–1915.
30. Lyu L, Cai Y, Xiao M, et al. Causal relationships of general and abdominal adiposity on osteoarthritis: a two-sample mendelian randomization study. J Clin Med 2022;12(1):320.
31. Elmaleh-Sachs A, Schwartz JL, Bramante CT, et al. Obesity management in adults: a review. JAMA 2023;330(20):2000–2015.

American College of Rheumatology
Empowering Rheumatology Professionals

Arthritis & Rheumatology
Vol. 77, No. 11, November 2025, pp 1512–1523
DOI 10.1002/art.43238

Efficacy and Safety of Ivarmacitinib, a Selective JAK1 Inhibitor, in Patients With Active Ankylosing Spondylitis: Results From an Adaptive Seamless Phase 2/3 Trial

Xu Liu,[1] Liling Xu,[1] Cheng Zhao,[2] Shengyun Liu,[3] Lingyun Sun,[4] Lei Yang,[5] Xiaoyan Xu,[6] Rui Wu,[7] Xiumei Liu,[8] Jing Zhang,[9] Shengqian Xu,[10] Ping Zhu,[11] Haiying Chen,[12] Xiaoxia Wang,[13] Changsong Lin,[14] Jin Lin,[15] Feng Zhan,[16] Hua Wei,[17] Qingchun Huang,[18] Huaxiang Liu,[19] Xinmei Ma,[20] Guixiu Shi,[21] Yuewu Lu,[22] Xiuqin Geng,[23] Zhenyu Jiang,[24] Ning Zhang,[25] Kaijiang Tang,[26] Ronghua Zhang,[27] Yi Zhao,[28] Luan Xue,[29] Shulin Song,[30] Xiaofei Shi,[31] Zhiyi Zhang,[32] Pan Liu,[33] Hui Wang,[33] and Zhanguo Li[1]

Objective. This randomized, double-blind, adaptive phase 2/3 trial aimed to evaluate the efficacy and safety of ivarmacitinib, a novel selective JAK1 inhibitor, in patients with active ankylosing spondylitis (AS).

Methods. In phase 2, patients were randomized (1:1:1:1) to receive ivarmacitinib at a dose of 2, 4, or 8 mg or placebo once daily for 12 weeks. Based on interim analysis, ivarmacitinib 4 mg was selected as the recommended dose. In phase 3, patients were randomized (1:1) to receive ivarmacitinib 4 mg or placebo for 12 weeks; from week 12 onward, all patients received ivarmacitinib 4 mg once daily through week 24. The primary end point was the proportion of patients achieving a ≥20% improvement in the Assessment of SpondyloArthritis international Society (ASAS20) response criteria at week 12.

Results. During the entire study, 504 patients were randomized (ivarmacitinib 4 mg, n = 187; placebo, n = 186). At week 12, the ASAS20 response rate was significantly higher in the ivarmacitinib 4 mg group compared to the placebo group (48.7% vs 29.0%; one-sided $P = 0.0001$). The ASAS40 response rate (32.1% vs 18.3%) and all other secondary end points also favored ivarmacitinib 4 mg. Efficacy was sustained through 24 weeks. During the placebo-controlled period, treatment-emergent adverse events occurred in 79.7% of the ivarmacitinib group and 65.6% of the placebo group.

Conclusion. Ivarmacitinib 4 mg significantly improved the signs and symptoms of AS at week 12 compared to placebo, with sustained efficacy through 24 weeks and a tolerable safety profile. These findings support ivarmacitinib 4 mg as a new treatment option for active AS.

ClinicalTrials.gov identifier: NCT04481139.
Supported by Jiangsu Hengrui Pharmaceuticals Co, Ltd.
[1]Xu Liu, MD, Liling Xu, MD, Zhanguo Li, MD: Department of Rheumatology and Immunology, Peking University People's Hospital, Beijing, China; [2]Cheng Zhao, MD: Department of Rheumatology and Immunology, The First Affiliated Hospital of Guangxi Medical University, Nanning, China; [3]Shengyun Liu, MD: Department of Rheumatology and Immunology, The First Affiliated Hospital of Zhengzhou University, Zhengzhou, China; [4]Lingyun Sun, MD: Department of Rheumatology and Immunology, Nanjing Drum Tower Hospital, Nanjing, China; [5]Lei Yang, MM: Department of Rheumatology and Immunology, Zhengzhou Central Hospital, Zhengzhou, China; [6]Xiaoyan Xu, PhD: Department of Rheumatology and Immunology, Zhongda Hospital Southeast University, Nanjing, China; [7]Rui Wu, MD: Department of Rheumatology and Immunology, The First Affiliated Hospital of Nanchang University, Nanchang, China; [8]Xiumei Liu, MD: Department of Rheumatology and Immunology, First Hospital of Shanxi Medical University, Taiyuan, China; [9]Jing Zhang, MD: Department of Rheumatology and Immunology, Sichuan Provincial People's Hospital, Chengdu, China; [10]Shengqian Xu, PhD: Department of Rheumatology and Immunology, The First Affiliated Hospital of Anhui Medical University, Hefei, China; [11]Ping Zhu, PhD: Department of Clinical Immunology, The First Affiliated Hospital of Air Force Military Medical University, Xi'an, China; [12]Haiying Chen, MD: Department of Rheumatology and Immunology, The Third Hospital of Hebei Medical University, Shijiazhuang, China; [13]Xiaoxia Wang, MD: Department of Rheumatology and Immunology, The Second Hospital of Shanxi Medical University, Taiyuan, China; [14]Changsong Lin, MD: Department of Rheumatology and Immunology, The First Affiliated Hospital of Guangzhou University of Chinese Medicine, Guangzhou, China; [15]Jin Lin, MD: Department of Rheumatology and Immunology, The First Affiliated Hospital, Zhejiang University School of Medicine, Hangzhou, China; [16]Feng Zhan, MD: Department of Rheumatology and Immunology, Hainan Provincial People's Hospital, Haikou, China; [17]Hua Wei, PhD: Department of Rheumatology and Immunology, North Jiangsu People's Hospital, Yangzhou, China; [18]Qingchun Huang, PhD: Department of Rheumatology and Immunology, Guangdong Provincial Hospital of Chinese Medicine, Guangzhou, China; [19]Huaxiang Liu, MD: Internal Medicine - Immunology, Qilu Hospital of Shandong University, Jinan, China; [20]Xinmei Ma, MM: Department of Rheumatology and Immunology, Zaozhuang Municipal Hospital, Zaozhuang, China; [21]Guixiu Shi, PhD: Department of Rheumatology and Immunology, The First Affiliated Hospital of Xiamen University, Xiamen, China; [22]Yuewu Lu, MD: Department of Rheumatology and Immunology, Beijing Chao-Yang Hospital, Capital Medical University, Beijing, China; [23]Xiuqin Geng, MD: Department of Rheumatology

INTRODUCTION

Axial spondyloarthritis (axSpA) is a chronic, progressive inflammatory disease characterized by inflammatory back pain, reduced spinal mobility, enthesitis, and various peripheral and extra-articular manifestations.[1–3] It is classified into two forms: ankylosing spondylitis (AS; also known as radiographic axSpA), which is defined by radiographic evidence of sacroiliitis, and nonradiographic axSpA, which has similar clinical features but does not meet the radiographic criteria for definitive sacroiliitis (bilateral grade ≥2 or unilateral grade ≥3).[1,4,5] Given its potential for irreversible structural damage and substantial impact on quality of life, long-term pharmacologic management is essential for disease control.[6]

Current treatment guidelines from the Assessment of SpondyloArthritis international Society (ASAS), the EULAR, the American College of Rheumatology, the Spondylitis Association of America, and the Spondyloarthritis Research and Treatment Network recommend nonsteroidal anti-inflammatory drugs (NSAIDs) as the first-line treatment for AS.[6–8] For patients with inadequate responses to NSAIDs, biologic disease-modifying antirheumatic drugs (bDMARDs), primarily tumor necrosis factor inhibitors (TNFi) and interleukin-17 (IL-17) inhibitors, are equally recommended, except for patients with concomitant inflammatory bowel disease (IBD), in whom monoclonal antibodies to TNF are preferred.[1,7–11] Although TNFi and IL-17 inhibitors have improved outcomes, many patients fail to achieve sustained disease control despite these treatments.[12,13] This unmet need has driven the development of alternative therapeutic options, particularly oral therapies that offer greater convenience and adherence benefits.

JAK inhibitors have emerged as a promising oral treatment for AS by targeting inflammatory pathways. The US Food and Drug Administration, the European Medicines Agency, and Chinese regulatory authorities have approved two oral JAK inhibitors, tofacitinib and upadacitinib, for use in active AS.[14–17] Tofacitinib is a pan-JAK inhibitor primarily targeting JAK1 and JAK3, with lesser effects on JAK2 and minimal inhibition[18] of TYK2. Upadacitinib, a more selective JAK1 inhibitor, demonstrates greater specificity[17] for JAK1 over JAK3 and TYK2.

Ivarmacitinib (formerly SHR0302) is a highly selective JAK1 inhibitor with more than tenfold greater specificity for JAK1 compared to JAK2 and even higher selectivity over[19] JAK3 and TYK2. It is under development for several autoimmune conditions, including rheumatoid arthritis, AS, psoriatic arthritis, and ulcerative colitis. A phase 2 clinical trial (ClinicalTrials.gov identifier NCT03254966) demonstrated that ivarmacitinib at 4 or 8 mg once daily was well tolerated and provided rapid symptom improvement in patients with moderate to severe rheumatoid arthritis.[20] This adaptive seamless phase 2/3 trial evaluated the efficacy and safety of ivarmacitinib at a 4 mg daily dose, the recommended phase 3 dose identified by the Independent Data Monitoring Committee (IDMC), compared to placebo in patients with active AS. Here, we present the overall study findings, with a focus on outcomes at the recommended dose.

PATIENTS AND METHODS

Study design. This randomized, double-blind, placebo-controlled, adaptive seamless phase 2/3 trial (ClinicalTrials.gov identifier NCT04481139, registered July 21, 2020) was conducted at 51 sites in China. Both phase 2 (stage 1) and phase 3 (stage 2) included a 4-week screening, a 12-week core treatment, a 12-week extension, and a 4-week safety follow-up period (Supplementary Figure 1). During stage 1, three dosing regimens of ivarmacitinib (2, 4, and 8 mg) were evaluated to determine the optimal dose for clinical development in AS. In stage 2, the efficacy and safety of ivarmacitinib at the recommended dose were further assessed. An IDMC selected the optimal regimen based on an interim analysis conducted after all stage 1 patients completed the core treatment period.

The study was conducted in accordance with the ethical principles of the Declaration of Helsinki, the International Council for Harmonization guidelines, and applicable local regulations. The trial protocol and all amendments were approved by an institutional review board or independent ethics committee at each study site. All patients provided written consent before enrollment.

Patients. Eligible patients aged 18 to 75 years with a body mass index ≥18 had to meet the modified New York criteria for AS,[29] confirmed by radiographic evaluation of the sacroiliac joints. Active disease was defined by a Bath Ankylosing Spondylitis Disease Activity Index (BASDAI) score ≥4 and a back pain score ≥40 mm on a 0 to 100 mm visual analog scale at both screening

and Immunology, Xinxiang Central Hospital, Xinxiang, China; [24]Zhenyu Jiang, MD: Department of Rheumatology and Immunology, The First Hospital of Jilin University, Changchun, China; [25]Ning Zhang, PhD: Department of Rheumatology and Immunology, ShengJing Hospital of China Medical University, Shenyang, China; [26]Kaijiang Tang, MD: Department of Rheumatology and Immunology, Liuzhou Workers' Hospital, Liuzhou, China; [27]Ronghua Zhang, MD: Department of Traditional Chinese Medicine and Rheumatology, First Affiliated Hospital, Army Medical University (Third Military Medical University), Chongqing, China; [28]Yi Zhao, MD: Department of Rheumatology, Immunology and Allergology, Xuanwu Hospital, Capital Medical University, Beijing, China; [29]Luan Xue, PhD: Rheumatism Department, Shanghai Yueyang Integrated Traditional Chinese and Western Medicine Hospital, Shanghai, China; [30]Shulin Song, MD: Department of Rheumatology and Immunology, Xiling Campus of Yichang Central People's Hospital, Yichang, China; [31]Xiaofei Shi, MD: Department of Rheumatology and Immunology, The First Affiliated Hospital and College of Clinical Medicine of Henan University of Science and Technology, Luoyang, China; [32]Zhiyi Zhang, MD: Department of Rheumatology and Immunology, The First Affiliated Hospital of Harbin Medical University, Harbin, China; [33]Pan Liu, MS, Hui Wang, MM: Clinical Research and Development, Jiangsu Hengrui Pharmaceuticals Co, Ltd, Shanghai, China.

Xu Liu and Liling Xu contributed equally to this work.

Additional supplementary information cited in this article can be found online in the Supporting Information section (https://acrjournals.onlinelibrary.wiley.com/doi/10.1002/art.43238).

Author disclosures are available at https://onlinelibrary.wiley.com/doi/10.1002/art.43238.

Address correspondence via email to Zhanguo Li, MD, at li99@bjmu.edu.cn.

Submitted for publication January 3, 2025; accepted in revised form April 24, 2025.

and baseline. Patients were required to have an inadequate response to two or more NSAIDs or a contraindication or intolerance to NSAIDs. Concomitant medications were allowed if administered at a stable dose: NSAIDs or analgesics for ≥14 days prebaseline, conventional synthetic DMARDs (methotrexate, sulfasalazine, or hydroxychloroquine) for ≥3 months (and stable for ≥28 days), or oral glucocorticoids (≤10 mg/day of prednisone or equivalent) for ≥28 days. Key exclusion criteria were total spinal ankylosis; prior exposure to any JAK inhibitor or bDMARD within six months before randomization; a history of inflammatory or autoimmune diseases other than AS; selected laboratory abnormalities; and current or recent clinically significant comorbid conditions, including infections. Additionally, patients who received a BCG vaccination within 12 months before screening or received (or planned to receive) live or attenuated vaccines within 3 months before randomization or during the study were excluded. Complete eligibility criteria are provided in the Supplementary Protocol.

Randomization and procedures. Randomization in both study stages was performed using a centralized interactive response system with block sizes of 8 for the stage 1 core treatment period, 6 for the stage 1 extension period, and 4 for stage 2. Stratification was based on prior use of biologic agents and/or JAK inhibitors for treating AS (yes or no). In stage 1 (phase 2), patients were randomized (1:1:1:1) to receive ivarmacitinib at 2, 4, or 8 mg or placebo once daily for a 12-week core treatment period. After week 12, placebo-assigned patients were rerandomized (1:1:1) to receive ivarmacitinib (2, 4, or 8 mg once daily) during an additional 12-week extension, whereas patients initially taking ivarmacitinib continued their assigned dose until week 24. In stage 2 (phase 3), patients were randomized 1:1 to receive either ivarmacitinib at the recommended dose or placebo once daily for 12 weeks, after which all patients received ivarmacitinib during the extension period. All patients, investigators, study personnel, and outcome assessors remained blinded to treatment assignment until the last patient completed assessment at week 24 in stage 2; at the interim analysis, only the IDMC and the independent statisticians involved in the analysis were unmasked.

End points. In both study stages, the primary end point was the proportion of patients achieving ≥20% improvement in the ASAS (ASAS20) response criteria at week 12. Secondary end points included the proportion of patients achieving ASAS20 response at week 24, ASAS40 response at weeks 12 and 24, and ASAS5/6 response at weeks 12 and 24, alongside changes from baseline in the BASDAI score, the Bath Ankylosing Spondylitis Functional Index (BASFI) score, Bath Ankylosing Spondylitis Metrology Index (BASMI) linear scores, the Short Form-36 (SF-36) physical component summary (PCS) and mental component summary (MCS) scores, and the Ankylosing Spondylitis Quality of Life (ASQoL) score, all assessed at weeks 12 and 24.[30]

Additional efficacy end points assessed changes from baseline at weeks 12 and 24 in the following: C-reactive protein (CRP) level, erythrocyte sedimentation rate (ESR), the Ankylosing Spondylitis Disease Activity Score (ASDAS) based on CRP, total back pain, nocturnal pain, patient global assessment of disease activity (PtGA), physician global assessment of disease activity (PhGA), swollen and tender joint counts in 44 joints (SJC44 and TJC44), the Maastricht Ankylosing Spondylitis Enthesitis Score (MASES), and the Spondyloarthritis Research Consortium of Canada (SPARCC) magnetic resonance imaging (MRI) sacroiliac joint score. Safety outcomes included treatment-emergent adverse events (TEAEs), laboratory test results, vital signs, and 12-lead electrocardiograms monitored from the time of informed consent until 28 days after the last administration of the study treatment.

Statistical analysis. The sample size calculation for the primary end point of the ASAS20 response rate at week 12 was based on the following assumptions: 50% for ivarmacitinib 2 mg, 60% for ivarmacitinib 4 mg, 62% for ivarmacitinib 8 mg, and 40% for placebo. The study design allocated 50% of the total patients to each stage, with a randomization ratio of 1:1:1:1 for ivarmacitinib 2 mg, 4 mg, 8 mg and placebo in stage 1 and a 1:1 ratio for ivarmacitinib at the recommended dose and placebo in stage 2. For the primary end point analysis of the overall study, the *P* values for comparing ivarmacitinib at the recommended dose versus placebo from the two study stages were combined using the inverse normal method.[21] A total of 408 patients for the entire study (stage 1: 51 patients in each ivarmacitinib group and 51 in the placebo group; stage 2: 102 patients in each ivarmacitinib group and 102 in the placebo group) would provide at least 90% power at a one-sided significance level of $\alpha = 0.025$ to detect the superiority of ivarmacitinib at the recommended dose over placebo. Assuming a dropout rate of 15%, the final planned sample size was 480 patients: 60 each in the ivarmacitinib 2 mg, 4 mg, and 8 mg groups and 60 in the placebo group in stage 1 and 120 in the recommended ivarmacitinib dose group and 120 in the placebo group in stage 2.

A prespecified interim analysis was planned after the last patient completed the efficacy assessment at week 12 in stage 1. Under the premise that the IDMC judged the safety profile as acceptable, both the decision on whether to proceed to phase 3 and the recommended dose of ivarmacitinib were based on the efficacy results. If the ASAS20 response rates in all ivarmacitinib groups differed from placebo by <10% in stage 1, the study would be terminated owing to insufficient efficacy. A detailed decision tree is provided in Supplementary Figure 2. The interim analysis was performed on October 19, 2021, and the IDMC recommended the 4 mg dose of ivarmacitinib for stage 2 based on its favorable efficacy and safety profile, which fulfilled all predefined criteria (Supplementary Tables 1–3).

All randomized patients who received at least one dose of the assigned study treatment were included in the full analysis set. Patients who received at least one dose of the study treatment were included in the safety analysis set.

For the primary end point analysis in each stage, the comparison between ivarmacitinib and placebo was performed using a Z-test (based on normal approximation), with between-group differences in ASAS20 response rates and associated 95% confidence intervals (CIs) calculated using normal approximation. For the overall study's primary end point analysis, the final one-sided *P* value was obtained by combining the *P* values from stage 1 and stage 2 using the inverse normal method.[21] In stage 1, the results were adjusted for multiplicity using the Simes method before being combined with stage 2 data to calculate the overall study's primary end point *P* value. A one-sided *P* value ≤0.025 was considered statistically significant. The weighted average was used to calculate the between-group difference in the proportion of patients achieving ASAS20 at week 12, along with a one-sided 97.5% simultaneous CI. Additionally, patients who discontinued treatment early for non–COVID-19 reasons or who increased their background medication before the week 12 efficacy assessment were also analyzed using nonresponder imputation (NRI). A prespecified subgroup analysis of the ASAS20 response at week 12 was conducted using the same method as the primary end point analysis.

For the analysis of all secondary and other efficacy end points in the overall study, pooled data from stage 1 and stage 2 were used. No further multiplicity adjustment was applied to the combined data from both stages. The ASAS40 and ASAS5/6 response rates and other binary end points at week 12 were analyzed using a Z-test (based on normal approximation), with NRI used to address missing data.

Changes from baseline at week 12 in BASDAI, BASFI, BASMI (linear), and ASQoL scores were analyzed using a mixed-effects model for repeated measures with restricted maximum likelihood, which included baseline as a covariate and treatment group, visit, randomization strata, and treatment–visit interaction as fixed effects. Patients were modeled as random effects with an unstructured covariance matrix; if convergence failed, a compound symmetry structure was used. Changes from baseline in SF-36 PCS and MCS scores at week 12 were analyzed using analysis of covariance, with treatment group and randomization strata as independent variables and baseline value as a covariate. Missing data were imputed using the last observation carried forward method.

Adjustments for multiplicity for secondary end points were not performed; all *P* values presented are nominal in nature. Safety data were summarized descriptively. All statistical analyses were performed using SAS version 9.4 or higher. Please refer to the Supplementary Statistical Analysis Plan for additional details.

RESULTS

Patients. A total of 717 patients were screened for eligibility, and 504 were randomized across the two study stages (Supplementary Figure 3). Among these, 373 patients were assigned to either the placebo group (n = 186) or the ivarmacitinib at the recommended dose of 4 mg group (the dose selected for clinical development, n = 187), and all received at least one dose of the study treatment. These patients form the basis of the current analysis. Of the 373 patients, 350 (93.8%) completed the initial 12-week treatment period, and 304 of the 311 patients (97.7%) who either switched from placebo to the ivarmacitinib 4 mg or continued with ivarmacitinib 4 mg after week 12 completed the entire 24-week treatment (Figure 1). During the core treatment period, discontinuations due to TEAEs were higher in the ivarmacitinib 4 mg group (2.7%, n = 5) compared with the placebo group (1.1%, n = 2), whereas discontinuations due to patient decision were more frequent in the placebo group (4.8%, n = 9) than in the ivarmacitinib 4 mg group (1.1%, n = 2).

Baseline characteristics were generally balanced between groups (Table 1). The mean age was 33.8 years, and the mean AS symptom duration was 9.3 years; 259 patients (69.4%) had symptoms for ≥5 years. Among the patients, 297 (79.6%) were male and 327 (87.7%) were HLA–B27 positive. Additionally, 313 patients (83.9%) were receiving concomitant NSAIDs at baseline, and 120 patients (32.2%) had prior exposure to JAK inhibitors and/or bDMARDs. Treatment compliance was high across all treatment groups and remained consistent during both the core and extension treatment periods (Supplementary Table 4).

Efficacy (core treatment period). The study met its primary end point, with significantly more patients achieving an ASAS20 response at week 12 in the ivarmacitinib 4 mg group compared to the placebo group (91 of 187 [48.7%] vs 54 of 186 [29.0%]; one-sided *P* = 0.0001), yielding a treatment difference of 19.6% (one-sided 97.5% CI 8.3–100.0) (Table 2 and Figure 2A). Furthermore, a consistent benefit in ASAS20 response at week 12 was observed with ivarmacitinib 4 mg across baseline subgroups, regardless of age, sex, baseline body mass index, prior exposure to bDMARDs or JAK inhibitors, baseline CRP level, AS symptom duration, or previous TNFi usage (Supplementary Tables 5 and 6). Specifically, among patients with prior bDMARD exposure, the ASAS20 response rate was 41.0% with ivarmacitinib 4 mg versus 22.4% with placebo, and among those without, it was 52.4% versus 32.0%.

The primary end point's clinical benefit was accompanied by improvements in all secondary efficacy end points. At week 12, a higher proportion of patients achieved ASAS40 responses (32.1% vs 18.3%; one-sided nominal *P* = 0.0011) and ASAS5/6 responses (42.8% vs 15.6%; one-sided nominal *P* < 0.0001) with ivarmacitinib 4 mg compared to placebo (Table 2 and Figure 2A). Ivarmacitinib also demonstrated a rapid onset of action, with consistently higher ASAS20, ASAS40, and ASAS5/6 response rates from the first assessment at week 2 through all scheduled visits during the core treatment period (Figure 2B–D). Moreover,

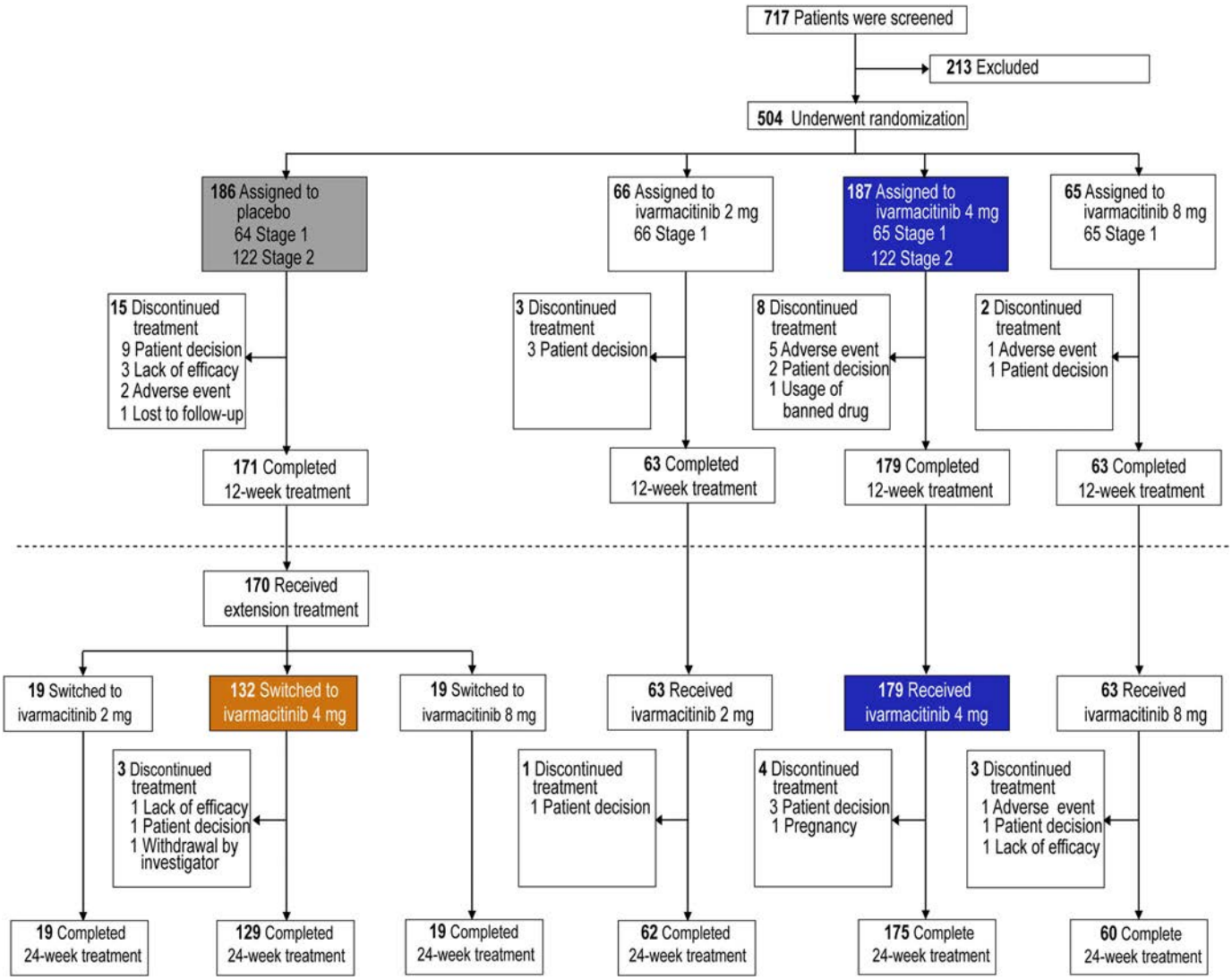

Figure 1. Trial profile for the overall study.

improvements in disease symptoms, physical function, and spinal mobility (as indicated by reductions in BASDAI, BASFI, and BASMI [linear] scores) and gains in quality of life (as measured by ASQoL, SF-36 PCS, and SF-36 MCS scores) were greater with ivarmacitinib 4 mg at week 12 (all one-sided nominal $P < 0.05$; Table 2 and Figure 3A).

At week 12, patients treated with ivarmacitinib 4 mg demonstrated improvements compared to patients receiving placebo in most additional efficacy end points, including changes from baseline in CRP level, ESR, ASDAS based on CRP, back pain, nocturnal pain, PtGA, and PhGA (all one-sided nominal $P < 0.0001$; Supplementary Table 7). A higher proportion of patients achieved ASDAS clinically important improvement (ASDAS-CII, 51.3% vs 18.3%) and ASDAS major improvement (22.5% vs 2.2%) with ivarmacitinib 4 mg compared with placebo (all one-sided nominal $P < 0.0001$). No clinically relevant differences were observed between the ivarmacitinib 4 mg and placebo groups in least squares mean changes from baseline in SJC44, TJC44, or MASES (Supplementary Table 7). At week 12, patients receiving ivarmacitinib 4 mg demonstrated a greater reduction in SPARCC MRI sacroiliac joint scores from baseline compared to those receiving placebo (–7.56 vs –3.34; one-sided nominal $P < 0.0001$; Supplementary Figure 4).

Efficacy (extension treatment period). During the extension period, the ASAS20, ASAS40, and ASAS5/6 response rates continued to improve from week 12 to week 24 in patients receiving continuous ivarmacitinib (Figure 2B–D). At week 24, the response rates were 66.7%, 48.3%, and 59.5%, respectively (Supplementary Table 8). The benefits observed with ivarmacitinib in other efficacy end points at week 12 were also sustained, with further numerical improvements in most of these end points by week 24 (Supplementary Table 8). In patients initially randomized to placebo and switched to ivarmacitinib 4 mg,

Table 1. Demographics and baseline disease characteristics*

	Placebo (n = 186)	Ivarmacitinib 4 mg (n = 187)
Age, y	33.5 ± 10.5	34.1 ± 10.0
Sex		
Female	40 (21.5)	36 (19.3)
Male	146 (78.5)	151 (80.7)
Body mass index	24.1 ± 4.0	24.4 ± 4.3
HLA–B27 positive	161 (86.6)	166 (88.8)
Time of AS symptoms, y	9.2 ± 6.8	9.5 ± 7.0
≥5 y	126 (67.7)	133 (71.1)
<5 y	60 (32.3)	54 (28.9)
Prior exposure to any JAK inhibitor and/or bDMARD	59 (31.7)	61 (32.6)
bDMARD	59 (31.7)	61 (32.6)
JAK inhibitor	2 (1.1)	0
Smoking status		
Never	114 (61.3)	110 (58.8)
Former	7 (3.8)	13 (7.0)
Current	65 (34.9)	64 (34.2)
History of psoriasis	0	0
History of uveitis[a]	5 (2.7)	2 (1.1)
Concomitant NSAID use	158 (84.9)	155 (82.9)
Concomitant csDMARD use	22 (11.8)	21 (11.2)
Sulfasalazine	21 (11.3)	21 (11.2)
Methotrexate	1 (0.5)	1 (0.5)
Concomitant glucocorticoid use	1 (0.5)	0
Back pain[b]	65.6 ± 13.1	66.8 ± 13.7
Nocturnal pain	59.0 ± 18.1	61.9 ± 18.5
Patient global assessment of disease activity	63.9 ± 14.2	65.2 ± 15.2
Physician global assessment of disease activity	59.4 ± 14.3	61.6 ± 14.6
Morning stiffness (inflammation)	60.3 ± 18.1	60.8 ± 17.7
ASDAS based on CRP[c]	3.5 ± 0.7	3.6 ± 0.7
BASDAI	6.4 ± 1.2	6.4 ± 1.2
BASFI	48.7 ± 19.3	48.0 ± 19.9
BASMI (linear)[d]	3.7 ± 1.6	3.8 ± 1.7
MASES[e]	3.0 ± 2.3	2.8 ± 2.0
SPARCC MRI sacroiliac joint score[f]	12.9 ± 17.3	11.8 ± 15.9
SJC44[g]	1.5 ± 0.9	1.7 ± 0.9
TJC44[h]	3.2 ± 3.3	4.0 ± 5.1
CRP, mg/L[i]	11.7 ± 14.7	13.2 ± 15.7
ESR, mm/h	21.4 ± 19.0	25.2 ± 22.3
SF-36 PCS score	37.0 ± 7.0	37.6 ± 6.0
SF-36 MCS score	41.2 ± 11.0	41.2 ± 10.3
ASQoL score	8.6 ± 4.6	9.0 ± 4.1

* Data are presented as n (%) or mean ± SD unless noted otherwise. AS, axial spondyloarthritis; ASDAS, Ankylosing Spondylitis Disease Activity Score; ASQoL, Ankylosing Spondylitis Quality of Life; BASDAI, Bath Ankylosing Spondylitis Disease Activity Index; BASFI, Bath Ankylosing Spondylitis Functional Index; BASMI, Bath Ankylosing Spondylitis Metrology Index; bDMARD, biologic disease-modifying antirheumatic drug; CRP, C-reactive protein; csDMARD, conventional synthetic disease-modifying antirheumatic drug; ESR, erythrocyte sedimentation rate; MASES, Maastricht Ankylosing Spondylitis Enthesis Score; MCS, mental component summary; MRI, magnetic resonance imaging; NSAID, nonsteroidal anti-inflammatory drug; PCS, physical component summary; SF-36, Short Form-36; SJC44, swollen joint count in 44 joints; SPARCC, Spondyloarthritis Research Consortium of Canada; TJC44, tender joint count in 44 joints.

[a] Uveitis is defined as a clustered medical history of iritis, uveitis, and iridocyclitis.

[b] Back pain was defined on a visual analog scale (0–100 mm) based on the question "What was the level of back pain you experienced at any time during the last week?"

[c] ASDAS was assessed in 185 patients in the placebo group and 186 in the ivarmacitinib 4 mg group.

[d] BASMI was assessed in 185 patients in the placebo group and 186 in the ivarmacitinib 4 mg group.

[e] MASES was assessed in 107 patients in the placebo group and 112 in the ivarmacitinib 4 mg group (all with MASES >0 at baseline).

[f] SPARCC MRI sacroiliac joint score involved 162 patients in the placebo group and 164 in the ivarmacitinib 4 mg group.

[g] SJC44 was assessed in 26 patients in the placebo group and 21 in the ivarmacitinib 4 mg group (all with SJC44 >0).

[h] TJC44 was assessed in 73 patients in the placebo group and 69 in the ivarmacitinib 4 mg group (all with TJC44 >0).

[i] CRP was measured in 185 patients in the placebo group and 187 in the ivarmacitinib 4 mg group.

Table 2. Primary end point and secondary efficacy end points at wk 12 in the full analysis set*

End points	Placebo (n = 186)	Ivarmacitinib 4 mg (n = 187)
Primary end point		
ASAS20 response		
n[a]	54	91
Proportion of patients, % (95% CI)[b]	29.0 (22.5 to 35.6)	48.7 (41.5 to 55.8)
Difference vs placebo, % (97.5% CI); *P* value[c]	–	19.6 (8.3 to 100.0); 0.0001
Secondary efficacy end points		
ASAS40 response		
n[a]	34	60
Proportion of patients, % (95% CI)[b]	18.3 (12.7 to 23.8)	32.1 (25.4 to 38.8)
Difference vs placebo, % (95% CI)[b]; *P* value[c]	–	13.8 (5.1 to 22.5); 0.0011
ASAS5/6 response		
n[a]	29	80
Proportion of patients, % (95% CI)[b]	15.6 (10.4 to 20.8)	42.8 (35.7 to 49.9)
Difference vs placebo, % (95% CI)[b]; *P* value[c]	–	27.2 (18.4 to 36.0); <0.0001
BASDAI score		
n[a]	168	178
Change from baseline, LS mean difference (95% CI)	−1.43 (−1.69 to −1.16)	−2.21 (−2.48 to −1.95)
Change vs placebo, LS mean difference (95% CI); *P* value[d]	–	−0.79 (−1.16 to −0.42); <0.0001
BASFI score		
n[a]	169	178
Change from baseline, LS mean difference (95% CI)	−0.79 (−1.03 to −0.55)	−1.33 (−1.57 to −1.09)
Change vs placebo, LS mean difference (95% CI); *P* value[d]	–	−0.54 (−0.87 to −0.21); 0.0007
BASMI score (linear)		
n[a]	155	171
Change from baseline, LS mean difference (95% CI)	−0.29 (−0.37 to −0.20)	−0.40 (−0.48 to −0.32)
Change vs placebo, LS mean difference (95% CI); *P* value[d]	–	−0.11 (−0.23 to 0.00); 0.0289
SF-36 PCS score		
n[a]	186	187
Change from baseline, LS mean difference (95% CI)	3.33 (2.55 to 4.11)	4.43 (3.65 to 5.21)
Change vs placebo, LS mean difference (95% CI); *P* value[e]	–	1.10 (0.03 to 2.16); 0.0217
SF-36 MCS score		
n[a]	186	187
Change from baseline, LS mean difference (95% CI)	0.97 (−0.06 to 1.99)	2.32 (1.30 to 3.34)
Change vs placebo, LS mean difference (95% CI); *P* value[e]	–	1.35 (−0.04 to 2.75); 0.0285
ASQoL score		
n[a]	169	178
Change from baseline, LS mean difference (95% CI)	−2.18 (−2.71 to −1.64)	−3.13 (−3.65 to −2.61)
Change vs placebo, LS mean difference (95% CI); *P* value[d]	–	−0.95 (−1.68 to −0.23); 0.0052

* ASAS20, 20% improvement in the Assessment of SpondyloArthritis international Society response criteria; ASAS40, 40% improvement in the Assessment of SpondyloArthritis international Society response criteria; ASAS5/6, 20% improvement in 5 of 6 domains of the Assessment of SpondyloArthritis international Society response criteria; ASQoL, Ankylosing Spondylitis Quality of Life; BASDAI, Bath Ankylosing Spondylitis Disease Activity Index; BASFI, Bath Ankylosing Spondylitis Functional Index; BASMI, Bath Ankylosing Spondylitis Metrology Index; CI, confidence interval; LS, least squares; MCS, mental component summary; PCS, physical component summary; SF-36, Short Form-36.

[a] The number of patients with observed values at wk 12.

[b] 95% CIs were calculated using the normal approximation method.

[c] For the primary end point and binary secondary end points, the inverse normal method was used to combine *P* values from Z-tests across stage 1 and stage 2, with nonresponder imputation (NRI) applied for missing values. Additionally, for the primary end point, patients who discontinued treatment early because of non–COVID-19 reasons or who increased their background medication before the wk 12 assessment were also analyzed using NRI.

[d] Comparisons for BASDAI, BASFI, BASMI, and ASQoL scores were performed using a mixed-effects model for repeated measures based on the restricted maximum likelihood method, with baseline values as covariates. Treatment group, visit, randomization strata, and the interaction between treatment and visit were treated as fixed effects, with patients as random effects. An unstructured covariance matrix was used (or a compound symmetry structure if convergence issues arose).

[e] Comparisons for SF-36 PCS and MCS scores were performed using analysis of covariance, with the change from baseline as the dependent variable, treatment group and randomization strata as independent variables, baseline as a covariate, and missing data imputed using the last observation carried forward method.

improvements in ASAS response rates and other end points were also observed during the extension period. By week 24, their outcomes were numerically similar to those of patients initially randomized to ivarmacitinib 4 mg (Figure 2B–D, Figure 3B–D, and Supplementary Table 8).

Safety. During the 12-week core treatment period, TEAEs occurred in 79.7% (149 of 187) of patients in the ivarmacitinib 4 mg group compared to 65.6% (122 of 186) in the placebo group. The most frequently reported TEAEs in the ivarmacitinib 4 mg group were hyperuricemia (16.0% [30 of 187] vs 5.9%

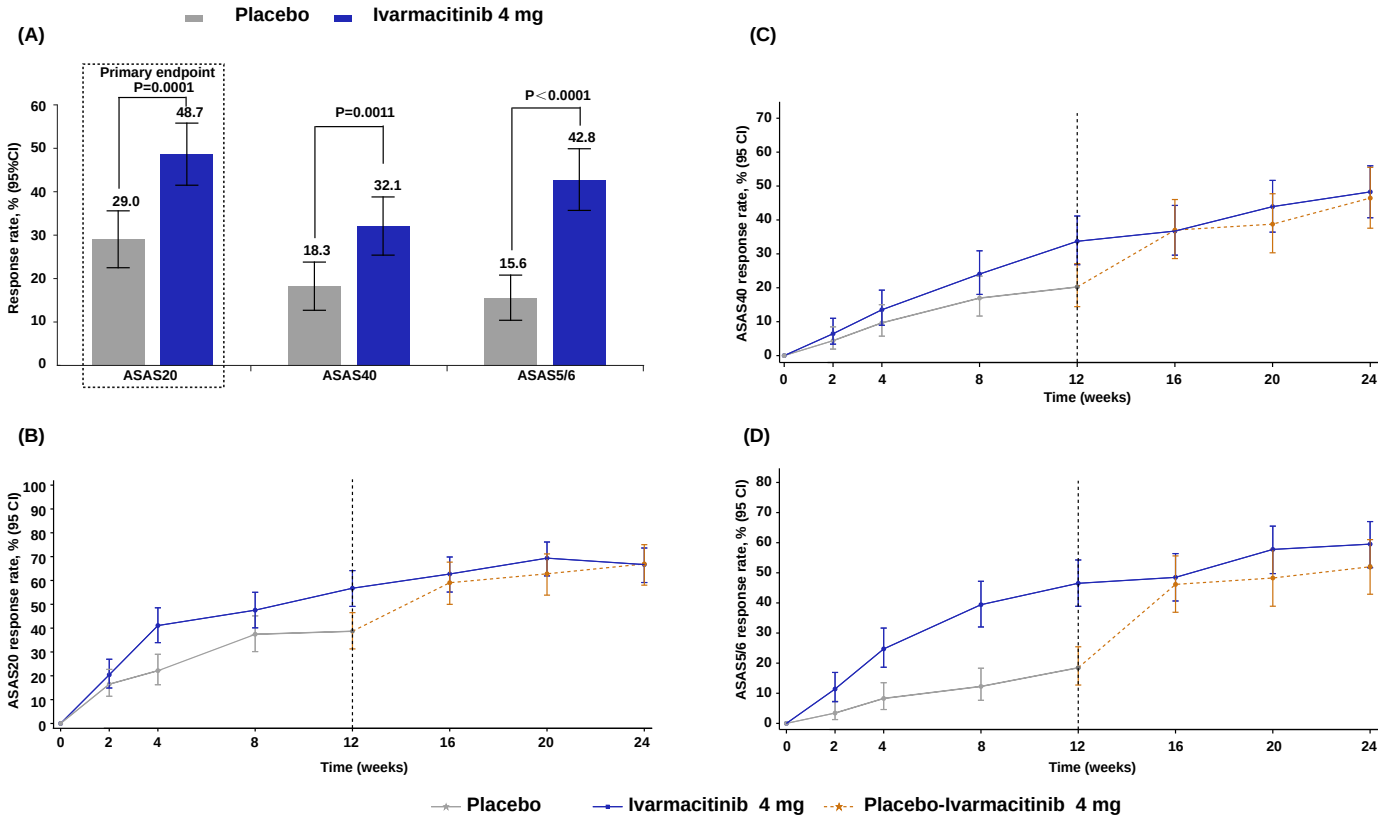

Figure 2. Proportions of patients achieving ASAS20, ASAS40, and ASAS5/6 responses at the scheduled visits. (A) Proportions of patients achieving ASAS20, ASAS40, and ASAS5/6 responses at week 12, using NRI. Additionally, for the primary end point, patients who discontinued treatment early because of non–COVID-19 reasons or who increased their background medication before the week 12 assessment were also analyzed using NRI. (B) Proportions of patients achieving ASAS20 responses over 24 weeks (observed case analysis). (C) Proportions of patients achieving ASAS40 responses over 24 weeks (observed case analysis). (D) Proportions of patients achieving ASAS5/6 responses over 24 weeks (observed case analysis). Data are presented as percentages (95% CI). ASAS20/40, 20%/40% improvement in the Assessment of SpondyloArthritis international Society response criteria; ASAS5/6, 20% improvement in 5 of 6 domains of the ASAS response criteria; CI, confidence interval; NRI, nonresponder imputation.

[11 of 186] receiving placebo) and upper respiratory tract infections (13.4% [25 of 187] vs 12.9% [24 of 186] receiving placebo) (Table 3). Aside from the higher hyperuricemia rate, other TEAE incidences differed by less than 5% between groups. Mean hemoglobin levels were similar, and changes in other laboratory parameters were generally transient and clinically insignificant. Overall, the type, frequency, and severity of TEAEs in patients treated with ivarmacitinib, whether they continued treatment or switched from placebo during the extension period, were consistent with those observed during the initial 12-week period.

During the core treatment period, 2.2% (4 of 186) of patients in the placebo group experienced treatment-emergent serious adverse events (TESAEs): cholelithiasis, spondylolisthesis, cubital tunnel syndrome, and concurrent infective cholangitis, and obstructive pancreatitis (n = 1 for each). In the ivarmacitinib 4 mg group, 1.1% (2 of 187) of patients experienced TESAEs: one with pneumonia and concurrent chest pain and one with increased blood creatine phosphokinase (Supplementary Table 9). During the extension period, 2.3% (3 of 132) of patients in the placebo to ivarmacitinib 4 mg group (vertebrobasilar insufficiency, ureterolithiasis, and benign breast neoplasm; n = 1 for each) reported TESAEs, whereas no TESAEs were reported in the ivarmacitinib 4 mg group (Supplementary Table 10).

During the core treatment period, prespecified TEAEs of special interest occurred in 1.1% (2 of 187) of patients receiving ivarmacitinib 4 mg and 0.5% (1 of 186) of those receiving placebo. In the ivarmacitinib 4 mg group, one patient experienced a systemic opportunistic infection (mild herpes simplex), and another had a liver function abnormality (moderate liver injury). In the placebo group, one patient experienced a serious infection (severe infective cholangitis). Additionally, one patient (0.5%) in the placebo group reported herpes zoster, and uveitis was reported in three (1.6%) patients in the ivarmacitinib group and two (1.1%) patients in the placebo group. During the extension period, no prespecified TEAEs of special interest were reported in either group; one patient (0.8%) in the placebo to ivarmacitinib 4 mg group experienced herpes zoster, and uveitis was reported in two (1.5%) patients in the placebo to ivarmacitinib 4 mg group

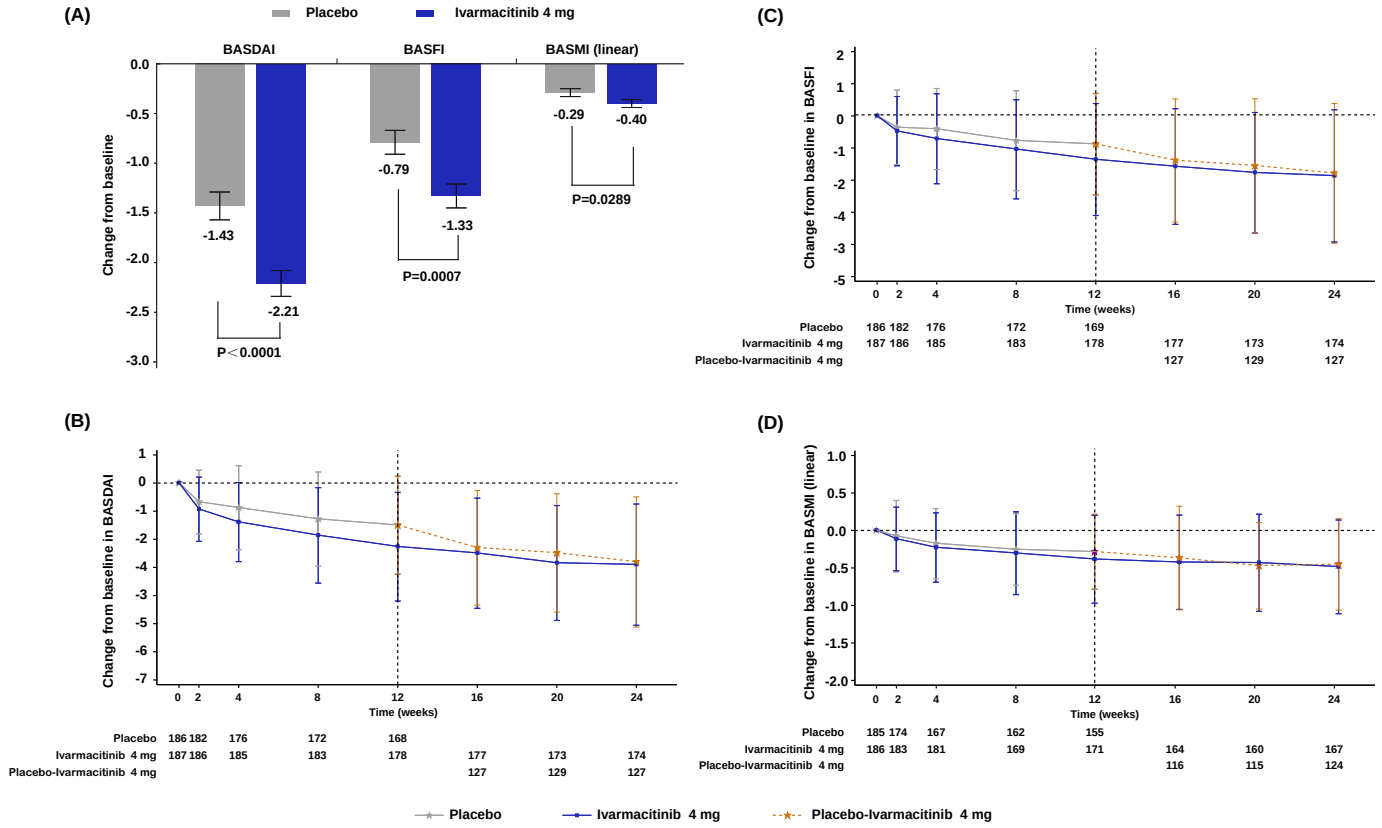

Figure 3. Change from baseline in BASDAI, BASFI, and BASMI (linear) scores at the scheduled visits. (A) Change from baseline in BASDAI, BASFI, and BASMI (linear) scores at week 12. (B) Change from baseline in BASDAI score over 24 weeks (observed case analysis). (C) Change from baseline in BASFI score over 24 weeks (observed case analysis). (D) Change from baseline in BASMI (linear) score over 24 weeks (observed case analysis). Data are presented as least squares mean ± SE (A) and as mean ± SD (B–D). BASDAI, Bath Ankylosing Spondylitis Disease Activity Index; BASFI, Bath Ankylosing Spondylitis Functional Index; BASMI, Bath Ankylosing Spondylitis Metrology Index.

and two (1.1%) patients in the ivarmacitinib 4 mg group. No newly diagnosed malignancies, thromboembolic events, major cardiovascular events, IBD, or deaths were reported throughout the study (Table 3).

Up to week 12, treatment discontinuations due to TEAEs were low, occurring in 2.7% (5 of 187) of patients in the ivarmacitinib 4 mg group and 1.6% (3 of 186) in the placebo group (Supplementary Table 11). During the extension period, no patients in either the placebo to ivarmacitinib 4 mg group or the ivarmacitinib 4 mg group experienced TEAEs that led to dose discontinuation.

DISCUSSION

In this registrational phase 2/3 trial, the primary end point for the overall study was met, with ivarmacitinib demonstrating an ASAS20 response rate of 48.7% at week 12 at the recommended dose of 4 mg, compared to 29.0% with placebo in patients with active AS. The improvement in ASAS20 response with ivarmacitinib was generally consistent across subgroups, including the challenging-to-treat populations with high disease activity and prior use of bDMARDs or TNFi.

Ivarmacitinib showed a rapid onset of action, with significant improvements in ASAS20, ASAS40, and ASAS5/6 responses as early as week 2, the first postbaseline assessment, which were maintained through week 12. At week 12, the ASAS40 and ASAS5/6 response rates were 32.1% and 42.8%, respectively, for ivarmacitinib, compared to 18.3% and 15.6% for placebo. By week 24, response rates for ASAS20, ASAS40, and ASAS5/6 continued to improve, reaching 66.7%, 48.3%, and 59.5%, respectively, in patients receiving continuous ivarmacitinib.

These trends align with findings from studies of other JAK inhibitors in active AS.[15,16,22] In a phase 3 study of tofacitinib, a 5-mg twice daily dose resulted in ASAS20 and ASAS40 response rates of 56.4% (vs 29.5% for placebo) and 40.6% (vs 12.5% for placebo), respectively, at week 16 in patients with active AS, regardless of prior bDMARD use.[15] Similarly, upadacitinib 15 mg once daily led to ASAS20 and ASAS40 response rates of 65% (vs 40% for placebo) and 52% (vs 26% for placebo), respectively, at week 14 in bDMARD-naive patients in the SELECT-AXIS 1 trial.[16] In the SELECT-AXIS 2 trial, bDMARD-inadequate

Table 3. TEAEs through wk 0–12 and wk 12–24 (safety population)*

	Placebo-controlled period (wk 0–12)		Extension period (wk 12–24)	
	Placebo (n = 186)	Ivarmacitinib 4 mg (n = 187)	Placebo–ivarmacitinib 4 mg (n = 132)	Ivarmacitinib 4 mg (n = 179)
TEAEs	122 (65.6)	149 (79.7)	100 (75.8)	134 (74.9)
TESAEs	4 (2.2)	2 (1.1)	3 (2.3)	0
Infection-related TEAEs	47 (25.3)	54 (28.9)	47 (35.6)	58 (32.4)
TEAEs leading to dose discontinuation	3 (1.6)	5 (2.7)	0	0
TEAEs leading to dose interruption	10 (5.4)	9 (4.8)	11 (8.3)	6 (3.4)
TEAEs that required the use of antimicrobial therapy	14 (7.5)	22 (11.8)	16 (12.1)	17 (9.5)
Deaths	0	0	0	0
Prespecified TEAEs of special interest	1 (0.5)	2 (1.1)	0	0
Serious infection[a]	1 (0.5)	0	0	0
Any systemic opportunistic infection[b]	0	1 (0.5)	0	0
Newly diagnosed malignancy	0	0	0	0
Thromboembolic event[c]	0	0	0	0
Major cardiovascular event[d]	0	0	0	0
Liver function abnormality[e]	0	1 (0.5)	0	0
Other TEAEs of special interest				
Herpes zoster	1 (0.5)	0	1 (0.8)	0
Inflammatory bowel disease	0	0	0	0
Uveitis[f]	2 (1.1)	3 (1.6)	2 (1.5)	2 (1.1)
TEAEs occurring in ≥5% of patients in any treatment group				
Upper respiratory tract infection	24 (12.9)	25 (13.4)	27 (20.5)	23 (12.8)
Hyperuricemia	11 (5.9)	30 (16.0)	8 (6.1)	23 (12.8)
Blood creatine phosphokinase level increased	7 (3.8)	15 (8.0)	14 (10.6)	22 (12.3)
Hyperlipidemia	14 (7.5)	19 (10.2)	10 (7.6)	21 (11.7)
COVID-19	8 (4.3)	7 (3.7)	6 (4.5)	18 (10.1)
ALT increased	7 (3.8)	4 (2.1)	7 (5.3)	17 (9.5)
AST increased	4 (2.2)	1 (0.5)	1 (0.8)	10 (5.6)
Weight increased	0	4 (2.1)	1 (0.8)	9 (5.0)
Hypertriglyceridemia	5 (2.7)	11 (5.9)	3 (2.3)	3 (2.3)

* Data are presented as n (%). Adverse events were coded using Medical Dictionary for Regulatory Activities Version 26.0. A TEAE is defined as an adverse event that either first occurred or worsened in severity after the initial dose of the study treatment. ALT, alanine aminotransferase; AST, aspartate aminotransferase; TEAE, treatment-emergent adverse event; TESAE, treatment-emergent serious adverse event.
[a] Severe infection is defined as an infection requiring systemic antimicrobial therapy for more than two weeks, including sepsis, pyemia, and septic shock.
[b] Includes any systemic opportunistic infection (eg, active tuberculosis, disseminated herpes zoster).
[c] Includes venous thrombosis (eg, deep vein thrombosis), pulmonary thromboembolism, arterial thrombosis, and cerebrovascular events (eg, thrombotic stroke, transient ischemic attacks).
[d] Major cardiovascular events include cardiovascular death, nonfatal myocardial infarction, nonfatal stroke, unstable angina requiring hospitalization, and heart failure requiring hospital admission.
[e] Liver function abnormality is defined as follows: (1) ALT or AST level more than five times the upper limit of normal (ULN); (2) ALT or AST level more than three times ULN, with total bilirubin level more than two times ULN; or (3) ALT or AST level more than three times ULN, accompanied by clinical symptoms/signs of hepatitis or an eosinophil count >5%.
[f] Uveitis is defined as a clustered term for iritis, uveitis, and iridocyclitis.

responders treated with upadacitinib had ASAS20 and ASAS40 response rates of 65.4% (vs 38.3% for placebo) and 44.5% (vs 18.2% for placebo), respectively.[22] Direct comparisons between our study and these trials should be made with caution because of differences in patient characteristics, study designs, patient populations, assessment time points, and the proportion of bDMARD-naive patients, as well as the ASAS20 and ASAS40 response rates in the placebo groups. Our placebo-controlled period lasted 12 weeks, shorter than the 14- to 16-week periods in the tofacitinib and upadacitinib studies.[15,16,22] Despite these differences, the efficacy of ivarmacitinib 4 mg aligns with that of currently approved JAK inhibitors and is supported by its consistent efficacy across varying baseline disease activity levels and prior bDMARD status.

During the core treatment period, ivarmacitinib 4 mg showed consistent improvements over placebo across other secondary and additional efficacy end points, including disease activity, mobility, function, and health-related quality of life. Clinically relevant treatment goals, such as achieving ASDAS-CII, were met by 51.3% of patients receiving ivarmacitinib 4 mg at week 12, compared to 18.3% with placebo. Additionally, ivarmacitinib's efficacy in alleviating the signs and symptoms of AS was

supported by reductions in objective markers of inflammation, such as CRP level and ESR, and active inflammation seen in MRI scans of the sacroiliac joints. These benefits were sustained through week 24, with patients who switched from placebo to ivarmacitinib after week 12 showing improved clinical responses from weeks 12 to 16, which were maintained through week 24.

Collectively, these results support the rapid, durable, and clinically meaningful improvements in disease manifestations with ivarmacitinib 4 mg in treating active AS. Along with findings from studies in alopecia areata, ulcerative colitis, and rheumatoid arthritis, these results suggest a potential role for ivarmacitinib in treating a range of inflammatory diseases associated with JAK pathways.[23–25] Ivarmacitinib is currently under investigation for the treatment of active psoriatic arthritis (ClinicalTrials.gov identifier NCT04957550) and nonradiographic axSpA (ClinicalTrials.gov identifier NCT05324631).

Regarding safety, during the 12-week placebo-controlled period, hyperuricemia was more frequent in the ivarmacitinib 4 mg group (16.0%) than the placebo group (5.9%). However, all cases were mild, and uric acid levels remained stable throughout the study. The incidence of other TEAEs was similar between the groups, with differences of less than 5%. No new safety findings were observed compared to previous ivarmacitinib trials in other autoimmune diseases,[20,23,24] with most TEAEs being mild and resolving without treatment discontinuation. The incidence of TEAEs leading to discontinuation was low and comparable between groups (2.7% for ivarmacitinib 4 mg vs 1.6% for placebo), as was the incidence of TESAEs (1.1% vs 2.2%).

Infection-related TEAEs are notable adverse events associated with JAK inhibitors.[26–28] In our study, upper respiratory tract infections were the most common TEAEs in both groups, with similar incidence rates (13.4% in the ivarmacitinib 4 mg group vs 12.9% in the placebo group). The incidence of COVID-19 was also comparable (3.7% vs 4.3%), with no severe cases reported. The frequency of herpes zoster was very low and consistent across treatment arms through week 24.

Laboratory values, including hemoglobin levels, creatine kinase levels, uric acid levels, liver enzyme levels, lipid levels, platelet counts, and neutrophil counts, showed trends similar to those observed with other JAK inhibitors in patients with AS.[15,16,26] These changes were transient, clinically insignificant, and generally asymptomatic, with most abnormalities reversible without treatment interruption. No cases of active tuberculosis, newly diagnosed malignancies, major cardiovascular events, or deaths were reported during the trial; however, further investigation in studies with longer follow-up is warranted.

Several limitations of our study should be acknowledged. First, although the study evaluated ivarmacitinib over a 24-week period, further research is needed to assess its long-term efficacy and safety because AS is a chronic disease requiring ongoing management. Second, the lack of an active comparator limits direct comparisons with other bDMARDs for AS. Third, radiographic outcomes by MRI were optional and not assessed in all patients. Fourth, the study included only Chinese patients with radiographic axSpA, so the treatment effects of ivarmacitinib in other ethnic groups and in patients with nonradiographic axSpA remain to be determined. Finally, although preclinical evaluations revealed no reproductive organ toxicity, ivarmacitinib's impact on male fertility has not been examined in humans, and dedicated clinical research is warranted.

In conclusion, ivarmacitinib 4 mg once daily provided rapid, sustained, and clinically meaningful improvements in disease activity, signs and symptoms, function, and MRI-detected inflammation in patients with active AS who had an inadequate response to NSAIDs, with a manageable safety profile. Our findings support ivarmacitinib as a new treatment option for patients with active AS.

ACKNOWLEDGMENTS

We are grateful to all participants and their families and all members of the study group.

AUTHOR CONTRIBUTIONS

All authors contributed to at least one of the following manuscript preparation roles: conceptualization AND/OR methodology, software, investigation, formal analysis, data curation, visualization, and validation AND drafting or reviewing/editing the final draft. As corresponding author, Dr Li confirms that all authors have provided the final approval of the version to be published and takes responsibility for the affirmations regarding article submission (eg, not under consideration by another journal), the integrity of the data presented, and the statements regarding compliance with institutional review board/Declaration of Helsinki requirements.

ROLE OF THE STUDY SPONSOR

Jiangsu Hengrui Pharmaceuticals Co, Ltd, designed the trial and collaborated with external authors on data collection, analysis, and interpretation. There were confidentiality agreements between the authors and the sponsor. All authors had full access to the trial data, participated in the interpretation of the data and development of the draft, approved the final draft before submission, and vouch for adherence of the trial to the protocol, completeness and accuracy of the data and analyses, and reporting of adverse events. Publication of this article was not contingent upon approval by Jiangsu Hengrui Pharmaceuticals Co, Ltd. Medical writing support was provided by Lin Dong, PhD (a medical writer at Jiangsu Hengrui Pharmaceuticals Co, Ltd), according to Good Publication Practice Guidelines.

REFERENCES

1. Sieper J, Poddubnyy D. Axial spondyloarthritis. Lancet 2017; 390(10089):73–84.
2. Dean LE, Jones GT, MacDonald AG, et al. Global prevalence of ankylosing spondylitis. Rheumatology (Oxford) 2014;53(4):650–657.
3. Poddubnyy D, Sieper J. Treatment of axial spondyloarthritis: what does the future hold? Curr Rheumatol Rep 2020;22(9):47.
4. Sieper J, Braun J, Dougados M, et al. Axial spondyloarthritis. Nat Rev Dis Primers 2015;1(1):15013.

5. Bohn R, Cooney M, Deodhar A, et al. Incidence and prevalence of axial spondyloarthritis: methodologic challenges and gaps in the literature. Clin Exp Rheumatol 2018;36(2):263–274.
6. Ward MM, Deodhar A, Gensler LS, et al. 2019 Update of the American College of Rheumatology/Spondylitis Association of America/Spondyloarthritis Research and Treatment Network recommendations for the treatment of ankylosing spondylitis and nonradiographic axial spondyloarthritis. Arthritis Rheumatol 2019;71(10): 1599–1613.
7. van der Heijde D, Ramiro S, Landewé R, et al. 2016 update of the ASAS-EULAR management recommendations for axial spondyloarthritis. Ann Rheum Dis 2017;76(6):978–991.
8. Ward MM, Deodhar A, Gensler LS, et al. 2019 Update of the American College of Rheumatology/Spondylitis Association of America/Spondyloarthritis Research and Treatment Network recommendations for the treatment of ankylosing spondylitis and nonradiographic axial spondyloarthritis. Arthritis Care Res (Hoboken). 2019; 71(10):1285–1299.
9. Sieper J, Deodhar A, Marzo-Ortega H, et al; MEASURE 2 Study Group. Secukinumab efficacy in anti-TNF-naive and anti-TNF-experienced subjects with active ankylosing spondylitis: results from the MEASURE 2 Study. Ann Rheum Dis 2017;76(3):571–592.
10. Deodhar A, Poddubnyy D, Pacheco-Tena C, et al; COAST-W Study Group. Efficacy and safety of ixekizumab in the treatment of radiographic axial spondyloarthritis: sixteen-week results from a phase III randomized, double-blind, placebo-controlled trial in patients with prior inadequate response to or intolerance of tumor necrosis factor inhibitors. Arthritis Rheumatol 2019;71(4):599–611.
11. Menegatti S, Bianchi E, Rogge L. Anti-TNF Therapy in Spondyloarthritis and Related Diseases, Impact on the Immune System and Prediction of Treatment Responses. Frontiersin Immunology 2019;10:382.
12. Veale DJ, McGonagle D, McInnes IB, et al. The rationale for Janus kinase inhibitors for the treatment of spondyloarthritis. Rheumatology (Oxford) 2019;58(2):197–205.
13. McInnes IB, Szekanecz Z, McGonagle D, et al. A review of JAK-STAT signalling in the pathogenesis of spondyloarthritis and the role of JAK inhibition. Rheumatology (Oxford) 2022;61(5):1783–1794.
14. van der Heijde D, Deodhar A, Wei JC, et al. Tofacitinib in patients with ankylosing spondylitis: a phase II, 16-week, randomised, placebo-controlled, dose-ranging study. Ann Rheum Dis 2017;76(8):1340–1347.
15. Deodhar A, Sliwinska-Stanczyk P, Xu H, et al. Tofacitinib for the treatment of ankylosing spondylitis: a phase III, randomised, double-blind, placebo-controlled study. Ann Rheum Dis 2021;80(8):1004–1013.
16. van der Heijde D, Song IH, Pangan AL, et al. Efficacy and safety of upadacitinib in patients with active ankylosing spondylitis (SELECT-AXIS 1): a multicentre, randomised, double-blind, placebo-controlled, phase 2/3 trial. Lancet 2019;394(10214):2108–2117.
17. European Medicines Agency. RINVOQ (upadacitinib): EPAR – Product Information. First published December 18, 2019; Accessed June 10, 2025. https://www.ema.europa.eu/en/documents/product-information/rinvoq-epar-product-information_en.pdf
18. Clark JD, Flanagan ME, Telliez JB. Discovery and development of Janus kinase (JAK) inhibitors for inflammatory diseases. J Med Chem 2014;57(12):5023–5038.
19. Gu YJ, Sun WY, Zhang S, et al. Targeted blockade of JAK/STAT3 signaling inhibits proliferation, migration and collagen production as well as inducing the apoptosis of hepatic stellate cells. Int J Mol Med 2016;38(3):903–911.
20. Zeng X, Jiang Y, Yang Y, et al. A multicenter, randomized, placebo-controlled, double-blind phase 2 study of SHR0302 versus placebo in Chinese subjects with moderate to severe active rheumatoid arthritis (RA) [abstract]. Arthritis Rheumatol 2020;72(suppl 10). Accessed January 25, 2024. https://acrabstracts.org/abstract/a-multicenter-randomized-placebo-controlled-double-blind-phase-2-study-of-shr0302-versus-placebo-in-chinese-subjects-with-moderate-to-severe-active-rheumatoid-arthritis-ra/
21. Posch M, Koenig F, Branson M, et al. Testing and estimation in flexible group sequential designs with adaptive treatment selection. Stat Med 2005;24(24):3697–3714.
22. van der Heijde D, Baraliakos X, Sieper J, et al. Efficacy and safety of upadacitinib for active ankylosing spondylitis refractory to biological therapy: a double-blind, randomised, placebo-controlled phase 3 trial. Ann Rheum Dis 2022;81(11):1515–1523.
23. Zhou C, Yang X, Yang B, et al. A randomized, double-blind, placebo-controlled phase II study to evaluate the efficacy and safety of ivarmacitinib (SHR0302) in adult patients with moderate-to-severe alopecia areata. J Am Acad Dermatol 2023;89(5):911–919.
24. Chen B, Zhong J, Li X, et al. Efficacy and safety of ivarmacitinib in patients with moderate-to-severe, active, ulcerative colitis: a phase II study. Gastroenterology 2022;163(6):1555–1568.
25. Liu J, Jiang Y, Zhang S, et al. Ivarmacitinib, a selective Janus kinase 1 inhibitor, in patients with moderate-to-severe active rheumatoid arthritis and inadequate response to conventional synthetic DMARDs: results from a phase III randomised clinical trial. Ann Rheum Dis 2025; 84(2):188–200.
26. Akkoc N, Khan MA. JAK inhibitors for axial spondyloarthritis: what does the future hold? Curr Rheumatol Rep 2021;23(6):34.
27. Bechman K, Subesinghe S, Norton S, et al. A systematic review and meta-analysis of infection risk with small molecule JAK inhibitors in rheumatoid arthritis. Rheumatology (Oxford) 2019;58(10):1755–1766.
28. Nash P, Kerschbaumer A, Dörner T, et al. Points to consider for the treatment of immune-mediated inflammatory diseases with Janus kinase inhibitors: a consensus statement. Ann Rheum Dis 2021; 80(1):71–87.
29. van der Linden S, Valkenburg HA, Cats A. Evaluation ofdiagnostic criteria for ankylosing spondylitis. A proposal for modification ofthe New York criteria. Arthritis andrheumatism 1984;27(4):361-368.
30. Sieper J, Rudwaleit M, Baraliakos X, et al. The Assessment of SpondyloArthritis international Society (ASAS) handbook: a guide to assess spondyloarthritis. Annals of the rheumatic diseases 2009;68 (Suppl 2):ii1-ii44.

American College of Rheumatology
Empowering Rheumatology Professionals

Arthritis & Rheumatology
Vol. 77, No. 11, November 2025, pp 1524–1532
DOI 10.1002/art.43227

Genetics of Childhood-Onset Systemic Lupus Erythematosus

Raffaella Carlomagno,[1] Nicholas Gold,[2] Fangming Liao,[3] Jingjing Cao,[3] Paul D. Arnold,[4] Christie L. Burton,[5] Jennifer Crosbie,[6] Daniela Dominguez,[2] Dafna D. Gladman,[7] Mariko Ishimori,[8] Caroline Jefferies,[9] Diane L. Kamen,[10] Sylvia Kamphuis,[11] Marisa S. Klein-Gitelman,[12] Andrea M. Knight,[2] Chia-Chi J. Lee,[13] Deborah M. Levy,[2] Karen B. Onel,[14] Andrew D. Paterson,[15] Christine A. Peschken,[16] Janet E. Pope,[17] Russell J. Schachar,[6] Earl D. Silverman,[2] Lisa Strug,[15] Zahi Touma,[7] Murray B. Urowitz,[18] Daniel J. Wallace,[13] Cheng Wang,[3] Declan Webber,[2] Joan E. Wither,[7] and Linda T. Hiraki[19]

Objective. Genome-wide association studies (GWAS) have identified >100 loci for systemic lupus erythematosus (SLE). These loci may also affect age at diagnosis. We aimed to identify genetic variants for age at SLE diagnosis and to complete a GWAS of childhood-onset SLE (cSLE) in children diagnosed <18 years of age.

Methods. Patients met American College of Rheumatology and/or Systemic Lupus Erythematosus International Collaborative Clinics classification criteria, had documented age at diagnosis, and were genotyped on multiethnic arrays. Ungenotyped single nucleotide polymorphisms (SNPs) and HLA alleles were imputed to multiethnic referents. Ancestry was genetically inferred. We tested known SLE loci (142 non-HLA, 166 HLA) with log-transformed age of SLE diagnosis, adjusted for sex and five principal components (significance threshold $P < 1.6 \times 10^{-4}$). We also completed a GWAS of 346 patients with cSLE and 4,080 children and adolescents without SLE of European and East Asian ancestry (genome-wide significance $P < 5 \times 10^{-8}$).

Results. We included 1,489 patients with SLE, 51% of patients had cSLE, 88% of patients were female, 39% of patients were of European ancestry, 19% of patients were of East Asian ancestry, and 17% of patients were of Admixed ancestry. The median age at diagnosis was 17.7 years (interquartile range 14.0–30.9). One SLE-risk SNP, intronic to coiled-coil domain containing 113 (*CCDC113*) (chromosome 16), was associated with younger age at SLE diagnosis ($\beta = -0.12$, SE = 0.03, $P = 6.3 \times 10^{-6}$) and with cSLE versus adult-onset SLE (aSLE). GWAS of cSLE compared to controls without SLE identified significant chromosome 6 SNP rs9268469, intronic to *TSBP1-AS1* (odds ratio 2.04 [95% confidence interval 1.59–2.63], $P = 1.79 \times 10^{-8}$) and *HLA-DQA1*.

Conclusion. We identified a significant locus for younger age at SLE diagnosis, intronic to *CCDC113*, among a large multiancestral cohort of children and adults with SLE. In the first GWAS of cSLE, we identified a *TSBP1-AS1* locus and an *HLA-DQA1* previously identified for aSLE.

Dr Carlomagno's work was supported by Funds Eugenio Litta, Fondation Genevoise de Bienfaisance Valeria Rossi di Montelera, Hospital General Administration and Pediatrics Department of Lausanne University Hospital (Centre Hospitalier Universitaire Vaudois), and Société Académique Vaudoise. Supported by the CIHR, grant MOP-106573 to Dr Arnold, grant MOP-93696 to Dr Schachar. Dr Burton, Dr Crosbie, and Dr Schachar's work was supported by the Canadian Institutes of Health Research (CIHR). Dr Knight's work was supported by grants from the Lupus Foundation of America and the Lupus Research Alliance. Dr Peschken's work was supported by grants from Lupus Research Alliance, CIHR, and Lupus Canada; Dr Hiraki and part of the work was supported by The Arthritis Society Stars Career Development award, CIHR, and a Canada Research Chair.

[1]Raffaella Carlomagno, MD: Division of Rheumatology, The Hospital for Sick Children, Toronto, Ontario, Canada, and Unit of Rheumatology, Immunology and Allergology, Department of Pediatrics, Lausanne University Hospital, Lausanne, Switzerland; [2]Nicholas Gold, BSc, Daniela Dominguez, MD, Andrea M. Knight, MD, Deborah M. Levy, MS, MD, Earl D. Silverman, MD, Declan Webber, MD: Division of Rheumatology, The Hospital for Sick Children, Toronto, Ontario, Canada; [3]Fangming Liao, MSc, Jingjing Cao, MSc, Cheng Wang, MSc: Genetics & Genome Biology, Research Institute, The Hospital for Sick Children, Toronto, Ontario, Canada; [4]Paul D. Arnold, MD, PhD: Mathison Centre for Mental Health Research and Education, Departments of Psychiatry, and Hotchkiss Brain Institute, Cumming School of Medicine, University of Calgary, Calgary, Alberta, Canada; [5]Christie L. Burton, PhD: Neurosciences and Mental Health, Research Institute, Hospital for Sick Children, Toronto, Ontario, Canada; [6]Jennifer Crosbie, PhD, Russell J. Schachar, MD: Neurosciences and Mental Health, Research Institute, Hospital for Sick Children, and Department of Psychiatry, University of Toronto, Toronto, Ontario, Canada; [7]Dafna D. Gladman, MD, Zahi Touma, MD, PhD, Joan E. Wither, MD, PhD: Schroeder Arthritis Institute, Toronto Western Hospital, University of Toronto, and Krembil Research Institute, Toronto Western Hospital, Toronto, Ontario, Canada; [8]Mariko Ishimori, MD: Kao Autoimmunity Institute, Cedars-Sinai Medical Center, Los Angeles, California; [9]Caroline Jefferies, MD, PhD: Kao Autoimmunity Institute, Cedars-Sinai Medical Center, Los Angeles,

INTRODUCTION

Systemic lupus erythematosus (SLE) is a complex, chronic autoimmune disease that affects both children and adults, with the majority diagnosed in young adulthood. The etiopathogenesis of SLE is not completely understood, but it is thought to be a complex interaction between genetic susceptibility loci and environmental factors,[1] with heritability estimates up to 66% in family-based studies.[2,3] Genome-wide association studies (GWAS) of SLE have identified more than 100 loci associated with SLE risk.[4–8] These studies included diverse ancestral populations, with the majority being of European or East Asian ancestry. All these studies have primarily included patients diagnosed with adult-onset SLE (aSLE).

Approximately 20% of those with SLE are diagnosed in childhood or adolescence (childhood-onset SLE [cSLE]). Previous studies have observed an inverse association between the number of SLE-risk alleles a person carries and the age at SLE diagnosis.[4,9–11] Yet, no study to date has completed a GWAS of cSLE specifically.

The goals of our study were to examine the effect of known SLE-risk alleles on age at SLE diagnosis in a multiancestral cohort of children and adults with SLE. We also aimed to complete the first GWAS of cSLE.

PATIENTS AND METHODS

Age at SLE diagnosis. The study population included patients with cSLE and aSLE who met American College of Rheumatology and/or Systemic Lupus Erythematosus International Collaborative Clinics classification criteria for lupus.[12–14] These patients were observed at tertiary care centers across North America and Europe (Supplemental Methods and Table S1).

Collaborating centers provided deidentified DNA samples from consented participants. Demographics and clinical and laboratory SLE features were extracted from dedicated SLE databases supplemented by medical chart review from each center. We included patients with documented age at SLE diagnosis. Patients were not involved in the development of the research question, outcome measures, and design of the study. Local institutional review board approval was obtained at each site (The Hospital for Sick Children [SickKids] ethics approval number: 1000058324).

Participants were genotyped on the Illumina Multi-Ethnic Global Array (MEGA) (v.8x1-Infinium-LCG-iSelect-MEGA_Consortium_v2) (~2*M* single nucleotide polymorphisms [SNPs]) or the Illumina Global Screening Array (GSA) (GSA-24v2-0_A1) (~0.6*M* SNPs), in accordance with the recommended protocols specified by The Centre for Applied Genomics at SickKids, Toronto. Quality control measures, principal component (PC) analysis, imputation of non-HLA and HLA SNPs, and ancestral estimation are reported in the Supplemental Methods.[15–17]

We genetically inferred ancestry with PCs and ancestral proportions with ADMIXTURE, using all 1000 Genome Project ancestral groups as a referent.[18] Global PCs were included in genetic analyses for the total cohort and ancestry-specific local PCs for European and East Asian populations for ancestry-stratified analyses. Demographic estimates assigned a participant to an ancestral group when ≥80% of ancestral proportion was ascribed to that group. Those with <80% of single ancestral proportion were classified as "Admixed."

The main outcome of interest was age at SLE diagnosis (years). We log-transformed age at diagnosis to improve normality of the residuals ensuring appropriateness for linear regression (Figure S1). A secondary outcome was cSLE (diagnosis <18 years) compared to aSLE (diagnosis ≥18 years). We tested different thresholds of age at diagnosis to define cSLE. We chose 18 years because it was the median age at diagnosis in the total cohort and is a commonly used definition for cSLE.[19,20] Demographic and clinical information included sex, SLE manifestations, and follow-up time, defined as the time between SLE diagnosis and the last documented clinical encounter.

We calculated medians and interquartile ranges (IQRs) for continuous variables and counts and proportions for categorical variables; in addition, we conducted chi-square tests using R (version 4.2.2). We focused on 142 non-HLA and 166 HLA SLE-risk alleles from three of the largest SLE GWAS to date[4–6] and tested each SNP with age at SLE diagnosis in our SLE cohort, as well

California, and Division of Rheumatology, Department of Medicine, Cedars Sinai Medical Center, Los Angeles; [10]Diane L. Kamen, MD: Division of Rheumatology and Immunology, Medical University of South Carolina, Charleston; [11]Sylvia Kamphuis, MD, PhD: Department of Pediatric Rheumatology, Sophia Children's Hospital, Erasmus University Medical Center, Rotterdam, The Netherlands; [12]Marisa S. Klein-Gitelman, MD: Division of Rheumatology, Department of Pediatrics, Ann & Robert H. Lurie Children's Hospital of Chicago, Chicago, Illinois; [13]Chia-Chi J. Lee, MD, Daniel J. Wallace, MD: Division of Rheumatology, Department of Medicine, Cedars Sinai Medical Center, Los Angeles, California; [14]Karen B. Onel, MD: Pediatric Rheumatology, Hospital for Special Surgery, New York, New York; [15]Andrew D. Paterson, MB, ChB, Lisa Strug, PhD: Genetics & Genome Biology, Research Institute, The Hospital for Sick Children, and Divisions of Biostatistics and Epidemiology, Dalla Lana School of Public Health, University of Toronto, Toronto, Ontario, Canada; [16]Christine A. Peschken, MD, MSc: Departments of Medicine and Community Health Sciences, University of Manitoba, Winnipeg, Manitoba, Canada; [17]Janet E. Pope, MD: Department of Medicine, University of Western Ontario, St. Joseph's Health Centre, London, Ontario, Canada; [18]Murray B. Urowitz, MD: Schroeder Arthritis Institute, Toronto Western Hospital, University of Toronto, Toronto, Ontario, Canada; [19]Linda T. Hiraki, MD, ScD: Division of Rheumatology, The Hospital for Sick Children, Toronto, Ontario, Canada, and Genetics & Genome Biology, Research Institute, The Hospital for Sick Children, Toronto, Ontario, Canada, and Division of Epidemiology, Dalla Lana School of Public Health, University of Toronto, Toronto, Ontario, Canada.

Additional supplementary information cited in this article can be found online in the Supporting Information section (https://acrjournals.onlinelibrary.wiley.com/doi/10.1002/art.43227).

Author disclosures are available at https://onlinelibrary.wiley.com/doi/10.1002/art.43227.

Address correspondence via email to Linda T. Hiraki, MD, FRCPC, ScD, at linda.hiraki@sickkids.ca.

Submitted for publication April 15, 2024; accepted in revised form April 18, 2025.

as with cSLE (vs aSLE). Results were considered significant at a Bonferroni corrected threshold of $P < 1.6 \times 10^{-4}$, accounting for 308 tests. We completed analyses of cSLE versus aSLE diagnosis using logistic regression models, and linear regression of age at SLE diagnosis including five PCs to control for populations stratification. We also investigated the entire genome for age at SLE diagnosis loci using GENESIS,[21] an R/Bioconductor package that has improved control for population stratification by creating a genetic relatedness matrix (significant threshold $P < 5 \times 10^{-8}$). Chromosome (chr) X was analyzed using a genetic dominance model, adjusted for sex and five PCs, in accordance with best practices for sex-chromosome analyses.[22] We ran an HLA-wide analysis of age at SLE diagnosis with HLA-Typing At Protein coding positions for Associated Studies (HLA-TAPAS), an HLA-focused pipeline, using a large-scale multiancestry HLA imputation reference panel from the Michigan Imputation server (Four-digit-Multi-ethnic-HLA_v.1.0-2021).[17] For HLA-wide analyses, from 42,924 HLA markers, we focused on the 80 classic HLA alleles with 2- and 4-digit resolution. For non-HLA and HLA-wide analyses, we ran marginal and multivariable adjusted regression models with covariates for sex and five PCs, first using linear regression models for continuous age at SLE diagnosis in years (log-transformed). We repeated analyses of cSLE versus aSLE diagnosis using logistic regression models and a threshold of $P < 5 \times 10^{-8}$.

We calculated polygenic risk scores (PRSs) for SLE using all independent SNP associations within a region as reported by one of the largest SLE GWAS.[4] We compared non-HLA and HLA SLE PRS distributions in cSLE and aSLE using analysis of variance (Supplemental Methods).

We completed sensitivity analyses to explore possible differences in the genetic architecture for age of SLE diagnosis by subgroups. We repeated analyses of age at SLE diagnosis stratified by cSLE and aSLE, ancestral groups (European, East Asian, African, and American or Admixed) and meta-analyzed the results using inverse variance weighting and tested for heterogeneity (Meta Analysis Helper, METAL).[23] The South Asian population was not included in the stratified analysis because of limited sample size. We also repeated analyses adding the non-HLA SLE PRS as a covariate to test whether conditioning on SLE-risk SNPs would improve the power to discover new loci for age at SLE diagnosis.

We examined the allele frequency of our top SNP for age of diagnosis across sex and ancestral groups. We also ran models with an interaction term between the top SNP and sex to test for effect modification of the top SNP by age group (cSLE vs aSLE) and by sex.

To investigate the functional consequence of the most significant locus, we examined all SNPs within 100 kb of the top SNP using LocusFocus (version 1.4.9-alpha), a web-based colocalization tool for exploration of GWAS signals. We ran analyses using two different single-cell RNA sequencing (RNAseq) referents (Supplemental Methods).[24–26] The threshold for significance was based on the number of genes and hematopoietic single-cell gene expressions tested.

cSLE GWAS. We completed a cSLE GWAS comparing the cSLE cohort and a population-based cohort of children from the Spit for Science study. We restricted to participants of European and East Asian ancestry, who comprised the largest genotyped ancestral groups from the Spit for Science study and ran ancestry-stratified cSLE GWAS (Supplemental Methods).[27,28]

Spit for Science participants without SLE were genotyped on the Illumina Human Core Exome (HCE) (HCE-v.1-0_12-bead-chip).[28] We harmonized the MEGA and HCE platforms by restricting to SNPs present on both MEGA and HCE arrays before imputation using TOPMed-r2@1.0.0 as imputation referent (version 1.3.3).[29] We retained SNPs with minor allele frequency (MAF) ≥0.1 and imputation quality R^2 ≥0.3. GSA genotyped participants with SLE were not included (Supplemental Methods).

For cSLE GWAS of Europeans, we used the Scalable and Accurate Implementation of Generalized mixed models (SAIGE_v0.29.5) method designed for unbalanced case-control ratios.[30] For GWAS of East Asian patients, we used GENESIS.[21] We ran marginal and multivariable adjusted GWAS of cSLE with sex and PCs. PCs were calculated in European (three PCs) and East Asian ancestral cohorts (five PCs), each accounting for >99% variability in individual ancestral group. We meta-analyzed results using inverse variance weighting (METAL_v2011-03-25).[23] Chr. X was analyzed using a genetic dominance model, adjusted for sex and PCs.[22] We also completed an HLA-wide association study of cSLE using HLA-TAPAS. From 34,619 HLA markers (Supplemental Methods), we focused on 44 classic HLA alleles with 2- and 4-digit resolution. Results from GWAS analyses were considered significant at a threshold of $P < 5 \times 10^{-8}$.

We used meta-analyzed GWAS for cSLE results in Locus Focus (version 1.4.9-alpha) to examine all SNPs within 100 kb of the top chr. 6 SNP.[24,25] Threshold for significance was again based on the number of genes and hematopoietic single-cell gene expression tested (Supplemental Methods).

We tested the association between HLA and non-HLA SLE PRSs and cSLE in logistic regression analyses in European and East Asian participants. These models were additionally adjusted for sex and PCs as covariates and then meta-analyzed.

RESULTS

Age at SLE diagnosis. Our study included 1,489 patients with SLE; 88% of patients were female (n = 1,306), and 51% of patients had cSLE (n = 761). Overall, the median age at diagnosis was 17.7 years (IQR 14–30.9 years), 14.1 years (IQR 11.8–15.8 years) in the cSLE group and 31.2 years (IQR 24.7–42 years) in the aSLE group (Table 1, Figure S1). The majority of our cohort was of European ancestry (39%), East Asian ancestry (19%), and Admixed ancestry (17%) (Table 1). The ancestral distribution

Table 1. Demographics and clinical characteristics of patients with SLE*

Characteristics	Total (N = 1,489)	cSLE (n = 761)	aSLE (n = 728)	*P* value
Age at SLE diagnosis, median (IQR), y	17.7 (14–30.9)	14.1 (11.8–15.8)	31.2 (24.7–42)	
Female, n (%)	1,306 (88)	646 (85)	660 (91)	9×10^{-5}
Ancestry, n (%)				1.94×10^{-22}
European	576 (39)	279 (37)	297 (41)	
East Asian	278 (19)	163 (21)	115 (16)	
African	232 (16)	88 (12)	144 (20)	
South Asian	87 (6)	43 (6)	44 (6)	
Amerindian	63 (4)	38 (5)	25 (3)	
Admixed	253 (17)	150 (20)	103 (14)	
SLE features, n (%)				
Mucocutaneous	1,256 (85)	652 (86)	604 (83)	0.34
Hematologic	1,170 (79)	613 (81)	557 (77)	0.18
Musculoskeletal	1,101 (74)	534 (70)	567 (78)	0.003
Renal	634 (43)	328 (43)	306 (42)	0.72
Serositis	403 (27)	159 (21)	244 (34)	2.62×10^{-6}
Neuropsychiatric	221 (15)	143 (19)	78 (11)	2.9×10^{-5}
Low C3 and/or C4	836 (64)[a]	425 (62)[a]	411 (66)[a]	0.003
ANA	1,457 (98)	745 (98)	712 (98)	0.82
Follow-up time, median (IQR), y	9.2 (4.7–16.5)	6.8 (3.7–12.7)	12.2 (6.6–20.4)	2.81×10^{-244}

* ANA, antinuclear antibody; aSLE, adult-onset systemic lupus erythematosus; cSLE, childhood-onset systemic lupus erythematosus; IQR, interquartile range; SLE, systemic lupus erythematosus.
[a] Hypocomplementemia data were available for 1,310 patients in the total cohort, 688 in the cSLE group and 622 in the aSLE group.

differed between patients with cSLE and patients with aSLE ($P = 1.9 \times 10^{-22}$; Table 1). There was a larger proportion of patients with East Asian (21%) and Admixed Admixed (20%) ancestries in the cSLE cohort compared to the adult group (16% East Asian and 14% Admixed ancestries), whereas the aSLE cohort had a higher proportion of patients with African ancestry (20%) than the cSLE cohort (12%).

Regarding SLE features, neuropsychiatric involvement was more prevalent in the cSLE group compared to the aSLE group (19% vs 11%, $P = 2.9 \times 10^{-5}$). Serositis was more prevalent in aSLE compared with cSLE (34% vs 21%, $P = 2.62 \times 10^{-6}$), as was hypocomplementemia (66% in aSLE vs 51% in cSLE, $P = 0.003$) and musculoskeletal involvement (78% in aSLE vs 70% in cSLE, $P = 0.003$). The median follow-up time was 9.2 years (IQR 4.7–16.5 years) for the total cohort, 6.8 years (IQR 3.7–12.7 years) for the cSLE group, and 12.2 years (IQR 6.6–20.4 years) for the aSLE group (Table 1).

Analysis of the 142 non-HLA risk loci for SLE by age at diagnosis identified rs2550333, intronic to coiled-coil domain containing 113 (*CCDC113*) (chr.16), as significantly associated with age of lupus diagnosis ($\beta = -0.12$, SE = 0.03, $P = 6.3 \times 10^{-6}$, risk allele frequency [RAF] = 0.25). Similarly, rs2550333 was significantly associated with increased odds of developing cSLE as opposed to developing SLE as an adult (odds ratio [OR] 1.50 [95% confidence interval (CI) 1.12–1.83], $P = 1.85 \times 10^{-5}$). When stratified by age group, RAF was greater in those diagnosed at younger ages ($P = 4.95 \times 10^{-10}$, Figure 1 and Figure S2). However, there was no evidence for different SNP rs2550333 effect on age at diagnosis when stratified by those diagnosed at <18 years and at ≥18 years (*P* heterogeneity [het] = 0.31). When we tested the RAF by age category stratified by ancestry, we only observed a significantly greater prevalence at young ages for the Admixed population (Admixed $P = 5.94 \times 10^{-4}$; East Asian $P = 0.013$; European $P = 0.041$; American $P = 0.17$; South Asian $P = 0.44$; African $P = 0.77$) (Figure S2).

Genome-wide testing of loci for age of diagnosis (6.8 million SNPs) identified an additional *CCDC113* SNP in high linkage

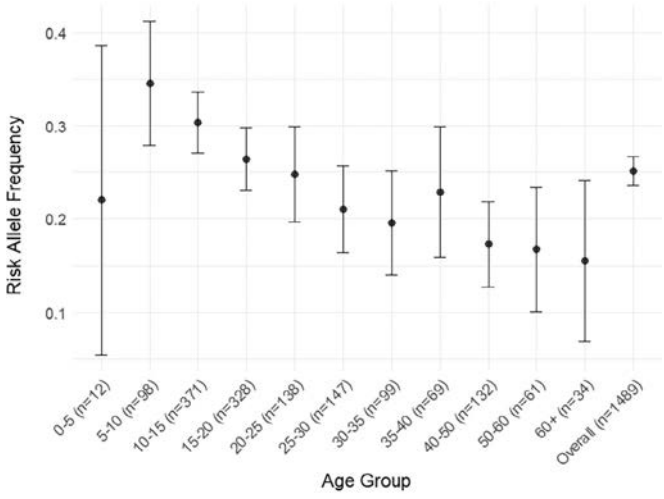

Figure 1. *CCDC113* risk allele rs2550333 frequency by age of systemic lupus erythematosus (SLE) diagnosis. The risk allele frequency (y-axis) is plotted for each age group (x-axis) of SLE diagnosis. The dots represent the mean and the whiskers represent the confidence intervals of SDs.

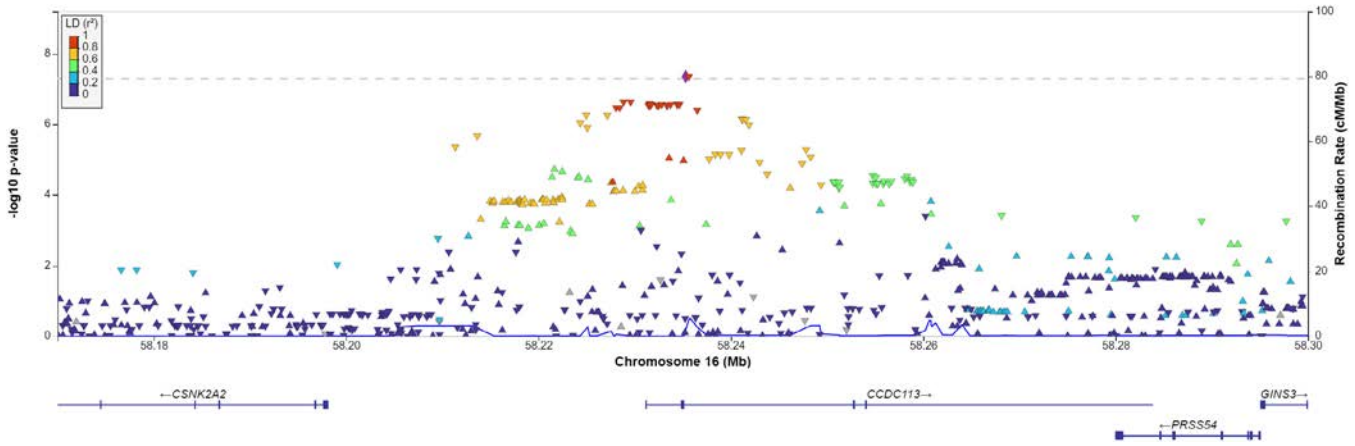

Figure 2. Locus plot of top single nucleotide polymorphisms (SNPs) on chr. 16 on log-transformed age of systemic lupus erythematosus (SLE) diagnosis, in multivariate models adjusted for sex and five principal components. The index SNP is in high linkage disequilibrium (LD) with rs2550333 (D' 0.99, r^2 0.8). The locus plot represents a zoomed-in plot of *P* values for analyses of age of SLE diagnosis in which each triangle/circle represents an SNP, and the diamond represents the index SNP (rs11641349), which is in high LD with rs2550333. The area of focus in the locus plot is 0.12 Mb upstream and downstream the genome-wide significant SNP for age of SLE diagnosis is on chr.16.

disequilibrium (LD) with rs2550333, with a stronger effect on age of diagnosis (rs11641349 [r^2 = 0.8, D' = 0.99]: effect allele C [RAF = 0.20], β = –0.15, SE = 0.03, $P = 3.32 \times 10^{-8}$) (Figure 2). Sensitivity analyses stratified by sex and ancestry and meta-analyzed showed similar results. The RAF of rs2550333 was higher in the East Asian population (RAF = 0.46) and Admixed (RAF = 0.28) compared to European (RAF = 0.15; $P = 9.2 \times 10^{-47}$). Yet, there was no significant difference of the effect of rs2550333 on age at diagnosis between ancestral groups (*P* het = 0.92). In sex-stratified analyses, although the RAF was similar in females (RAF = 0.25) and males (RAF = 0.25; *P* = 0.86), the SNP had a significantly greater effect on age of diagnosis among males (β = –0.30, SE = 0.07, $P = 2.56 \times 10^{-6}$) compared with females (β = –0.12, SE = 0.03, $P = 1.17 \times 10^{-6}$, *P* het = 0.014) (Figure S3). When we added the non-HLA SLE PRS as covariate to the analyses, results were similar. We also specifically investigated the association between rs2550333 and the SNPs on chr.16 included in the PRS, and found they were not correlated. Analysis of the X chromosome did not identify SNPs for age at SLE diagnosis. Analysis of the 166 HLA SLE-risk alleles and HLA-wide analyses did not identify associations with age of diagnosis or with cSLE (vs aSLE).

LocusFocus analysis of the chr.16 top SNP region, with OneK1K[25] as reference (Bonferroni corrected $P < 2.2 \times 10^{-4}$, Supplemental Methods), identified significant differential *CSNK2A2* expression in $CD8^+$ T effective memory (TEM) cells ($P = 2.7 \times 10^{-7}$) and in natural killer (NK) cells ($P = 6.2 \times 10^{-6}$) (Figure S4). Repeated LocusFocus analyses using single-cell sequencing data from a cohort of 162 patients with SLE[26] did not identify significant associated gene expression changes.

The non-HLA SLE PRS was significantly associated with younger age at diagnosis in the univariate model (β = –0.09, SE = 0.02, $P = 1.84 \times 10^{-6}$), and multivariable adjusted model (β = –0.09, SE = 0.02, $P = 3.63 \times 10^{-10}$). Similarly, the non-HLA SLE PRS was significantly associated with cSLE in both univariate (OR 1.38 [95% CI 1.2–1.59], $P = 3.7 \times 10^{-6}$) and multivariable adjusted models (OR 1.33 [95% CI 1.15–1.54], $P = 1.75 \times 10^{-4}$) (Supplemental Results and Figure S5).

Regression of HLA SLE PRS and age of SLE diagnosis showed a significant positive association in the total cohort in the univariate model (β = 0.06, SE = 0.02, *P* = 0.02) and the multivariable adjusted model (β = 0.04, SE = 0.02, *P* = 0.04). Yet, there was no significant association between HLA SLE PRS and cSLE in the total cohort (univariate analysis *P* = 0.09, multivariate analysis *P* = 0.48) (Supplemental Results). The joint analysis of non-HLA and HLA SLE PRS demonstrated similar results to the independent analyses, suggesting that their associations with age of SLE diagnosis are independent of one another.

Table 2. Demographics of patients with cSLE and participants without SLE included in the cSLE risk analysis*

Characteristics	cSLE (n = 346)	Spit for Science (n = 4,080)
Female, n (%)	287 (83)	1,993 (49)
Ancestry, n (%)		
European	199 (58)	3,671 (90)
East Asian	147 (42)	409 (10)
Age at SLE diagnosis or enrollment, median (IQR), y		
European	14.3 (12–16.1)	10.7 (8.8–13.1)
East Asian	14.3 (12–16.1)	11.8 (9.4–13.3)

* cSLE, childhood-onset systemic lupus erythematosus; IQR, interquartile range; SLE, systemic lupus erythematosus.

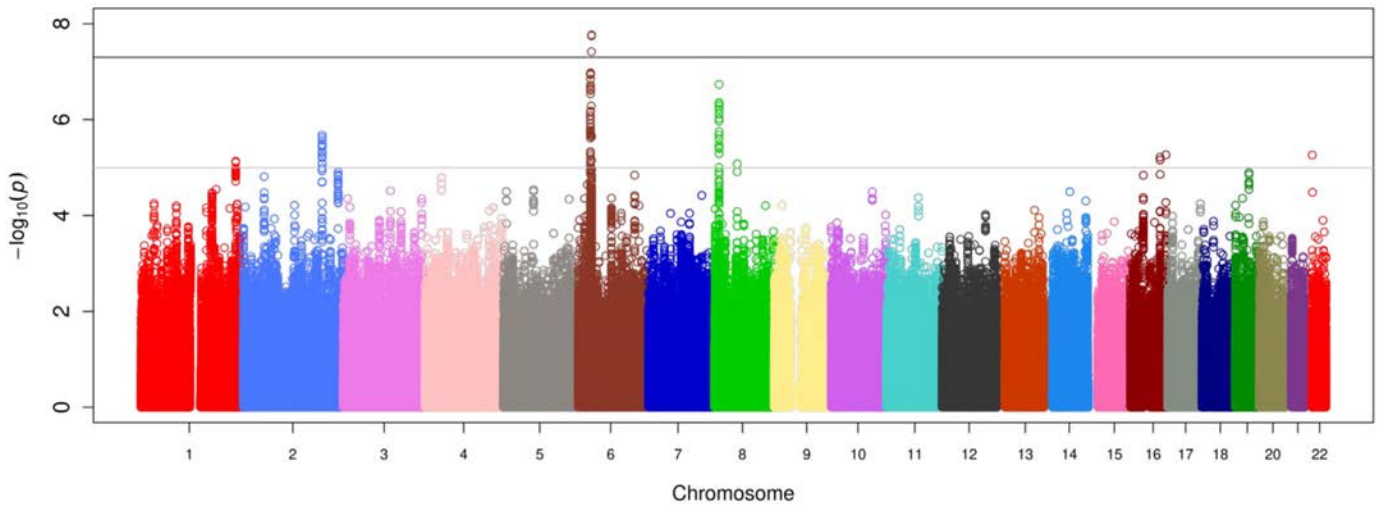

Figure 3. Manhattan plot of meta–genome-wide association studies of childhood-onset systemic lupus erythematosus (cSLE) risk (patients with cSLE vs healthy controls), in European and East Asian populations adjusted for including covariates for sex and three principal components (PCs). There is a genome-wide significant peak on chr. 6. Each circle on the Manhattan plot represents a single nucleotide polymorphism (SNP). The gray line represents marginal significance ($P < 5 \times 10^{-5}$) and the black line represents genome-wide significance ($P < 5 \times 10^{-8}$). The genome-wide significant SNP for cSLE risk is on chr. 6. Color figure can be viewed in the online issue, which is available at http://onlinelibrary.wiley.com/doi/10.1002/art.43227/abstract.

cSLE GWAS. The cSLE GWAS included 4,426 participants, 346 with cSLE, 3,870 (87%) of European ancestry (199 [5%] cSLE, and 3,671 [95%] non-SLE group), and 556 (13%) of East Asian ancestry (147 [26%] cSLE, and 409 [74%] non-SLE group) (Table 2). We included 4.9 million SNPs in the European cohort analysis (lambda genomic control [λgc] = 1.02), and 4.7 million SNPs in the East Asian cohort analysis (λgc = 1.02). The meta-GWAS included 3.8 million overlapping SNPs (λgc = 0.997). Multiple SNPs on chr. 6 reached genome-wide significance, the most significant being rs139299944, intronic to *HLA-DQA1* (OR 1.68 [95% CI 1.41–2.01], $P = 1.71 \times 10^{-8}$), and rs9268469, intronic to gene *TSBP1-AS1* (OR 2.04 [95% CI 1.59–2.63], $P = 1.79 \times 10^{-8}$) (Figure 3). Outside of chr. 6, rs2736336 on chr. 8 (upstream to B-lymphoid tyrosine kinase [*BLK*]) was the most significant SNP associated with cSLE, although it did not reach genome-wide significance (OR 1.69 [95% CI 1.39–2.04], $P = 4.45 \times 10^{-7}$) (Figure S6). GWAS stratified by ancestry identified a significant signal in chr. 16 in the European population (rs1143679, OR 3.67 [95% CI 2.58–5.22], $P = 1.75 \times 10^{-13}$) (Figure S7a). This SNP is intronic to *ITGAM* (MAF = 0.13). This SNP was not present in the East Asian population (Figure S7b) and therefore was not included in the meta-GWAS (Figure 3). In order to analyze the relationship of this locus with age at SLE diagnosis, we ran a regression analysis of this SNP by log-transformed age at diagnosis in our cSLE and aSLE cohort (n = 1,489). Although it was associated with younger age at diagnosis, it did not reach our threshold of significance ($P < 2 \times 10^{-4}$; β = –0.1, SE = 0.04, $P = 7.12 \times 10^{-4}$). Analysis of X chr. did not identify a significant locus for cSLE.

When we ran the 4-digit resolution HLA-wide meta-analysis of cSLE in European and East Asian populations, we did not identify genome-wide significant alleles (Supplemental Results and Table S2).

Testing the top chr. 6 locus from meta-GWAS in LocusFocus identified significant colocalization for gene expression (Bonferroni corrected $P < 2.2 \times 10^{-4}$) of *HLA-DRB5* in B lymphocytes ($P = 2.2 \times 10^{-6}$) and classic dendritic cells (cDCs) ($P = 1.3 \times 10^{-5}$) when using data from the cohort of patients with SLE (Figure S8). Analyses using OneK1K as reference did not identify significant gene expression changes.

The non-HLA PRS analysis showed a significant association with cSLE in multivariable adjusted models in both European (OR 2.19 [95% CI 1.86–2.59], $P = 6.99 \times 10^{-21}$) and East Asian groups (OR 2.06 [95% CI 1.49–2.86], $P = 1.4 \times 10^{-5}$), as well as in the meta-analysis (OR 2.17 [95% CI 1.87–2.51], $P = 5.48 \times 10^{-25}$). A total of 25 of the 39 non-HLA SNPs were significantly associated with cSLE (Table S3).

The multivariate HLA PRS logistic regression showed a significant association with cSLE risk in the European group (OR 2.27 [95% CI 1.67–3.08], $P = 1.56 \times 10^{-6}$) and in the total cohort (OR 1.81 [95% CI 1.42–2.32], $P = 2.03 \times 10^{-6}$). Yet, it was not significant in the East Asian groups (OR 1.46 [95% CI 0.92–2.33], $P = 0.11$). The HLA allele *DQA1*01:02*, the top SNP of the cSLE-risk GWAS, was included in the SLE HLA PRS (Table S4).

DISCUSSION

We tested known HLA and non-HLA SLE-risk loci for association with age of SLE diagnosis in a multiancestral cohort of

children and adults with SLE and identified a locus intronic to *CCDC113* significantly associated with younger age at SLE diagnosis. Colocalization testing demonstrated significant association with *CSNK2A2* expression in CD8$^+$TEM and NK cells. We also completed a GWAS of cSLE in European and East Asian children and adolescents. We identified a chr.6 SNP for cSLE, intronic to *TSBP1-AS1* and a *HLA-DQA1* allele previously identified for aSLE.[31–35] Colocalization testing showed a significant association with the expression of *HLA-DRB5* in B and cDC cells. Our findings highlight shared HLA susceptibility loci for SLE in children and adults, as well as novel locus for younger age at SLE diagnosis.

Our cohort study included a large, multiancestral cSLE and aSLE population genotyped with access to detailed phenotypic data that are rarely available for larger cohorts, including age at diagnosis and clinical SLE features. In our study cohort, age at diagnosis had a bimodal distribution consistent with previous studies, with a median of 14.1 years (IQR 11.8–15.8 years) in the cSLE group and 31.2 years (IQR 24.7–42 years) in the aSLE group (Table 1 and Figure S1).[36,37] We tested different thresholds of age of diagnosis to define cSLE and chose 18 years because it was the median age of diagnosis in the total cohort and is a commonly used definition for cSLE.[20] Comparison of ancestry distribution in cSLE and aSLE cohorts demonstrated a higher prevalence of East Asian and Admixed patients in the cSLE cohort and African ancestry patients in the aSLE cohort. These differences reflect the ancestral differences between contributing cohorts to the study.

Clinical features of our cSLE and aSLE cohorts were similar to those reported in the literature.[36,38] The cSLE group had a higher prevalence of neuropsychiatric involvement compared to adults, and the aSLE group had a higher prevalence of musculoskeletal involvement and serositis. Contrary to previous studies, we did not see a significantly higher proportion of renal and hematologic features in cSLE compared to aSLE. Follow-up time in the aSLE group was significantly longer compared to the cSLE group. This may impact the observed prevalence of clinical features, as a longer follow-up could lead to a higher prevalence of features.

We identified SNP rs2550333 on chr. 16 as the sole locus associated with younger age at SLE diagnosis, and with risk of cSLE compared to aSLE, from more than 300 SLE-risk loci tested. In a previous SLE GWAS, rs2550333 was associated with SLE in the Hispanic American cohort (OR 1.28 [95% CI 1.16–1.41], $P = 9.52 \times 10^{-7}$), but not in the total cohort[4] (OR 1.13 [95% CI 1.07–1.18], $P = 2.58 \times 10^{-6}$). In our ancestry-stratified analyses, the RAF of SNP rs2550333 was higher in East Asian and Admixed ancestral groups compared with those of European ancestry (East Asian 0.46 and Admixed 0.28 vs European 0.15 [$P = 9.2 \times 10^{-47}$]). Although there was variation in RAF across ancestries, sensitivity analyses demonstrated no significant difference in allelic effect on age of diagnosis by ancestry. When stratifying the RAF by age groups of SLE diagnosis, there was a greater prevalence of the RAF in younger age at diagnosis. We also observed that rs2550333 had a greater effect on younger age at diagnosis among males compared to females. It is unclear the mechanism by which rs2550333 has a stronger effect on age of diagnosis among males.

CCDC113, encodes a component of centriolar satellites, a protein highly expressed in organs containing cells that assemble motile cilia.[39] Colocalization testing of our GWAS results identified significantly increased expression of one gene proximal to *CCDC113: CSNK2A2* in CD8$^+$TEM and NK cells. *CSNK2A2*, mainly expressed in EBV–transformed lymphocytes, encodes the ubiquitous enzyme CK2, serine/threonine kinase that plays an important role in the JAK-STAT activation.[40] A variant in *CSNK2A2* (rs2731783) was associated with SLE risk in a large Chinese and European GWAS.[41] When the authors applied a fine-mapping algorithm, two LD linked variants residing in a lymphoblastoid cell line were identified upstream of *CSNK2A2* and *CCDC113*. These variants were in the enhancer region of *CSNK2A2* and were associated with reduced expression of both genes in B lymphocytes.[41]

The HLA-wide analysis did not identify significant alleles for age at SLE diagnosis. This may in part be due to limited power with highly polymorphic regions such as HLA.

We completed a meta-GWAS of cSLE in European and East Asian populations and identified an SNP (rs9268469) intronic to gene *TSBP1-AS1*, located in the major histocompatibility complex region. *TSPB1-AS1* is a long noncoding RNA gene, identified as a putative pleiotropic gene shared by immune and skeletal diseases.[42] Colocalization studies demonstrated a significant association with differential *HLA-DRB5* expression in B and cDCs. Previous studies have implicated *HLA-DRB5* alleles for SLE,[43] with recent single-cell gene expression studies similarly linking differential expression with SLE.[44]

The meta-GWAS also identified a marginally significant SNP upstream of *BLK*, which encodes a tyrosine kinase of the SRC family. Previous studies demonstrated a significant association of variants in BLK with several autoimmune disorders,[45,46] including SLE.[45,47] This allele did not reach significance in our study, likely due to our modest cSLE sample size compared to aSLE GWASs, yet, this underlines the genetic similarity between cSLE and aSLE. GWAS of cSLE in the European ancestry group identified a significant SNP rs1143679, intronic to *ITGAM*. However, this SNP was not significant in the cSLE GWAS among people of East Asian ancestry or meta-GWASs. This may reflect reduced power for discovery in the East Asian cohort compared to the European cohort. However, it may also represent a European-specific risk SNP, as the frequency in East Asian populations is much lower compared to European populations (11% vs 0.2%) (gnomADv4.1.0).

We also identified *HLA-DQA1* for cSLE compared to population-based controls without SLE. The top loci from HLA-wide analysis, *HLA-DQA1*01:02*, *HLA-DRB1*15* as cSLE risk alleles, and *HLA-DQB1*03:01* as a protective allele, did not reach genome-wide significance, potentially due to lower frequency of

these variants in the polymorphic region of the genome. The non-HLA SLE PRS was significantly associated with cSLE risk in both European and East Asian cohorts. However, the HLA SLE PRS was associated with cSLE only in the European and total cohorts. This may be due to the limited East Asian sample size and missing East Asian–specific HLA alleles for SLE.

We acknowledge some limitations of the study. In our multiancestral cohort, some ancestral groups were limited in size, particularly for the cSLE cohort. However, our study represents the largest cSLE cohort genotyped to date. Age at diagnosis was our main outcome, rather than age at disease onset, arguably the outcome of biologic interest. However, age at onset was not consistently documented by each cohort and is susceptible to recall bias. The use of age at SLE diagnosis enabled harmonization across collaborating sites. When testing for age thresholds defining cSLE, age <18 years corresponded to the median age of diagnosis in our cohort. Although this cSLE age definition is commonly used,[20] our findings may be specific to our cohort and require replication. We applied a primarily European-derived PRS to populations that are not European,[48] thereby excluding SLE-risk SNPs of populations that are not European. However, this would lead to reduced power to detect an association and was unlikely to induce spurious associations. For the cSLE GWAS, we harmonized array data by restricting to SNPs genotyped on both the MEGA and HCE arrays before imputation. This may have resulted in exclusion of variants that were not in high LD with genotyped SNPs. Conversely, we are confident that our cSLE GWAS findings do not reflect technical artifact. Chr. X analyses used a genetic dominance model, adjusted for sex[22] rather than a sex-stratified analysis. We chose the dominance model because there was an expected predominance of females compared to males, and this approach has been demonstrated to be robust against false inferences. We acknowledge we may have missed significant chr. Y signals due to the relatively smaller number of males, which also precluded analysis of chr. Y. Regarding the colocalization analyses, LocusFocus was run using data from the OneK1K cohort, of predominantly people of Northern European ancestry without SLE. Analyses run using single-cell RNAseq referent data from patients with SLE[26] demonstrated significant differential gene expression for *HLA-DRB5* only. Future studies using gene expression from larger cohorts of people with SLE may yield different results.

Our study had a number of strengths. We completed a genome-wide, multiethnic study of both age at SLE diagnosis and cSLE risk. To our knowledge, this is the largest cohort of children and adolescents with SLE included in a GWAS to date. We also completed a comprehensive study of age at SLE diagnosis and cSLE including both non-HLA and HLA loci along with detailed phenotypic data. Colocalization analyses of SNP associations from our top locus for age at SLE diagnosis and cSLE risk with gene expression data led to identification of expression quantitative trait loci as a first step toward elucidating the causal mechanisms by which the locus affects age at SLE diagnosis.

In conclusion, we found a significant locus for younger age at SLE diagnosis, on chr. 16, intronic to *CCDC113*, with significant colocalization for differential expression of *CSNK2A2* in $CD8^{+}$TEM and NK cells. The first GWAS for cSLE identified a locus intronic to *TSPB1-AS1*, not previously reported for aSLE, with significant colocalization for *HLA-DRB5* differential expression in B cells and cDCs, and a previously identified HLA risk allele. Our study highlights the genetic similarities and differences between cSLE and aSLE.

ACKNOWLEDGMENTS

We thank the families and children who participated in the SLE cohort studies and the Ontario Science Centre for their collaboration and support.

AUTHOR CONTRIBUTIONS

All authors contributed to at least one of the following manuscript preparation roles: conceptualization AND/OR methodology, software, investigation, formal analysis, data curation, visualization, and validation AND drafting or reviewing/editing the final draft. As corresponding author, Dr Hiraki confirms that all authors have provided the final approval of the version to be published and takes responsibility for the affirmations regarding article submission (eg, not under consideration by another journal), the integrity of the data presented, and the statements regarding compliance with institutional review board/Declaration of Helsinki requirements.

REFERENCES

1. Woo JMP, Parks CG, Jacobsen S, et al. The role of environmental exposures and gene-environment interactions in the etiology of systemic lupus erythematous. J Intern Med 2022;291(6):755–778.
2. Lawrence JS, Martins CL, Drake GL. A family survey of lupus erythematosus. 1. Heritability. J Rheumatol 1987;14(5):913–921.
3. Alarcón-Segovia D, Alarcón-Riquelme ME, Cardiel MH, et al; Grupo Latinoamericano de Estudio del Lupus Eritematoso (GLADEL). Familial aggregation of systemic lupus erythematosus, rheumatoid arthritis, and other autoimmune diseases in 1,177 lupus patients from the GLADEL cohort. Arthritis Rheum 2005;52(4):1138–1147.
4. Langefeld CD, Ainsworth HC, Cunninghame Graham DS, et al. Transancestral mapping and genetic load in systemic lupus erythematosus. Nat Commun 2017;8(1):16021.
5. Bentham J, Morris DL, Graham DSC, et al. Genetic association analyses implicate aberrant regulation of innate and adaptive immunity genes in the pathogenesis of systemic lupus erythematosus. Nat Genet 2015;47(12):1457–1464.
6. Yin X, Kim K, Suetsugu H, et al; Japanese Research Committee on Idiopathic Osteonecrosis of the Femoral Head. Meta-analysis of 208370 East Asians identifies 113 susceptibility loci for systemic lupus erythematosus. Ann Rheum Dis 2021;80(5):632–640.
7. Morris DL, Sheng Y, Zhang Y, et al. Genome-wide association meta-analysis in Chinese and European individuals identifies ten new loci associated with systemic lupus erythematosus. Nat Genet 2016;48(8):940–946.
8. Sun C, Molineros JE, Looger LL, et al. High-density genotyping of immune-related loci identifies new SLE risk variants in individuals with Asian ancestry. Nat Genet 2016;48(3):323–330.
9. Webb R, Kelly JA, Somers EC, et al. Early disease onset is predicted by a higher genetic risk for lupus and is associated with a more severe phenotype in lupus patients. Ann Rheum Dis 2011;70(1):151–156.

10. Dominguez D, Kamphuis S, Beyene J, et al; Canadian Network for Improved Outcomes in SLE (CaNIOS) and APPLE Investigators. Relationship between genetic risk and age of diagnosis in systemic lupus erythematosus. J Rheumatol 2021;48(6):852–858.
11. Kwon YC, Ha E, Kwon HH, et al. Higher genetic risk loads confer more diverse manifestations and higher risk of lupus nephritis in systemic lupus erythematosus. Arthritis Rheumatol 2023;75(9):1566–1572.
12. Tan EM, Cohen AS, Fries JF, et al. The 1982 revised criteria for the classification of systemic lupus erythematosus. Arthritis Rheum 1982;25(11):1271–1277.
13. Hochberg MC. Updating the American College of Rheumatology revised criteria for the classification of systemic lupus erythematosus. Arthritis Rheum 1997;40(9):1725.
14. Petri M, Orbai AM, Alarcón GS, et al. Derivation and validation of the Systemic Lupus International Collaborating Clinics classification criteria for systemic lupus erythematosus. Arthritis Rheum 2012;64(8): 2677–2686.
15. Conomos MP, Miller MB, Thornton TA. Robust inference of population structure for ancestry prediction and correction of stratification in the presence of relatedness. Genet Epidemiol 2015;39(4):276–293.
16. Jia X, Han B, Onengut-Gumuscu S, et al. Imputing amino acid polymorphisms in human leukocyte antigens. PLoS One 2013;8(6):e64683.
17. Luo Y, Kanai M, Choi W, et al; NHLBI Trans-Omics for Precision Medicine (TOPMed) Consortium. A high-resolution HLA reference panel capturing global population diversity enables multi-ancestry fine-mapping in HIV host response. Nat Genet 2021;53(10):1504–1516.
18. Abecasis GR, Altshuler D, Auton A, et al; 1000 Genomes Project Consortium. A map of human genome variation from population-scale sequencing. Nature 2010;467(7319):1061–1073.
19. Hiraki LT, Benseler SM, Tyrrell PN, et al. Clinical and laboratory characteristics and long-term outcome of pediatric systemic lupus erythematosus: a longitudinal study. J Pediatr 2008;152(4):550–556.
20. Silva CA, Avcin T, Brunner HI, et al. Taxonomy for systemic lupus erythematosus with onset before adulthood. Arthritis Care Res (Hoboken) 2012;64(12):1787–1793.
21. Gogarten SM, Sofer T, Chen H, et al. Genetic association testing using the GENESIS R/Bioconductor package. Bioinformatics 2019; 35(24):5346–5348.
22. Chen B, Craiu RV, Strug LJ, et al. The X factor: A robust and powerful approach to X-chromosome-inclusive whole-genome association studies. Genet Epidemiol 2021;45(7):694–709.
23. Willer CJ, Li Y, Abecasis GR. METAL: fast and efficient meta-analysis of genomewide association scans. Bioinformatics 2010;26(17): 2190–2191.
24. Panjwani N, Wang F, Mastromatteo S, et al. LocusFocus: web-based colocalization for the annotation and functional follow-up of GWAS. PLoS Comput Biol 2020;16(10):e1008336.
25. Yazar S, Alquicira-Hernandez J, Wing K, et al. Single-cell eQTL mapping identifies cell type-specific genetic control of autoimmune disease. Science 2022;376(6589):eabf3041.
26. Perez RK, Gordon MG, Subramaniam M, et al. Single-cell RNA-seq reveals cell type-specific molecular and genetic associations to lupus. Science 2022;376(6589):eabf1970.
27. Crosbie J, Arnold P, Paterson A, et al. Response inhibition and ADHD traits: correlates and heritability in a community sample. J Abnorm Child Psychol 2013;41(3):497–507.
28. Burton CL, Wright L, Shan J, et al. SWAN scale for ADHD trait-based genetic research: a validity and polygenic risk study. J Child Psychol Psychiatry 2019;60(9):988–997.
29. McCarthy S, Das S, Kretzschmar W, et al; Haplotype Reference Consortium. A reference panel of 64,976 haplotypes for genotype imputation. Nat Genet 2016;48(10):1279–1283.
30. Zhou W, Nielsen JB, Fritsche LG, et al. Efficiently controlling for case-control imbalance and sample relatedness in large-scale genetic association studies. Nat Genet 2018;50(9):1335–1341.
31. Hanscombe KB, Morris DL, Noble JA, et al. Genetic fine mapping of systemic lupus erythematosus MHC associations in Europeans and African Americans. Hum Mol Genet 2018;27(21):3813–3824.
32. Hernández-Doño S, Jakez-Ocampo J, Márquez-García JE, et al. Heterogeneity of genetic admixture determines SLE susceptibility in Mexican. Front Genet 2021;12:701373.
33. Molineros JE, Looger LL, Kim K, et al. Amino acid signatures of HLA class-I and II molecules are strongly associated with SLE susceptibility and autoantibody production in Eastern Asians. PLoS Genet 2019; 15(4):e1008092.
34. Morris DL, Taylor KE, Fernando MM, et al; International MHC and Autoimmunity Genetics Network; Systemic Lupus Erythematosus Genetics Consortium. Unraveling multiple MHC gene associations with systemic lupus erythematosus: model choice indicates a role for HLA alleles and non-HLA genes in Europeans. Am J Hum Genet 2012;91(5):778–793.
35. Miglioranza Scavuzzi B, van Drongelen V, Kaur B, et al. The lupus susceptibility allele DRB1*03:01 encodes a disease-driving epitope. Commun Biol 2022;5(1):751.
36. Brunner HI, Gladman DD, Ibañez D, et al. Difference in disease features between childhood-onset and adult-onset systemic lupus erythematosus. Arthritis Rheum 2008;58(2):556–562.
37. Rees F, Doherty M, Grainge MJ, et al. The worldwide incidence and prevalence of systemic lupus erythematosus: a systematic review of epidemiological studies. Rheumatology (Oxford) 2017;56(11):1945–1961.
38. Kamphuis S, Silverman ED. Prevalence and burden of pediatric-onset systemic lupus erythematosus. Nat Rev Rheumatol 2010;6(9): 538–546.
39. Bazan R, Schröfel A, Joachimiak E, et al. Ccdc113/Ccdc96 complex, a novel regulator of ciliary beating that connects radial spoke 3 to dynein g and the nexin link. PLoS Genet 2021;17(3):e1009388.
40. Zheng Y, Qin H, Frank SJ, et al. A CK2-dependent mechanism for activation of the JAK-STAT signaling pathway. Blood 2011;118(1): 156–166.
41. Wang YF, Zhang Y, Zhu Z, et al. Identification of ST3AGL4, MFHAS1, CSNK2A2 and CD226 as loci associated with systemic lupus erythematosus (SLE) and evaluation of SLE genetics in drug repositioning. Ann Rheum Dis 2018;77(7):1078–1084.
42. He P, Cao RR, Deng FY, et al. Identification of potential pleiotropic genes for immune and skeletal diseases using multivariate metaCCA analysis. Curr Genomics 2021;22(8):596–606.
43. Laurynenka V, Harley JB. The 330 risk loci known for systemic lupus erythematosus (SLE): a review. Front Lupus 2024;2:1398035.
44. Guo Q, Fan YN, Xie M, et al. Exploring the transcriptomic landscape of moyamoya disease and systemic lupus erythematosus: insights into cross-talk genes and immune relationships. Front Immunol 2024;15:1456392.
45. Delgado-Vega AM, Dozmorov MG, Quirós MB, et al. Fine mapping and conditional analysis identify a new mutation in the autoimmunity susceptibility gene BLK that leads to reduced half-life of the BLK protein. Ann Rheum Dis 2012;71(7):1219–1226.
46. Zuo XB, Sheng YJ, Hu SJ, et al. Variants in TNFSF4, TNFAIP3, TNIP1, BLK, SLC15A4 and UBE2L3 interact to confer risk of systemic lupus erythematosus in Chinese population. Rheumatol Int 2014;34(4):459–464.
47. Guthridge JM, Lu R, Sun H, et al. Two functional lupus-associated BLK promoter variants control cell-type- and developmental-stage-specific transcription. Am J Hum Genet 2014;94(4):586–598.
48. Martin AR, Kanai M, Kamatani Y, et al. Clinical use of current polygenic risk scores may exacerbate health disparities. Nat Genet 2019;51(4): 584–591.

Arthritis & Rheumatology
Vol. 77, No. 11, November 2025, pp 1533–1547
DOI 10.1002/art.43235

Activin A–Activated ALK4 Induces Pathogenic Th17-Involved Endothelial–Mesenchymal Transition in Systemic Lupus Erythematosus–Associated Pulmonary Arterial Hypertension

Shuliang Jing,[1] Junyan Qian,[2] Hongjie Ying,[1] Pei Mao,[1] Mingxin Yao,[1] Zhihong Wu,[3] Harm J. Bogaard,[4] Lie Wang,[5] Mengtao Li,[2] and Jun Yang[6]

Objective. Autoimmune diseases, such as systemic lupus erythematosus (SLE), are associated with pulmonary arterial hypertension (PAH), a condition that can lead to heart failure. However, whether T cells also contribute to the occurrence of PAH in SLE has not been clarified. The objective of this study was to elucidate the role of Activin A and activated receptor signaling in SLE-PAH.

Methods. Mass Cytometry (CyTOF) analysis was performed to identify the major affected immune cell population in patients with SLE-PAH. Serum Activin A and interleukin-17 (IL-17) levels in patients with SLE-PAH, patients with SLE, and healthy donors were determined by enzyme-linked immunosorbent assay. Cocultures of Th17 cells with pulmonary microvascular endothelial cells (PMECs) and relevant rodent models were used to identify the converged target.

Results. The reduced $CD4^+$ T cell number was detected in patients with SLE-PAH after treatment with immunosuppressant and vasodilator. Increased Th17 cells population and higher serum Activin A and IL-17 levels were found in patients with SLE-PAH compared to patients with SLE only or donors. Activin A signals via activin receptor–like kinase 4 (ALK4) in both Th17 cells and PMECs. Overexpressing ALK4 in Th17 cells increased IL-6 and endothelial–mesenchymal transition (EndoMT) marker levels in cocultured PMECs. We found severe SLE–pulmonary hypertension (PH) in mice by overexpressing ALK4, and alleviated hemodynamic changes in $CD4^+$ T cells depletion mice. ALK4 inhibitor vactosertib (TEW-7197) effectively treated SLE-PH mice by repressing connective tissue growth factor (*CTGF*) transcription, which was induced by ALK4 activated pSmad2 and pSTAT3.

Conclusion. Our findings suggest that Activin A activates ALK4 in Th17 cells, thereby inducing IL-17 secretion. Concurrently, activated ALK4 induces EndoMT in human PMECs (hPMECs) via CTGF up-regulation. It suggests that ALK4 is a promising therapeutic target for SLE-PAH.

INTRODUCTION

Autoimmune diseases, including connective tissue disease (CTD), are strongly associated with the development of irreversible end-stage pulmonary arterial remodeling, leading to pulmonary arterial hypertension (PAH) (defined as a mean pulmonary artery pressure [mPAP] > 20 mm Hg) at rest.[1] Although CTD-PAH in White populations primarily relates to systemic sclerosis, systemic lupus erythematosus (SLE)–associated PAH is a more common form of CTD-PAH in Asian individuals.[1] Current treatments have yet to achieve complete cure for SLE-PAH, and the patients continue to face a challenged prognosis.[2,3] Therefore,

Supported by the National Fundation Science of China (grant 82470431), the National Key Research and Development Program of China (grants 2023YFC2507100, 2023YFC2507103, and 2021YFA1100500), and Beijing Nova Program of Peking Union Medical College Hospital Young Reserve Talent Development Program (UHB11839).

[1]Shuliang Jing, MD, Hongjie Ying, BS, Pei Mao, BS, Mingxin Yao, MS: Department of Physiology and Department of Cardiology, the Second Affiliated Hospital, Zhejiang University School of Medicine, Hangzhou China; [2]Junyan Qian, MD, Mengtao Li, MD: Department of Rheumatology, Peking Union Medical College Hospital, Beijing, China; [3]Zhihong Wu, MD: Stem Cell Facility of National Infrastructures for Translational Medicine, Institute of Clinical Medicine, Peking Union Medical College Hospital, Chinese Academy of Medical Sciences and Peking Union College, Beijing, China; [4]Harm J. Bogaard, MD, PhD: Department of Pulmonary Medicine, Amsterdam University Medical Center Vrije University, Amsterdam, The Netherlands; [5]Lie Wang, PhD: Department of Immunology, School of Basic Medical Sciences, Zhejiang University School of Medicine, Hangzhou, China; [6]Jun Yang, PhD: Department of Physiology, and Department of Cardiology of the Second Affiliated Hospital, Zhejiang University School of Medicine and State Key Laboratory of Transvascular Implantation Devices, Hangzhou, China.
Drs Jing and Qian are co-first authors and contributed equally to this work.

identifying molecular targets closely related to the progression of SLE-PAH is important for the development of interventions.

In patients with SLE, the presence of PAH coincides with significantly higher serum protein levels of interleukin-17 (IL-17).[4,5] IL-17 is primarily secreted by Th17 cells, which are a subtype of $CD4^+$ T cells associated with many inflammatory and autoimmune diseases. Transforming growth factor β (TGFβ) and IL-6 induce $CD4^+$ T cells differentiate to Th17 cells and secrete[6–8] IL-17. Pathogenic Th17 cells were also found to exacerbate local inflammation in an animal model of autoimmune encephalomyelitis.[7] However, further investigation is necessary to determine whether the induction of pathogenic Th17 cell differentiation is involved in SLE-PAH.

Mutations at members of the TGFβ family of receptors, including bone morphogenetic protein type II receptor (BMPR2) and activin receptor–like kinase 1 (ALK1), have been implicated in the development of idiopathic and heritable PAH.[9–11] BMPR2 plays a vital role in maintaining pulmonary vascular endothelial integrity.[12,13] In contrast, Activin A, another TGFβ family member, and its receptor ALK4/5 coordinately mediate the abnormal proliferation of pulmonary vascular endothelial cells, which is related to elevated pulmonary artery pressure.[14–17] Patients with PAH have increased Activin A levels in peripheral blood and elevated levels of proinflammatory cytokines[18–20] such as IL-6. Furthermore, on exposure of $CD4^+$ T cells to cytokines, such as IL-6, IL-1β, and IL-23, Activin A was up-regulated in $CD4^+$ T cells, and activated ALK4 in an autocrine manner to induce pathogenic Th17 cells.[7] Therefore, we hypothesized that ALK4 activation can induce pathogenic Th17 to produce IL-17 in SLE-PAH.

Current treatments for SLE-PAH include endothelin receptor antagonists, phosphodiesterase type 5 inhibitors, and prostacyclin analogs, which are often administered in combination. In 2023, a fourth potential therapy for PAH,[1] sotatercept, which is a recombinant human activin receptor type II A (ACTRIIA) fusion protein that acts as a ligand trap for Activin A, was introduced to rebalance growth-inhibiting BMPR2 signaling. It was reported to significantly decrease pulmonary vascular resistance in patients with PAH and improve their performance on a six-minute walk test.[21,22] However, whether this approach is effective for a broader population of patients with CTD, especially those with SLE-PAH, which has a high regional incidence rate, is still unclear. It suggests specific therapeutic strategies for CTD-PAH must be considered.

In this study, we used patient-derived blood samples, cell cocultures, and a rodent model of SLE–pulmonary hypertension (PH) to delineate the mechanism of Activin A–activated signaling in the inflamed pulmonary vasculature and to investigate the role of specific receptors in the pathogenic effects of Th17 cells involved in SLE-PAH. Our study revealed a significant reduction in the $CD4^+$ T cell population in the SLE-PAH (after treatment compared with before treatment) and confirmed the involvement of $CD4^+$ T cells in PH mice. Increased IL-17 and Activin A levels in the peripheral blood samples of patients with SLE-PAH promoted the activation of target genes such as connective tissue growth factor (CTGF) in human pulmonary microvascular endothelial cells (PMECs). More severe PH was developed by overexpressing ALK4 in pristane-induced mice exposed to hypoxia. We treated the mice with a novel ALK4 inhibitor, Vactosertib (small molecule TEW-7197, shorten as TEW), and found a significant improvement in hemodynamic indices and vascular remodeling.

MATERIALS AND METHODS

Patient enrollment. Before the study began, all individuals provided written informed permission by the principles established in the Declaration of Helsinki approved by the Ethics Committee of Zhejiang University Medical College (no. 014-2015). Patients with SLE-PAH (total n = 45) and patients with SLE without PAH (total n = 46, age- and sex-matched) and patients with primary Sjögren disease (pSjD)–associated PAH (total n = 24) and patients with PAH without pSjD (total n = 27) were enrolled at Peking Union Medical College Hospital between November 2016 and May 2021. PAH was diagnosed based on the 2015 European Society of Cardiology and the European Respiratory Society guidelines by right-sided heart catheterization, with an mPAP of 25 mm Hg at rest and pulmonary vascular resistance (PVR) of >2 Wood units.[23] All patients with SLE were diagnosed using the American College of Rheumatology 1997 criteria.[24] All patients with pSjD were diagnosed using the 2016 American College of Rheumatology/EULAR classification criteria for pSjD.[25,26] Patients with additional overlapping CTDs, interstitial lung disease, pulmonary thromboembolism, left heart insufficiency, infection, or acute organ dysfunction were excluded.

Animal study design. All animal study protocols were in accordance with the Animals in Research: Reporting In Vivo Experiments 2.0 Guidelines.[27] All animal study protocols were reviewed and approved by Animal Care & Use Committee of Zhejiang University (numbers ZJU20210036 and ZJU20240927, AIRB-2023-0317). Animals were randomly assigned to experimental groups. Following the principle of equal opportunity, the random number table method was used

Additional supplementary information cited in this article can be found online in the Supporting Information section (http://onlinelibrary.wiley.com/doi/10.1002/art.43235).

Author disclosures and graphical abstract are available at https://onlinelibrary.wiley.com/doi/10.1002/art.43235.

Address correspondence via email to Mengtao Li, MD, at mengtao.li@cstar.org.cn; or to Jun Yang, PhD (lead contact), at yang_jun@zju.edu.cn.

Submitted for publication December 4, 2024; accepted in revised form May 2, 2025.

to assign each animal. No samples or animals were excluded from the analysis. All quantitative analyses and measurements (gene expression analysis, enzyme-linked immunosorbent assay [ELISA], right ventricular systolic pressure [RVSP] measurement, Western blot analysis) were performed in a masked manner. All figures are representative of at least three experiments unless otherwise noted. At the time of killing, mice were anesthetized with pentobarbital sodium (1% in 0.9% saline, 0.1 mL/10 g body weight) injected intraperitoneally once. Rats were anesthetized with pentobarbital sodium (2% in 0.9% saline, 0.2 mL/100 g body weight) injected intraperitoneally once. The anesthesia depth was monitored with pedal reflex. At the end of the experiment, all animals were killed by cervical dislocation.

SLE-PH mouse model establishment. Female wild type (WT) C57BL/6J mice (18–20 g, Charles River, n = 8 mice per group) were randomly grouped according to the experiments. The mice in the SLE and SLE-PH groups were intraperitoneally injected with 0.5 mL of pristane (MedChemExpress), whereas saline was also intraperitoneally administered to the mice in the normoxia and hypoxia groups. Then, the mice in the hypoxia and SLE-PH groups were placed in a 10% O_2 chamber and maintained under hypoxic conditions for four weeks to establish the SLE-PH model.

All animals were housed in a specific pathogen-free facility (three to four mice per cage) in a room with a temperature of 25°C (SD ± 2°C), were maintained on a 12-hour light/dark cycle, and were allowed free access to a standard rodent chow diet and water. At the end point of model establishment, the Vevo 2100 system (VisualSonics) was used for transthoracic echocardiography.

Statistical analysis. All the statistical analyses were performed using GraphPad Prism 8 (GraphPad Software). All the data were analyzed without the exclusion of any data points. All experimental data were subjected to a normality (Shapiro-Wilk) test. Unless otherwise noted, statistical comparisons of samples were conducted using Student's *t*-test or one-way repeated measures analysis of variance with the Dunn–Bonferroni correction for multiple comparisons followed by Dunnett's post hoc test. For nonnormally distributed data, statistical comparisons of samples were conducted using the Mann-Whitney U-test. Correlations were evaluated by Spearman's correlation analysis, with the strength of relationships quantified by the correlation coefficient (r_s). P values < 0.05 (two-tailed) were considered to indicate statistical significance. In the corresponding figures, "*," "**," and "***" indicate $P < 0.05$, $P < 0.01$, and $P < 0.001$, respectively. Each figure legend mentions the test used, the criteria for statistical significance, and the number of experimental and biologic replicates.

Data availability statement. The data that support the findings of this study are available on request from the corresponding author. All data relevant to the study are included in the article or uploaded as supplemental information.

RESULTS

Th17 cells and IL-17 levels elevated in patients with SLE-PAH, with increased Activin A to drive Th17 cell differentiation. To identify the major affected immune cell type in patients with SLE-PAH, we applied mass cytometry to determine the proportions of immune cells in the peripheral blood samples of patients with SLE-PAH before and after six months of treatment with vasodilator and immunosuppressant (Figure 1A and Figure S1A); details are listed in Supplemental Table 1. Compared to that in the pretherapy group, the proportion of $CD4^+$ T cells was significantly reduced in posttherapy patients, but not for $CD8^+$ T cells and other subsets, indicating that $CD4^+$ T cells might be the major immune cells involved in the pathogenesis of SLE-PAH (Figure 1B and Figure S1B and C). To confirm the involvement of Th17 cells in SLE-PAH, we analyzed Th17 cells proportion in peripheral blood mononuclear cells (PBMCs) from five healthy controls and six patients with SLE-PAH by flow cytometry (Figure 1C). Quantitative analysis revealed a significant elevation in Th17 cell frequency in patients with SLE-PAH compared to controls. In addition, we detected elevated IL-17 levels in SLE-PAH serum samples compared with control and SLE without PAH serum samples (Figure 1D).

To investigate the potential involvement of Activin A in CTD-PAH pathogenesis, we measured the levels of Activin A in serum samples from 33 healthy controls, 34 patients with SLE, 27 patients with pSjD without PAH, 33 patients with SLE-PAH, and 24 patients with pSjD-PAH by ELISA (Supplemental Table 2), and detected highest readouts in patients with SLE-PAH and pSjD-PAH than healthy controls and non-PAH groups (Figure 1D and Figure S1D). Then we analyzed the correlation between Activin A levels and key clinical parameters in patients with SLE-PAH. Pearson correlation analysis revealed that Activin A levels were positively correlation with N-Termimal-pro–brain natriuretic peptide (r_s = 0.904), mPAP (r_s = 0.902), and PVR (r_s = 0.896) and negatively correlation with cardiac index (r_s = –0.920) (Figure 1E). Similar correlation was also observed for IL-17 (Supplemental Figure 1E), suggesting Activin A and IL-17 may contribute to SLE-associated PAH progression and serve as potential biomarkers for SLE-PAH.

Then, to clarify how IL-17 was produced in the context of increased Activin A in SLE-PAH, we isolated $CD4^+$ T cells from human PBMCs and stimulated with Activin A alone or in combination with IL-6 for 18 hours.[7] We found that retinoic acid receptor-related orphan receptor γ t and IL-17, signatures of Th17 cells,[28,29] were up-regulated in Activin A–treated $CD4^+$ T cells, with further elevation in the Activin A with IL-6 group

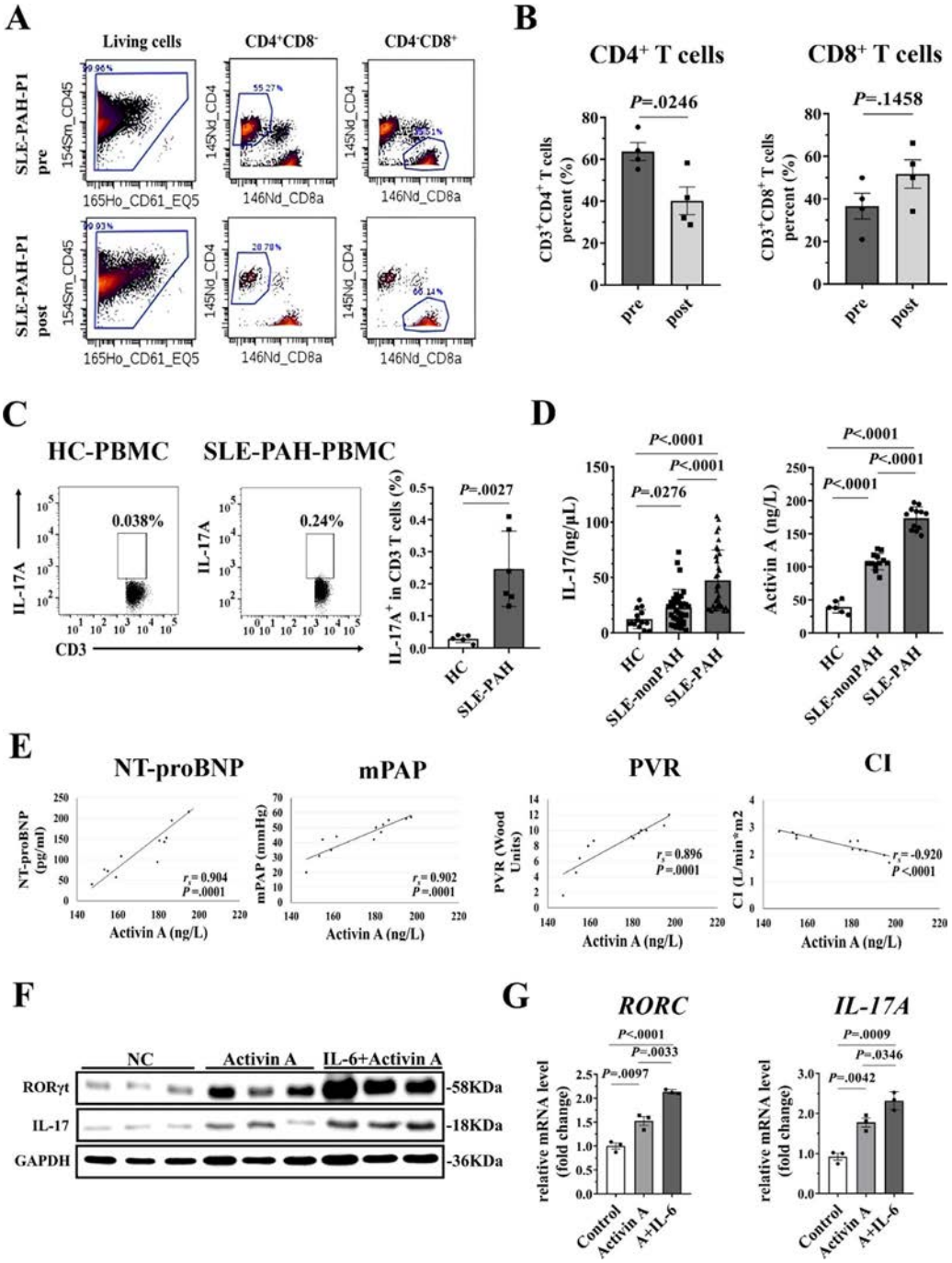

Figure 1. Th17 cells and IL-17 were elevated in patients with SLE-PAH, with increased Activin A to drive Th17 cells differentiation. (A) The percentages of $CD4^+$ T cells and $CD8^+$ T cells in the peripheral blood of the patients before and after therapy were analyzed by mass cytometry. (B) The quantification of analyzed cells from the four patients. (C) Representative flow cytometry dot plots of PBMCs from five HCs and six patients with SLE-PAH, and the quantification of Th17 cells is shown on the right. (D) Enzyme-linked immunosorbent assays were conducted with serum samples from HCs, patients with SLE without PAH (n = 46), and patients with SLE-PAH (n = 45). (E) Correlation analysis between Activin A level and clinical parameters in patients with SLE-PAH. (F) The human PBMC-derived $CD4^+$ T cells stimulated by Activin A or Activin A with IL-6 were collected and examined by Western blot for IL-17 and RORγt (left) and densitometric quantification was shown in right (n = 3). (G) The mRNA expression of *RORC* and *IL-17A* in human $CD4^+$ T cells activated by Activin A or Activin A with IL-6 (n = 3). Data are shown as means ± SEMs, and *P* values (Bonferroni corrected) are depicted in the panels throughout all figures as $^*P < 0.05$, $^{**}P < 0.01$ and $^{***}P < 0.001$ using one-way analysis of variance with repeated measures, followed by Bonferroni correction for multiple comparisons. A, Activin A; CI, cardiac index; HC, healthy control; IL-6, interleukin-6; mPAP, mean pulmonary artery pressure; mRNA, messenger RNA; NC, negative control; NT-proBNP, NT-pro–brain natriuretic peptide; PAH, pulmonary arterial hypertension; PBMC, peripheral blood mononuclear cell; PVR, pulmonary vascular resistance; *RORC*, RAR-related orphan receptor C; RORγt, receptor-related orphan receptor γ t; SLE, systemic lupus erythematosus.

(Figure 1F and Figure S1F). At the same time, extracellular signal–regulated kinase 1 or 2 phosphorylation, a pathogenic Th17 activation signal,[7] was significantly increased after Activin A stimulation (Figure S1G). We also detected increased RAR-related orphan receptor C (*RORC*), *IL-17A*, and granulocyte–macrophage colony-stimulating factor (*GM-CSF*) at the messenger RNA (mRNA) level in Activin A–treated groups (Figure 1G and Figure S1H). To confirm the dependence of Activin A on Th17 differentiation, WT C57BL/6J mouse spleen $CD4^+$ T cells were differentiated into Th17 cells. Suppressing Activin A with Follistatin (a natural Activin A antagonist)[15,30] dose-dependently reduced *RORC* and *IL-17A* mRNA levels (Supplemental Figure 1H). These findings implied that in the context of SLE-PAH, elevated Activin A might contribute to $CD4^+$ T cells differentiation into Th17 cell with IL-17 expression.

Activin A receptor ALK4 mediating the release of IL-17 from Th17 cells and induced endothelial–mesenchymal transition in cocultured PMECs. Activin A binds to naïve $CD4^+$ T cells to drive them to produce IL-17 through activation of the type I receptor ALK4 in the context of SLE-PAH. At the same time, Activin A may also induce endothelial–mesenchymal transition (EndoMT) in endothelial cells. Considering the complexity of the inflammatory conditions in PAH, we investigated the interaction between PMECs and Th17 cells by coculture assays. In these assays, we further examined the role of the possible key player ALK4 by modulating its expression on Th17 cells to confirm its effect on cocultured PMECs.[7] We isolated $CD4^+$ T cells from WT C57BL/6J mice, treated these cells with ALK4–short hairpin RNA (shRNA), scramble-shRNA, or ALK4-Overexpression (OE) lentiviruses with or without Activin A in the presence of IL-6, and then cocultured differentiated Th17 cells with PMECs isolated from WT C57BL/6J mice (Figure 2A). The knockdown efficiency of ALK4-shRNA in Th17 cells was evaluated by quantitative polymerase chain reaction (qPCR) and immunoblotting, as the efficiency of ALK4 overexpression (Figure 2B and Figure S2). Further analysis of gene expression in Th17 cells revealed that the levels of *IL-17*, *GM-CSF*, and *RORC* were elevated in the ALK4-OE group, whereas *IL-10* was increased in the ALK4-shRNA group compared with the ALK4-OE and scramble-shRNA groups, respectively (Figure 2C).

To further confirm that the interaction between Th17 cells and PMECs is mediated by ALK4, we cocultured PMECs and Th17 cells for a prolonged period. We found that the expression of genes related to Activin A-ALK4 signaling, such as *CTGF* and plasminogen activator inhibitor 1 (*PAI1*), extracellular matrix (ECM)–related genes *Col1α1*, and *Fn1*, inflammatory factor *IL-6* and mesenchymal markers, including α-smooth muscle actin (*α-SMA*) and *Vimentin* were significantly increased in the ALK4-OE coculture group but significantly decreased in the ALK4-shRNA coculture group. Oppositely, the expression of vascular endothelial (*VE*)-*Cadherin*, an endothelial marker, was decreased in the ALK4-OE coculture group and increased in the ALK4-shRNA coculture group (Figure 2D). We also examined smooth muscle cell marker 22α (SM22α) expression in mouse pulmonary endothelial cells determined by immunofluorescent staining. We demonstrated that SM22α was highly expressed in ALK4-OE coculture group and decreased in ALK4-shRNA coculture group (Figure 2E). These data suggested that Activin A exerted its effects through ALK4 to drive the differentiation of pathogenic Th17 cells to induce inflammation and detrimental EndoMT in cocultured PMECs.

$CD4^+$ T cell depletion alleviating hemodynamic changes in hypoxia mice. To further investigate the involvement of $CD4^+$ T cells in SLE-PAH, we generated $CD4^+$ T cell–depleted mice by using anti-CD4 antibody GK1.5 in WT C57BL/6J mice and isotype antibody in control mice under chronic hypoxia (10% O_2) exposure for three weeks (Figure 3A). The effectiveness of $CD4^+$ T cells depletion was confirmed by a reduction in $CD4^+$ T cells from approximately 13% to 5% of total splenic cells examined by flow cytometry (Figure 3B). Compared with the hypoxia group, $CD4^+$ T cell–depleted mice exhibited a significant decrease in RVSP, total pulmonary vascular resistance index (TPVRI), and right heart hypotrophy index (Fulton index) (Figure 3C–E). The serum level of IL-17 was also reduced in $CD4^+$ T cell–depleted mice (Figure 3F). However, $CD4^+$ T cell depletion had less effect on reversing remodeled small pulmonary arteries with only partially reduced wall thickness (Figure 3G–I). A marked decrease in IL-17 levels was observed in the $CD31^+$ pulmonary vasculature endothelium cells in $CD4^+$ T cell–depleted mice (Figure 3I). Furthermore, immunoblotting of homogenized lungs demonstrated that a reduction in IL-6 and Smad2 phosphorylation, which was accompanied by decreased CTGF in $CD4^+$ T cell–depleted mice (Figure 3J). The analysis of genes expression in lungs showed decreased expression levels of *IL-17A*, *GM-CSF*, *Rorc*, inhibin beta A (*INHBA*), *CTGF*, *Col1α1*, *IL-6*, and *Fn1* in $CD4^+$ T cell–depleted mice (Figure S3). These findings suggested that CD4 depletion protected against inflammation and hemodynamic changes in hypoxia-induced PH but exerted less effects on reversing vascular remodeling.

Aberrant activation of ALK4 but not ALK5 inducing proinflammatory factor and EndoMT gene expression in hPMECs. To investigate Activin A signaling associated with SLE-PAH pathogenesis, we analyzed the downstream mediator in human PMECs (hPMECs) exposed to patients' serum samples or Activin A. Immunoblotting revealed significant up-regulation of pSmad2, along with elevated IL-6 and CTGF expression, known to induce EndoMT,[31] following stimulation with SLE without PAH serum, SLE-PAH serum, or Activin A (Figure 4A and Figure S4A). Notably, SLE-PAH serum induced greater protein activation than non-SLE PAH serum. To confirm Activin A dependent effect, we

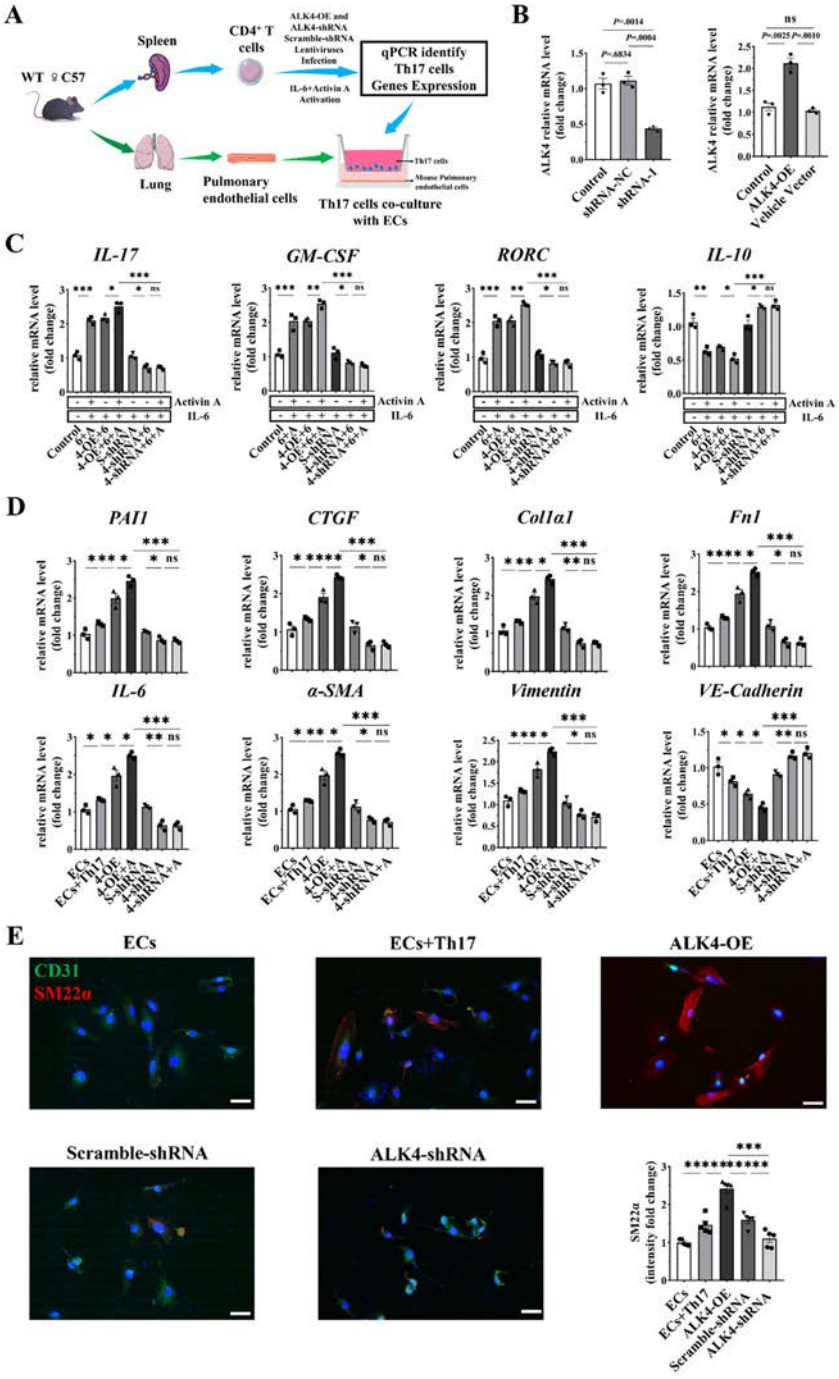

Figure 2. The Activin A receptor ALK4 mediated the release of IL-17 from Th17 cells and induced endothelial–mesenchymal transition in cocultured pulmonary microvascular ECs (PMECs). (A) Schematic illustration of $CD4^+$ T cells interaction with hPMECs. (B) The mRNA expression of *ALK4* after treated with ALK4-shRNA and ALK4-OE lentiviruses in $CD4^+$ T cells (n = 3). (C) The mRNA expression in $CD4^+$ T cells treated with ALK4-shRNA, ALK4-OE, and scramble-shRNA lentivirus after 48 hours (n = 3). (D) The mRNA expression in mouse PMECs cocultured with Th17 cells (n = 3). (E) Representative images showing CD31 (green) and SM22α (red) with DAPI (blue) counterstain for nuclei in mouse pulmonary ECs cocultured with Th17 cells assessed by immunofluorescence microscopy from the indicated groups. Scale bar = 50 μm. SM22α was quantified using ImageJ (right) (n = 5). Data are shown as means ± SEMs, and *P* values (Bonferroni corrected) are depicted in the panels throughout all figures as $^*P < 0.05$, $^{**}P < 0.01$, and $^{***}P < 0.001$ using one-way analysis of variance with repeated measures, followed by Bonferroni correction for multiple comparisons. 4-OE, activin receptor–like kinase 4 overexpression; 4-shRNA, activin receptor–like kinase 4–short hairpin RNA; 6, IL-6; ALK4, activin receptor–like kinase 4; α-SMA, α-smooth muscle actin; *Col1α1*, Collagen Type I Alpha 1 Chain; *CTGF*, connective tissue growth factor; EC, endothelial cell; *Fn1*, Fibronectin 1; *GM-CSF*, granulocyte–macrophage colony-stimulating factor; hPMECS, human PMECs; IL-17, interleukin-17; mRNA, messenger RNA; ns, not significant; *PAI1*, plasminogen activator inhibitor 1; qPCR, quantitative polymerase chain reaction; *RORC*, RAR-related orphan receptor C; S-shRNA, scramble–short hairpin RNA; shRNA, short hairpin RNA; SM22α, smooth muscle 22α; VE, vascular endothelial; WT, wild type. Color figure can be viewed in the online issue, which is available at http://onlinelibrary.wiley.com/doi/10.1002/art.43235/abstract.

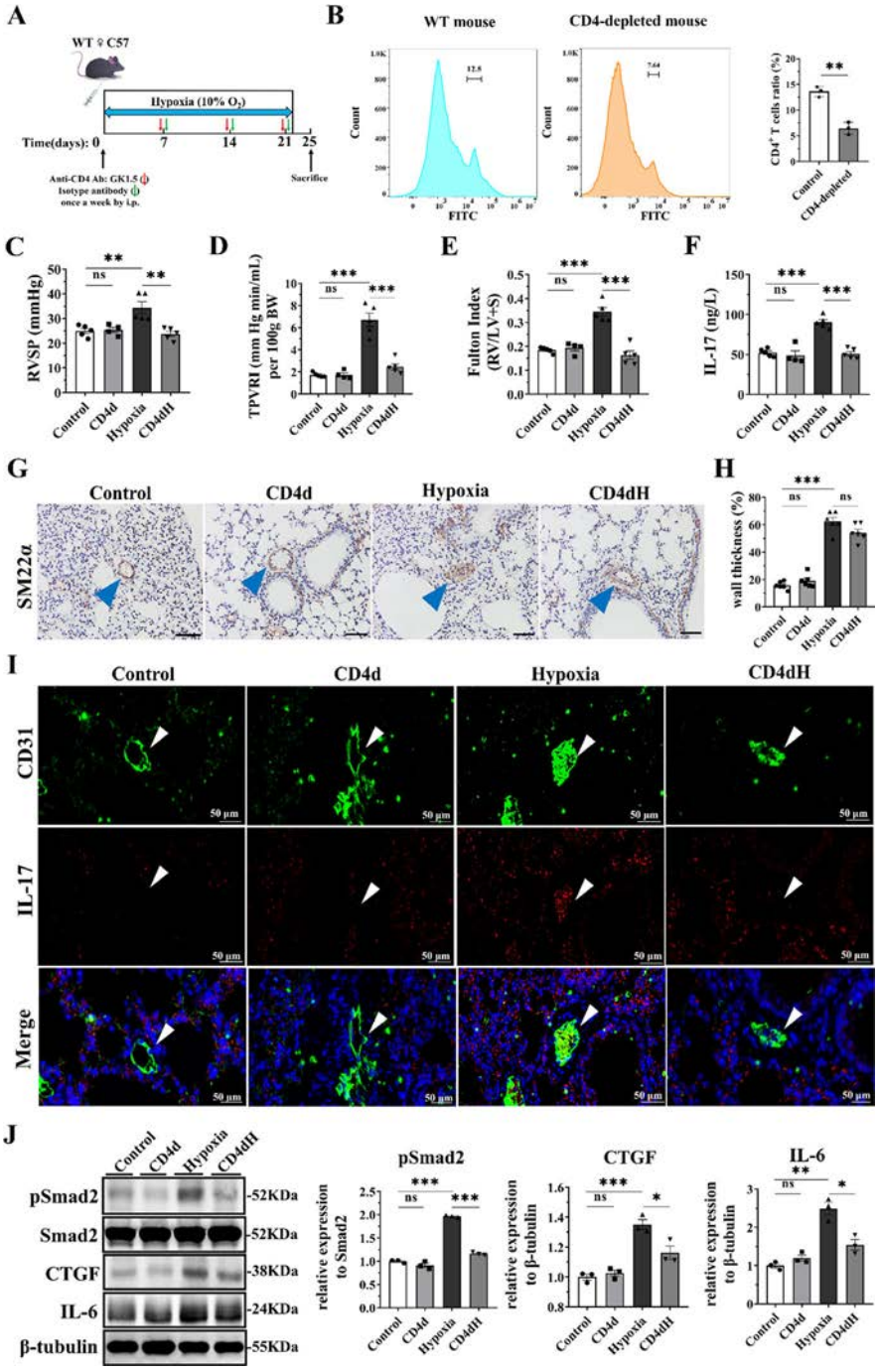

Figure 3. CD4$^+$ T cell depletion alleviates hemodynamic changes in hypoxia mice. (A) The schematic diagram of chronic hypoxia model in CD4$^+$ T cell–depleted mice. (B) Representative flow cytometry histogram of CD4$^+$ T cells from spleens and quantification of CD4$^+$ T cells (n = 3). (C, D, E) Pulmonary hypertension parameters were as follows: RVSP, TPVRI, and Fulton index (n = 6 mice for each group). (F) Enzyme-linked immunosorbent assay showing IL-17 level in the serum of different groups. (G) The representative images of pulmonary arteries by immunohistochemistry staining of SM22α of each group indicated in the panel. Scale bar = 50 μm. Blue arrow indicates small pulmonary arteries. (H) Medial wall thickness of small pulmonary arteries. (I) Representative images showing CD31 (green) and IL-17 (red) with DAPI (blue) counterstain for nuclei in systemic lupus erythematosus pulmonary hypertension mice. White arrow indicates the pulmonary small arterial. Scale bar = 50 μm. (J) The Western blot result showed that pSmad2, CTGF, and IL-6 expression in lungs of each group (left) and densitometric quantification is shown in the right (n = 3). Data are shown as means ± SEMs, and *P* values (Bonferroni corrected) are depicted in the panels throughout all figures as $^*P < 0.05$, $^{**}P < 0.01$, and $^{***}P < 0.001$ using one-way analysis of variance with repeated measures, followed by Bonferroni correction for multiple comparisons. CD4d, CD4-deleted; CD4dH, CD4-depleted and hypoxia; CTGF, connective tissue growth factor; FITC, fluorescein Isothiocyanate; IL-17, interleukin-17; LV, left ventricle; ns, not significant; RVSP, right ventricular systolic pressure; RV, right ventricle; SM22α, smooth muscle 22α; TPVRI, total pulmonary vascular resistance index; WT, wild type. Color figure can be viewed in the online issue, which is available at http://onlinelibrary.wiley.com/doi/10.1002/art.43235/abstract.

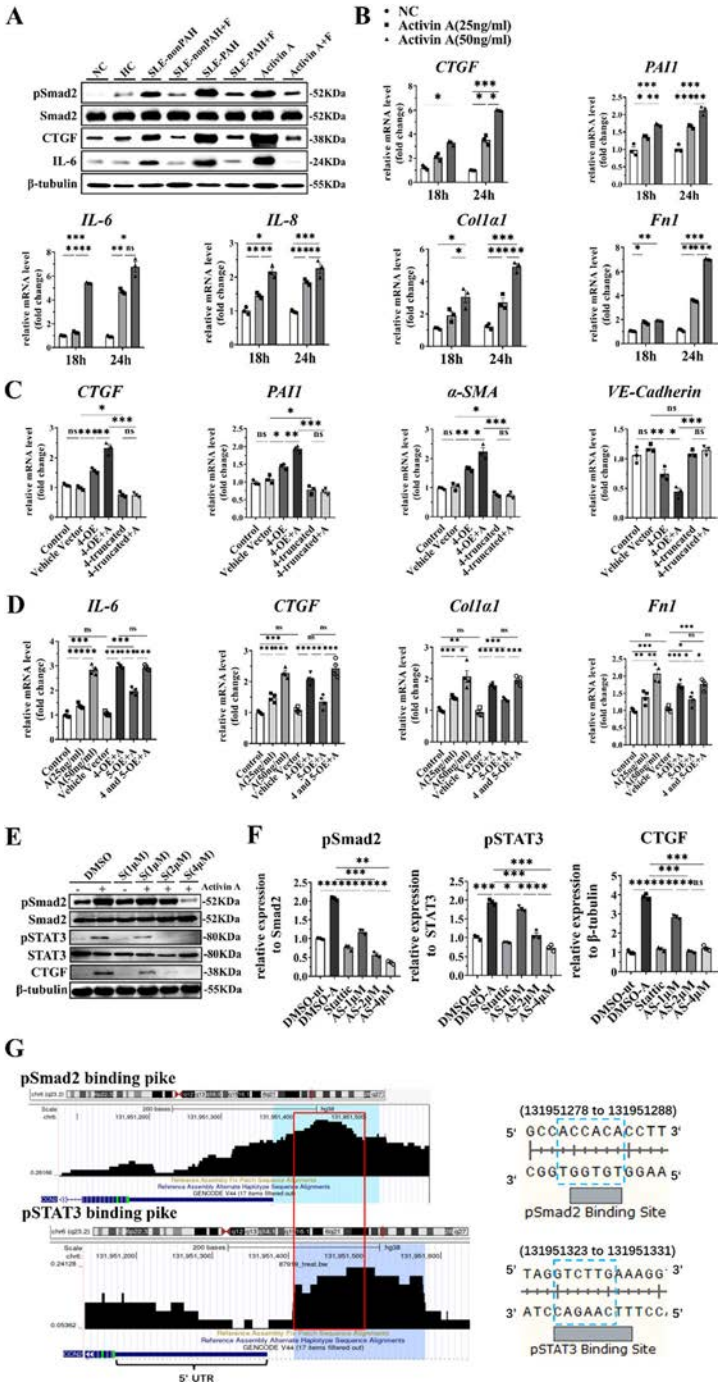

Figure 4. The aberrant activation of ALK4 not ALK5 induced pro-inflammatory factor and endothelial–mesenchymal transition gene expression in h-pulmonary microvascular endothelial cells (hPMECs). (A) hPMECs stimulated by serum samples from HCs, patients with SLE, and patients with SLE-PAH, Activin A (25 ng/mL) and Follistatin (100 ng/mL) for 24 hours were collected and examined by western blot. (B) The mRNA expression in hPMECs induced by Activin A (25 ng/mL and 50 ng/mL) for indicated time (n = 3). (C) The mRNA expression in control, ALK4-OE, ALK4-truncated, and vehicle vector groups (n = 3). (D) The mRNA expression in hPMECs transfected with ALK4-OE and ALK5-OE plasmid. (E) The pSTAT3, pSmad2, and CTGF expression in hPMECs treated with Stattic were examined by Western blot. (F) The densitometric quantification of protein levels of pSmad2, pSTAT3, and CTGF (n = 3). (G) The overlapping binding region of pSmad2 and pSTAT3 in *ctgf* promoter region was indicated by red line. Data are shown as means ± SEMs, and *P* values (Bonferroni corrected) are depicted in the panels throughout all figures as $^{*}P < 0.05$, $^{**}P < 0.01$, and $^{***}P < 0.001$ using one-way analysis of variance with repeated measures, followed by Bonferroni correction for multiple comparisons. Each data point in the panels represents one independent participant. 4-OE, activin receptor–like kinase 4 overexpression; ALK4, activin receptor–like kinase 4; AS, Activin A+Stattic; α-SMA, α-smooth muscle actin; *Col1α1*, col1α1, collagen type I alpha 1 chain; CTGF, connective tissue growth factor; F, Follistatin; *Fn1*, fibronectin 1; hPMECS, human PMECs; HC, healthy control; IL-6, interleukin-6; mRNA, messenger RNA; NC, negative control; ns, not significant; PAH, pulmonary arterial hypertension; *PAI1*, plasminogen activator inhibitor 1; S, Stattic; SLE, systemic lupus erythematosus; ut, untreated by Activin A; VE, vascular endothelial. Color figure can be viewed in the online issue, which is available at http://onlinelibrary.wiley.com/doi/10.1002/art.43235/abstract.

also used Follistatin and found it reduced Smad2 phosphorylation, IL-6, and CTGF expression in the presence of Activin A.

To examine the direct effect of Activin A on hPMECs, hPMECs were subjected to dose and time gradients assay (25–50 ng/mL for 18–24 hours) (Figure 4B). The results revealed up-regulation of the Activin A target genes (*CTGF*, *PAI1*),[32] proinflammatory factors (*IL-6*, *IL-8*), and ECM-related genes (*Fn1*, *Col1α1*) in a time- and dose-dependent manner. We also detected increased expression of *α-SMA* and *Vimentin* coupled with decreased *VE-Cadherin* (Supplemental Figure 4B), paralleled by CTGF expression and Smad2 phosphorylation over time (Supplemental Figure 4C and D).

Given the role of ALK4 in IL-17 regulation in $CD4^+$ T cells, we engineered ALK4 functional domains through lentiviral constructs, including canonical ALK4 full-length and kinase-defective truncation[33] (Figure S5A). Transfection efficiency in hPMECs was validated by qPCR (Figure S5B). ALK4 overexpression led to significant elevation of ECM-related genes (*CTGF*, *Fn1*, *Col1α1*), *PAI1*, and proinflammatory factors (*IL-6*, *IL-8*) when compared to controls. Conversely, kinase-truncated ALK4 reversed these expression patterns (Figure 4C and Figure S5C). Both ALK4 and ALK5 mediate Activin A/TGFβ signaling through Smad2 phosphorylation,[13] and their different roles in Activin A–induced vascular pathology remain undefined. Our studies revealed ALK4 overexpression specifically enhanced ECM genes expression (*CTGF*, *Fn1*, *Col1α1*) and *IL-6* and EndoMT progression (*α-SMA* and *Vimentin*) in hPMECs, concurrent with Bmpr2 down-regulation and endothelial marker loss (*VE-Cadherin*). Notably, these pathologic changes were more pronounced with ALK4 versus ALK5 activation (Figure 4D and Figure S5D), the protein expression of pSmad2, IL-6, and CTGF by overexpression ALK4 and ALK5 were also confirmed with immunoblotting (Figure S5E).

Considering the key role of CTGF in EndoMT and ECM genes expression,[34] we investigated its transcriptional regulation in Activin A–stimulated hPMECs. The results revealed Stat3 inhibition, via selective antagonist Stattic,[35] attenuated Smad2 phosphorylation and CTGF expression (Figure 4E and F), establishing STAT3 as a synergistical signal molecule for Smad2-mediated CTGF activation. Mining of chromatin profiling data sets (GSM2635691 and GSM2752894) identified colocalized pSmad2/pSTAT3 binding motifs within the CTGF promoter on chromosome 6 (Figure 4G). These transcription factors exhibited overlapping occupancy at CTGF promoter region, indicating with red rectangles in Figure 4G. These findings suggested ALK4 rather than ALK5 in up-regulating ECM-related genes and IL-6, which activated pSTAT3 to synergize with pSmad2 to induce CTGF expression in hPMECs.

ALK4 overexpression inducing severe PH in SLE mice. To confirm the importance of ALK4 in vivo, we aimed to examine the detrimental role of ALK4 by establishing an SLE-PH mouse model (Figure 5A). In our previous study, mice with SLE-PH induced with pristane and exposure to hypoxic conditions (10% O_2) (SLE-PH mice) exhibited only a mild increase in RVSP without right heart hypotrophy. Therefore, we treated mice weekly with an ALK4-overexpressing lentivirus via intranasal instillation to reproduce the increased activation of Activin A in the SLE-PH mouse model and further monitored the mice for five weeks. We observed an increase in the RVSP to approximately 35 mm Hg and a significant increase in the Fulton index (Figure 5B–D).

We also applied ALK4 shRNA to confirm the reversal effects of knocking down ALK4. Compared with that in the control group, ALK4 knockdown resulted in considerable amelioration of the increase in the RVSP, a reduced TPVRI and a decreased Fulton index (Figure 5B–D). The serum levels of Activin A, IL-17, and mouse anti–double stranded DNA (anti-dsDNA) antibody, which are markers of SLE in humans,[36] were also decreased (Figure 5E). Alleviation of pulmonary inflammation and decreased perivascular IL-17 levels were observed in the ALK4 knockdown group, accompanied by reduced infiltration of immune cells, as assessed by hematoxylin and eosin staining and immunohistochemistry staining of IL-17 (Figure 5F), and the wall thickness of the small pulmonary arteries was markedly decreased (Figure S6A). The decrease in pSmad2 levels was observed in ALK4 knockdown PMECs (Figure 5G). A reduction in ALK4 and Smad2 phosphorylation was accompanied by reduced CTGF protein levels in the ALK4 knockdown group (Figure 5H). Further gene expression analysis revealed significant decreases in the expression levels of *IL-17*, *Rorc*, *CTGF*, *Col1α1*, *IL-6*, *GM-CSF*, and *PAI1* in the ALK4 knockdown group, whereas the expression of *IL-10* was increased in this group (Figure S6B). In addition, the expression levels of EndoMT markers (*a-SMA* and *Vimentin*) decreased and the expression of *VE-cadherin* was restored in the ALK4 knockdown group. Our results showed that ALK4 had a detrimental effect on pulmonary vascular remodeling in SLE-PH mice and that decreasing ALK4 expression reversed pulmonary hypertension in vivo.

The potent ALK4 inhibitor TEW reversing PH by suppressing IL-17 expression in the lungs and EndoMT in hPMECs. To evaluate whether inhibition of ALK4 can suppress inflammation and reverse SLE-PAH, we used the ALK4 inhibitor TEW, which is in a phase 2 clinical trial for breast cancer therapy with low half maximal inhibitory concentration (IC50) (13 n*M*) and minimal side effects.[37,38] In SLE-PH mice, TEW treatment with reported dose,[39,40] reduced lung edema (Figure 6A) and reversed elevated RVSP, TPVRI, and Fulton index (Figure 6B–D). Serum IL-17, Activin A, and anti-dsDNA autoantibody levels, elevated in SLE or SLE-PH groups, were significantly reduced by TEW (Figure 6E). TEW reduced perivascular IL-17, lung inflammation, and immune cell infiltration (Figure 6F), as well as pulmonary artery wall thickness (Figure 6G). TEW also reversed SLE-PH-induced

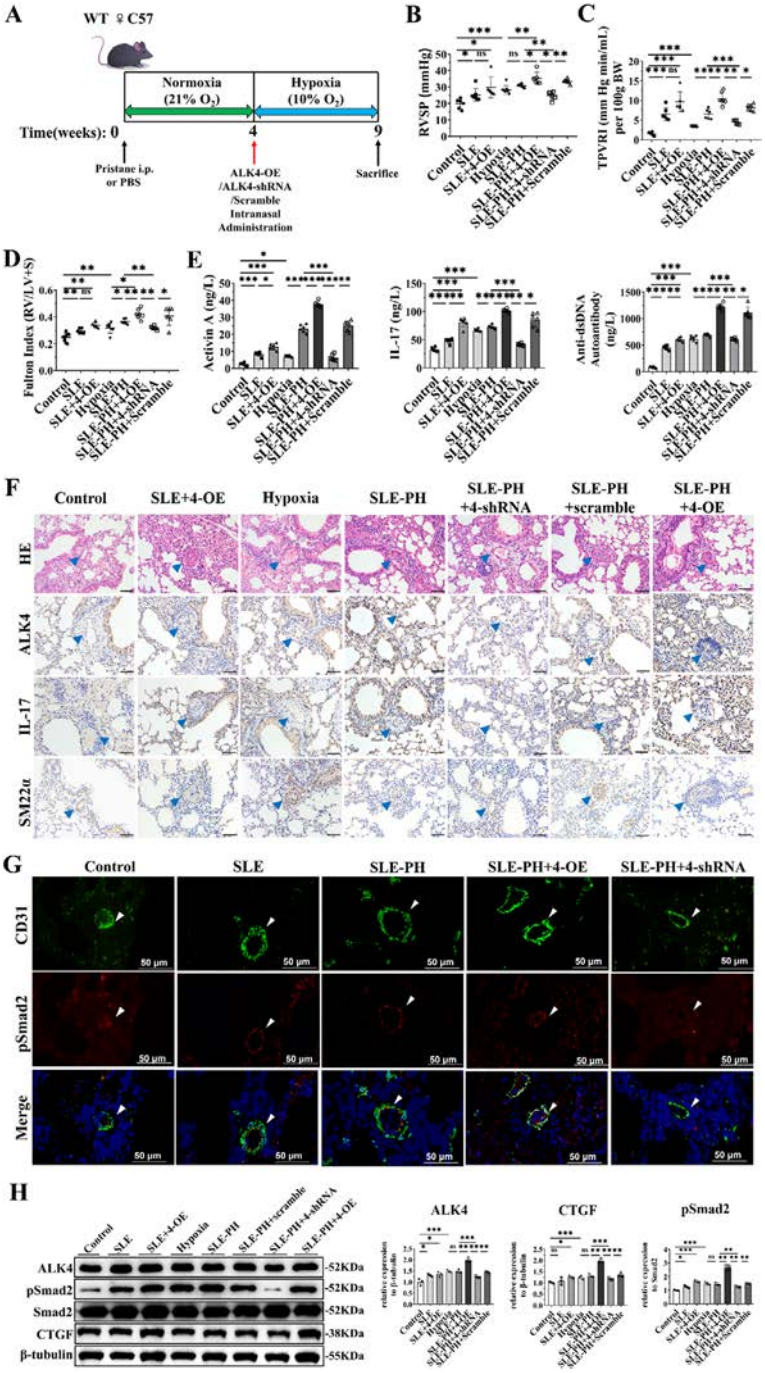

Figure 5. ALK4 overexpression induced severe pulmonary hypertension in SLE mice. (A) Schematic illustration of ALK4 overexpression and knockdown in SLE-PH mice. (B, C, D) Hemodynamic indices including RVSP, TPVRI, and Fulton index were measured in the SLE-PH mice (n = 6 each). (E) Enzyme-linked immunosorbent assay showing Activin A, IL-17, and anti-dsDNA autoantibody level in the serum of different groups. (F) The representative images of pulmonary arteries (Scale bar = 50 μm) by HE and immunohistochemistry staining of SM22α, ALK4, and IL-17 in each group. Blue arrows indicated small pulmonary arteries. (G) Representative images showed CD31 (green) and pSmad2 (red) with DAPI (blue) in SLE-PH mice. White arrows indicated the pulmonary small arteries. Scale bar = 50 μm. (H) The western blot result showed that ALK4, pSmad2, and CTGF expression in the lungs of each group (left) with quantification (right). Data are shown as means ± SEMs, and *P* values (Bonferroni corrected) are depicted in the panels throughout all figures as $^{*}P < 0.05$, $^{**}P < 0.01$ and $^{***}P < 0.001$ using one-way analysis of variance with repeated measures, followed by Bonferroni correction for multiple comparisons. 4-OE, activin receptor–like kinase 4 overexpression; 4-shRNA, activin receptor–like kinase 4–short hairpin RNA; ALK4, activin receptor–like kinase 4; anti-dsDNA, anti–double-stranded DNA; CTGF, connective tissue growth factor; HE, hematoxylin and eosin; IL-17, interleukin-17; LV, left ventricle; ns, not significant; PH, pulmonary hypertension; RV, right ventricle; RVSP, right ventricular systolic pressure; S-shRNA, scramble–short hairpin RNA; shRNA, short hairpin RNA; SLE, systemic lupus erythematosus; SM22α, smooth muscle 22α; TPVRI, total pulmonary vascular resistance index; WT, wild type. [Correction added on 10 September 2025, after first online publication: Figure 5 has been updated in this version.] Color figure can be viewed in the online issue, which is available at http://onlinelibrary.wiley.com/doi/10.1002/art.43235/abstract.

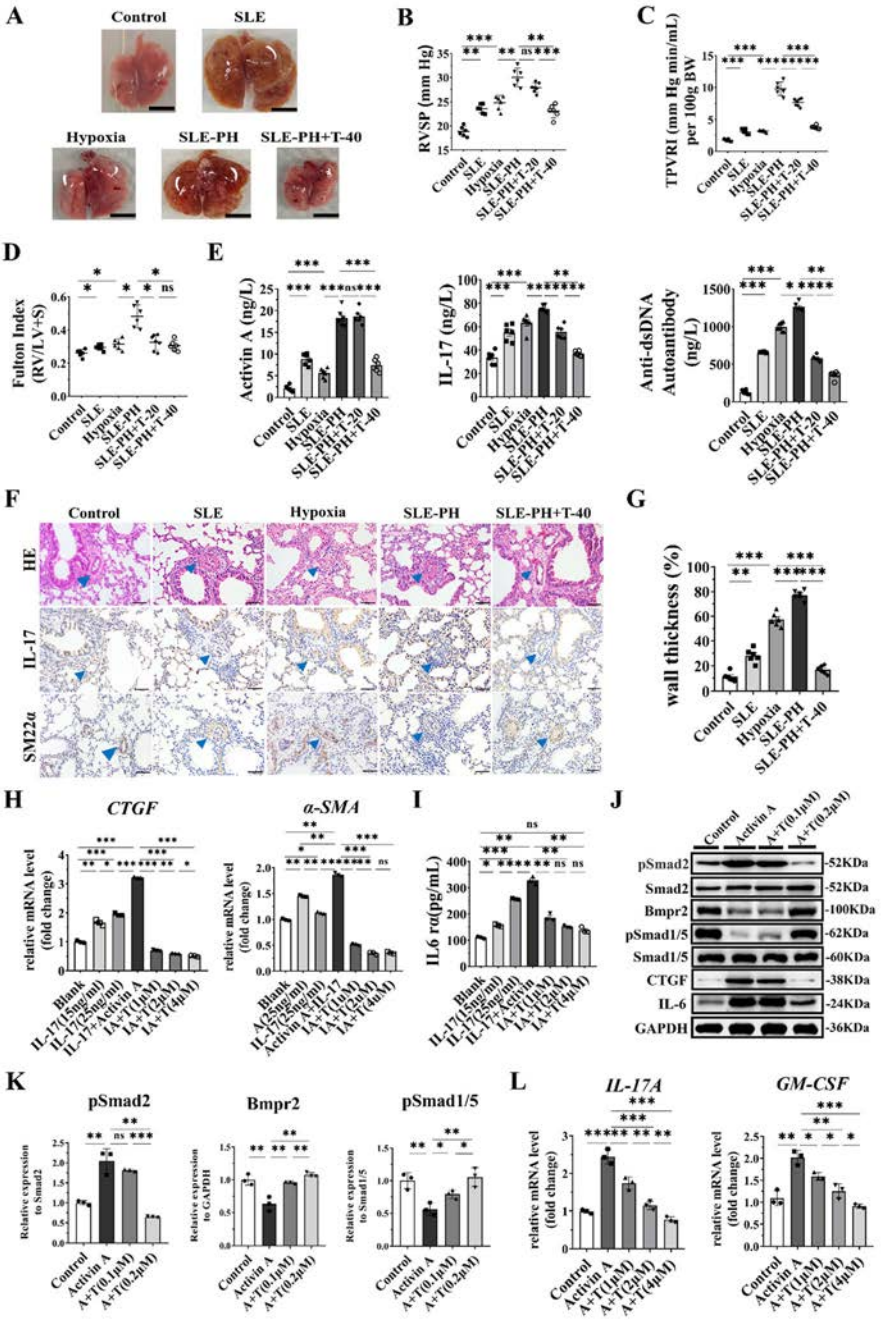

Figure 6. The potent ALK4 inhibitor TEW reversed pulmonary hypertension. (A) Representative images of the lung of control and treated mice (Scale bars = 1cm). (B, C, D) Hemodynamic indices including RVSP, TPVRI, and Fulton index in each group (n = 6). (E) Enzyme-linked immunosorbent assay showing IL-17, anti-dsDNA autobody, and Activin A level in the serum from different groups. (F) The representative images of pulmonary arteries (scale bar = 50 μm) by HE and IL-17 and SM22α immunohistochemistry staining of each group. Blue arrows indicated the small pulmonary arteries. (G) Medial wall thickness of small pulmonary arteries. (H) The mRNA expression in h-pulmonary microvascular endothelial cells (hPMECs) treated with TEW after stimulation with IL-17 and Activin A (n = 3). (I) IL-6rα level in the supernatant of hPMECs treated with TEW (n = 3). (J) The protein expressions of pSmad2, Bmpr2, pSmad1/5, CTGF and IL-6 in hPMECs treated with TEW were examined by western blot. (K) The densitometric quantification of protein levels of pSmad2, CTGF, Bmpr2, and pSmad1/5 (n = 3). (L) The mRNA expression in Th17 cells treated with TEW after stimulation with Activin A (n = 3). Data are shown as means ± SEMs, and *P* values (Bonferroni corrected) are depicted in the panels as $^{*}P < 0.05$, $^{**}P < 0.01$, and $^{***}P < 0.001$ using one-way analysis of variance with repeated measures, followed by Bonferroni correction for multiple comparisons. ALK4, activin receptor–like kinase 4; anti-dsDNA, anti–double-stranded DNA; α-SMA, α-smooth muscle actin; AT, Activin A with TEW; Bmpr2, bone morphogenetic protein type II receptor; CTGF, connective tissue growth factor; *GM-CSF*, granulocyte–macrophage colony-stimulating factor; HE, hematoxylin and eosin; HPMECS, human PMECs; IA, IL-17 with Activin A; IL-17, interleukin-17; LV, left ventricle; mRNA, messenger RNA; ns, not significant; PH, pulmonary hypertension; RV, right ventricle; RVSP, right ventricular systolic pressure; SLE, systemic lupus erythematosus; SM22α, smooth muscle 22α; T-20, TEW (20 mg/kg); T-40, TEW (40 mg/kg); TEW, vactosertib (TEW-7197, shorten as TEW); TPVRI, total pulmonary vascular resistance index. Color figure can be viewed in the online issue, which is available at http://onlinelibrary.wiley.com/doi/10.1002/art.43235/abstract.

elevations in *IL-17*, *IL-6*, and ECM genes (*CTGF*, *Col1α1*, *Fn1*), and PAI1 and suppressed EndoMT markers (*α-SMA*, *Vimentin*), restoring *VE-cadherin* expression in lung tissues (Figure S6C).

Specifically, TEW inhibits phosphorylation of Smad2.[37,41,42] Based on the efficient doses reported previously,[40,43] we applied three different doses for the in vitro assay. A significant increase in *CTGF*, *IL-6*, and *α-SMA* expression was observed in hPMECs activated by IL-17 and Activin A, whereas the expression of the endothelial marker *VE-Cadherin* was decreased. Treatment with TEW effectively reversed the IL-17– and Activin A–induced alterations in gene expression (Figure 6H and Figure S7A) and IL-6rα secretion (Figure 6I) from hPMECs. We further assessed the effects of TEW on CTGF, IL-6, and BMPR2 signaling in hPMECs. As shown in Figure 6J and K and Figure S7B, TEW suppressed Activin A–induced pSmad2, CTGF, and IL-6 expression while restoring BMPR2 levels and pSmad1/5 signaling impaired by Activin A. *IL-17*, *GM-CSF*, and *RORC* expression were significantly reduced, whereas *IL-10* expression was recovered in TEW-treated Th17 cells derived from mice $CD4^+$ T cells (Figure 6L and Figure S7C). These results demonstrated that TEW treatment reversed pathologic pulmonary vascular remodeling and the development of SLE-PH. It effectively suppressed Th17 cells induced inflammation and EndoMT in hPMECs while balancing BMPR2 signaling.

TEW reversing PAH in Monocrotaline (MCT)-treated rats by rebalancing signaling through the Activin A/ALK4 and BMPR2 pathways. To further confirm that TEW alleviated PAH in an inflammation-related rat model in which the animals could be catheterized more accurately, we used a rat model of MCT-induced PAH to reproduce the pathologic characteristics of patients, including the infiltration of inflammatory cells in the pulmonary vasculature.[44] Severe lung damages were observed in the MCT group, whereas TEW treatment groups displayed less pulmonary hemorrhage (Figure S8A and B). The survival rates of all groups of rats are demonstrated in Figure S8C. TEW treatment with 40 mg/kg significantly improved the survival rate of MCT-induced rats.

Our results showed a significant improvement in RVSP, the Fulton index, and the TRVRI in MCT rats treated with TEW (Supplemental Figure 8D–F). We observed that RVSP reduced to nearly 35 mm Hg with lower Fulton index and total pulmonary vascular resistance index (TPVRI) in the Tew-40 mg/kg group than in the MCT group. Serum IL-17 and Activin A levels were significantly elevated in the MCT group and decreased in the rats administered TEW (Figure S8G). TEW treatment also significantly reduced lung inflammation and perivascular IL-17 expression in the pulmonary vascular and significantly decreased the wall thickness of small pulmonary arteries (Figure S9A). Additionally, the gene expression of *IL-17*, *CTGF*, *IL-6*, *Inhba*, *Rorc*, *GM-CSF*, *Col1α1*, *Fn1*, *Cxcr1*, and *PAI1* decreased with TEW treatment (Figure S8H and Figure S9B). We also found that TEW alleviated EndoMT in MCT rats. *α-SMA* and *Vimentin* decreased, and *VE-Cadherin* increased. Western blot analysis revealed a reduction in pSmad2 protein level and an elevation in Bmpr2 in the TEW-treated group (Figure S8I). Immunofluorescence staining showed decreased pSmad2 in TEW-treated rats (Figure S8J).

We also conducted TEW in SU5416-induced PH with hypoxia in rats, which blocked vascular endothelial growth factor receptor 2 and caused severe pulmonary vascular remodeling (Figure S10A). Images of the lung from each group are shown in Figure S10B. The whole lungs showed poor blood circulation and supply in the Sugen5416 with hypoxia (SuHx) group. Our results showed a significant improvement in hemodynamic indices in the TEW-treated group, which RVSP decreased from 40 to 35 mm Hg with a lower Fulton index and TPVRI than in the SuHx group (Figure S10C–E). With TEW treatment, serum IL-17 and Activin A levels were significantly reduced (Figure S10F); moreover, immune cell infiltration and perivascular IL-17 levels decreased (Figure S10G). The wall thickness of pulmonary small arteries was significantly reduced with TEW treatment (Figure S10H), as was the gene expression of *IL-17*, *IL-6*, *Inhba*, *Col1α1*, and *PAI1* decreased with TEW treatment as well as mesenchymal markers (*α-SMA* and *Vimentin*) and *VE-Cadherin* increased (Figure S10I). The previously mentioned results confirmed the cell signaling by which TEW inhibits Activin A/ALK4 signaling in immunologically dysfunctional PAH rat models.

DISCUSSION

This study aimed to elucidate the role of Activin A-ALK4 signaling in SLE-PAH, with a special focus on the molecular targets that alleviate the initial inflammatory insult on the most vulnerable endothelial layer during the onset of PAH. The reduced $CD4^+$ T cell population in patients after treatment and elevated Th17 cells in PBMCs of patients with SLE-PAH suggested that Th17 cells are involved in SLE-PAH. We observed significantly higher levels of IL-17 and Activin A in serum of patients with SLE-PAH than in those of patients with SLE without PAH. Coculture experiments revealed that ALK4 mediates the interaction between immune cells and endothelial cells. We observed increased expression of CTGF and proinflammatory genes downstream of the Activin A/ALK4 pathway in vitro and in vivo, which suggested the detrimental role of ALK4 in promoting a pathogenic behavior of Th17 cells to induce inflammation and pulmonary vascular remodeling. The specific ALK4 inhibitor TEW effectively suppressed the release of IL-17 by Th17 cells and prevented EndoMT in hPMECs in an SLE-PH mouse model and an MCT-PAH rat model. Finally, we confirmed that *CTGF* gene transcription is regulated by Activin A/pSmad2 and IL-6/pSTAT3 in hPMECs. We first addressed the importance of targeting Activin A/ALK4, which also relies on suppressing pathogenic Th17 cells, to strongly contribute to alleviating PAH in the context of inflammation-related disorders, such as SLE.

We used mass cytometry to observe the dynamic involvement of immune cells before and after treatment. Mass cytometry enables the analysis of immune cells at the single-cell level, allowing the examination of the intricate immune status of patients with SLE-PAH. Following immunosuppressant and vasodilator combination therapy, we observed reductions in the populations of $CD4^+$ T cells in patients with SLE-PAH, which allowed us to identify the source of the increase in the IL-17 level.

The current therapeutic strategy for SLE-PAH involves combination treatment including immunosuppressants along with conventional vasodilator for PAH, which increases the risk of side effects.[1] So far, no therapy has been shown to achieve the "one stone kills two birds" effect for SLE-PAH in the clinic. Immunosuppressive medications, primarily glucocorticoids, cyclophosphamide, and cyclosporine A, are fundamental for SLE treatment. However, these treatments fail to reverse pulmonary vascular remodeling. To improve the prognosis of patients with SLE-PAH, recent efforts have been made to restore the balance between Activin A and BMPR2 signaling during PH progression.[45] Hydroxychloroquine and tacrolimus were not only immunosuppressants but also reported to balance BMPR2 signaling in PAH.[46,47] For patient 1 with SLE-PAH, tacrolimus was applied to replace cyclophosphamide, and patient 4 with SLE-PAH reached low-risk PAH even without vasodilator in this study. A Study of Sotatercept for the Treatment of Pulmonary Arterial Hypertension (STELLAR) trial,[22,48] suggesting the clinical effectiveness of targeting the Activin A signaling pathway in the context of CTD-PAH.[21] Our findings implied the potentiality of Activin A–BMPR2 balance modulator in addition to the immunosuppressive effect in SLE-PAH treatment.

Elevated levels of IL-6, which plays an important role in autoimmune diseases, have also been found in patients with PAH.[1,49] IL-6 is produced by macrophages and T cells through pSTAT3 to facilitate Smad2 phosphorylation upon Activin A activation. Our findings revealed that inhibiting pSTAT3 in hPMECs with Stattic led to decreased pSmad2 and CTGF levels. Thus, it is worth further exploring the interaction between the Activin A/pSmad2/CTGF pathway and IL-6/pSTAT3 to determine the functional significance of the activation of pSTAT3 in hPMECs. Although we predicted the pSmad2 and pSTAT3 binding sites in the *ctgf* promoter region via database searches and JASPAR, the precise binding sites of pSmad2 and pSTAT3 in the *ctgf* promoter on chromosome 6 in hPMECs and the epigenetic modifications of this promoter remain to be confirmed. Although our data suggested a potential association between Activin A signaling and Th17 cell differentiation in SLE-PAH, the mechanistic interplay between ALK4 and Th17 cells remains to be fully elucidated. The limitations of this study also include the development of targeted therapies, for example, whether the source of Activin A in patients with SLE-PAH is the same as that in patients with PAH. Further profiling Activin A expression in PBMCs in patients with SLE-PAH may be able to provide direct evidence.

In conclusion, our research revealed that abnormally activated ALK4 inducing IL-17 production and secretion in pathogenic Th17 cells in the context of SLE-PAH. Meanwhile, Activin A binds to ALK4 and promotes the expression of CTGF, α-SMA, and IL-6 in hPMECs. Moreover, IL-6 and pSTAT3 synergistically induce CTGF expression in hPMECs. TEW effectively inhibits ALK4 activity in hPMECs and Th17 cells to alleviate inflammation and EndoMT in the context of SLE-PAH and PAH associated with other inflammatory conditions. Furthermore, we intend to use Activin A as a biomarker to identify the most suitable patient cohort and explore the potential development of TEW for therapeutic application.

ACKNOWLEDGMENT

We would like to gratefully thank the participation of patients, Hangzhou Leading Pharmatech Co, Ltd, and the Centre for Experimental Animal Research of Zhejiang University. We also thank Nan Zhou from the Core Facilities, Zhejiang University School of Medicine for her technical support, Professor Qingqing Wang for the advice and discussion, Jingyuan Zhang helped with animal catheterization and experiment design, and Yufang Ding and Qizhi Yuan collected patient samples.

AUTHOR CONTRIBUTIONS

All authors contributed to at least one of the following manuscript preparation roles: conceptualization AND/OR methodology, software, investigation, formal analysis, data curation, visualization, and validation AND drafting or reviewing/editing the final draft. As corresponding author, Drs Li and Yang confirm that all authors have provided the final approval of the version to be published and take responsibility for the affirmations regarding article submission (eg, not under consideration by another journal), the integrity of the data presented, and the statements regarding compliance with institutional review board/Declaration of Helsinki requirements.

REFERENCES

1. Zhao J, Wang Q, Deng X, et al. The treatment strategy of connective tissue disease associated pulmonary arterial hypertension: evolving into the future. Pharmacol Ther 2022;239:108192.
2. Chaisson NF, Hassoun PM. Systemic sclerosis-associated pulmonary arterial hypertension. Chest 2013;144(4):1346–1356.
3. Nihtyanova SI, Schreiber BE, Ong VH, et al. Prediction of pulmonary complications and long-term survival in systemic sclerosis. Arthritis Rheumatol 2014;66(6):1625–1635.
4. Gaowa S, Zhou W, Yu L, et al. Effect of Th17 and Treg axis disorder on outcomes of pulmonary arterial hypertension in connective tissue diseases. Mediators Inflamm 2014;2014:247372.
5. Maston LD, Jones DT, Giermakowska W, et al. Central role of T helper 17 cells in chronic hypoxia-induced pulmonary hypertension. Am J Physiol Lung Cell Mol Physiol 2017;312(5):L609–L624.
6. Singh RP, Hasan S, Sharma S, et al. Th17 cells in inflammation and autoimmunity. Autoimmun Rev 2014;13(12):1174–1181.
7. Wu B, Zhang S, Guo Z, et al. The TGF-β superfamily cytokine Activin-A is induced during autoimmune neuroinflammation and drives pathogenic Th17 cell differentiation. Immunity 2021;54(2):308–323.e6.

8. Park H, Li Z, Yang XO, et al. A distinct lineage of CD4 T cells regulates tissue inflammation by producing interleukin 17. Nat Immunol 2005; 6(11):1133–1141.
9. Cuthbertson I, Morrell NW, Caruso P. BMPR2 mutation and metabolic reprogramming in pulmonary arterial hypertension. Circ Res 2023; 132(1):109–126.
10. Aldred MA, Morrell NW, Guignabert C. New mutations and pathogenesis of pulmonary hypertension: progress and puzzles in disease pathogenesis. Circ Res 2022;130(9):1365–1381.
11. Ryanto GRT, Ikeda K, Miyagawa K, et al. An endothelial activin A-bone morphogenetic protein receptor type 2 link is overdriven in pulmonary hypertension. Nat Commun 2021;12(1):1720.
12. Parichatikanond W, Luangmonkong T, Mangmool S, et al. Therapeutic targets for the treatment of cardiac fibrosis and cancer: focusing on TGF-β signaling. Front Cardiovasc Med 2020;7:34.
13. Derynck R, Budi EH. Specificity, versatility, and control of TGF-β family signaling. Sci Signal 2019;12(570):12.
14. Bloise E, Ciarmela P, Dela Cruz C, et al. Activin A in mammalian physiology. Physiol Rev 2019;99(1):739–780.
15. de Kretser DM, O'Hehir RE, Hardy CL, et al. The roles of activin A and its binding protein, follistatin, in inflammation and tissue repair. Mol Cell Endocrinol 2012;359(1–2):101–106.
16. Tam AYY, Horwell AL, Trinder SL, et al. Selective deletion of connective tissue growth factor attenuates experimentally-induced pulmonary fibrosis and pulmonary arterial hypertension. Int J Biochem Cell Biol 2021;134:105961.
17. Xing Y, Zhao S, Wei Q, et al. A novel piperidine identified by stem cell-based screening attenuates pulmonary arterial hypertension by regulating BMP2 and PTGS2 levels. Eur Respir J 2018;51(4):51.
18. Guignabert C, Savale L, Boucly A, et al. Serum and pulmonary expression profiles of the Activin signaling system in pulmonary arterial hypertension. Circulation 2023;147(24):1809–1822.
19. Nihtyanova SI, Denton CP. Pathogenesis of systemic sclerosis associated interstitial lung disease. J Scleroderma Relat Disord 2020;5(2) (suppl):6–16.
20. Yndestad A, Larsen KO, Oie E, et al. Elevated levels of activin A in clinical and experimental pulmonary hypertension. J Appl Physiol (1985) 2009;106(4):1356–1364.
21. Humbert M, McLaughlin V, Gibbs JSR, et al; PULSAR Trial Investigators. Sotatercept for the treatment of pulmonary arterial hypertension. N Engl J Med 2021;384(13):1204–1215.
22. Hoeper MM, Badesch DB, Ghofrani HA, et al; STELLAR Trial Investigators. Phase 3 trial of sotatercept for treatment of pulmonary arterial hypertension. N Engl J Med 2023;388(16):1478–1490.
23. Galiè N, Humbert M, Vachiery JL, et al; ESC Scientific Document Group. 2015 ESC/ERS Guidelines for the diagnosis and treatment of pulmonary hypertension: The Joint Task Force for the Diagnosis and Treatment of Pulmonary Hypertension of the European Society of Cardiology (ESC) and the European Respiratory Society (ERS): Endorsed by: Association for European Paediatric and Congenital Cardiology (AEPC), International Society for Heart and Lung Transplantation (ISHLT). Eur Heart J 2016;37(1):67–119.
24. Hochberg MC. Updating the American College of Rheumatology revised criteria for the classification of systemic lupus erythematosus. Arthritis Rheum 1997;40(9):1725.
25. Shiboski CH, Shiboski SC, Seror R, et al; International Sjögren's Syndrome Criteria Working Group. 2016 American College of Rheumatology/European League Against Rheumatism Classification Criteria for Primary Sjögren's Syndrome: a consensus and data-driven methodology involving three international patient cohorts. Arthritis Rheumatol 2017;69(1):35–45.
26. Seror R, Bowman SJ, Brito-Zeron P, et al. EULAR Sjögren's syndrome disease activity index (ESSDAI): a user guide. RMD Open 2015;1(1):e000022.
27. Percie du Sert N, Hurst V, Ahluwalia A, et al. The ARRIVE guidelines 2.0: updated guidelines for reporting animal research. PLoS Biol 2020;18(7):e3000410.
28. Bedoya SK, Lam B, Lau K, et al. Th17 cells in immunity and autoimmunity. Clin Dev Immunol 2013;2013:986789.
29. Mills KHG. IL-17 and IL-17-producing cells in protection versus pathology. Nat Rev Immunol 2023;23(1):38–54.
30. Hedger MP, de Kretser DM. The activins and their binding protein, follistatin-diagnostic and therapeutic targets in inflammatory disease and fibrosis. Cytokine Growth Factor Rev 2013;24(3):285–295.
31. He M, Chen Z, Martin M, et al. miR-483 targeting of CTGF suppresses endothelial-to-mesenchymal transition: therapeutic implications in Kawasaki disease. Circ Res 2017;120(2):354–365.
32. Chen B, Chang HM, Zhang Z, et al. ALK4-SMAD3/4 mediates the effects of activin A on the upregulation of PAI-1 in human granulosa lutein cells. Mol Cell Endocrinol 2020;505:110731.
33. Attisano L, Wrana JL, Montalvo E, et al. Activation of signalling by the activin receptor complex. Mol Cell Biol 1996;16(3):1066–1073.
34. Zhang Z, Wang J, Chen Y, et al. Activin a promotes myofibroblast differentiation of endometrial mesenchymal stem cells via STAT3-dependent Smad/CTGF pathway. Cell Commun Signal 2019;17(1):45.
35. Schust J, Sperl B, Hollis A, et al. Stattic: a small-molecule inhibitor of STAT3 activation and dimerization. Chem Biol 2006;13(11):1235–1242.
36. Freitas EC, de Oliveira MS, Monticielo OA. Pristane-induced lupus: considerations on this experimental model. Clin Rheumatol 2017; 36(11):2403–2414.
37. Jung SY, Yug JS, Clarke JM, et al. Population pharmacokinetics of vactosertib, a new TGF-β receptor type Iota inhibitor, in patients with advanced solid tumors. Cancer Chemother Pharmacol 2020;85(1): 173–183.
38. Anderson R, Blidner AG, Rapoport BL. Frontiers in pharmacology: review manuscript targeting of the neutrophil as an adjunctive strategy in non-small cell lung cancer. Front Pharmacol 2021;12: 676399.
39. Hong E, Barczak W, Park S, et al. Combination treatment of T1-44, a PRMT5 inhibitor with Vactosertib, an inhibitor of TGF-β signaling, inhibits invasion and prolongs survival in a mouse model of pancreatic tumors. Cell Death Dis 2023;14(2):93.
40. Hong E, Park S, Ooshima A, et al. Inhibition of TGF-β signalling in combination with nal-IRI plus 5-Fluorouracil/Leucovorin suppresses invasion and prolongs survival in pancreatic tumour mouse models. Sci Rep 2020;10(1):2935.
41. Son JY, Park SY, Kim SJ, et al. EW-7197, a novel ALK-5 kinase inhibitor, potently inhibits breast to lung metastasis. Mol Cancer Ther 2014; 13(7):1704–1716.
42. Jin CH, Krishnaiah M, Sreenu D, et al. Discovery of N-((4-([1,2,4]triazolo[1,5-a]pyridin-6-yl)-5-(6-methylpyridin-2-yl)-1H-imidazol-2-yl) methyl)-2-fluoroaniline (EW-7197): a highly potent, selective, and orally bioavailable inhibitor of TGF-β type I receptor kinase as cancer immunotherapeutic/antifibrotic agent. J Med Chem 2014; 57(10):4213–4238.
43. Lee SY, Byeon S, Ko J, et al. Reducing tumor invasiveness by ramucirumab and TGF-beta receptor kinase inhibitor in a diffuse-type gastric cancer patient-derived cell model. Cancer Med 2021;10(20): 7253–7262.
44. Nogueira-Ferreira R, Vitorino R, Ferreira R, et al. Exploring the monocrotaline animal modelfor the study of pulmonary arterial hypertension: a network approach. Pulm Pharmacol Ther 2015; 35:8–16.

45. Westerhof BE, Saouti N, van der Laarse WJ, et al. Treatment strategies for the right heart in pulmonary hypertension. Cardiovasc Res 2017;113(12):1465–1473.
46. Spiekerkoetter E, Tian X, Cai J, et al. FK506 activates BMPR2, rescues endothelial dysfunction, and reverses pulmonary hypertension. J Clin Invest 2013;123(8):3600–3613.
47. Dunmore BJ, Drake KM, Upton PD, et al. The lysosomal inhibitor, chloroquine, increases cell surface BMPR-II levels and restores BMP9 signalling in endothelial cells harbouring BMPR-II mutations. Hum Mol Genet 2013;22(18):3667–3679.
48. Souza R, Badesch DB, Ghofrani HA, et al. Effects of sotatercept on haemodynamics and right heart function: analysis of the STELLAR trial. Eur Respir J 2023;62(3):62.
49. Florentin J, Zhao J, Tai YY, et al. Interleukin-6 mediates neutrophil mobilization from bone marrow in pulmonary hypertension. Cell Mol Immunol 2021;18(2):374–384.

American College of Rheumatology
Empowering Rheumatology Professionals

Arthritis & Rheumatology
Vol. 77, No. 11, November 2025, pp 1548–1559
DOI 10.1002/art.43243

Trio Whole Exome Sequencing in Chinese Childhood-Onset Lupus Reveals Novel Candidate Genes

Jianyang Ma,[1] Yuting Qin,[1] Soon-Min Hong,[2] Thuvaraka Ware,[3] Guojun Hou,[2] Jingjing Tan,[4] Chengmei Xie,[1] Pingjing Zhang,[1] Xiaoqian Wu,[1] Todor Arsov,[5] Lanfang Cao,[6] T. Daniel Andrews,[4] Philip Wu,[4] Qian Shen,[7] Huihua Ding,[2] Nan Shen,[1] Carola G. Vinuesa,[7] and Yuke He[1]

Objective. Systemic lupus erythematosus (SLE) is an autoimmune disease in which rare and common gene variants contribute to pathogenesis. Severe sporadic disease in children is often explained by "de novo" variants that can be uncovered by trio sequencing.

Methods. Whole-exome sequencing was performed in 50 Chinese trios with childhood-onset SLE (cSLE). Rare coding variants in SLE-associated genes and all de novo variants were investigated. Gene pathway and expression analysis and interferon-β (IFNβ) luciferase assays were used to predict contribution to disease.

Results. Each proband carried at least one rare variant in an SLE-associated gene, with a median of six per child. At least two probands had monogenic disease, and one-third of probands carried novel or rare variants in genes well accepted to cause monogenic SLE: *ACP5*, *C3*, *C4A*, *C4B*, *DNASE1*, *IFIH1*, *NRAS*, *RNASEH2B*, *RNASEH2C*, and *SAMHD1*. Probands carried a median of one de novo, rare, coding variant. Intriguingly, although only two de novo variants occurred in genes previously associated with SLE, 12 of the 50 genes were enriched in the top 20 SLE-related pathways and were highly expressed in age-associated B cells and plasma B cells. These genes represent promising candidate lupus genes. Two de novo variants occurring in genes not previously linked to SLE or autoimmunity, *DHX8* and *ACTR5*, enhanced type I IFN signaling.

Conclusion. This study highlights the abundance of lupus-relevant rare gene variants in cSLE, supports frequent contribution of de novo variants to disease, and identifies genes that may constitute novel therapeutic targets of relevance to Chinese patients.

INTRODUCTION

Systemic lupus erythematosus (SLE) is the prototypic systemic autoimmune disease, driven by a combination of genetic and environmental factors. Over the past decades, genome-wide association studies (GWASs) have identified hundreds of variants with statistically significant association to SLE ($P < 1 \times 10^{-8}$). However, most of these variants are common variants and located in noncoding regions, generally exerting small effects on disease susceptibility.[1] With the advent of next-generation sequencing technologies, many novel and rare variants have been identified in recent years. Some, but not all, of these variants are found within genes previously implicated in SLE.[2] Generation of mouse models carrying the orthologous variants has identified

Supported by the National Natural Science Foundation of China (grants 32270946, 32170903, 31930037, and 32141004) and a Royal Society Wolfson Fellowship as well as the Francis Crick Institute (grant C2228), which receives its core funding from Cancer Research UK, the UK Medical Research Council, and the Wellcome Trust.

[1]Jianyang Ma, PhD, Yuting Qin, PhD, Chengmei Xie, PhD, Pingjing Zhang, BS, Xiaoqian Wu, MSc, Nan Shen, MD, PhD, Yuke He, PhD: China-Australia Centre for Personalized Immunology, Department of Rheumatology and Shanghai Institute of Rheumatology, School of Medicine, Renji Hospital, Shanghai Jiao Tong University, Shanghai, China; [2]Soon-Min Hong, PhD, Guojun Hou, PhD, Huihua Ding, MD, PhD: Shanghai Institute of Rheumatology, School of Medicine, Renji Hospital, Shanghai Jiao Tong University, Shanghai, China; [3]Thuvaraka Ware, PhD: The Francis Crick Institute, London, United Kingdom; [4]Jingjing Tan, MSc, T. Daniel Andrews, PhD, Philip Wu, PhD: Division of Immunology and Infectious Disease, John Curtin School of Medical Research, The Australian National University, Canberra, Australian Capital Territory, Australia; [5]Todor Arsov, PhD: Faculty of Medical Sciences, Goce Delcev University, Shtip, North Macedonia; [6]Lanfang Cao, MD, PhD: Department of Pediatrics, Renji Hospital, Shanghai Jiao Tong University, Shanghai, China; [7]Qian Shen, PhD, Carola G. Vinuesa, MD, PhD: China-Australia Centre for Personalized Immunology, Department of Rheumatology, Renji Hospital, Shanghai Jiao Tong University School of Medicine, Shanghai, China, and The Francis Crick Institute, London, United Kingdom.

Drs Ma and Qin are co-first authors and contributed equally to this work. Drs N. Shen, Vinuesa, and He are co-last authors and contributed equally to this work.

Additional supplementary information cited in this article can be found online in the Supporting Information section (https://acrjournals.onlinelibrary.wiley.com/doi/10.1002/art.43243).

Author disclosures are available at https://onlinelibrary.wiley.com/doi/10.1002/art.43243.

Address correspondence via email to Yuke He, PhD, at hyk@mail.ustc.edu.cn; to Carola G. Vinuesa, MD, PhD, at carola.vinuesa@crick.ac.uk; or to Nan Shen, MD, PhD, at nanshensibs@gmail.com.

Submitted for publication September 26, 2024; accepted in revised form April 30, 2025.

novel genes[3–6] causing monogenic or oligogenic SLE such as *TLR7*, *UNC93B1*, *SAT1*, and *TNIP1*, expanding the list of monogenic lupus causes. Functional validation of variants has also revealed how rare variants in genes such as *PACSIN1*, *SH2B3*, and *P2RY8* likely contribute to SLE susceptibility.[7–9]

Trio testing increases rare disease diagnosis rates, enabling identification of biallelic, homozygous, and de novo variants. The latter have been shown to explain two-thirds of severe sporadic genetic disease in childhood.[10] Several small studies have investigated the presence of de novo variants in White cohorts, revealing putative novel causes of monogenic disease. In this study, we set out to investigate the presence, mode of inheritance, and putative contribution of rare gene variants in 50 Chinese probands with childhood-onset SLE (cSLE), which is known to present with more severe phenotype and have a higher genetic risk.[11]

MATERIALS AND METHODS

Human samples collection and sequencing. This study includes 50 unrelated cSLE probands from the pediatric department of Shanghai Renji Hospital. All patients fulfilled American College of Rheumatology criteria for SLE.[12] The study was approved by the Renji Hospital Ethics Committee of Shanghai Jiaotong University School of Medicine (KY2022-023-B). Written informed consents were obtained from all participants. Detailed patient characteristics are included in Supplementary Table 1.

Genomic DNA was extracted by using QIAamp DNA Blood kit (QIAGEN) according to the manufacturer's instructions. Whole-exome sequencing (WES) was performed using the Illumina HiSeq X platform. Bioinformatic analysis was undertaken by the China-Australia Center for Personalized Immunology (CACPI) pipeline.[9] Deleterious of variants were predicted based on PolyPhen-2, SIFT, and CADD. Variants with low minor allele count (<5) were filtered out.

Gene selection and variant screening. We generated a list of all identified lupus-associated genes including 49 monogenic causes of SLE[13,14] and 213 GWAS SLE loci[13,15] (Supplementary Table 2). In the case of parent-proband trios, de novo origin of variants was established by comparison with their parents' WES data. Relatedness of probands and parents was confirmed using Peddy.[16] We refer to variants with minor allele frequency (MAF) <0.005 as "rare variants." Variants with MAF greater than 0.005 in gnomAD version 4.0 and gnomAD version 4.0 East Asian databases were excluded.

Gene enrichment analysis. All genes with rare variants were analyzed by MetaScape online analysis tool (https://metascape.org/). The top 20 pathway enrichment plots and gene lists clustered in each pathway were automatically generated by the tool.

Luciferase reporter assay. HEK293 cells were transfected with interferon-β (IFN-β) reporter, renilla reporter, myeloid differentiation factor 88 (MYD88) plasmid, IFN regulatory factor 7 (IRF7) plasmid, and indicated plasmids. Cells were lysed 24 hours after transfection, and luciferase activity was detected by using Dual-Glo Luciferase Assay System (Promega).

Quantitative real-time reverse transcriptase–polymerase chain reaction. Complementary DNA was prepared using PrimeScript RT Reagent Kit (Takara) and amplified with the primers shown in Supplementary Table 3. Threshold cycle (Ct) values was normalized by GAPDH and relative expression was calculated using the $2^{-\Delta\Delta Ct}$ method.

Statistical analysis. For all the experiments, *P* values were determined by an unpaired *t*-test, Mann-Whitney U-test, or chi-square test. *P* values less than 0.05 were considered significant. Data analysis was performed using Graph Prism 8.0.

This research was done without direct patient involvement beyond sample collection. Patients did not participate in designing the study, analyzing the data, or drafting the article.

RESULTS

Characteristics of the cSLE cohort. We performed WES of 50 Chinese trios, which included a total of 50 probands and one identical twin sister with cSLE. Genetically determined ethnicity revealed that 86% of probands were of Eastern Chinese descent, whereas Dai of South China and Yi of Southwest China each accounted for 4% (Figure 1A); one child had detectable Japanese ancestry. The mean age at disease onset was 10.8 years, and 78.4% of the probands were female (Table 1). The mean Systemic Lupus Erythematosus Disease Activity Index (SLEDAI) score of 50 probands is 9.96, as determined by the SLEDAI 2000 (Table 1).

Landscape of rare variants identified by WES. Following WES and subsequent data analysis of the 50 trios, we filtered variants by MAF <0.005 according to gnomAD v4.0 East Asian. Four types of variants were included: missense variants, nonsense variants, coding region indels, and splice site variants with a high likelihood of resulting in alternative splicing. We identified 45 rare variants across 49 genes implicated in monogenic SLE and 224 rare variants across 213 SLE GWAS genes (Figure 1C and Supplementary Table 4). The probands carried a combined 125 de novo rare variants (Figure 1C and Supplementary Table 4). More than 90% of the identified variants were missense variants, and the remainder were nonsense, insertion/deletion, or splice variants (Figure 1D). Pathogenicity assessments revealed that 21.6% of de novo rare variants and 42% of rare variants in SLE-associated genes were predicted to be likely damaging based on PolyPhen-2, SIFT, and CADD scores (Supplementary Figure 1A). Stratification of probands by age at

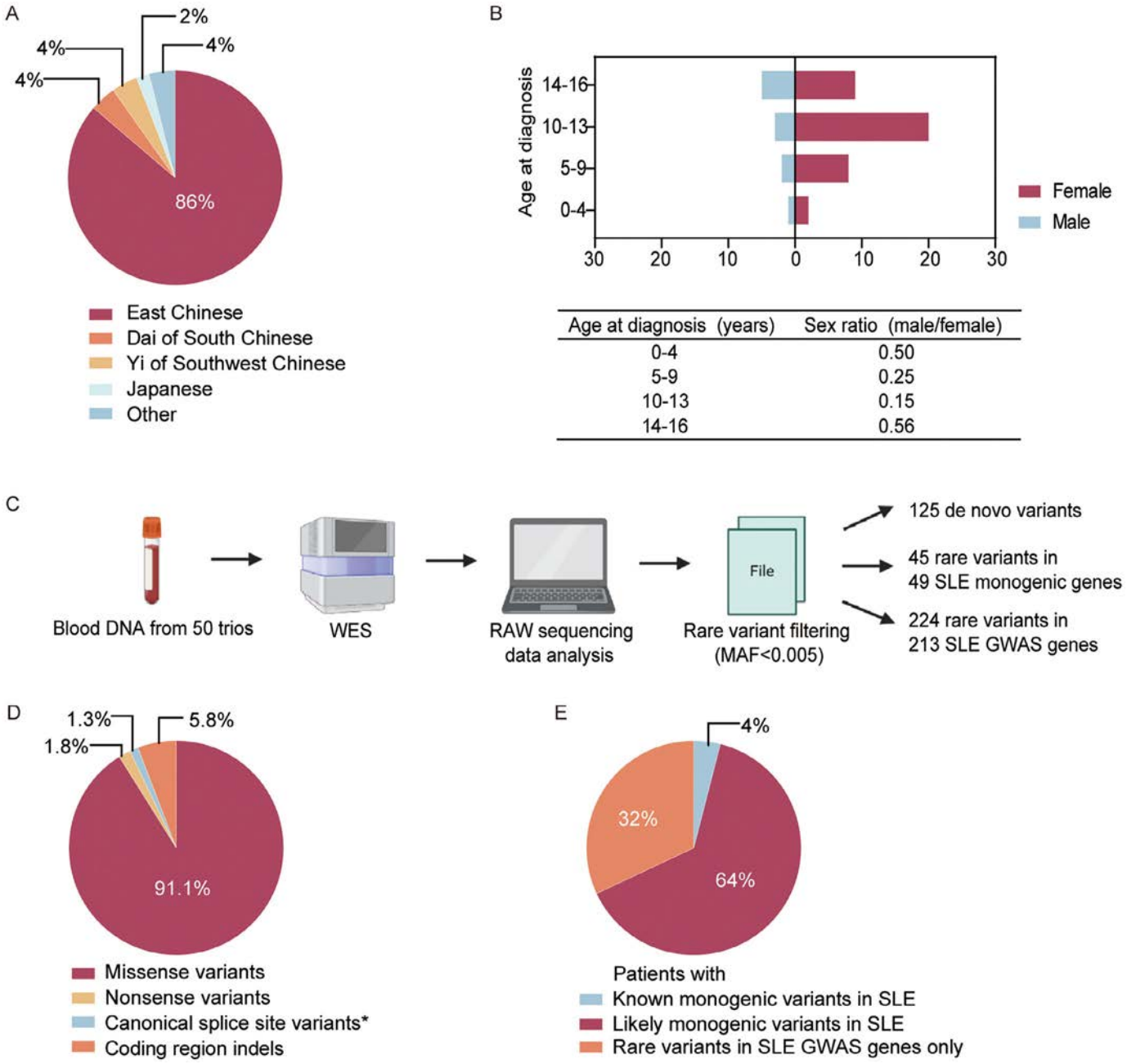

Age at diagnosis (years)	Sex ratio (male/female)
0-4	0.50
5-9	0.25
10-13	0.15
14-16	0.56

Figure 1. Patient characteristics and analysis pipeline. (A) Ethnicity of the 50 SLE probands. (B) Age and sex distribution. (C) Schematic representation of the pipeline for rare variant identification. Rare variants are defined as variants with an MAF of <0.005 (gnomAD East Asian version 4.0). De novo origin of variants was established by comparison with their parents' sequence data. Putative lupus–associated variants were selected based on filtering rare variants in 49 SLE monogenic genes and 213 GWAS genes. (D) Proportion of variants called by WES. *Splice site variants affecting +1 and +2 nucleotides at the 5′ donor splice site and −1 and −2 residues at the 3′ acceptor splice site. (E) Proportion of patients with different types of variants. GWAS, genome-wide association study; MAF, minor allele frequency; SLE, systemic lupus erythematosus; WES, whole-genome sequencing.

diagnosis showed that the 0- to 9-years group had a slightly higher number of rare variants in SLE genes compared to the 10- to 15-years group, although the difference was not statistically significant (Supplementary Figure 1B).

Pathogenic variants. Among the 50 lupus trios, we could only confidently identify two probands with monogenic SLE, without further functional validation (Figure 2). Proband 26 carried a de novo G12D variant in *NRAS* that is pathogenic in Noonan syndrome according to ClinVar (Variation ID: 39648); Noonan syndrome can present with SLE.[17] This variant has also been found in patients with myeloproliferative disorder[18] and as a somatic variant in multiple types of cancer such as non-small-cell lung

Table 1. Clinical features of patients with cSLE*

Characteristic	Patients with cSLE
Female, % (n/N)	78.4 (40/51)
Age at onset, mean ± SD, y	10.8 ± 3.46
SLEDAI-2K, mean ± SD	9.96 ± 4.91
Alopecia, % (n/N)	25.4 (13/51)
Arthritis, % (n/N)	35.3 (18/51)
Serositis, % (n/N)	3.9 (2/51)
Leukopenia, % (n/N)	19.6 (10/50)
Lymphopenia, % (n/N)	7.8 (4/51)
Renal, % (n/N)	39.2 (20/51)
ANA, % (n/N)	100 (24/24)
Anti-dsDNA, % (n/N)	69 (29/42)
Anti-SM, % (n/N)	9.8 (5/51)
Anti-RNP, % (n/N)	17.6 (9/51)
Anti-SSA, % (n/N)	27.5 (14/51)
Anti-SSB, % (n/N)	13.7 (7/51)
Cardiolipin antibodies, % (n/N)	6.1 (3/49)
β-2 glycoprotein I antibodies, % (n/N)	0 (0/45)
Consumed C3, % (n/N)	52.9 (27/51)
Consumed C4, % (n/N)	37.2 (19/51)
Seizures, % (n/N)	0 (0/51)
Psychosis, % (n/N)	0 (0/51)
Myelitis, % (n/N)	0 (0/51)

* ANA ≥1:80 was defined as positive, and anti-dsDNA ≥15 IU/mL was defined as positive. ANA, antinuclear antibody; anti-dsDNA, anti–double-stranded DNA; anti-SM, anti-Smith; C3, complement C3; C4, complement C4; cSLE, childhood-onset systemic lupus erythematosus; RNP, ribonucleoprotein; SLEDAI-2K, Systemic Lupus Erythematosus Disease Activity Index 2000.

carcinoma,[19] multiple myeloma, and acute myeloid leukemia.[20] Proband 31 had compound heterozygous variants in *ACP5*—G290V and R46Q—as well as an R24H variant in *SAMHD1* that we have previously reported.[21] ACP5 deficiency has been shown to cause SLE in an autosomal recessive manner. ACP5 and SAMHD1 variants may act synergistically to augment type I IFN production.

We also previously reported the damaging L257F variant in *P2RY8* in proband[9] 11. This is a novel de novo variant resulting in a complete loss of function, which leads to a reduced ability to repress AKT activation and migration, along with deregulated extracellular signal–regulated kinase (ERK) activation. This disruption is likely to disrupt B cell tolerance and contribute to the cSLE. Given the lack of a mouse *P2RY8* orthologue and in the absence of other kindreds where monogenic disease can be clearly established, it is not possible at this stage to state that P2RY8 loss-of-function causes monogenic SLE.

Although proband 35 was homozygous for a novel C4A missense variant (rs28357076), only complete C4 deficiency, which requires four null C4A and C4B alleles, has a 75% incidence of SLE.[22] Although this variant had an MAF of 0.002091 according to gnomAD 4.0 East Asian, gnomAD 2.0 recorded a variant frequency of 0.03653 in East Asian individuals. The variant was also predicted to be benign by three algorithms. Thus, it is unlikely this variant causes monogenic disease.

Rare variants in putative lupus–causing genes. We next looked at rare variants reported in the literature to cause monogenic SLE or lupus-like disease. Of the 50 kindreds and excluding the probands described previously, an additional 12 probands had rare variants in genes that are well accepted to cause monogenic SLE via either the complement pathway (*C3*, *C4A*, and *C4B*) or via metabolism of nucleic acids (*DNASE1*, *IFIH1*, *RNASEH2B*, *RNASEH2C*, and *SAMHD1*). All variants were of unknown or uncertain significance except for one *IFIH1* variant in two probands (17 and 37) reported as likely benign in ClinVar. When we included the remaining list of genes suggested to cause SLE in at least one publication, we identified an additional 19 probands. These additional putative mono- and oligogenic SLE genes are involved in type I IFN regulation (*DDX58*, *NLRC4*, and *PACSIN1*), disruption of B cell and T cell tolerance (*DOCK8*, *FAS*, and *LRBA*), and metabolic disorders (*CYBB*, *MAN2B1*, and *SLC7A7*) (Figure 2). Thus, a total of 64% (Figure 1E) of the probands had rare variants of unknown significance in genes with the potential to cause SLE.

Additionally, we identified 224 rare variants in genes associated with SLE by GWAS. Notably, all 50 probands carried rare variants in SLE GWAS genes, with a median of 4.5 per proband (and a total median of 6 variants per proband in SLE-associated genes). In 16 of these probands, rare variants were identified exclusively in SLE GWAS genes, representing 32% of the cohort (Figure 1E).

We also conducted a comparative analysis using 105 control samples of Han Chinese Southeast Asian ancestry from the 1000 Genomes Project database. This analysis revealed a significant increase in the number of rare variants in known SLE genes within the SLE cohort compared to controls (Figure 3A). These results add to other published evidence that SLE patients carry a higher burden of rare variants in SLE-associated genes.[23] Even though unaffected parents do not constitute an adequate control group for this analysis due to sharing ∼50% of their genetic material with probands—this can obscure a disease—specific signal, the parents versus probands comparison remained significant in our cohort (Figure 3A). A more restricted analysis focused on 64 well established SLE-associated genes that colocalize with expression quantitative trait loci (eQTL) signals[24] (Supplementary Table 2), revealed a total of 53 rare variants in 30 genes (underscored in Figure 2), distributed across 33 kindreds (33/50 = 66%).

Our previous analyses in White SLE enriched in childhood- and juvenile-onset disease identified 10 SLE-associated genes validated by eQTL analysis present in more than 5% of SLE probands, with *BLK*, *LYST*, *TYK2*, *UHRF1BP1*, and *IKBKE* being the genes most commonly harboring rare variants.[25] In our Chinese cohort, *TYK2*, *C4A*, and *C4B* were the genes most frequently containing rare variants in Chinese cohort (Figure 3B). TYK2 promulgates signaling downstream of many cytokines including type I and type III IFNs. None of the TYK2 variants were predicted to be pathogenic by our in-silico prediction tools; however, these algorithms are often poor

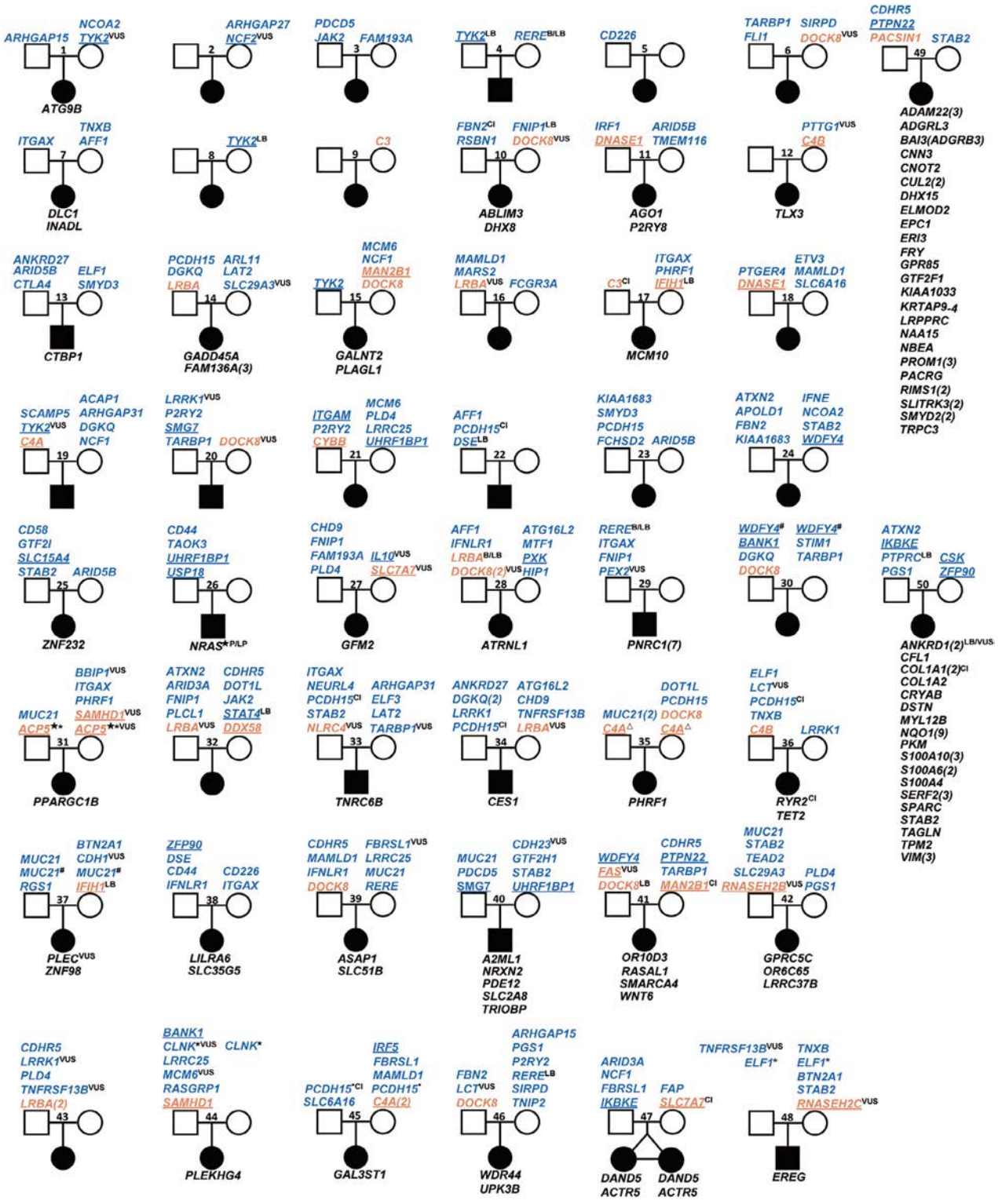

Figure 2. Landscape of rare variants identified by whole-genome sequencing in 50 systemic lupus erythematosus (SLE) trios. Rare/novel variants in monogenic SLE genes (orange), genome-wide association study (blue) SLE genes, and genes with de novo variants (black), carried by each proband were shown in the pedigree. Paternally inherited gene variants (present in the proband) are listed in the upper left, maternally inherited gene variants (present in the proband) are listed in the upper right, and genes with de novo variants are listed below each proband. For genes with multiple variant sites, the number of variants are shown in parentheses. Monogenic SLE genes with known causal variants. SLE genes validated by expression quantitative trait loci analysis are underlined. ★Variants inherited paternally or maternally; #compound heterozygous; *homozygous; △ClinVar categories. B, benign; CI, conflicting interpretations of pathogenicity; LB, likely benign; P/LP, pathogenic/likely pathogenic; VUS, variant of uncertain significance. Color figure can be viewed in the online issue, which is available at http://onlinelibrary.wiley.com/doi/10.1002/art.43243/abstract.

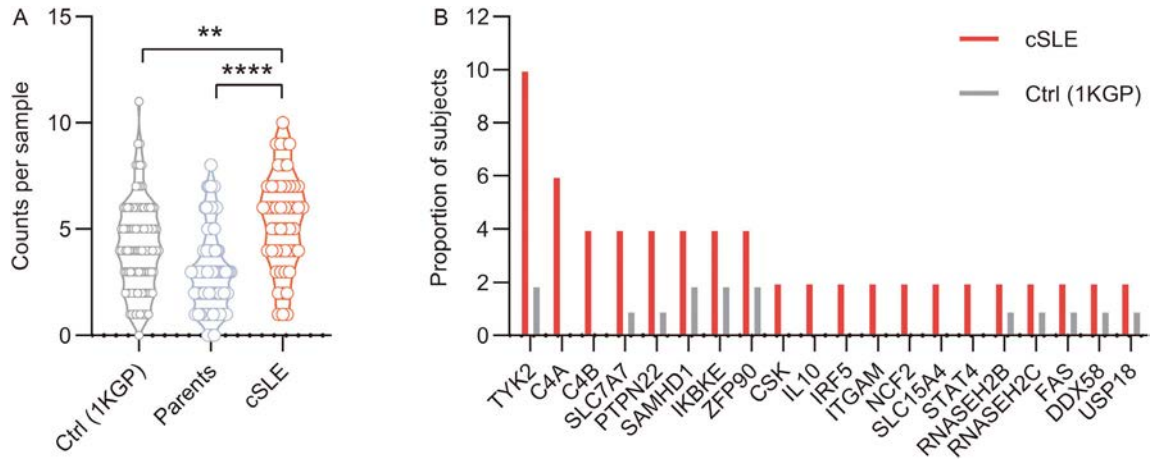

Figure 3. The most frequently mutated genes in 50 SLE trios. (A) Number of rare variants in known SLE genes (monogenic and genome-wide association study SLE genes) per individual in SLE cohort compared with unaffected parents and controls from the 1KGP. *P* values determined by chi-square test (*$P < 0.05$, ****$P < 0.0001$). (B) Most frequently mutated genes in SLE cohort, shown as the proportion of patients with SLE and controls carrying rare variants in each indicated SLE-associated gene. Data are based on 64 SLE genes validated by expression quantitative trait loci analysis. Genes with variants occurring at ≥2 times the prevalence in controls were shown. 1KGP, 1000 Genomes Project; cSLE, childhood-onset systemic lupus erythematosus; Ctrl, control. Color figure can be viewed in the online issue, which is available at http://onlinelibrary.wiley.com/doi/10.1002/art.43243/abstract.

predictors of pathogenic gain-of-function variants, which compared with loss-of-function variants tend to interfere less with protein structures.[26]

De novo rare variants. De novo variants are known to explain two-thirds of severe genetic disease[10] and are a fertile ground for understanding disease pathogenesis and discovering novel drug targets. By comparing the sequencing data of the proband and their parents, we identified a total of 125 de novo variants in 93 genes among 33 probands. Seventeen probands did not carry bona fide rare coding de novo variants. We found two probands (49 and 50) had an unusual number of de novo variants, 67 in total in 42 genes (Figure 2); relatedness was confirmed genetically, as was the absence of variant reads in the parents of these two trios. By comparing the variant allele frequency (VAF) of de novo variants in the two families with an unusually high number of such variants to the remaining 48 families, we found a higher proportion of low VAF (10–26%) de novo variants in these two families (Supplementary Figure 2A and Supplementary Table 4). This suggests a greater likelihood of somatic mutations, as opposed to gonadal parental mosaicism, in these cases.[27] Although neither patient in family 49 and 50 has developed neoplastic disease to date, the possibility of undetected preneoplastic processes cannot be ruled out. Further investigation and long-term follow-up of these patients will be essential to clarify the clinical significance of these genetic findings.

We took advantage of the Gene4denovo WES database to analyze de novo rare variants in healthy control samples. Using the same filtering criteria used for our cSLE cohort, we identified a total of 1,619 de novo rare variants (including missense, nonsense, canonical splice site variants, and coding region indels), distributed in the coding regions of 1,454 genes in 2,049 healthy control individuals. The total number of de novo rare variants in our cSLE cohort was significantly higher compared to the control group. This difference remained statistically significant even after excluding two probands (families 49 and 50) who carried an unusually high number of de novo variants (Supplementary Figure 2B and Supplementary Table 5). A comparison of per-sample counts of rare de novo variants between the SLE cohort and controls also suggested a significantly higher genetic burden in patients with cSLE (Supplementary Figure 2C). These results must nevertheless be taken with caution given the use of different sequencing platforms in SLE versus healthy controls.

In addition to the aforementioned variants in *NRAS* and *P2RY8*, three genes carrying de novo variants—*GADD45A*, *TET2*, and *PHRF1*—have been previously associated with SLE. GADD45A plays a crucial role in DNA repair and cellular stress responses, and its dysregulation has been linked to autoimmunity, including lupus.[28] TET2, a key regulator of DNA demethylation, has been implicated in immune dysregulation and lupus pathogenesis.[29] *PHRF1* is a well-established SLE GWAS gene, and an E3 ubiquitin ligase involved in genome integrity.[30] Additionally, leukocyte Ig–like receptor A6 (LILRA6) has been implicated in rheumatoid arthritis and multiple sclerosis, whereas minichromosome maintenance protein 10 (MCM10) has been identified in the context of immunodeficiency disease, with or without congenital cardiomyopathy. Thus, collectively, six genes (12%) show direct ties to immune diseases. For genes without established direct links to immune diseases, 23 genes (46%) are relevant to immunity (Supplementary Figure 2D and Supplementary Table 6).

We have previously shown that except for complement genes, most genes causing monogenic SLE or associated to lupus in GWAS are expressed in B cells, and a significant fraction of them are most highly expressed in age-associated B cells (ABCs). To investigate the likelihood that the genes carrying de novo variants in our cohort are contributing to the SLE phenotype, we first investigated their expression pattern. Using the online transcriptome GENEVESTIGATOR database, we plotted immune cell–specific expression of genes with de novo variants. We were intrigued to see 50 genes carrying de novo variants were expressed in B cells. Among them, 19 genes (*ACTR5*, *AGO1*, *ASAP1*, *CTBP1*, *DHX8*, *FAM136A*, *GFM2*, *LRRC37B*, *NRAS*, *P2RY8*, *PDE12*, *PHRF1*, *PLAGL1*, *PNRC1*, *PPARGC1B*, *TET2*, *TNRC6B*, *WDR44*, and *ZNF232*) were highly expressed in ABCs, and 12 genes (*ABLIM3*, *ATRNL1*, *DAND5*, *GPRC5C*, *LILRA6*, *OR10D3*, *PLEC*, *RASAL1*, *SLC35G5*, *SLC51B*, *TLX3*, and *WNT6*) were highly expressed in plasma cells (Supplementary Figure 3A). Among the 42 genes carrying de novo variants in the two outlier probands, 26 showed expression in immune cells, with endothelial progenitor cell 1 (EPC1) and WASH complex subunit 4 (WASHC4) (Supplementary Figure 3B) being highly expressed in ABCs and stabilin-2 (STAB2) highly expressed in plasma cells. Highly expression in ABCs together with its role in DNA repair makes *EPC1* a possible SLE contributing gene. *WASHC4* encodes a component of the WASH complex, which functions in the intracellular transport of endosomes.

Pathway enrichment analysis and visualization of rare variants. To obtain further insights as to potential contribution of de novo variants to SLE in the probands, we asked whether the genes harboring the variants belong to SLE-related pathways. For this, we conducted a pathway enrichment analysis using the online tool Metascape. A first analysis included Gene Ontology (GO) pathways, Kyoto Encyclopedia of Genes and Genomes pathways, Reactome pathways, and Wiki pathways, including all the genes with rare variants identified in the probands, including SLE monogenic genes, SLE GWAS genes, and the 50 genes with de novo variants. Two probands that had an unusual number of de novo variants, 42 in total, and were excluded from this analysis. Metascape generated the top 20 statistically significant pathways, with "positive regulation of immune response" emerging as the most significant pathway (Figure 4A and B). Other SLE-related pathways included innate immune response, immune cell activation, cytokine signaling, cellular responses to virus, nucleic acid metabolism, inflammatory response, regulation of immune effector process, and regulation of phosphorylation. Nearly half of the genes (21 of 50 genes) with de novo variants clustered among these top 20 pathways (Figure 4B), with some genes such as *PDE12*, *EREG*, *NRAS*, *PPARGC1B*, *GADD45A*, and *LILRA6* appearing in seven, five, five, five, four, and four clusters, respectively. Besides *DLC1* and *EREG*, RAS protein activator-like 1 (*RASAL1*) also formed part of the top SLE pathway (positive regulation of the immune response). The novel *RASAL1* W203X variant is predicted to change the length of the protein. RASAL1 belongs to the GAP1 family, acting as a suppressor of RAS function to control cellular proliferation and differentiation.[31] Considering its high expression in plasma cells, a loss-of-function variant in *RASAL1* would be a good candidate to contribute to cSLE. Together these results suggest that a significant proportion of de novo variants in cSLE probands may contribute to disease pathogenesis and are worth investigating further.

Functional validation of the promising de novo variants. To further probe whether some of the de novo variants occurring in genes not previously linked with SLE may contribute to disease, we selected two genes for functional analysis among the 12 genes that are both expressed most highly in ABCs and plasma cells and belong to the top 20 SLE pathways identified through enrichment analysis: *DHX8* and *ACTR5* (Figure 4C). DHX8 is an ATP-dependent RNA helicase involved in precursor messenger RNA (pre-mRNA) splicing.[32] It is required for the release of mature mRNA from the spliceosome.[32] The de novo variant I879V is located in the RecA2 domain, which forms the helicase core responsible for its helicase activity. This variant is evolutionarily conserved among species and predicted to be damaging by Polyphen, SIFT, and CADD algorithms (Figure 5A–C). DHX8 mRNA expression levels were elevated in untreated SLE patients compared to those receiving treatment (Figure 5H and I). A parallel trend was observed in the expression of IFN-stimulated genes (ISGs) in these patients (Supplementary Figure 4). A luciferase assay on transfection of wild type or mutant protein into HEK293 cells demonstrated that the DHX8 I879V variant causes increased IFN-β activity compared to the wild-type protein (Figure 5D), suggesting that the variant may positively regulate type I IFN pathway.

Acting-related protein 5 (ACTR5) is one of the subunits of the ATPase-dependent chromatin remodeling complex INO80, which is involved in repair of UV-damaged DNA and double-strand breaks in DNA.[33] This gene forms part of the "nucleic acid metabolism and innate immune sensing" pathway. Of note, two identical twins from proband 47 both carry the novel and de novo variant E424Q in *ACTR5*, and both twins exhibit a UV-sensitive clinical lupus phenotype. The variant is evolutionarily conserved and predicted to be deleterious by CADD (Figure 5E and F). A luciferase assay showed that E424Q in ACTR5 led to increased IFN-β activity (Figure 5G). Additionally, *ACTR5* mRNA was higher in untreated compared to treated patients with SLE (Figure 5H and I). A similar trend was observed in ISG expression in these SLE patients (Supplementary Figure 4). Together, these findings suggest that the function of ACTR5 in DNA repair may be important to maintain immune tolerance and prevent SLE, particularly upon UV damage.

A

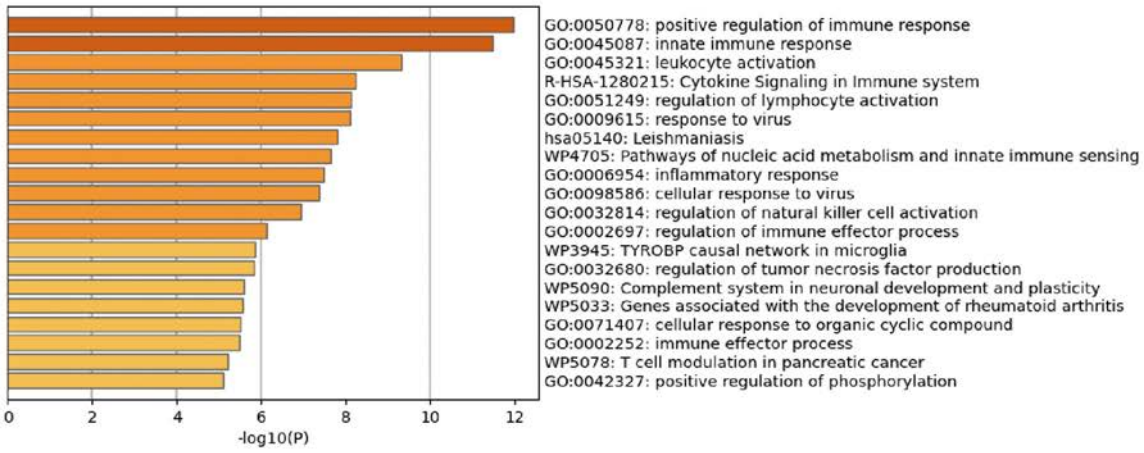

B

	Top 20 pathways		Clustered genes with de novo variants
1	GO:0050778	Positive regulation of immune response	*DLC1, EREG, LILRA6, RASAL1, SMARCA4*
2	GO:0045087	Innate immune response	*EREG, PDE12*
3	GO:0045321	Leukocyte activation	*TET2*
4	R-HSA-1280215	Cytokine Signaling in Immune system	*NRAS, SMARCA4, PDE12, EREG, LILRA6*
5	GO:0051249	Regulation of lymphocyte activation	*SMARCA4, NRAS, PPARGC1B, TRIOBP*
6	GO:0009615	Response to virus	*PDE12*
7	hsa05140	Leishmaniasis	*DLC1, NRAS, LILRA6*
8	WP4705	Pathways of nucleic acid metabolism and innate immune sensing	*GADD45A, TET2, MCM10, ACTR5*
9	GO:0006954	Inflammatory response	
10	GO:0098586	Cellular response to virus	*NRAS, GADD45A, PDE12, DHX8, PPARGC1B*
11	GO:0032814	Regulation of natural killer cell activation	*PDE12*
12	GO:0002697	Regulation of immune effector process	
13	WP3945	TYROBP causal network in microglia	
14	GO:0032680	Regulation of tumor necrosis factor production	*EREG, PDE12, RYR2, SLC2A8*
15	WP5090	Complement system in neuronal development and plasticity	*RYR2, TLX3, PPARGC1B*
16	WP5033	Genes associated with the development of rheumatoid arthritis	*GADD45A*
17	GO:0071407	Cellular response to organic cyclic compound	*CES1, PDE12, PPARGC1B, RYR2, WNT6*
18	GO:0002252	Immune effector process	*LILRA6, PLEC*
19	WP5078	T cell modulation in pancreatic cancer	*DLC1*
20	GO:0042327	Positive regulation of phosphorylation	*EREG, PPARGC1B, GADD45A, SLC51B, NRAS*

C

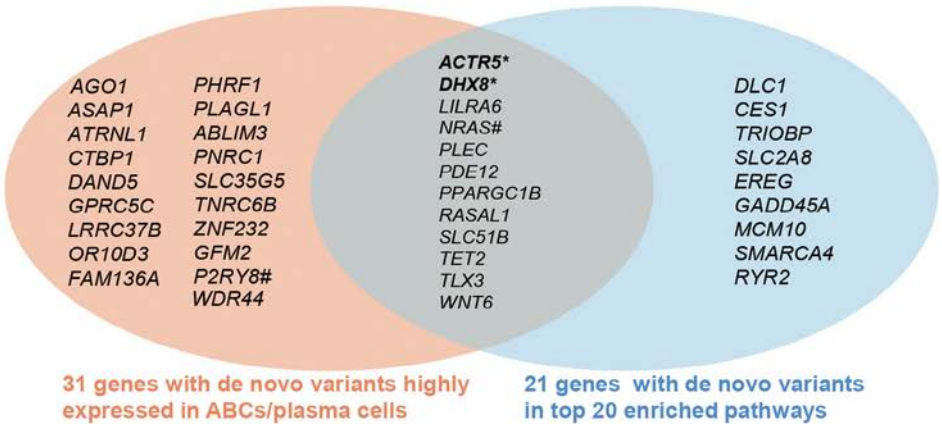

Figure 4. Variants based signaling pathway gene set for enrichment analysis. All selected genes with rare variants carried by patients were processed with online tool Metascape for enrichment analysis. Four pathway analyses were included: Gene Ontology, Kyoto Encyclopedia of Genes and Genomes, Reactome, and Wiki. (A) The top 20 pathways were automatically generated with the –log10 *P* value >4 after the enrichment analysis. (B) List of genes of de novo variants that clustered in each of the top 20 pathways. (C) Venn diagram showing the overlap between the 31 genes carrying de novo variants highly expressed in age-associated B cells and plasma cells and the 21 genes carrying de novo variants belonging to the top 20 enriched pathways. *Taken further for functional validation genes, #Genes with variants already reported to be pathogenic. Color figure can be viewed in the online issue, which is available at http://onlinelibrary.wiley.com/doi/10.1002/art.43243/abstract.

DISCUSSION

Unlike the common variants identified through GWAS, rare variants tend to have a larger effect size and are frequently found within protein-coding regions, offering insights into disease mechanisms that may be missed by traditional approaches. Notably, de novo rare variants, which arise spontaneously and are not

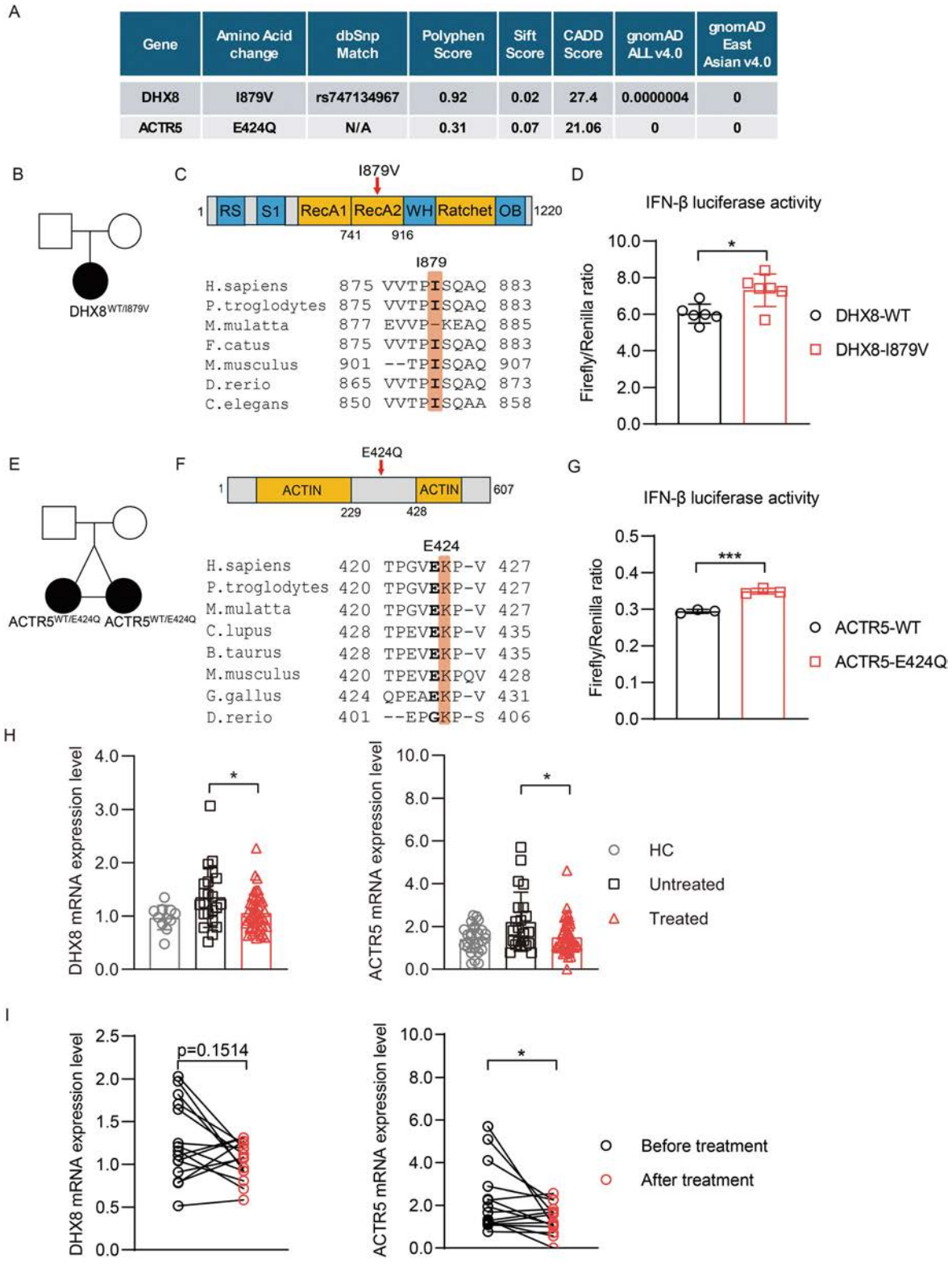

Figure 5. Legend on next page.

found in the somatic genome of either parents, can be especially informative in understanding severe forms of sporadic cSLE. Trio-based genetic analysis provides valuable information into the pattern of inheritance of gene variants and uncovers the presence of de novo variants. The latter, when shown to be pathogenic, can offer profound insights into the mechanisms underpinning disease. Although some studies have investigated the burden of rare gene and de novo variants in cSLE, this is the first study in a Chinese cohort.

In our cohort, all probands carried at least 1 rare variant in a known SLE gene, with some children carrying up to 10 rare variants. We only call monogenic SLE in two probands (4%) with sufficient degree of confidence. This is within the 3.5% to 7% monogenic diagnostic range in published British and French cohorts.[23,34] Our focus on Asian populations is particularly important given the known ethnic variations in SLE prevalence and severity. For example, Asian populations generally show higher SLE prevalence and more severe disease manifestations compared to European populations.[35]

In our analysis, *TYK2* emerged among the top five genes in both Chinese and White cohorts.[25] TYK2 binds to the type I IFN receptor complex and gain-of-function variants in TYK2 enhance cytokine signaling.[36] These findings carry significant therapeutic implications, as selective TYK2 inhibitors could mitigate IFN-driven responses in SLE.[37] Current clinical trials, including those of deucravacitinib, have shown promising results in SLE treatment.[38] The cross-population identification of rare TYK2 variants highlights its crucial role in SLE pathogenesis, paving the way for more precise genetic testing, personalized therapies, and novel targeted treatments.

In this study, rare and coding de novo variants were identified in all probands from 50 trios. The median number of de novo coding variants was 1, which coincides with reports in the literature,[39] with a range of 0 to 16 variants per proband. In the context of cSLE, de novo variants are especially informative because they can explain more severe forms of the disease. Because these mutations are not inherited (or they are inherited from parents with gonadal mosaicism), they frequently escape evolutionary filtering, resulting in more damaging effects on essential biologic processes. Consequently, pathogenic de novo variants in cSLE are often found in genes involved in immune regulation, DNA repair, and other critical cellular functions. Disruptions in these pathways can lead to an overactive immune response, increasing the risk of severe manifestations. Thus, studying de novo variants in cSLE can uncover novel genes and pathways essential to disease development, paving the way for targeted therapeutic interventions. Notably, in the past two years, three different reports have described de novo variants in TLR7 that confer gain-of-function in children with early-onset lupus-like disease.[3,40,41]

We took a combination of two approaches to prioritize the de novo variants: (1) being among the top 20 SLE GO-pathways (21/50 = 42%) and (2) expression in ABC and plasma B cells (31/50 = 62%). This identified 12 genes (12/50 = 24%) that fulfilled both criteria and thus constitute promising candidate lupus genes. Notably, this group contained a gene previously implicated in the causation of SLE (*NRAS*).[17–20] Initial functional validation of ACTR5 and DHX8 showed that both enhanced type I IFN signaling. Increased type I IFN activity is a hallmark of SLE, promoting immune activation and autoantibody production.[42] Monogenic forms of SLE often involve mutations in genes that modulate the metabolism of nucleic acids (eg, *DNASE1*, *DNASE1L3*, *IFIH1*, *RNASEH2A/B/C*, *ADA2*, and *SAMHD1*) or mediate nucleic acid sensing (eg, *TLR7*, *UNC93B1*, *IFIH1*, *ACP5*, and *TMEM173*), leading to excessive type I IFN signaling.[43] Type I IFN reporter assays effectively prioritize variants for further investigation. Once promising variants are identified through functional screening, definitive evidence of SLE causation may be obtained by assessing the effects of these variants in primary immune cells and animal models of lupus. Our multifaceted approach, combining bioinformatic predictions and functional assays, offers a strategy to identify and prioritize de novo variants that may contribute to SLE pathogenesis and uncover potential therapeutic targets.

It was interesting that more than half of de novo variants occurred in genes that were not previously associated with SLE or autoimmunity but were highly expressed in ABCs, a B cell subpopulation thought to be pathogenic in SLE.[44] ABCs are known to be enriched in patients with SLE and exhibit a strong correlation with autoantibodies and disease activity scores. ABCs have been shown to efficiently differentiate into (plasma cells) PCs, and their absence is associated with a reduction in autoantibodies and histologic manifestations of disease.[45,46] The detailed mechanisms governing ABC function and their complex interactions with other immune cells are currently the focus of intensive investigation.[13,47]

Figure 5. Characteristics of de novo rare variants in two systemic lupus erythematosus (SLE) trios. (A) Bioinformatic predictions of protein damage for each de novo variant based on PolyPhen, SIFT, and CADD score. The gnomAD version 4.0 allele frequency, and dbSNP match are shown. (B and E) Pedigrees of probands carrying de novo rare variants in DHX8 and ACTR5. (C and F) Schematic representation of protein domain and evolutionary conservation of each residue. (D and G) IFN-β luciferase assay with indicated WT and mutant complementary DNA. (H and I) Left: DHX8 mRNA expression in peripheral blood mononuclear cells (PMBCs) of patients with SLE. HC (n = 11), untreated patients (n = 22), treated patients (n = 47), and patients before and after treatment (n = 15). Right: ACTR5 mRNA expression in PMBCs of patients with SLE. HC (n = 27), untreated patients (n = 22), treated patients (n = 47), and patients before and after treatment (n = 15). *P* values determined by (D and G) unpaired *t*-test, (H and I) Mann-Whitney U-test. $^{*}P < 0.05$; $^{**}P < 0.01$; $^{***}P < 0.001$; Graphs depict means with SDs. ACTR5, acting-related protein 5; dbSNP, single-nucleotide polymorphism database; HC, healthy control; IFNβ, interferon-β; mRNA, messenger RNA; N/A, not available; WT, wild type. Color figure can be viewed in the online issue, which is available at http://onlinelibrary.wiley.com/doi/10.1002/art.43243/abstract.

Our study focused on rare coding variants associated with SLE, employing an MAF threshold of <0.005 for variant filtration. Although this cutoff value allowed us to concentrate on rare variants, we acknowledge that the choice of 0.005 is somewhat arbitrary and may exclude potentially relevant variants above this threshold. It has been very well established that noncoding and more common variants identified by GWAS can also exert functional effects and act in a polygenic manner to confer SLE risk and larger studies using WGS will be needed to investigate the contribution of rare and common alleles in coding and noncoding regions combined, ideally including polymorphisms in the HLA region. Some of the novel putative SLE candidate genes and variants reported here may help further our understanding of SLE pathogenesis relevant to Asian populations and once validated, harnessed for development of personalized therapies. Although our sample size of 50 trios may seem limited for a complex disease, our findings represent an important first step toward elucidating the intricate genetic contributions to SLE. Future large-scale, collaborative studies across diverse populations will be essential to validate and extend these findings, ultimately refining our understanding of SLE pathogenesis.

ACKNOWLEDGMENTS

For access to human samples, we thank the National Human Genetic Resources Sharing Service Platform construction of Shanghai innovation center (YCZYPT [2017]02) and the professional technical service platform for the physical database of clinical biologic samples of major diseases in Shanghai (18DZ2294100).

AUTHOR CONTRIBUTIONS

All authors contributed to at least one of the following manuscript preparation roles: conceptualization AND/OR methodology, software, investigation, formal analysis, data curation, visualization, and validation AND drafting or reviewing/editing the final draft. As corresponding authors, Drs He, Vinuesa, and N. Shen confirm that all authors have provided the final approval of the version to be published and take responsibility for the affirmations regarding article submission (eg, not under consideration by another journal), the integrity of the data presented, and the statements regarding compliance with institutional review board/Declaration of Helsinki requirements.

REFERENCES

1. Cirulli ET, Goldstein DB. Uncovering the roles of rare variants in common disease through whole-genome sequencing. Nat Rev Genet 2010;11(6):415–425.
2. Lo MS. Monogenic lupus. Curr Rheumatol Rep 2016;18(12):71.
3. Brown GJ, Cañete PF, Wang H, et al. TLR7 gain-of-function genetic variation causes human lupus. Nature 2022;605(7909):349–356.
4. David C, Arango-Franco CA, Badonyi M, et al. Gain-of-function human UNC93B1 variants cause systemic lupus erythematosus and chilblain lupus. J Exp Med 2024;221(8):e20232066.
5. Xu L, Zhao J, Sun Q, et al. Loss-of-function variants in *SAT1* cause X-linked childhood-onset systemic lupus erythematosus. Ann Rheum Dis 2022;81(12):1712–1721.
6. Medhavy A, Athanasopoulos V, Bassett K, et al. A TNIP1-driven systemic autoimmune disorder with elevated IgG4. Nat Immunol 2024;25(9):1678–1691.
7. Xie C, Zhou H, Athanasopoulos V, et al. De novo PACSIN1 gene variant found in childhood lupus reveals a role for PACSIN1/TRAF4 complex in TLR7 activation. Arthritis Rheumatol 2023;75(6):1058–1071.
8. Zhang Y, Morris R, Brown GJ, et al. Rare SH2B3 coding variants in lupus patients impair B cell tolerance and predispose to autoimmunity. J Exp Med 2024;221(4):e20221080.
9. He Y, Gallman AE, Xie C, et al. P2RY8 variants in lupus patients uncover a role for the receptor in immunological tolerance. J Exp Med 2022;219(1):e20211004.
10. French CE, Delon I, Dolling H, et al; NIHR BioResource—Rare Disease; Next Generation Children Project. Whole genome sequencing reveals that genetic conditions are frequent in intensively ill children. Intensive Care Med 2019;45(5):627–636.
11. Webb R, Kelly JA, Somers EC, et al. Early disease onset is predicted by a higher genetic risk for lupus and is associated with a more severe phenotype in lupus patients. Ann Rheum Dis 2011;70(1):151–156.
12. Aringer M, Costenbader K, Daikh D, et al. 2019 European League Against Rheumatism/American College of Rheumatology Classification Criteria for Systemic Lupus Erythematosus. Arthritis Rheumatol 2019;71(9), 1400–1412. Portico. https://doi.org/10.1002/art.40930
13. Vinuesa CG, Shen N, Ware T. Genetics of SLE: mechanistic insights from monogenic disease and disease-associated variants. Nat Rev Nephrol 2023;19(9):558–572.
14. Qin Y, Ma J, Vinuesa CG. Monogenic lupus: insights into disease pathogenesis and therapeutic opportunities. Curr Opin Rheumatol 2024;36(3):191–200.
15. Guga S, Wang Y, Graham DC, et al. A review of genetic risk in systemic lupus erythematosus. Expert Rev Clin Immunol 2023;19(10):1247–1258.
16. Pedersen BS, Quinlan AR. Who's who? Detecting and resolving sample anomalies in human DNA sequencing studies with peddy. Am J Hum Genet 2017;100(3):406–413.
17. Cirstea IC, Kutsche K, Dvorsky R, et al. A restricted spectrum of NRAS mutations causes Noonan syndrome. Nat Genet 2010;42(1):27–29.
18. Altmüller F, Lissewski C, Bertola D, et al. Genotype and phenotype spectrum of NRAS germline variants. Eur J Hum Genet 2017;25(7):823–831.
19. Ohashi K, Sequist LV, Arcila ME, et al. Characteristics of lung cancers harboring NRAS mutations. Clin Cancer Res 2013;19(9):2584–2591.
20. Chang MT, Asthana S, Gao SP, et al. Identifying recurrent mutations in cancer reveals widespread lineage diversity and mutational specificity. Nat Biotechnol 2016;34(2):155–163.
21. Hong SM, Chen W, Feng J, et al. Novel mutations in ACP5 and SAMHD1 in a patient with pediatric systemic lupus erythematosus. Front Pediatr 2022;10:885006.
22. Du Clos TW, Mold C. Complement in host deficiencies and diseases. In: Rich RR, Fleisher TA, Shearer WT, et al, eds. Clinical Immunology: Principles and Practice. 4th ed. Elsevier; 2012:252–269.
23. Belot A, Rice GI, Omarjee SO, et al; FREX Consortium; GENIAL Investigators; UK JSLE Study Group. Contribution of rare and predicted pathogenic gene variants to childhood-onset lupus: a large, genetic panel analysis of British and French cohorts. Lancet Rheumatol 2020;2(2):e99–e109.
24. Ota M, Nagafuchi Y, Hatano H, et al. Dynamic landscape of immune cell-specific gene regulation in immune-mediated diseases. Cell 2021;184(11):3006–3021.e17.
25. Jiang SH, Athanasopoulos V, Ellyard JI, et al. Functional rare and low frequency variants in BLK and BANK1 contribute to human lupus. Nat Commun 2019;10(1):2201.

26. Gerasimavicius L, Livesey BJ, Marsh JA. Loss-of-function, gain-of-function and dominant-negative mutations have profoundly different effects on protein structure. Nat Commun 2022;13(1):3895.
27. Weinstock JS, Laurie CA, Broome JG, et al; NHLBI Trans-Omics for Precision Medicine (TOPMed) Consortium. The genetic determinants of recurrent somatic mutations in 43,693 blood genomes. Sci Adv 2023;9(17):eabm4945.
28. Salvador JM, Hollander MC, Nguyen AT, et al. Mice lacking the p53-effector gene Gadd45a develop a lupus-like syndrome. Immunity 2002;16(4):499–508.
29. Sung WY, Lin YZ, Hwang DY, et al. Methylation of *TET2* promoter is associated with global hypomethylation and hypohydroxymethylation in peripheral blood mononuclear cells of systemic lupus erythematosus patients. Diagnostics (Basel) 2022;12(12):3006.
30. Chang CF, Chu PC, Wu PY, et al. PHRF1 promotes genome integrity by modulating non-homologous end-joining. Cell Death Dis 2015; 6(4):e1716.
31. Chen H, Cheng ZY, Pan Y, et al. RASAL1 influences the proliferation and invasion of gastric cancer cells by regulating the RAS/ERK signaling pathway. Hum Cell 2014;27(3):103–110.
32. Felisberto-Rodrigues C, Thomas JC, McAndrew C, et al. Structural and functional characterisation of human RNA helicase DHX8 provides insights into the mechanism of RNA-stimulated ADP release. Biochem J 2019;476(18):2521–2543.
33. Kitayama K, Kamo M, Oma Y, et al. The human actin-related protein hArp5: nucleo-cytoplasmic shuttling and involvement in DNA repair. Exp Cell Res 2009;315(2):206–217.
34. Charras A, Haldenby S, Smith EMD, et al. Panel sequencing links rare, likely damaging gene variants with distinct clinical phenotypes and outcomes in juvenile-onset SLE. Rheumatology (Oxford) 2023; 62(SI2):SI210–SI225.
35. Wang YF, Lau YL, Yang W. Genetic studies on systemic lupus erythematosus in East Asia point to population differences in disease susceptibility. Am J Med Genet C Semin Med Genet 2019;181(2): 262–268.
36. Sigurdsson S, Nordmark G, Göring HH, et al. Polymorphisms in the tyrosine kinase 2 and interferon regulatory factor 5 genes are associated with systemic lupus erythematosus. Am J Hum Genet 2005;76(3):528–537.
37. Satoh-Kanda Y, Nakayamada S, Kubo S, et al. Modifying T cell phenotypes using TYK2 inhibitor and its implications for the treatment of systemic lupus erythematosus. RMD Open 2024;10(2):e003991.
38. Morand E, Pike M, Merrill JT, et al. Deucravacitinib, a tyrosine kinase 2 inhibitor, in systemic lupus erythematosus: a phase II, randomized, double-blind, placebo-controlled trial. Arthritis Rheumatol 2023; 75(2):242–252.
39. Jónsson H, Sulem P, Kehr B, et al. Parental influence on human germline de novo mutations in 1,548 trios from Iceland. Nature 2017; 549(7673):519–522.
40. Stremenova Spegarova J, Sinnappurajar P, Al Julandani D, et al. A de novo TLR7 gain-of-function mutation causing severe monogenic lupus in an infant. J Clin Invest 2024;134(13):e179193.
41. David C, Badonyi M, Kechiche R, et al. Interface gain-of-function mutations in TLR7 cause systemic and neuro-inflammatory disease. J Clin Immunol 2024;44(2):60.
42. Sim TM, Ong SJ, Mak A, et al. Type I interferons in systemic lupus erythematosus: a journey from bench to bedside. Int J Mol Sci 2022; 23(5):2505.
43. Psarras A, Wittmann M, Vital EM. Emerging concepts of type I interferons in SLE pathogenesis and therapy. Nat Rev Rheumatol 2022; 18(10):575–590.
44. Ma K, Du W, Wang X, et al. Multiple functions of B cells in the pathogenesis of systemic lupus erythematosus. Int J Mol Sci 2019;20(23): 6021.
45. Nickerson KM, Smita S, Hoehn KB, et al. Age-associated B cells are heterogeneous and dynamic drivers of autoimmunity in mice. J Exp Med 2023;220(5):e20221346.
46. Dai D, Gu S, Han X, et al. The transcription factor ZEB2 drives the formation of age-associated B cells. Science 2024;383(6681):413–421.
47. He Y, Vinuesa CG. Germinal center versus extrafollicular responses in systemic autoimmunity: who turns the blade on self? Adv Immunol 2024;162:109–133.

Arthritis & Rheumatology
Vol. 77, No. 11, November 2025, pp 1560–1572
DOI 10.1002/art.43219

American College of Rheumatology
Empowering Rheumatology Professionals

Differences in Dynamics of Specific Antinuclear Antibodies and Their Susceptibility to B Cell–Targeting Treatment in Patients With Systemic Lupus Erythematosus

Hugo J. van Dooren,[1] Mieke van Schaik,[1] Annemarie L. Dorjée,[1] Eline J. Arends,[1] Meggan Mackay,[2] Laura Cooney,[3] David A. Fox,[3] David Wofsy,[4] Dawn Smilek,[4] Cynthia Aranow,[2] Maria Dall'Era,[4] Tom W. J. Huizinga,[1] Cees van Kooten,[1] René E. M. Toes,[1] Betty Diamond,[2] Y. K. Onno Teng,[1] and Jolien Suurmond[1]

Objective. The presence of antinuclear antibodies (ANAs) is characteristic for systemic lupus erythematosus (SLE). Antibody dynamics over time are thought to reflect the cellular source of ANAs and their therapeutic targetability. Anti–double-stranded DNA (anti-dsDNA) is the most prevalent and well-studied of all ANAs, and fluctuations in anti-dsDNA serum levels are associated with disease activity. Antibody dynamics of other ANAs, such as antibodies targeting RNA-binding proteins (RBPs), are often considered more stable compared to anti-dsDNA. However, anti-RBPs may be heterogeneous in nature, and their fluctuation has not been extensively analyzed. Therefore, we aimed to study the dynamics of the different ANAs and their susceptibility to B cell–targeting treatments in patients with SLE.

Methods. Seroconversion of specific ANAs was analyzed using electronic health records from patients with SLE. Titers of specific ANAs and anti-varicella zoster virus (VZV) were determined in serum samples from a longitudinal cohort of patients with SLE and serum from patients with SLE treated with rituximab and belimumab.

Results. Anti-Smith (anti-Sm) and anti-RNP, similar to anti-dsDNA titers, seroconverted more frequently compared to anti–SS-A/SS-B. Furthermore, anti-Sm/RNP and anti-dsDNA titers, but not anti–SS-A/SS-B titers, fluctuated significantly compared to stable anti-VZV controls. Likewise, reductions in anti-dsDNA and anti-Sm/RNP titers after B cell–depleting treatment were comparable in magnitude. However, only anti-dsDNA titer reductions associated with clinical outcomes.

Conclusion. Together, these results show that anti-Sm/RNP and anti-dsDNA, in contrast to anti–SS-A/SS-B, frequently fluctuate and their levels can decrease following B cell–targeted treatments. Thus, distinct ANAs have variable kinetics, potentially reflecting their derivation from different B cell differentiation pathways.

INTRODUCTION

Systemic lupus erythematosus (SLE) is an autoimmune disease that can affect virtually every organ system. SLE can be perceived as a prototypical autoimmune disease in which autoantibodies directed to nuclear antigens (antinuclear antibodies [ANAs]) are a preponderant feature. Among ANAs, anti–double-stranded DNA (anti-dsDNA) antibodies are highly associated with SLE. They are present in the majority of patients with SLE and can reflect disease activity.[1,2] Anti-Smith (anti-Sm) is another ANA considered specific for SLE, although it is present less frequently than anti-dsDNA. Other SLE-associated antibodies are

Supported by Leiden University Medical Center funding (internal MSCA Seal-of-Excellence 2020 regulation). The Calibrate trial was conducted by the Immune Tolerance Network, supported by the National Institute of Allergy and Infectious Diseases, NIH (grant UM1-AI-109565).

[1]Hugo J. van Dooren, MSc, Mieke van Schaik, MD, Annemarie L. Dorjée, BAS, Eline J. Arends, MD, PhD, Tom W. J. Huizinga, MD PhD, Cees van Kooten, PhD, René E. M. Toes, PhD, Y. K. Onno Teng, MD, PhD, Jolien Suurmond, PhD: Leiden University Medical Center, Leiden, The Netherlands; [2]Meggan Mackay, MD, MSc, Cynthia Aranow, MD, Betty Diamond, MD: Institute of Molecular Medicine, The Feinstein Institutes for Medical Research, Manhasset, New York; [3]Laura Cooney, PhD, David A. Fox, MD: University of Michigan, Ann Arbor, and University of California, San Francisco; [4]David Wofsy, MD, Dawn Smilek, MD, PhD, Maria Dall'Era, MD: University of California, San Francisco.

Mr van Dooren and Dr van Schaik are co-first authors and contributed equally to this work. Drs Teng and Suurmond are co-senior authors and contributed equally to this work.

Additional supplementary information cited in this article can be found online in the Supporting Information section (https://acrjournals.onlinelibrary.wiley.com/doi/10.1002/art.43219).

Author disclosures and graphical abstract are available at https://onlinelibrary.wiley.com/doi/10.1002/art.43219.

Address correspondence via email to Jolien Suurmond, PhD, at j.suurmond@lumc.nl.

Submitted for publication June 21, 2024; accepted in revised form April 21, 2025.

anti-U1RNP, anti-SS-A (also called Ro), and anti-SS-B (also called La); these are also associated with other autoimmune diseases. Together with anti-Sm, these are grouped as antibodies against RNA-binding proteins (RBPs).

Regarding the origin of these autoantibodies in SLE, both the extrafollicular and germinal center pathways have been implicated in this disease.[3–6] Extrafollicular responses generally induce short-lived plasmablasts or plasma cells, whereas germinal center responses are associated with long-lived plasma cells that can produce antibodies stably for decades.[7] Both short- and long-lived plasma cells can contribute to anti-dsDNA production in lupus mouse models. However, whether these models accurately represent autoantibody sources in patients with SLE is not clear. For example, anti-dsDNA antibodies diminished to nearly undetectable levels following treatment with CD19 chimeric antigen receptor (CAR) T cells, in contrast to durable vaccination antibody responses produced by long-lived plasma cells.

It is often alleged that the dynamics of the anti-RBP response is inherently different from that of the anti-dsDNA response, in that dsDNA antibodies are considered to have a typical short-lived nature, with fluctuating titers and frequent seroconversion, whereas anti-RBPs are often said to be stable. Therefore, anti-RBP detection is often only performed at diagnosis.[8] Although it has been clear for a long time that anti-dsDNA antibodies are fluctuating, less is known about stability of anti-RBPs. Some studies showed stability of anti-RBP positivity.[9,10] However, several other studies indicate that anti-RBP levels can fluctuate substantially and can also seroconvert. Importantly, most of these studies lack a direct comparison of the degree of fluctuation between the different ANAs. These findings suggest that anti-RBP durability may be heterogeneous in nature, consisting of both short- and long-lived plasma cells. A possible explanation for discrepant findings is differences in treatments between the studies.

Two B cell–targeting treatments used in patients with SLE are rituximab and belimumab. Rituximab targets CD20, not expressed by plasma cells. Belimumab targets BAFF, a cytokine involved in B cell activation and survival. Long-lived plasma cells express receptors that can bind BAFF and APRIL, another member of the tumor necrosis factor ligand family. These cytokines are important in plasma cell differentiation and survival, but BAFF deficiency alone is not enough to diminish the survival of long-lived plasma cells.[11] Therefore, rituximab and belimumab treatments are hypothesized to affect only short-lived antibody responses while pre-existing vaccination-induced antibodies are maintained, and data on autoantibody levels in clinical trials with these B cell–targeting therapies may be used to delineate the lifespan of autoantibody-producing plasma cells.

Levels of anti-dsDNA often decrease following rituximab or belimumab treatment, in line with their fluctuating nature. Decreases of other ANAs following treatment with rituximab or belimumab have also been reported in some studies but not in others. In these studies, decreases in autoantibody levels varied considerably among patients. If autoantibody levels decrease, data on the magnitude of change combined with analysis of clinical outcomes can provide valuable insight into the contribution of autoantibodies to disease pathogenesis.

Reactivity toward multiple nuclear antigens is associated with increased disease severity and the presence of multiple disease manifestations.[12,13] Pathogenicity of autoantibodies has been most clearly established for anti-dsDNA and anti–SS-A/SS-B. Anti-dsDNA contribute to kidney pathogenesis in lupus mouse models by binding to chromatin in glomeruli and inducing complement-mediated inflammation.[14,15] SS-A/B antibodies can cause disease pathogenesis as well, most clearly exemplified in neonatal lupus, whereas for Sm/RNP antibodies, there is less evidence of direct pathogenicity, although they have the ability to induce type I interferon responses.[16] In SLE, rising anti-dsDNA levels are predictive of disease flares.[17,18] Furthermore, decreases of anti-dsDNA levels following B cell–targeting treatments are predictive of the clinical response.[19,20] The relationship between anti-RBP levels and clinical response have rarely been investigated, although a few studies report a concordance between changes in levels of specific anti-RBPs and clinical disease activity. However, differences between assays and upper limits of detection, which are frequently reached for anti-RBP in routine clinical assays, makes direct comparison between the specific ANA levels difficult.

In this study, we aimed to determine the dynamics of specific ANAs in patients with SLE. Firstly, we performed a retrospective observational study exploring the prevalence and seroconversion of ANAs over time in a very large cohort of patients with SLE. Subsequently, we analyzed ANA titer dynamics in a separate longitudinal SLE cohort and in patients with SLE who participated in clinical trials investigating B cell–targeted treatments. We used enzyme-linked immunosorbent assay (ELISA)–based titer determination for each specific ANA, allowing for more direct comparison of the degree of fluctuation of autoantibody levels. In the clinical trials, we analyzed ANA levels in response to treatment as well as their relationship with clinical outcomes.

MATERIALS AND METHODS

Electronic health record data. We performed a retrospective observational study exploring the frequencies and dynamics of autoantibodies over time, in a cohort of 856 patients with a clinical SLE diagnosis treated in the Leiden University Medical Center (LUMC) between January 2010 and March 2023. All data from the Leiden electronic health record (EHR) cohort were retrospectively collected, after pseudonymization. As a result, the Dutch Research Involving Human Subjects Act did not apply, and active individual patient consent was not required. Instead, approval was granted by the Internal Medicine Scientific Committee in December 2022, ensuring adherence to local codes of conduct for data use by the researchers involved. All 856 patients

were notified by letter about the use of pseudonymized data, with an option to opt out. Through this process, passive consent was obtained from 836 patients (97.7%). Of this patient cohort, 84.9% of patients were female, and the average age was 49 years at the time of data collection. Demographics and laboratory data were extracted from EHRs using CTcue software (CTcue version 4.8.1), a web-based data mining tool designed for the systematic and anonymized retrieval of medical data. No information on medication was available in this cohort. Comprehensive details about the assays employed in the LUMC clinical laboratory for ANA measurement are available in the Supplementary Methods and Supplementary Table 1. Because the EHR data were obtained in a routine clinical setting, the antigens on which the assay we based differ from those used for the longitudinal cohort and clinical trial samples.

Longitudinal SLE cohort. Serum was obtained from 72 patients with a clinical diagnosis of SLE and who fulfilled the 1997 revised American College of Rheumatology criteria[21] from The Feinstein Institutes for Medical Research Rheumatology Specimen and Clinical Data Bank. Of these, 61 participants were positive for at least one specific ANA. Two serum samples were selected from each patient, with ~1 year time difference (median 1.016 years; range 0.0767–6.647 years). Patients with SLE were excluded from the study if they received belimumab, rituximab, or cyclophosphamide 12 months before the study or during the one-year follow-up. Clinical and routine laboratory data were collected from the same time point as serum collection. Information regarding patient characteristics can be found in Supplementary Table 2. The study with patients with SLE and healthy participants from the Feinstein Institute was approved by the Northwell Health Institutional Review Board, and all participants gave written informed consent.

Clinical trials with rituximab or belimumab treatment. Serum samples from patients with SLE in the Calibrate and Synbiose trials[22,23] were obtained for ANA titer analysis before and after initiation of B cell–targeting treatments. In the Calibrate trial, patients were randomized to receive either rituximab and cyclophosphamide (RC) or rituximab, cyclophosphamide, and belimumab (RCB). Treatment in the single-arm Synbiose trial consisted of rituximab and belimumab (RB). Doses and timing of RB were similar up to 48 weeks in both trials; patients received 1,000 mg of rituximab at weeks 0 and 2 and intravenous belimumab at a dose of 10 mg/kg at weeks 4, 6, and 8 and every four weeks thereafter. Additional information regarding these clinical trials can be found in the Supplementary Methods and Supplementary Table 3.

Clinical trial data analysis. From both clinical trials, serum samples that were collected at baseline and at 24 and 48 weeks after initiation of the treatment regimen were used for analysis of ANA dynamics. Clinical data from these patients were previously published and obtained from TrialShare (ITN055AI CALIBRATE) or from the original study data (Synbiose study). Renal responses were analyzed in patients with lupus nephritis at baseline. Complete renal responses were defined as having a 24-hour urine protein creatinine ratio (UPCR) of <0.5, and additionally having an estimated glomerular filtration rate (eGFR) of either ≥120 mL/min/1.73 m^2, or >80% compared with baseline if the baseline value was <120 mL/min/1.73 m^2, and adherence to the prednisone dosing provisions (maximum 10 mg/day). Partial renal responses were defined as proteinuria <50% of baseline (even if above 0.5 g/24 h) and eGFR/prednisone as above for complete response. These definitions were taken from the Calibrate trial and applied to patients from both studies. The analyses were repeated using the Synbiose definitions of complete renal response (proteinuria of <0.7 g/24 h) and serum creatinine (eGFR) within 125% of the baseline.

Only patients positive for at least one specific ANA at baseline were included in the analysis. For analysis of antibody titer dynamics, patients treated per protocol were included, consisting of 14 RC patients, 13 RCB patients, and 14 RB patients at week 24 and 7 RC patients, 11 RCB patients, and 10 RB patients at week 48. For correlations with clinical outcomes, modified intention to treat patients were selected, consisting of 14 RC patients, 13 RCB patients, and 15 RB patients at week 24 and 13 RC patients, 13 RCB patients, and 9 RB patients at week 48.

Titer ELISA. Clear flat bottom polystyrene high bind 384-well microplates (Corning) were coated overnight at 4°C with 2 ug/mL of varicella zoster virus (VZV) Antigen, Native (East Coast Bio), 1 μg/mL of UltraPure Salmon Sperm DNA Solution (Thermo), 0.8 μg/mL of nonrecombinant bovine Sm, 0.6 μg/mL of recombinant human U1snRNP-68/70kDa, 0.5 μg/mL of 60-kDa recombinant human SS-A or 1.1 μg/mL of recombinant human SS-B, 0.5 ug/mL of nonrecombinant bovine nucleosome, and 2.5 ug/mL of nonrecombinant bovine histone (all from Diarect) diluted in phosphate buffered saline (PBS). All washing steps were performed by washing four times with 0.05% Tween20 (Sigma) in PBS using the Berthold Zoom HT LB 920 Plate Washer. Plates were washed and subsequently blocked with 1% bovine serum albumin (BSA) (Sigma) and 50 m*M* Tris (Roche, pH = 8.0) in PBS for one hour at room temperature (RT). Subsequently, the plates were washed, and the wells were incubated with serum titrations ranging from 1:100 to 1:102,400 in PBS/0.05% Tween20/1% BSA/Tris (pH = 8.0), for one hour at RT. After the incubation, the ELISA plates were washed and incubated with 1 μg/mL anti-IgG horse-radish peroxidase (Bethyl) and, subsequently, washed and incubated with ABTS (Sigma-Aldrich) with 1:2,000 hydrogen peroxide (Merck). All plates were measured at 415 nm on the SpectraMax i3x Multi-Mode Microplate Reader.

Serum samples from 10 healthy donors were obtained from the LUMC Voluntary Donor Service and were taken along at 1:200 to confirm the cutoff OD for titer determination. Cutoffs were rounded to one decimal and were established based on the mean plus two times the SD of healthy control ODs and ranged from 0.3 to 0.5. Positive controls were taken along on each plate, and interplate variability was <15%. Furthermore, samples from the same patient were always measured on the same plate. In-house ANA ELISAs were validated using SLE serum samples with known reactivities obtained from the anti-RBP SLE profile 2 ELISA kit (Euroimmune) or clinical diagnostic assays (data not shown). All ELISAs reached a sensitivity and a specificity of at least 0.8.

Five-parameter logistic curves were generated per sample to calculate each titer value by intrapolating the cutoff value for each specific antibody titer. For determination of titer change in the Feinstein cohort, positive seroconversions were excluded (VZV n = 1, Sm n = 1, RNP70 n = 2).

Statistics. Statistical analysis was performed in GraphPad version 9.3.1 and SPSS version 29. Fisher's exact test was used for comparison of fractions between groups. Mann-Whitney U-tests were used to compare two groups. The Kruskal-Wallis test with Dunn's post hoc test was used to compare multiple groups. Correlations were analyzed using repeated-measures correlation for the EHR data, and the nonparametric Spearman's correlation test for the longitudinal SLE cohort.[24] A two-tailed *P* value of <0.05 was considered statistically significant.

RESULTS

Distinct rates of seroconversion between specific ANAs. To study whether differences in seroconversion exist between specific ANAs, historical laboratory data from EHRs of patients with a clinical diagnosis of SLE were analyzed. For each ANA, more than 200 patients had multiple measurements for which the range of variation over time could be assessed (Supplementary Table 4). Representative examples of antibody fluctuations are shown in Figure 1A and B. Figure 1C–H displays the range of antibody levels per ANA, with each bar representing an individual patient. With the exception of anti-dsDNA, upper limits of routine care measurements are applicable; variation above this limit is unknown. Although restricted by this measurement limit, it appears that especially for anti–SS-A and anti–SS-B levels, fewer patients have a wide range of antibody levels. Anti-Sm/RNP, on the other hand, seem to display antibody level ranges similar to anti-dsDNA.

Per ANA, positive patients with serial measurements are shown in Table 1. Anti-dsDNA positivity changed considerably over time, with only 50% of the patients being positive at each time point ("always positive"). In contrast, anti–SS-A/SS-B positivity was significantly more stable, with 85% and 74% of the patients, respectively, being positive at each time point. Anti-Sm, anti-U1RNP, and anti-RNP70 displayed similar degrees of seroconversion as anti-dsDNA. In particular, negative seroconversion was observed in a significant proportion of patients (20–30%) for dsDNA and Sm/RNP antibodies.

Change of specific ANA titers over time. To further corroborate the explorative results on seroconversion and level ranges of specific ANAs, we analyzed ANA levels on two consecutive time points in 61 patients with SLE from the longitudinal SLE cohort. We performed titer ELISAs on two samples per patient, with a time window of approximately one year. Anti-VZV titers were measured as a positive control representing "stable titers," reflecting the induction of long-lived B cell responses against VZV.

Representative examples of titer measurements are shown in Figure 2A–F. Antibody dynamics were expressed as the fold change of the titer at year 1 compared to baseline (T1/T0). In Figure 2G, the changes are shown as absolute fold changes, meaning the change can be an increase or a decrease of the titer during the one-year follow-up. An absolute titer change of 1 indicates that no increase or decrease has occurred compared to baseline. In Figure 2H, only the decreasing titers are shown, in which T1 is displayed as a percentage decrease compared to T0. As expected, anti-VZV titers displayed only small titer changes over time (Figure 2G and H). In contrast, both anti-dsDNA and anti-Sm titers displayed greater changes over time whereas anti–SS-A remained stable like anti-VZV. Similarly, anti-nucleosome and anti-histone titers also displayed larger titer changes compared to anti-VZV (Supplementary Figure 1). SS-B results were somewhat unexpected, as they also showed significant titer changes in the longitudinal SLE cohort. However, numbers of anti–SS-B–positive patients were small.

We defined a fold change ≥2 as a changing titer, as virtually all VZV titers stayed below this cutoff, and a two-fold change would constitute a clinically relevant reduction in antibody production. Analysis of the frequency of ≥2-fold changes confirmed that anti-dsDNA and anti-Sm titers fluctuate more frequently compared to anti-VZV (Supplementary Table 5 and Figure 2I). Therefore, these findings show that anti-dsDNA and anti-Sm exhibit more frequent titer change compared to anti-VZV and SS-A.

Anti-dsDNA and anti-Sm/RNP70 titers changing in the same direction. We analyzed whether specific ANAs change in the same direction, as this would provide insight into their regulation. As a positive control, we confirmed the correlation between changes of anti-Sm and RNP70 titers (Supplementary Figure 2A), as we hypothesized that levels of antibody production directed against the same antigen complex would most likely correlate with each other. In the longitudinal SLE cohort, anti-dsDNA titer changes showed statistically significant correlations and with anti-Sm ($r = 0.477$ and anti-RNP70 $r = 0.532$) (Supplementary Figure 2B and C). In contrast, the correlation between anti-dsDNA

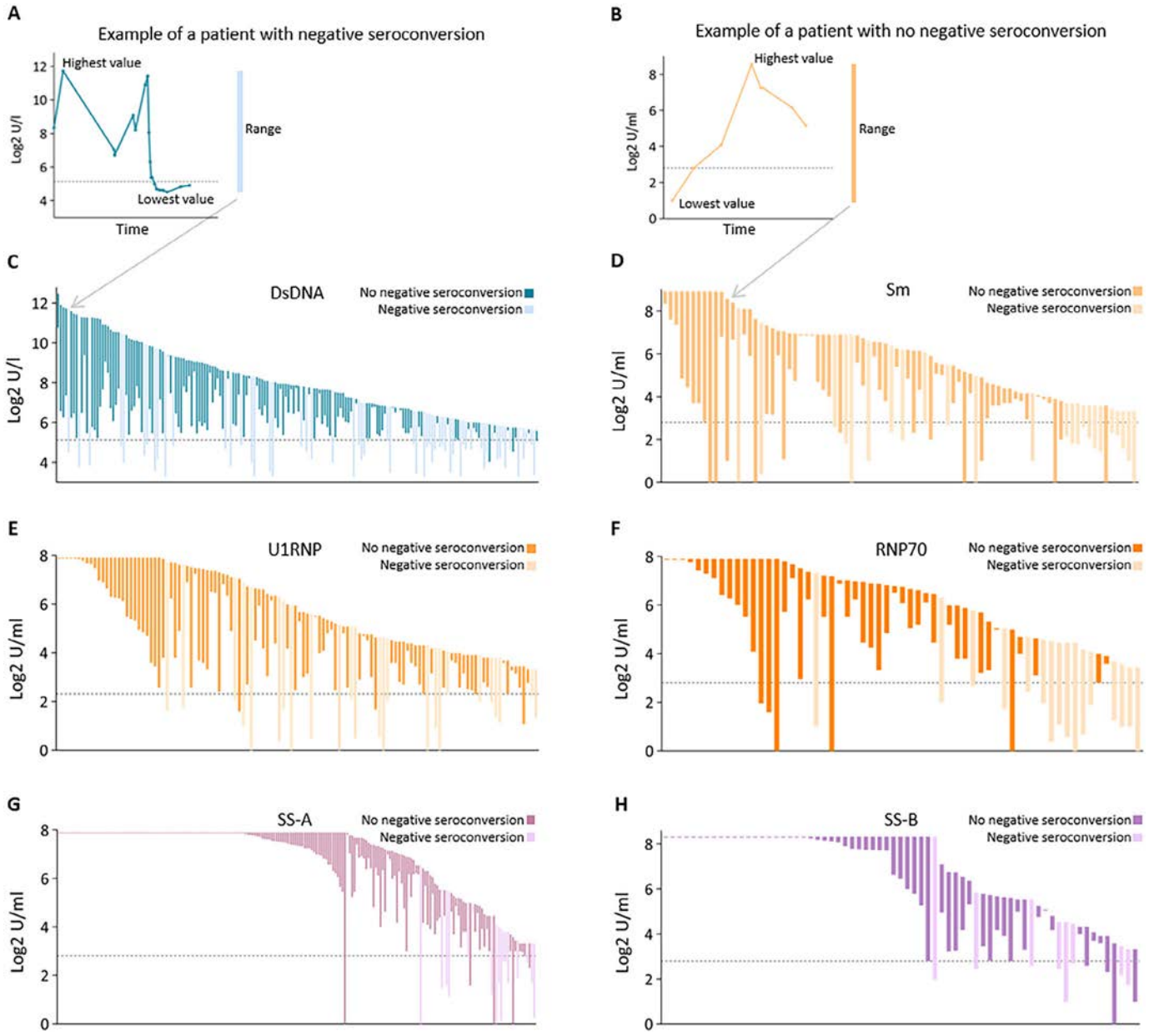

Figure 1. Ranges of specific ANA levels over time. Examples of individual patient trajectories for (A) anti-dsDNA and (B) anti-Sm levels. The resulting range is subsequently depicted as a dark-colored bar when negative seroconversion does not occur, and as a light-colored bar when seroconversion occurs. (C–H) Ranges of ANA levels for all patients with anti-dsDNA, anti-Sm, anti-U1RNP, anti-RNP70, anti–SS-A, and anti–SS-B. The x-axis represents patients, ordered by descending maximum measurement values, whereas the y-axis indicates autoantibody levels. Dashed lines denote the positivity cutoff value. Measurement limits are in place for all ANA except anti-dsDNA. Negatives seroconversion occurs progressively less frequently from anti-dsDNA to anti-SS-B. ANA, antinuclear antibody; anti-dsDNA, anti–double-stranded DNA; anti-Sm, anti-Smith.

and anti–SS-A was weaker and not significant (Supplementary Figure 2D). Because very few patients had simultaneous measurements of anti-dsDNA and anti–SS-B within the measurement range, correlation coefficients could not be accurately assessed.

We also analyzed directionality of ANA fluctuations in the EHR cohort. Again, we were able to confirm the correlation between the changes of anti-Sm and anti-RN70 titers in this cohort (Supplementary Figure 2E). Repeated-measures correlations between these antibodies confirmed that anti-dsDNA and anti-Sm frequently change in the same direction, in contrast to SS-A, which showed a much weaker correlation (Supplementary Figure 2F–H). Several patients exhibited a similar pattern over time for anti-dsDNA, anti-Sm, and anti-RNP70, of which representative examples can be seen in Supplementary Figure 2I and J. This is in contrast with anti–SS-A and anti–SS-B, in which anti-dsDNA can show remarkable changes

Table 1. Antinuclear antibody positivity over time in the electronic health record cohort*

Antibody	Anytime positive, n/N (%)	Follow-up, median (range), mo	Always positive, n/N (%)	Negative seroconversion, n/N (%)	Positive seroconversion, n/N (%)	Inconclusive, n/N (%)
Anti-dsDNA (n = 294)	184/294 (63)	32 (14–47)	92/184 (50)	58/184 (32)	21/184 (11)	28/184 (15)
Anti-Sm (n = 218)	84/218 (39)	41 (17–63)	42/84 (50), ns	24/84 (29), ns	19/84 (23)	5/84 (6)
Anti-U1RNP (n = 244)	120/244 (49)	44 (20–74)	61/120 (50), ns	25/120 (21), ns	6/120 (5)	31/120 (26)
Anti-RNP70 (n = 235)	61/235 (26)	45 (21–74)	36/61 (59), ns	16/61 (26), ns	7/61 (11)	4/61 (7)
Anti-SS-A (n = 273)	202/273 (74)	40 (17–71)	171/202 (85)**	16/202 (8)**	7/202 (3)	10/202 (5)
Anti-SS-B (n = 254)	69/254 (27)	43 (21–79)	51/69 (74)**	8/69 (12)**	4/69 (6)	6/69 (9)

* The first column lists the numbers of patients with repeated measurements. The remaining columns refer only to patients with at least one positive value. The frequency for each anti–RNA-binding protein was compared with that of anti-dsDNA. Patients not meeting the criteria for consistent positivity or seroconversion had measurements between the reference value and cutoff value for positivity and were designated inconclusive and excluded from analysis. Frequencies of negative seroconversion are similar for anti-Sm, anti-U1RNP, and anti-RNP70 and differ significantly for anti–SS-A and anti–SS-B. Please note patients can have both a positive and a negative seroconversion. Additional data are shown in Supplementary Table 4. Data are displayed as fraction (frequency), or median (range). False discovery rate–adjusted *P* values were obtained using Fisher's exact test; anti-dsDNA, anti-double-stranded DNA; anti-Sm, anti-Smith; ns; not significant.
** $P < 0.001$.

whereas anti–SS-A/SS-B remains stable, or they exhibit large changes in opposite directions (Supplementary Figure 2K and L). Together, these findings revealed that anti-DNA and anti-Sm/RNP antibodies often fluctuate in the same direction, in contrast to anti–SS-A.

Differences in susceptibility of specific ANAs to B cell–targeting therapy. Next, we addressed whether there was a difference in the degree of titer reduction of specific ANAs in response to B cell–targeted therapies, which are hypothesized to target B cells and short-lived plasma cells while leaving long-lived plasma cells intact. We studied samples from two clinical trials, the Calibrate trial and the Synbiose trial. In the Calibrate trial, patients were randomized to receive either RC or RCB. Treatment in the single-arm Synbiose trial consisted of RB.

Anti-VZV and ANA titers were measured at baseline and after 24 and 48 weeks of treatment. Representative examples of titer changes after treatment are shown in Figure 3A–F. For each specific ANA, we included only patients with a positive titer (≥200) at baseline. Although the treatment arms do not have exactly similar effects, they both target primarily short-lived B cell responses. However, all three treatment arms had roughly similar effects on antibody titers (Supplementary Figure 3). Therefore, the samples of all three treatment arms were combined. In each treatment arm, anti-dsDNA and anti-Sm significantly decreased at week 24 (Supplementary Figure 3A–C). At week 48, this decrease was less pronounced (Supplementary Figure 3D–F). After pooling all treatment arms together for direct comparison of the different antibodies, anti-VZV titers remained stable (within two–fold change) in most patients, whereas the anti-dsDNA titers decreased significantly at week 24 (Figure 3G and H). Anti-Sm titers also displayed a comparable decrease in titer, whereas anti–SS-A remained more stable compared to anti-VZV (Figure 3G and I). Although all specific ANAs decreased significantly compared to anti-VZV for both time points, there was a gradient in the degree of titer decreases, with anti-dsDNA decreasing most strongly and anti–SS-A/SS-B decreasing the least (Figure 3G–J and Supplementary Tables 6 and 7). The decrease in titer was comparable between Sm and dsDNA antibodies for both week 24 and week 48 (Figure 3G–J and Supplementary Tables 6 and 7). Anti-nucleosome and anti-histone titers showed similar decreases after treatment as anti-dsDNA (Supplementary Figure 4). Together, these results show that all ANAs decrease in titer in response to B cell–targeted treatment, with anti-Sm and anti-dsDNA titers displaying the strongest decreases.

Association of specific ANA titer changes with clinical and immunologic outcomes. Because of the significant reductions in anti-dsDNA and anti-Sm titers after B cell–targeting treatments, we investigated whether these reductions were associated with clinical responses. Patients were grouped based on their renal response as described in the Methods section. The degree of renal response was comparable between the treatment arms and trials (Supplementary Table 8). ANA titer changes were analyzed in nonresponders, partial responders, and complete renal responders at week 24 and 48 (Figure 4A–D). This analysis revealed that patients achieving complete renal responses had significantly larger reductions in anti-dsDNA titers at week 48 (Figure 4B).

Importantly, although a substantial group of anti-Sm–positive patients had a reduction in anti-Sm titer (Figure 3G and I), this decrease did not associate with the renal response at both weeks 24 and 48 (Figure 4C and D). Likewise, titer decreases for the other ANAs did not show a statistically significant correlation with renal response (data not shown). When analyzing the reduction in proteinuria, only anti-dsDNA titer reductions were associated with reduced UPCR (Supplementary Figure 5).

An important correlate of antibody effector functions and immune complex deposition is complement consumption, leading to decreased complement levels in serum. Most patients had a reduced C3 serum concentration at baseline, which increased

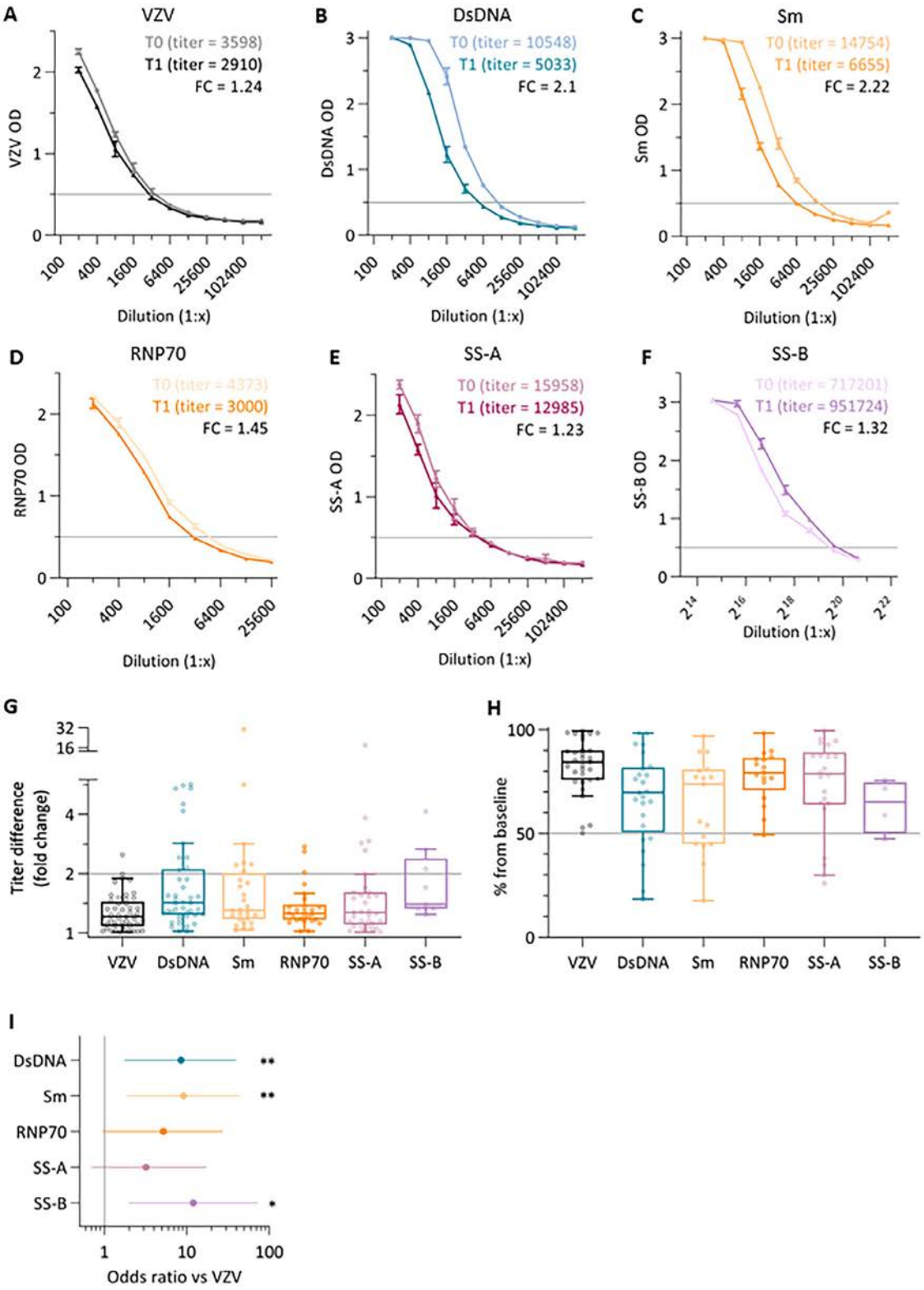

Figure 2. Anti-dsDNA and anti-Sm exhibit different titer dynamics compared to anti-VZV. (A–F) Representative examples of fold titer changes for anti-VZV, anti-dsDNA, anti-Sm, anti-RNP70, anti–SS-A, and anti–SS-B. (G and H) Summary of titer changes and titer decreases depicted as absolute fold change (G) or percentage decrease from baseline (H). Panel H only includes patients with a decrease in titer. (I) Frequencies of ≥2-fold titer changes of specific ANAs compared to VZV were visualized using Forest plots with 95% confidence intervals of the odds ratios compared to VZV. Each dot indicates an individual patient (G and H), and the boxplot represents the median and quartiles. *P* values were calculated using Kruskal-Wallis with Benjamini Hochberg's post hoc test (E and F) or Fisher's exact tests (G). *$P \leq 0.05$, **$P \leq 0.01$. ANA, antinuclear antibody; anti-dsDNA, anti–double-stranded DNA; anti-Sm, anti-Smith; VZV, varicella zoster virus. Color figure can be viewed in the online issue, which is available at http://onlinelibrary.wiley.com/doi/10.1002/art.43219/abstract.

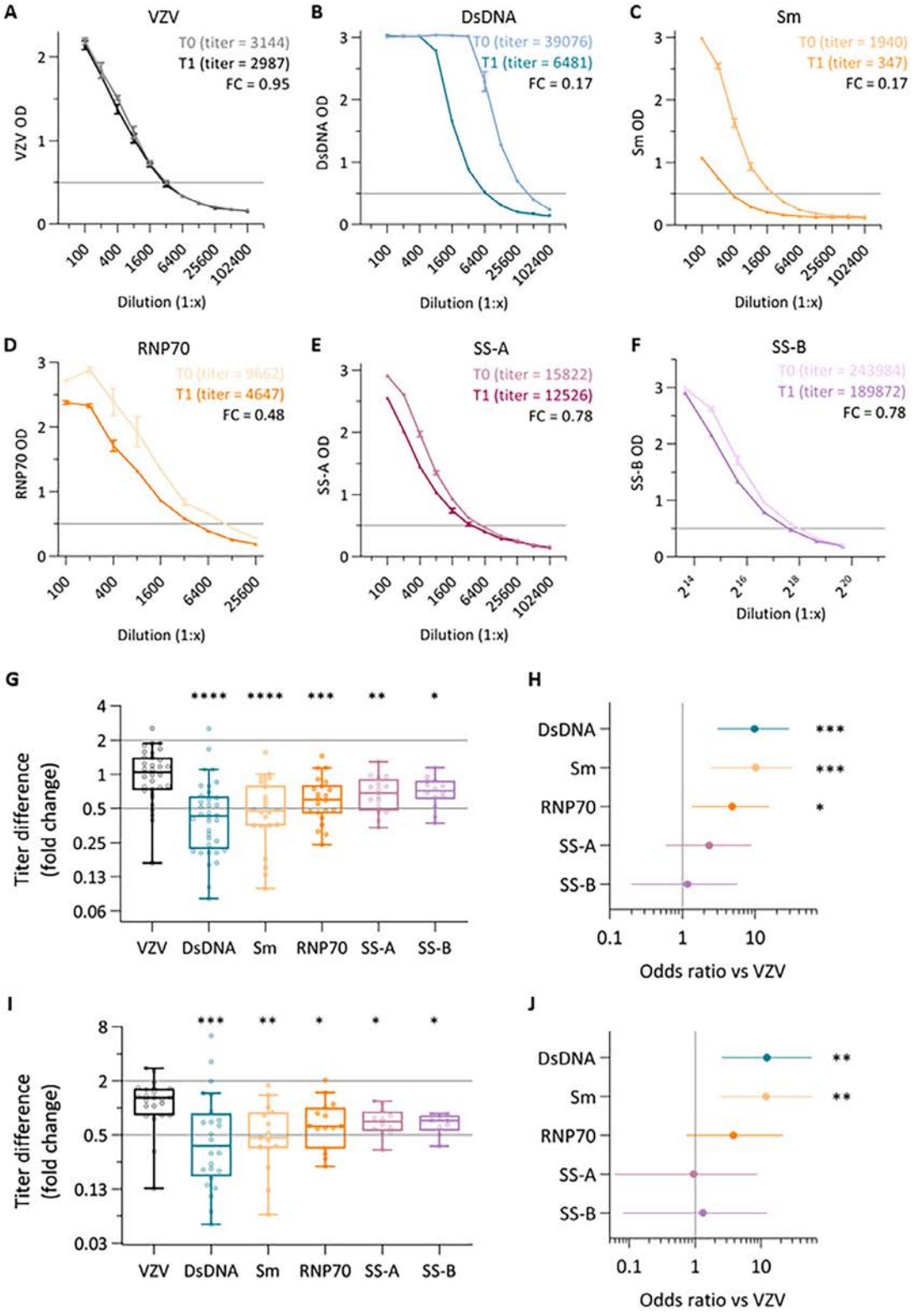

Figure 3. Effect of B cell–targeting therapies on specific ANA titers after 24 and 48 weeks of treatment. (A–F) Representative examples of fold titer changes for anti-VZV, anti-dsDNA, anti-Sm, anti-RNP70, anti–SS-A, and anti–SS-B. (G and I) Summarized results of fold titer changes of patients from all three treatment arms. Each dot indicates an individual, and the boxplots represent the median and quartiles. (H and J) Frequencies of ≥2-fold titer decreases of specific ANAs compared to VZV were visualized using Forest plots with 95% confidence intervals of the odds ratios compared to VZV. *P* values were calculated using Kruskal-Wallis test with Benjamini Hochberg's post hoc test (E and G). **P* ≤ 0.05, ***P* ≤ 0.01, ****P* ≤ 0.001, *****P* ≤ 0.0001. ANA, antinuclear antibody; anti-dsDNA, anti–double-stranded DNA; anti-Sm, anti-Smith; FC, fold change; VZV, varicella zoster virus. Color figure can be viewed in the online issue, which is available at http://onlinelibrary.wiley.com/doi/10.1002/art.43219/abstract.

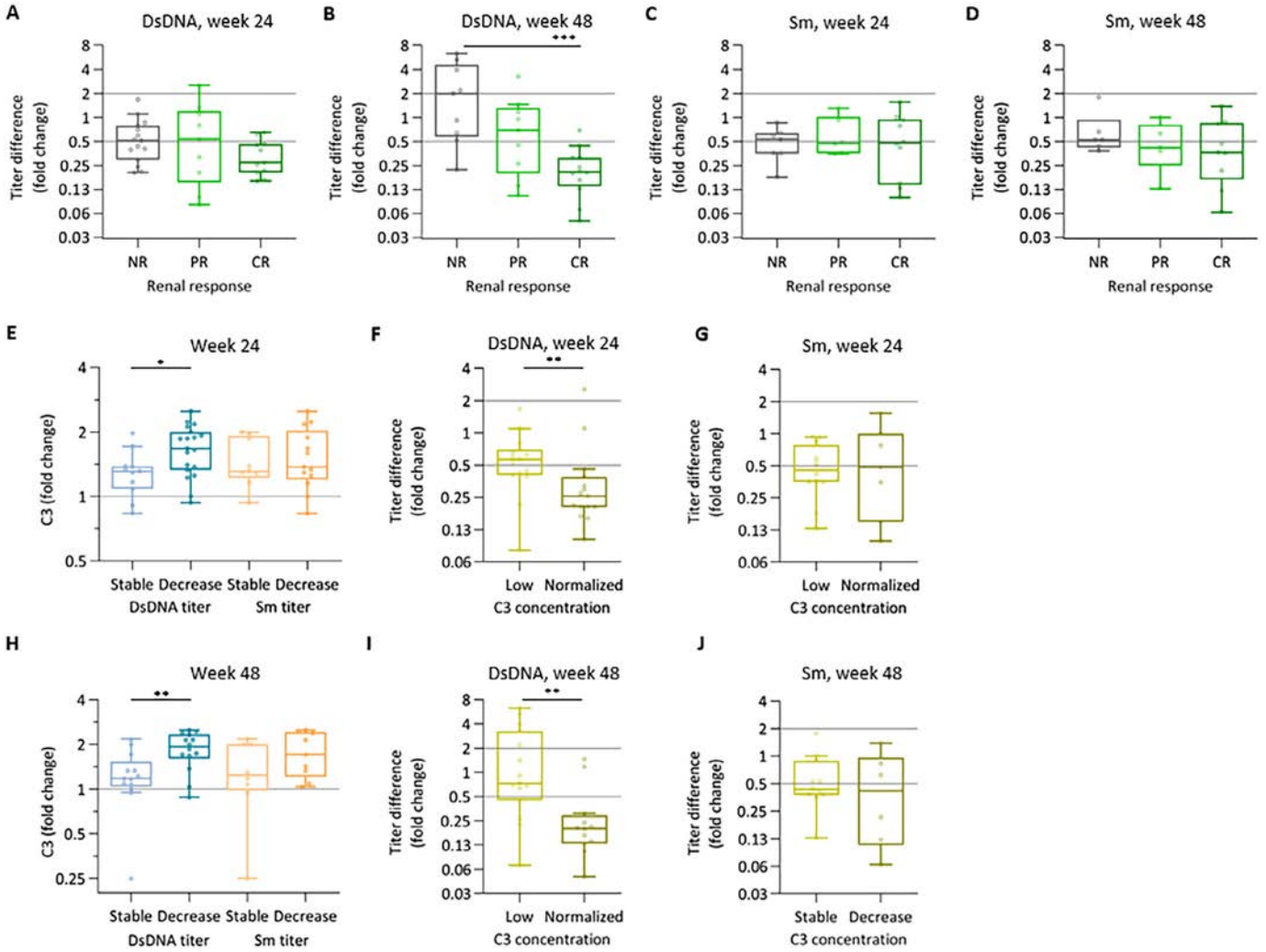

Figure 4. Association between clinical outcomes and titer dynamics in response to B cell–targeted therapies. (A–D) Changes in anti-dsDNA and anti-Sm titers in patients treated with B cell–targeted therapies after 24 and 48 weeks of treatment, stratified by responder status. Anti-dsDNA titer reductions are progressively greater in patients with better renal responses, with the most pronounced effects observed after 48 weeks. (E–G) Relationship between C3 concentration changes and autoantibody responses after 24 (E–G) and 48 (H–J) weeks of treatment. Larger (at least two-fold) decreases in anti-dsDNA titers are significantly associated with improvement of C3 concentrations. Conversely, anti-dsDNA titers decrease more significantly in patients whose C3 concentrations normalize. Dots indicate individual patients, and boxplots represent medians and quartiles. *P* values were calculated using the Mann-Whitney U-test or mixed-effects analysis. $^{*}P \leq 0.05$, $^{**}P \leq 0.01$, $^{***}P \leq 0.001$. ANA, antinuclear antibody; anti-dsDNA, anti–double-stranded DNA; anti-Sm, anti-Smith; CR, complete response; NR, nonresponse; PR, partial response. Color figure can be viewed in the online issue, which is available at http://onlinelibrary.wiley.com/doi/10.1002/art.43219/abstract.

in all three treatment arms at both weeks 24 and 48 (Supplementary Figure 6A and B). Normalization of C3 levels associated with stronger reductions in anti-dsDNA titers but not in anti-Sm titers (Figure 4E–J).

We next addressed whether the autoantibody titer changes at week 24 could predict clinical and immunologic responses at week 48. For anti-dsDNA, we found an association of titer decreases at week 24 with complete renal responses, UPCR, and C3 level increases at week 48 (Figure 5A, D, and G and Supplementary Tables 9 and 10). This association was not found for other ANAs or in cases of anti-Sm, even despite their decreasing titers (Figure 5B, C, and E–H). Thus, we conclude that despite the similar reductions of anti-dsDNA and anti-Sm titers in response to B cell–targeted therapy, only anti-dsDNA titer reductions were associated with renal responses and normalization of serum complement levels.

DISCUSSION

In this study, we observed distinct dynamics in groups of specific ANAs in three different cohorts. In particular, anti-Sm displays similar fluctuation and response to B cell–targeted therapies as anti-dsDNA, whereas anti–SS-A/SS-B levels were much more stable and less perturbed by therapy. Despite similar titer decreases following B cell–targeted therapies between anti-

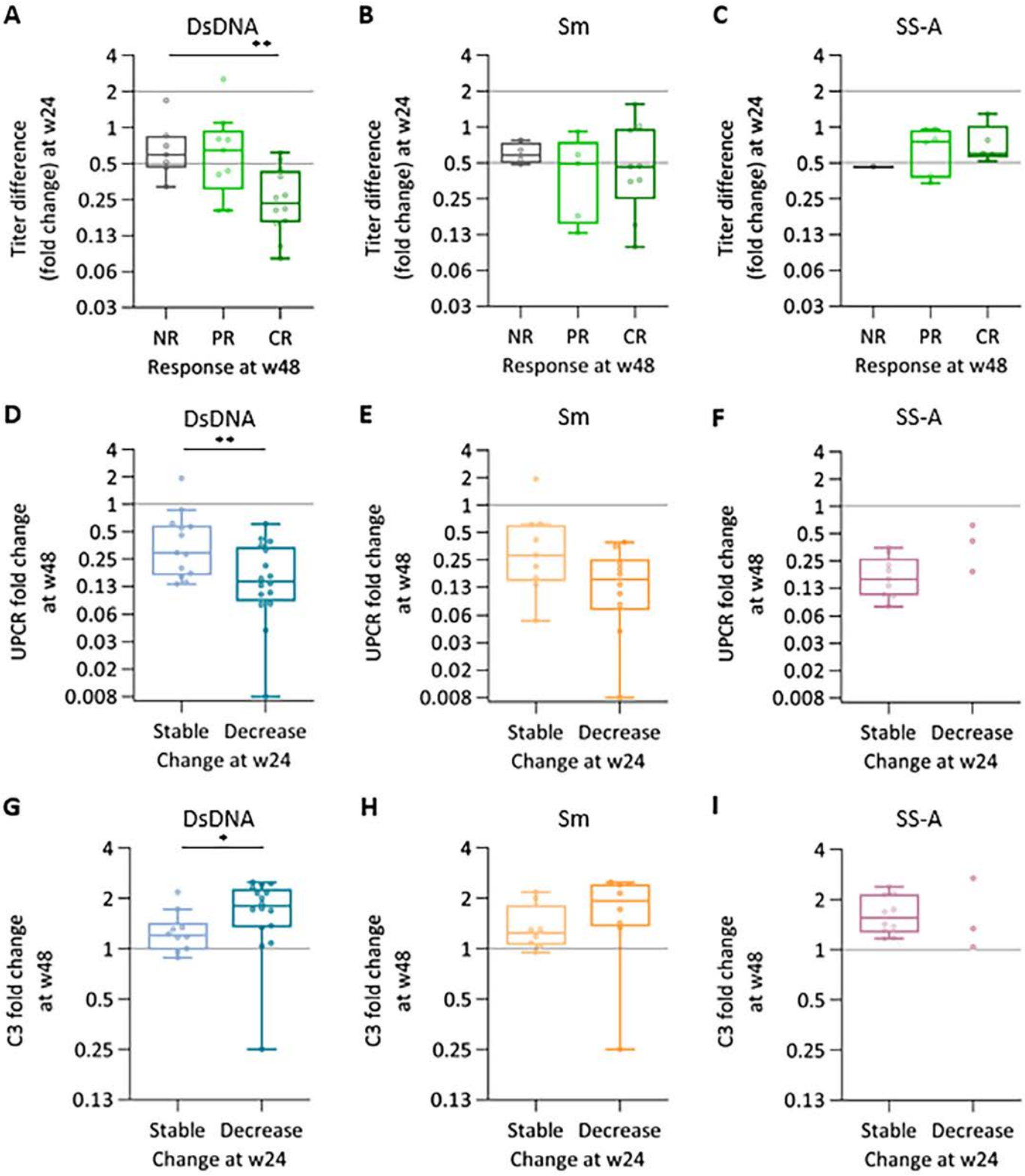

Figure 5. Association of titer changes at 24 weeks of B cell–targeted treatment with clinical responses at week 48. Titer changes of specific ANAs (dsDNA, Sm, and SS-A) at week 24 and their associations with renal responder status (A–C), UPCR fold changes (D–F), and C3 fold changes (G–I) at week 48. A titer was considered "stable" if it decreased less then two-fold compared to baseline. Each dot indicates an individual, and the boxplots represent the median and quartiles. *P* values were calculated using the Mann-Whitney U-test (A–E). $^{*}P \leq 0.05$, $^{**}P \leq 0.01$. ANA, antinuclear antibody; anti-dsDNA, anti–double-stranded DNA; anti-Sm, anti-Smith; CR, complete response; NR, nonresponse; PR, partial response; w24, week 24; UPCR, urine protein creatinine ratio. Color figure can be viewed in the online issue, which is available at http://onlinelibrary.wiley.com/doi/10.1002/art.43219/abstract.

dsDNA and anti-Sm, only reductions in anti-dsDNA titer associated with positive clinical outcomes following B cell–targeted therapies.

One of the strengths of our study is that we analyzed the specific ANA dynamics in three separate cohorts, with each cohort showing similar titer dynamics between anti-dsDNA and anti-Sm. Furthermore, in the longitudinal SLE cohort and the clinical trial samples, we measured titers using the same assay for each specific ANA, thereby allowing a direct comparison between the different ANAs. The results on seroconversion suggest that short-lived plasma cells have a considerable contribution to both anti-dsDNA and anti-Sm/RNP, as 25% to 30% of patients displayed a loss for these antibodies. Furthermore, treatment with RB led to a similar titer decrease of anti-dsDNA and anti-Sm, with approximately 60% of patients reaching a titer reduction of two-fold or more. Our results are in line with results from patients with SLE treated with CD19-CAR T cells, which suggested that anti-dsDNA levels (n = 5) and anti-Sm levels (n = 3) considerably decreased, in contrast to anti–SS-A (n = 4), which remained more or less stable.[25] In our study, a smaller percentage of patients displayed a negative seroconversion for anti-dsDNA and anti-Sm after treatment, suggesting that a part of the response may be derived from long-lived plasma cells. However, it could also be the consequence of incomplete B cell depletion or inhibition in peripheral tissues, as has been reported for rituximab.[26,27] In that context, the data on CD19-CAR T cell treatment are interesting, as negative seroconversion of anti-dsDNA and anti-Sm was found in the majority of patients.[25,28]

These data are in line with the notion that CD19-CAR T cells may lead to more complete depletion of B cells in tissue, and thus these findings could imply that most, if not all, of the anti-dsDNA and anti-Sm reactivity could reside in the short-lived plasma cell compartment. However, these findings could also be explained by differential expression of CD19 versus CD20 on (long-lived) plasma cell subsets. Several different plasma cell subsets have been described in bone marrow (BM), some of which express[29,30] CD19. Anti-dsDNA production by both $CD19^-$ and $CD19^+$ plasma cells in BM from one patient with SLE has been reported.[31] Although the general notion is that long-lived plasma cells reside in the $CD19^-$ population, there may be additional $CD19^+$ plasma cell subsets with an intermediate or long lifespan. Such a population would be less susceptible to rituximab than to $CD19^+$ CAR T cells as CD20 is down-regulated earlier than CD19 during plasma cell differentiation.

The variation in ANA dynamics previously observed across different studies may be attributed to three potential factors. First, several studies date back to the 1980s and 1990s, a period when treatment protocols differed significantly from contemporary practices, often involving medications with a lesser impact on autoantibodies.[9,32,33] Second, the studies employed different assay methodologies, such as the use of qualitative rather than quantitative approaches.[34] Lastly, some studies feature small sample sizes, particularly concerning SS-B, which increases the risk of bias.[35]

Regarding pathogenicity, analysis of the correlation between clinical outcomes and specific autoantibody titer reductions has been suggested as an approach to provide insight into the contribution of autoantibodies to disease pathogenesis.[36] The reasoning is that if an autoantibody is pathogenic and the titer is strongly reduced, it should coincide with the reduction of clinical symptoms. Such an analysis can only be performed for autoantibodies whose titers considerably diminish after treatment. In our study, we analyzed the association of anti-dsDNA and anti-Sm titer reduction with clinical outcomes and found only anti-dsDNA titer reductions to associate with renal responses, UPCR reduction, and normalization of complement levels. These results were somewhat unexpected because anti-Sm positivity has been associated with lupus nephritis and disease severity in some studies, anti-Sm antibodies have been eluted from lupus nephritis kidneys, and anti-Sm antibodies are capable of fixating complement.[37] The lack of association could be due to lower power for anti-Sm related to their lower frequency in SLE, leading to lower power to detect associations of titer changes to disease activity compared to anti-dsDNA. However, there was no trend of any kind for an association of anti-Sm titer reductions to clinical outcomes or normalization of complement levels.

The clinical implications of our study are that reductions in anti-dsDNA levels, can be used as a biomarker to predict efficacy following B cell–targeted treatment, whereas for anti-Sm, this needs to be addressed in larger studies. Another aspect is that anti-dsDNA and anti-Sm positivity are used to diagnose SLE. A considerable number of patients displayed a positive seroconversion for anti-Sm/RNP reactivity. We found this in 2 of the 61 patients in the longitudinal cohort with one-year follow-up but also in 20% of the anti-Sm–positive patients in the EHR data set. Regarding the observational data from the EHR, our immunology laboratory applies an algorithm that anti-RBPs are usually only remeasured if they were historically positive at least once in a patient's disease course, and therefore there may be an underestimation of the fraction of positive seroconversions. Monitoring Sm levels throughout the SLE disease course might not be cost-effective, although this will ultimately depend on whether anti-Sm titer changes are predictive for the disease course in larger studies.[10]

A limitation of our study are the small sample sizes for the least frequent ANAs, such as anti–SS-B. This may explain the discrepant findings in the longitudinal SLE cohort, in which anti–SS-B titers appeared to fluctuate whereas they were stable in the other two data sets. However, for the other ANAs, results were consistent in all three cohorts.

Similarly, we hypothesize that the smaller sample size at week 48 of the Synbiose and Calibrate trials may explain the less pronounced titer changes at this time point compared to week 24. However, it could also be possible that relapses occur over

the course of treatment leading to increases of these ANA titers and thus to a less observable titer decrease at week 48.

In conclusion, the results of this study show heterogeneity in the dynamics of ANA responses, with anti-dsDNA and anti-Sm showing most fluctuation and highest susceptibility to B cell–targeted therapies, in contrast to anti–SS-A/SS-B. These results suggest different contributions of short- and long-lived plasma cells to each specific ANA response, with a stronger contribution of short-lived plasma cells to anti-dsDNA and anti-Sm production. These insights could be used to develop treatments targeting specific ANAs while leaving other humoral responses intact.

ACKNOWLEDGMENT

We thank Dr Brigitte Wevers from the LUMC clinical chemistry and medical immunology laboratory for her invaluable contributions concerning the ANA assays used in clinical practice.

AUTHOR CONTRIBUTIONS

All authors contributed to at least one of the following manuscript preparation roles: conceptualization AND/OR methodology, software, investigation, formal analysis, data curation, visualization, and validation AND drafting or reviewing/editing the final draft. As corresponding author, Dr Suurmond confirms that all authors have provided the final approval of the version to be published and takes responsibility for the affirmations regarding article submission (eg, not under consideration by another journal), the integrity of the data presented, and the statements regarding compliance with institutional review board/Declaration of Helsinki requirements.

REFERENCES

1. Weitzman RJ, Walker SE. Relation of titred peripheral pattern ANA to anti-DNA and disease activity in systemic lupus erythematosus. Ann Rheum Dis 1977;36(1):44–49.
2. Bombardier C, Gladman DD, Urowitz MB, et al; The Committee on Prognosis Studies in SLE. A disease activity index for lupus patients. Arthritis Rheum 1992;35(6):630–640.
3. Cappione A III, Anolik JH, Pugh-Bernard A, et al. Germinal center exclusion of autoreactive B cells is defective in human systemic lupus erythematosus. J Clin Invest 2005;115(11):3205–3216.
4. Tipton CM, Fucile CF, Darce J, et al. Diversity, cellular origin and autoreactivity of antibody-secreting cell population expansions in acute systemic lupus erythematosus. Nat Immunol 2015;16(7):755–765.
5. Brown GJ, Cañete PF, Wang H, et al. TLR7 gain-of-function genetic variation causes human lupus. Nature 2022;605(7909):349–356.
6. Sakakibara S, Arimori T, Yamashita K, et al. Clonal evolution and antigen recognition of anti-nuclear antibodies in acute systemic lupus erythematosus. Sci Rep 2017;7(1):16428.
7. Malkiel S, Barlev AN, Atisha-Fregoso Y, et al. Plasma cell differentiation pathways in systemic lupus erythematosus. Front Immunol 2018;9:427.
8. Tozzoli R, Bizzaro N, Tonutti E, et al; Italian Society of Laboratory Medicine Study Group on the Diagnosis of Autoimmune Diseases. Guidelines for the laboratory use of autoantibody tests in the diagnosis and monitoring of autoimmune rheumatic diseases. Am J Clin Pathol 2002;117(2):316–324.
9. McCarty GA, Rice JR, Bembe ML, et al. Independent expression of autoantibodies in systemic lupus-erythematosus. J Rheumatol 1982; 9(5):691–695.
10. Raissi TC, Hewson C, Pope JE. Repeat testing of antibodies and complements in systemic lupus erythematosus: when is it enough? J Rheumatol 2018;45(6):827–834.
11. Benson MJ, Dillon SR, Castigli E, et al. Cutting edge: the dependence of plasma cells and independence of memory B cells on BAFF and APRIL. J Immunol 2008;180(6):3655–3659.
12. Alba P, Bento L, Cuadrado MJ, et al. Anti-dsDNA, anti-Sm antibodies, and the lupus anticoagulant: significant factors associated with lupus nephritis. Ann Rheum Dis 2003;62(6):556–560.
13. Kwon OC, Park MC. Risk of systemic lupus erythematosus flares according to autoantibody positivity at the time of diagnosis. Sci Rep 2023;13(1):3068.
14. Ehrenstein MR, Katz DR, Griffiths MH, et al. Human IgG anti-DNA antibodies deposit in kidneys and induce proteinuria in SCID mice. Kidney Int 1995;48(3):705–711.
15. Fenton KA, Tømmerås B, Marion TN, et al. Pure anti-dsDNA mAbs need chromatin structures to promote glomerular mesangial deposits in BALB/c mice. Autoimmunity 2010;43(2):179–188.
16. Savarese E, Chae OW, Trowitzsch S, et al. U1 small nuclear ribonucleoprotein immune complexes induce type I interferon in plasmacytoid dendritic cells through TLR7. Blood 2006;107(8):3229–3234.
17. Linnik MD, Hu JZ, Heilbrunn KR, et al; LJP 394 Investigator Consortium. Relationship between anti-double-stranded DNA antibodies and exacerbation of renal disease in patients with systemic lupus erythematosus. Arthritis Rheum 2005;52(4):1129–1137.
18. ter Borg EJ, Horst G, Hummel EJ, et al. Measurement of increases in anti-double-stranded DNA antibody levels as a predictor of disease exacerbation in systemic lupus erythematosus. A long-term, prospective study. Arthritis Rheum 1990;33(5):634–643.
19. Stohl W, Hiepe F, Latinis KM, et al; BLISS-52 Study Group; BLISS-76 Study Group. Belimumab reduces autoantibodies, normalizes low complement levels, and reduces select B cell populations in patients with systemic lupus erythematosus. Arthritis Rheum 2012;64(7): 2328–2337.
20. Rovin BH, Furie R, Latinis K, et al; LUNAR Investigator Group. Efficacy and safety of rituximab in patients with active proliferative lupus nephritis: the Lupus Nephritis Assessment with Rituximab study. Arthritis Rheum 2012;64(4):1215–1226.
21. Hochberg MC. Updating the American College of Rheumatology revised criteria for the classification of systemic lupus erythematosus. Arthritis Rheum 1997;40(9):1725.
22. Kraaij T, Arends EJ, van Dam LS, et al. Long-term effects of combined B-cell immunomodulation with rituximab and belimumab in severe, refractory systemic lupus erythematosus: 2-year results. Nephrol Dial Transplant 2021;36(8):1474–1483.
23. Kraaij T, Kamerling SWA, de Rooij ENM, et al. The NET-effect of combining rituximab with belimumab in severe systemic lupus erythematosus. J Autoimmun 2018;91:45–54.
24. Bakdash JZ, Marusich LR. Repeated measures correlation. Front Psychol 2017;8:456.
25. Müller F, Taubmann J, Bucci L, et al. CD19 CAR T-cell therapy in autoimmune disease - a case series with follow-up. N Engl J Med 2024;390(8):687–700.
26. Boumans MJ, Thurlings RM, Gerlag DM, et al. Response to rituximab in patients with rheumatoid arthritis in different compartments of the immune system. Arthritis Rheum 2011;63(11):3187–3194.
27. Crickx E, Chappert P, Sokal A, et al. Rituximab-resistant splenic memory B cells and newly engaged naive B cells fuel relapses in patients with immune thrombocytopenia. Sci Transl Med 2021; 13(589):eabc3961.

28. Mackensen A, Müller F, Mougiakakos D, et al. Anti-CD19 CAR T cell therapy for refractory systemic lupus erythematosus. Nat Med 2022; 28(10):2124–2132.
29. Duan M, Nguyen DC, Joyner CJ, et al. Understanding heterogeneity of human bone marrow plasma cell maturation and survival pathways by single-cell analyses. Cell Rep 2023;42(7):112682.
30. Halliley JL, Tipton CM, Liesveld J, et al. Long-lived plasma cells are contained within the CD19(–)CD38(hi)CD138(+) subset in human bone marrow. Immunity 2015;43(1):132–145.
31. Mei HE, Wirries I, Frölich D, et al. A unique population of IgG-expressing plasma cells lacking CD19 is enriched in human bone marrow. Blood 2015;125(11):1739–1748.
32. Barada FA Jr, Andrews BS, Davis JS IV, et al. Antibodies to Sm in patients with systemic lupus erythematosus. Correlation of Sm antibody titers with disease activity and other laboratory parameters. Arthritis Rheum 1981;24(10):1236–1244.
33. Wahren M, Tengnér P, Gunnarsson I, et al. Ro/SS-A and La/SS-B antibody level variation in patients with Sjögren's syndrome and systemic lupus erythematosus. J Autoimmun 1998;11(1):29–38.
34. Faria AC, Barcellos KSA, Andrade LEC. Longitudinal fluctuation of antibodies to extractable nuclear antigens in systemic lupus erythematosus. J Rheumatol 2005;32(7):1267–1272.
35. Frodlund M, Wetterö J, Dahle C, et al. Longitudinal anti-nuclear antibody (ANA) seroconversion in systemic lupus erythematosus: a prospective study of Swedish cases with recent-onset disease. Clin Exp Immunol 2020;199(3):245–254.
36. Hale M, Rawlings DJ, Jackson SW. The long and the short of it: insights into the cellular source of autoantibodies as revealed by B cell depletion therapy. Curr Opin Immunol 2018;55:81–88.
37. Kanayama Y, Peebles C, Tan EM, et al. Complement-activating abilities of defined antinuclear antibodies. Arthritis Rheum 1986;29(6): 748–754.

Arthritis & Rheumatology
Vol. 77, No. 11, November 2025, pp 1573–1584
DOI 10.1002/art.43236

American College of Rheumatology
Empowering Rheumatology Professionals

Regulatory Role of FGL-1 in Interorgan Communication by Controlling T Cell Homeostasis During the Onset of Sjögren Disease

Kunihiro Otsuka,[1] Aya Ushio,[2] Ruka Nagao,[3] Shigefumi Matsuzawa,[4] Rieko Arakaki,[3] Kazuki Fukuta,[3] Yasuhiro Mouri,[5] Takaaki Tsunematsu,[3] and Naozumi Ishimaru[2]

Objective. Autoimmunity occurs due to the tactics between pathogenic and regulatory factors in systemic organs. Although interorgan communication has been demonstrated in various diseases, the effects of the crosstalk between the immune system and other organs on autoimmune disease is unknown.

Methods. We analyzed the influence of interorgan communication on the cellular or molecular mechanism of autoimmunity using a mouse model of primary Sjögren disease (pSjD) and patients with pSjD by integrative genomic, bioinformatic, pathologic, and immunologic analyses.

Results. Fibrinogen-like protein-1 (FGL-1) was identified as a potent factor for interorgan communication between the liver and immune system in pSjD model mice. The production of FGL-1 of the liver is induced by interleukin-6 (IL-6) from $CD4^+$ T cells in these mice. The onset of autoimmune lesions in an *Fgl1*-deficient pSjD model mice was earlier than that in the wild type pSjD model mice. FGL-1 produced in the liver regulates naïve and memory T cell homeostasis. Further, FGL-1 was significantly up-regulated in patients with pSjD compared to the controls. Moreover, its concentration was closely related to the serum IL-6 levels in patients with pSjD.

Conclusion. FGL-1 plays a key role in the onset of autoimmunity by suppressing T cell activation in pSjD. Our results will facilitate the development of novel diagnostic or therapeutic strategies targeting the interorgan communication for autoimmune diseases.

INTRODUCTION

Primary Sjögren disease (pSjD) is a systemic autoimmune disease in which the exocrine glands, such as lacrimal and salivary glands (SGs), are mainly targeted by autoreactive immune cells.[1–3] Moreover, a variety of lesions in the extraglandular organs, including the gastrointestinal tract, lungs, kidneys, joint, lymph nodes, and nerve system, are also observed in pSjD.[4,5] Because of the complicated pathogenesis and diverse symptoms exhibited by each patient, pSjD is a refractory immune disease.[6,7] Among a variety of symptoms of pSjD, dry mouth and eye due to the dysfunction of salivary and lacrimal glands largely reduce quality of life in a lot of patients with pSjD. However, it is unclear why the exocrine gland is targeted among systemic organs in pSjD. In addition, any other organs may communicate with the target organ to control the pathogenesis of pSjD.

Interorgan communication occurs during physiologic homeostasis and various diseases, such as metabolic, neurologic, cardiovascular, infectious, immune disorders, and cancer.[8–11] The crosstalk between many organs via various mediators, including hormones, cytokines, chemokines, neuropeptides, or products

Dr Ishimaru's work was supported by the Japan Society for the Promotion of Science (JSPS) KAKENHI (grants 18K19648, 21K19605, 21J13008, and 23H00438).

[1]Kunihiro Otsuka, DDS, PhD: Department of Oral Pathology, Tokushima University Graduate School of Biomedical Sciences and Department of Interdisciplinary Researches for Medicine and Photonics, Institute of Post-LED Photonics, Tokushima University, Tokushima, Japan; [2]Aya Ushio, DDS, PhD, Naozumi Ishimaru, DDS, PhD: Department of Oral Pathology, Tokushima University Graduate School of Biomedical Sciences, Tokushima, Japan, and Department of Oral Pathology, Graduate School of Medical and Dental Sciences, Institute of Science Tokyo, Tokyo, Japan; [3]Ruka Nagao, DDS, Rieko Arakaki, PhD, Kazuki Fukuta, DDS, Takaaki Tsunematsu, DDS, PhD: Department of Oral Pathology, Tokushima University Graduate School of Biomedical Sciences, Tokushima, Japan; [4]Shigefumi Matsuzawa, DDS: Department of Oral Pathology, Tokushima University Graduate School of Biomedical Sciences, Tokushima, Japan, and Section of Oral and Maxillofacial Surgery, Division of Maxillofacial Diagnostic and Surgical Sciences, Faculty of Dental Science, Kyushu University, Fukuoka, Japan; [5]Yasuhiro Mouri, PhD: Department of Oral Bioscience, Tokushima University Graduate School of Biomedical Sciences, Tokushima, Japan.

Drs Otsuka and Ushio contributed equally to this work.

Additional supplementary information cited in this article can be found online in the Supporting Information section (https://acrjournals.onlinelibrary.wiley.com/doi/10.1002/art.43236).

Author disclosures and graphical abstract are available at https://onlinelibrary.wiley.com/doi/10.1002/art.43236.

Address correspondence via email to Naozumi Ishimaru, DDS, PhD, at ishimaru.naozumi@tmd.ac.jp.

Submitted for publication August 7, 2024; accepted in revised form May 6, 2025.

from microorganisms, orchestrates several functions of the target organ by controlling molecular dynamics, cell signaling, and gene expression.[12–15] However, the precise cellular or molecular mechanism underlying the onset of autoimmunity via interorgan communication is still unknown.

It is unclear why only exocrine glands are targeted by autoimmune mechanisms in pSjD. Moreover, the reason why the autoreactive cells never attack nontarget organs is also unknown in pSjD. Pathogenic or regulatory cytokines, chemokines, and hormones produced from nontarget organs, in addition to the target organs, have been reported in patients with pSjD and animal models.[16–19] Although the role of certain cytokines produced from nontarget cells is critical for the autoimmune response in the target organ in pSjD, the detailed interaction between the target and nontarget organs has during the pathogenesis of pSjD is unknown.

In this study, we hypothesized that the crosstalk between the target and nontarget organs might influence the onset or development of autoimmune lesions in pSjD. We attempted to identify the potent mediators produced by nontarget organs associated with interorgan communication that contribute to the pathogenesis of autoimmunity using a pSjD mouse model and samples from patients with pSjD. Our research might aid the development of novel diagnostic biomarkers or therapeutic strategies targeting pSjD.

MATERIALS AND METHODS

Mice. NFS/*sld* mice were obtained from the Central Institute for Experimental Animals (Kawasaki, Japan). Fibrinogen-like protein 1 (*Fgl1*) knockout (KO) mice were generated as described in the Supplementary Materials and Methods. This study was designed and undertaken by following the Fundamental Guidelines for Proper Conduct of Animal Experiments and Related Activities in Academic Research Institutions under the jurisdiction of the Ministry of Education, Culture, Sports, Science, and Technology of Japan. The protocol was approved by the Committee on Animal Experiments of Tokushima University (permit number T2021-48) and Institute of Science Tokyo (permit number A2024-134A). All experiments were performed under general anesthesia, and all efforts were made to minimize the suffering of the mice. The sample size of some experiments was determined to estimate the doubled number of experimental units. Inclusion and exclusion criteria were determined by the experimental protocol. All experimental units were randomly allocated to all mice during each experiment. In vitro and vivo experimental methods and materials are described in the Supplementary Materials and Methods and Supplementary Tables S1 and S2.

Integrative genomic analysis and bioinformatics. Microarray analysis was performed using the liver tissues from 10-week-old female control mice and pSjD model mice. Quality assessments and microarray experiments were completed as described in the Supplementary Materials and Methods.

Human participants. The Ethics Committee of the Tokushima University Hospital, Japan, granted approval for this study (no. 4252-1). Data from controls and patients with pSjD were used in this study, and all participants provided written informed consent in accordance with the principles outlined in the Declaration of Helsinki. All patients with pSjD were diagnosed by the Research Committee on pSjD of the Ministry of Health and Welfare of the Japanese Government (1999) and the 2016 American College of Rheumatology/EULAR Classification Criteria for Primary Sjogren's Syndrome. The serum samples of age-matched controls, including healthy individuals and non-pSjD controls, were used in this study. In addition, the patients had been untreated with any drug. We excluded patients with liver disease or severe infections from this cohort. The clinical information is shown in Supplementary Table S3.

Statistical analysis. The differences between individual groups were determined by using Student's *t*-test or one or two-way analyses of variance, in which P values of <0.05 were considered statistically significant. GraphPad Prism 8 software was used for all data analysis. Data are presented as means ± SDs.

RESULTS

Comprehensive analysis of genes in the liver of the pSjD model. We established a pSjD mouse model by performing neonatal thymectomy on newborn NFS/*sld* mice three days after birth.[20–23] The liver was chosen as a counterpart for interorgan communication with the target organ in pSjD. We performed microarray analysis to understand the changes in gene expression in the liver of the pSjD model compared with control mice. Further, by comparing the differentially expressed genes (DEGs) obtained from the microarray analysis with the marker genes in each cell type in the liver tissue, including hepatocytes, Kupffer cells, B cells, endothelial cells, and natural killer T cells derived from single-cell RNA sequencing data, we explored cell type–specific DEGs (Figure 1A and Supplementary Figure 1A). Notably, we identified hepatocyte-specific DEGs as candidate genes related to interorgan communication.

Among the candidate genes, *Fgl1* was chosen as an interorgan communication gene due to its up-regulated expression in liver tissues from the pSjD model mice (Figure 1B and Supplementary Figure 1B). FGL-1, an emerging hepatic factor in the fibrinogen superfamily,[24,25] is specifically expressed at a high proportion in hepatocytes (Figure 1C). Analysis of the plasma FGL-1 protein levels revealed that the FGL-1 levels of 4- to 12-week-old pSjD model mice were significantly higher than the control mice (Figure 1D). Moreover, FGL-1 was significantly up-regulated in the liver of pSjD model mice was observed compared with that of control mice (Figure 1E and F and Supplementary Figure 2A–D). In this pSjD model mouse, the onset of autoimmune

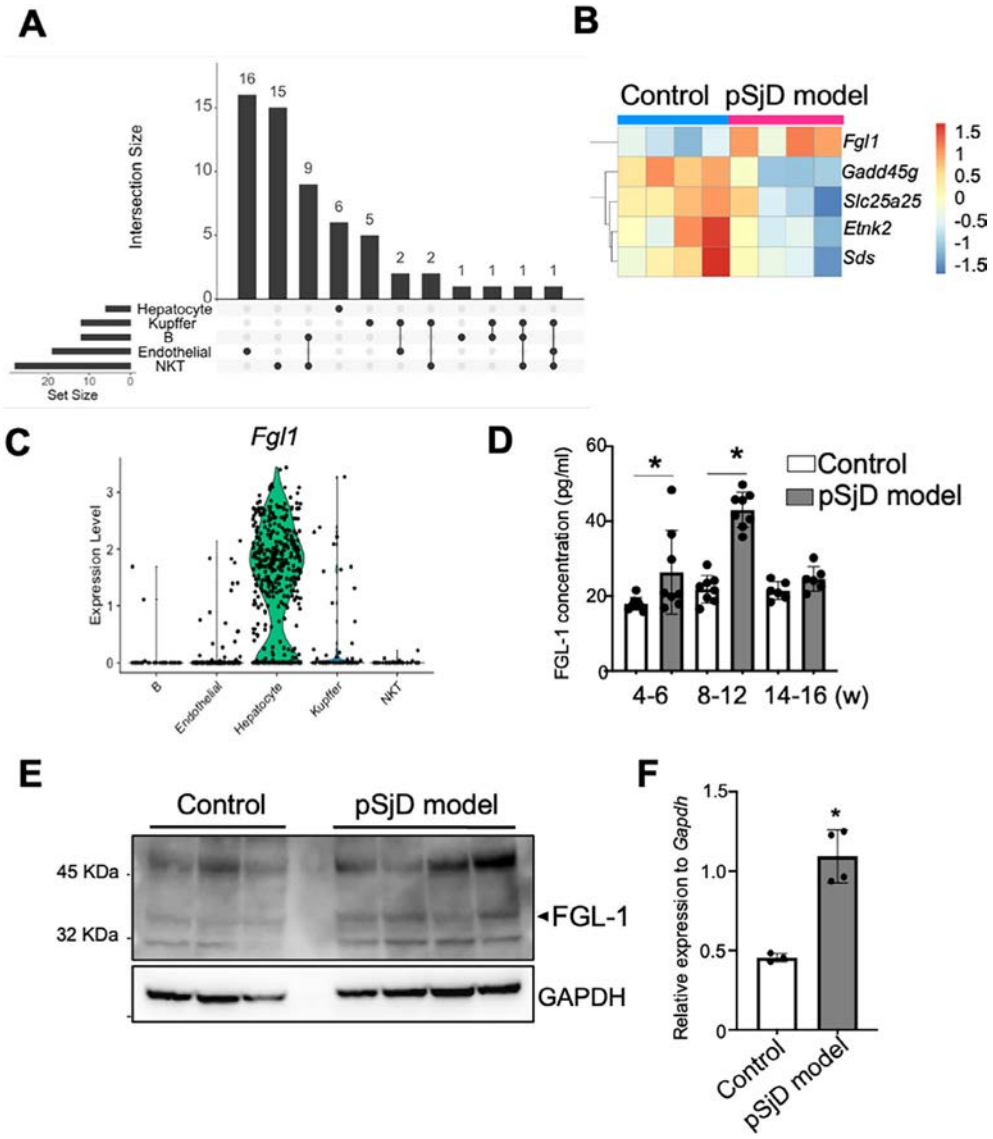

Figure 1. Identification of genes related to the interorgan communication from liver tissues in a pSjD mice model. (A) Visualization of the relationship between differentially expressed genes (DEGs) in liver tissues from the two groups and positive markers for various liver cell types. (B) Heat map showing the candidate gene expression between DEGs and hepatocyte markers in the liver from the pSjD model compared with control mice. The expression values of each gene were determined using the average expression value of all probes. (C) Expression of FGL-1 in each cell type of the liver. FGL-1 is highly expressed in the majority of hepatocytes. (D) FGL-1 concentration in the plasma from control and pSjD model mice was determined by enzyme-linked immunosorbent assay. Data are presented as averages ± SDs of six to eight mice per group. (E) Protein expression of FGL-1 was evaluated by Western blot analysis. Liver tissues of control (n = 3) and pSjD model mice (n = 4) were used, and GAPDH was used as a housekeeping protein. (F) The relative expression of FGL-1 to GAPDH was measured by densitometry intensity for the imaging. Data are presented as averages ± SDs. *$P < 0.05$, control versus pSjD model mice. *Etnk2*, ethanolamine kinase 2; FGL-1, fibrinogen-like protein-1; NKT, natural killer T; pSjD, primary Sjögren disease.

lesions in the salivary and lacrimal glands starts from four weeks old, and the inflammatory lesions are gradually developed until the mice were eight weeks old, in which the pSjD-like lesions were observed in almost 100% of the model mice.[20–23] FGL-1 might be up-regulated during the period of onset or development of the autoimmunity to regulate the lesions in the pSjD model mice. Therefore, FGL-1 expression and its regulatory mechanism in pSjD were further explored.

Change of FGL-1 expression by interleukin-6 in pSjD model mice. A previous study showed that interleukin-6 (IL-6) enhanced the messenger RNA (mRNA) and protein levels of FGL-1 in human hepatocytes in vitro.[26] The serum IL-6 levels were significantly higher in the pSjD model than in control mice (Figure 2A). Moreover, flow cytometric analysis of the intracellular IL-6 expression in the $CD4^+$ T cells in the spleen, liver, and SGs indicated that the proportion of IL-6 was significantly increased

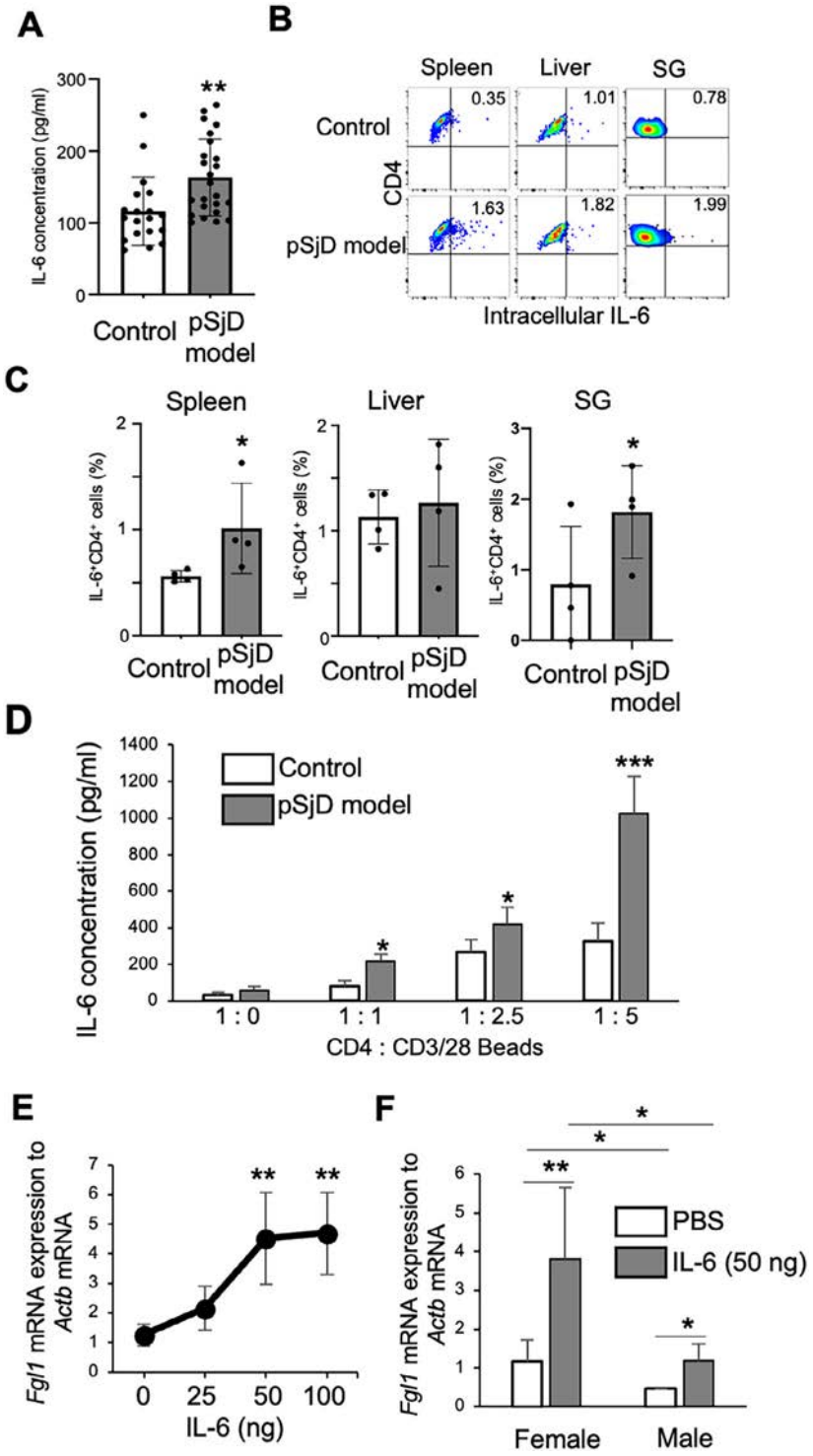

Figure 2. Relationship between IL-6 and FGL-1 in pSjD model mice. (A) IL-6 concentration was determined using the serum samples of 6- to 12-week-old control and pSjD model mice (n = 20 and 24, respectively). Data are shown as averages ± SDs. (B) Intracellular IL-6 expression was determined using spleen, liver and SGs form control and pSjD model mice (n = 4). (C) The proportion of IL-6$^+$CD4$^+$ T cells was evaluated, and data are shown as averages ± SDs. (D) IL-6 concentration was determined using the supernatants of splenic CD4$^+$ T cells stimulated with anti-CD3 and CD28 monoclonal antibody–coating beads. Data are shown as averages ± SDs of control and pSjD model mice (n = 4). (E) *Fgl1* mRNA expression was determined by quantitative transcriptase–polymerase chain reaction using the liver tissues from control female mice at 24 hours after peritoneal injection of IL-6 (0–100 ng/mouse). Data are shown as averages ± SDs of mice (n = 4 or 5). (F) *Fgl1* mRNA expression was determined using the liver tissues from female mice after peritoneal injection of PBS or IL-6 (50 ng/mouse). Data are shown as averages ± SDs of mice (n = 5). *P < 0.05 and **P < 0.005. ***P < 0.0005, versus control mice. IL-6, interleukin-6; FGL-1, fibrinogen-like protein-1; mRNA, messenger RNA; PBS, phosphate buffered saline; pSjD, primary Sjögren disease; SG, salivary gland.

in the spleen and SG in the pSjD model mice compared with that in the control mice (Figure 2B and C and Supplementary Figure 3A) without any significant difference in the liver tissue between the control and pSjD model mice (Figure 2B and C). However, there were no differences in the proportion of IL-6$^+$CD8$^+$ T cells of spleen, liver, and SG between control and pSjD model mice (Supplementary Figure 3B and C). In addition, no differences were found in CD11b$^+$IL-6$^+$ macrophages, CD11c$^+$IL-6$^+$ dendritic cells, and CD19$^+$IL-6$^+$ B cells in the spleen between control and pSjD model mice (Supplementary Figure 3B). In our pSjD mouse model, pulmonary lesions are also observed as well as the lesions in the salivary and lacrimal glands.[23] Therefore, we analyzed intracellular IL-6 expression of CD4$^+$ T cells from the lung tissues in control and pSjD model mice. A significantly increased proportion of IL-6$^+$CD4$^+$ T cells in pSjD model mice was detectable compared with that in control mice (Supplementary Figure 3D). Moreover, when the splenic CD4$^+$ T cells were stimulated with anti-CD3 and anti-CD28 monoclonal antibody (mAb)–conjugated beads for 24 hours, the IL-6 concentration was significantly higher in the supernatants of stimulated CD4$^+$ T cells from the pSjD model mice than that from the control mice (Figure 2D).

To examine whether IL-6 up-regulates FGL-1 expression in the liver, we injected recombinant IL-6 (0–100 ng/mouse) intraperitoneally into female control mice. The *Fgl1* mRNA was significantly up-regulated in the livers of mice injected with 50 and 100 ng IL-6 (Figure 2E). Additionally, the expression of *Fgl1* mRNA was significantly higher in the liver of both female and male mice after intraperitoneal injection of IL-6 (50 ng) (Figure 2F). The *Fgl1* mRNA expression in the liver of IL-6-injected female mice was significantly higher than in IL-6-injected male mice (Figure 2F). Similar results were seen in the *Fgl1* mRNA levels in the liver of phosphate buffered saline (PBS)–injected female mice compared with that in PBS-injected male mice (Figure 2F). On the other hand, as a control for IL-6, recombinant tumor necrosis factor α (TNFα) (50 ng/mouse) was intraperitoneally injected into female wild type (WT) mice. No difference was observed in *Fgl1* mRNA expression level between TNFα- and PBS-injected mice (Supplementary Figure 3E). These results demonstrate that IL-6 from CD4$^+$ T cells up-regulates FGL-1 expression in the liver of the pSjD model. In addition, *Fgl1* mRNA expression is higher in the liver of female mice than in male mice, implicating the role of sex dimorphism in female patients during the onset of autoimmunity.

Ligand for lymphocyte activation gene-3 expression on CD4$^+$ T cells in pSjD model mice. FGL-1 acts as a ligand for lymphocyte activation gene-3 (LAG-3), one of immune checkpoint molecules, on T cells.[27] Surface expression of LAG-3 on CD4$^+$ T cell subsets, including CD44^{high}CD62L$^-$ memory, CD44^{low}CD62L$^+$ naïve, and Foxp3$^+$ Treg cells, was detected by flow cytometric analysis. The expression intensity of LAG-3 on the T cell subsets in the spleen of control mice was in the following order: memory, Treg, and naïve CD4$^+$ T cells (Supplementary Figure 4A). When the geographic mean fluorescence intensity (gMFI) of LAG-3 on CD4$^+$ T cell subsets was evaluated, the gMFI was significantly higher on all the subsets in the pSjD model mice than in the control mice (Figure 3A and B). The CD4$^+$ T cell subsets in the pSjD model mainly included memory CD4$^+$ T cells, whereas naïve T cells were the main population in the control mice (Figure 3C). The proportion of LAG-3$^+$CD4$^+$ cells in the spleen of the pSjD model was significantly increased compared with that from control mice (Figure 3D and E) without any difference in these cells in the liver and SG between control and pSjD model mice (Figure 3D and E). Moreover, there was no difference in the proportion of LAG-3$^+$CD4$^+$ T cells of peripheral blood mononuclear cells (PBMCs) between control and pSjD model mice (Supplementary Figure 4B).

We performed an in vitro experiment by binding assay using recombinant FGL-1-Fc protein. When CD4$^+$ T cells were incubated with FGL-1-Fc (5 μg/mL) in vitro, the binding activity of CD4$^+$ T cells from pSjD model mice was significantly higher than that from control mice (Figure 3F). In addition, the suppressive effect of FGL-1 on CD4$^+$ T cell proliferation was evaluated by in vitro culture in which CD4$^+$ T cells were labeled with 5,6-carboxyfluorescein succinimidyl ester (CFSE) and then were stimulated with anti-CD3 and CD28 mAb in the presence of FGL-1-Fc protein for 72 hours. Proliferation of CD4$^+$ T cells from pSjD model was significantly inhibited by both 1 and 5 μg/mL of FGL-1-Fc, whereas proliferation of control CD4$^+$ T cells was significantly suppressed by only 5 μg/mL of FGL-1-Fc (Figure 3G). These findings showed both FGL-1 from the liver and its receptor LAG-3 on peripheral CD4$^+$ T cells are up-regulated in the pSjD model mice, suggesting that interorgan communication via FGL-1 between liver and peripheral T cells may control the onset or development of autoimmunity in pSjD model mice.

Immune phenotype of *FGL-1*KO mice. To further understand the role of FGL-1, we generated NFS/*sld* background *Fgl1*KO mice (Supplementary Figure 5A and Supplementary Figure 2A and B). Flow cytometric analysis of the spleen cells showed no differences in CD4$^+$ and CD8$^+$ T cell proportions between the WT and *Fgl1*KO mice at eight weeks of age (Supplementary Figure 5B–D). The proportion of CD44^{high}CD62L$^-$CD4$^+$ memory phenotype T cells of *Fgl1*KO mice was similar to that of WT mice (Supplementary Figure 5E and F). There was no difference in the proportion of CD44^{low}CD62L$^+$CD4$^+$ naïve phenotype T cells between WT and *Fgl1*KO mice (Supplementary Figure 5E and G) and the ratio of memory to naïve phenotype CD4$^+$ T cells between WT and *Fgl1*KO mice (Supplementary Figure 5H). In addition, no inflammatory lesions were found in the lacrimal and SGs of both WT and *Fgl1*KO mice (Supplementary Figure 5I and J). The results show that FGL-1 does not control the balance or

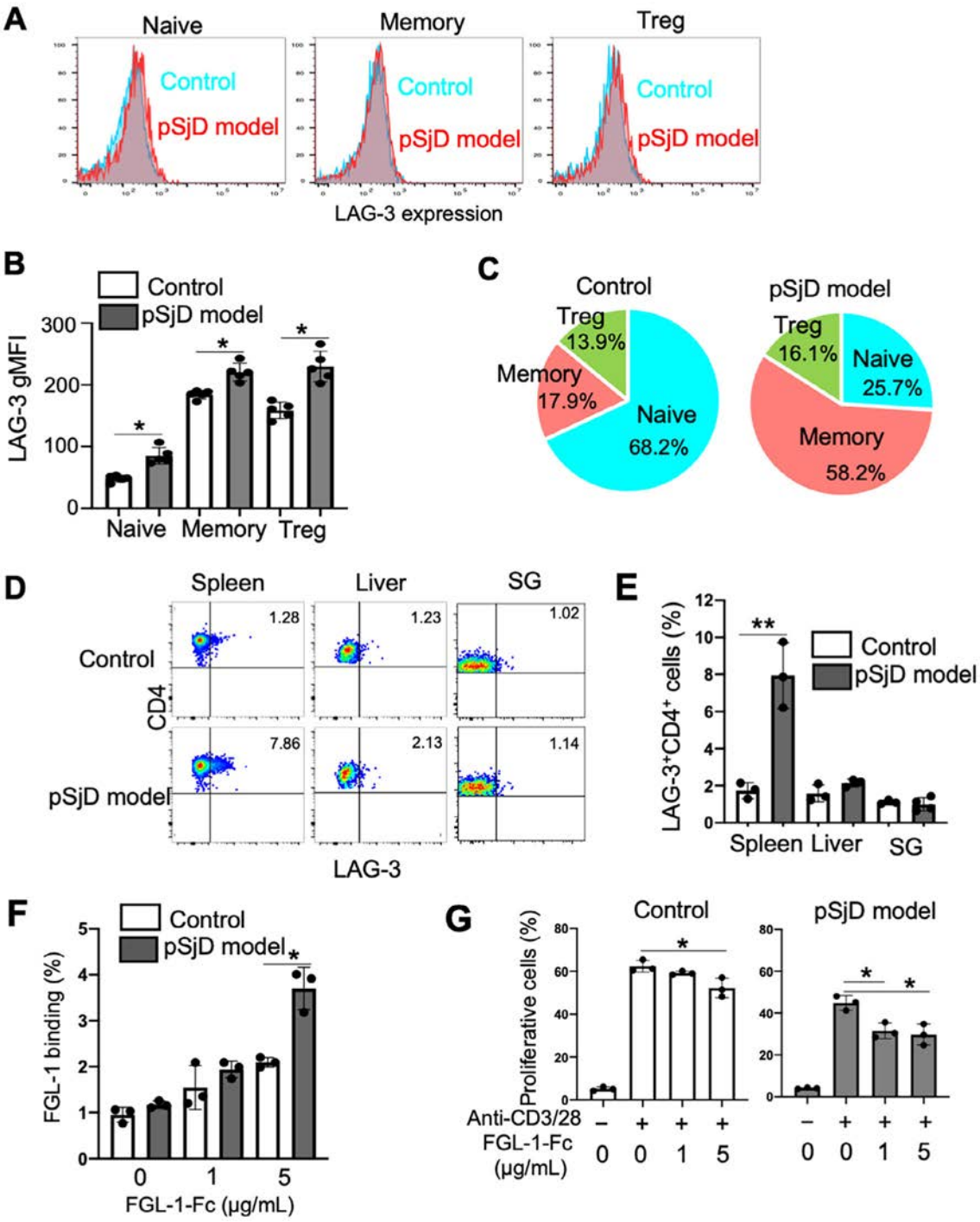

Figure 3. LAG-3 expression on CD4$^+$ T cells in pSjD model mice. (A) LAG-3 expression of naïve, memory, and Treg cells in the spleen was evaluated using eight-week-old female control and pSjD model mice. (B) The gMFI of each group was evaluated, and data are shown as averages ± SDs (n = 5). (C) Ratio of naïve, memory, and Treg cells in CD4$^+$ T cells in control and pSjD model mice was evaluated. (D) The proportion of LAG-3$^+$CD4$^+$ T cells in the spleen, liver, and SG in control and pSjD model mice was evaluated, and results are representative of each group. (E) Proportion of LAG-3$^+$CD4$^+$ T cells of spleen, liver, and SG in control and pSjD model mice are shown as averages ± SDs (n = 3). (F) Binding to FGL-1 of splenic CD4$^+$ T cells was evaluated using recombinant FGL-1-Fc protein. The proportion was detected using anti–Fc-IgG fluorescein isothiocyanate. Data are shown as averages ± SDs (n = 3). (G) Splenic CD4$^+$ T cells were labeled with 5,6-carboxyfluorescein succinimidyl ester and incubated with anti-CD3 and CD28 monoclonal antibody–bound beads with FGL-1-Fc for 72 hours. Proliferative cells are shown as averages ± triplicates. *$P < 0.05$, **$P < 0.005$. FGL-1, fibrinogen-like protein-1; gMFI, geographic mean fluorescence intensity; LAG-3, lymphocyte activation gene-3; pSjD, primary Sjögren disease; SG, salivary gland.

switching between naïve and memory CD4$^+$ T cells in the periphery under normal conditions.

Autoimmune pathology of *FGL-1*KO-pSjD model mice. To define the relationship between FGL-1 and autoimmune pathology in pSjD model mice, we performed neonatal thymectomy using *Fgl1*KO mice. The SGs and lacrimal glands of the *Fgl1*KO- and WT-pSjD model mice were subjected to histopathologic analysis. The onset of autoimmune lesions in the SGs and lacrimal glands occurs at four to six weeks of age in the pSjD model mice.[20–23] We detected a small area of lymphocyte infiltration in the SGs and lacrimal glands of the WT-pSjD model at four weeks of age (Figure 4A). Contrastingly, the pathologic score of the SGs in the *Fgl1*KO-pSjD model mice was significantly enhanced compared with that in the WT-pSjD model mice, without any difference in the pathologic score of the lacrimal glands between these mice (Figure 4A and C and Supplementary Figure 6A and B). Further, the number of inflammatory lesions/mm^2 (focus score) in the SGs and lacrimal glands in four-week-old *Fgl1*KO-pSjD model mice was significantly increased compared with that of the WT-pSjD model mice (Figure 4A and D and Supplementary Figure 6A and B). At eight weeks of age, the pathologic score and the focus score of SGs, but not lacrimal glands, were also higher in the *Fgl1*KO-pSjD model mice (Figure 4B–D and Supplementary Figure 6A and B). Conversely, there were no differences in the pathologic score and the focus score of SGs between WT-pSjD and *Fgl1*KO-pSjD model mice at 12 weeks old (Figure 4C and D). These pathologic findings suggest that interorgan communication via FGL-1 may control the onset of autoimmune pathology in the target organ of the pSjD model mice.

Immune phenotypes in *Fgl1*KO-pSjD model mice. To identify the peripheral T cell phenotypes in the *Fgl1*KO-pSjD model mice, we performed flow cytometric analysis to evaluate the proportion of T cell subsets in six-week-old mice. There were no differences in the proportions of CD4$^+$, CD8$^+$T cells, and CD19$^+$B cells between WT-pSjD and *Fgl1*KO-pSjD model mice (Figure 5A). However, the proportion of memory CD4$^+$ T cells was significantly higher in the *Fgl1*KO-pSjD model mice than in the WT-pSjD model mice (Figure 5B). Further, the proportion of naïve CD4$^+$ T cells was significantly lower in the *Fgl1*KO-pSjD model mice than in WT-pSjD model mice (Figure 5B). No difference was detected in the Treg cells between *Fgl1*KO-pSjD model mice (Figure 5B). Consequently, the ratio of memory to naïve CD4$^+$ T cells in the *Fgl1*KO-pSjD model mice was significantly increased compared with that in WT-pSjD model mice (Figure 5C).

To understand the activation or differentiation of CD4$^+$ T helper cells, the gene expression of inflammatory cytokines and master transcription factors of T helper cell subsets was analyzed using CD4$^+$ T cells isolated from the spleen. The mRNA expression levels of inflammatory cytokine genes, such as *Il2*, *Il4*, *Il10*, *Il17*, and *Ifn*g of the splenic CD4$^+$ T cells from WT-pSjD and *Fgl1*KO-pSjD model mice were measured by real-time reverse transcriptase–polymerase chain reaction. Among them, *Ifng* mRNA expression level of *Fgl1*KO-pSjD model mice was significantly higher than that of WT-pSjD model mice (Figure 5D). In addition, *Tbx21*, a master transcription factor gene for Th1 cells, mRNA expression of CD4$^+$ T cells from *Fgl1*KO-pSjD model mice was significantly up-regulated compared with that from WT-pSjD model mice (Figure 5E), suggesting that FGL-1 may control the activation of Th1 cells via interferon-γ during the onset of autoimmunity in pSjD model mice. Moreover, no differences were found in the proportions of LAG-3$^+$ on memory and naïve CD4$^+$ T cells, and Treg cells between WT-pSjD and *Fgl1*KO-pSjD model mice (Supplementary Figure 7A). Further, the serum levels of autoantibodies, including anti-SSA, anti-SSB, and anti–α-fodrin antibodies, were measured using enzyme-linked immunosorbent assay (ELISA) in the control, WT-pSjD model, and *Fgl1*KO-pSjD model mice at 10 to 16 weeks. Although these autoantibody levels were significantly higher in both WT-pSjD and *Fgl1*KO-pSjD model mice than in control mice, there were no differences in these autoantibody levels between WT-pSjD and *Fgl1*KO-pSjD model mice (Supplementary Figure 7B). The results demonstrate that the interorgan communication via FGL-1 influences the balance between naïve and memory T cell phenotype, but not autoantibody production in pSjD model mice.

In vivo role of FGL-1 on memory T cell homeostasis. To understand the in vivo role of FGL-1 in memory T cell homeostasis, we intraperitoneally injected anti-CD3 mAb into WT and *Fgl1*KO mice twice after IL-6 injection (Figure 5F). The T cell subsets, including CD4$^+$, CD8$^+$, CD44^{high}CD62L$^-$ memory CD4$^+$, and CD44^{low}CD62L$^+$ naïve CD4$^+$ cells, in PBMCs were evaluated by flow cytometric analysis. In addition, the ratio of memory-to-naïve CD4$^+$ cells (M/N) was evaluated for 47 days. The proportion of CD4$^+$ T cells in both WT and *Fgl1*KO mice reduced drastically and then gradually increased after the second injection of anti-CD3 mAb on day 4 (Figure 5G). The proportion of CD4$^+$ T cells was significantly lower in *Fgl1*KO mice than in WT mice from day 16 to 47, although CD4$^+$ T cells of WT mice recovered to the first level by day 40 (Figure 5G). Conversely, there was no difference in the proportion of CD8$^+$ T cells between WT and *Fgl1*KO mice from day 0 to 47 (Supplementary Figure 8). The proportion of memory CD4$^+$ T cells of *Fgl1*KO mice was significantly higher than that of WT mice from day 8 to 47 (Figure 5H), whereas the proportion of naïve CD4$^+$ T cells was significantly lower in *Fgl1*KO mice than in WT mice from day 8 to 47 (Figure 5I). Consequently, the M/N ratio was significantly increased compared with that of WT mice from day 8 to 47 (Figure 5J). The results suggest that FGL-1 may control naïve-to-memory T cell homeostasis after T cell activation.

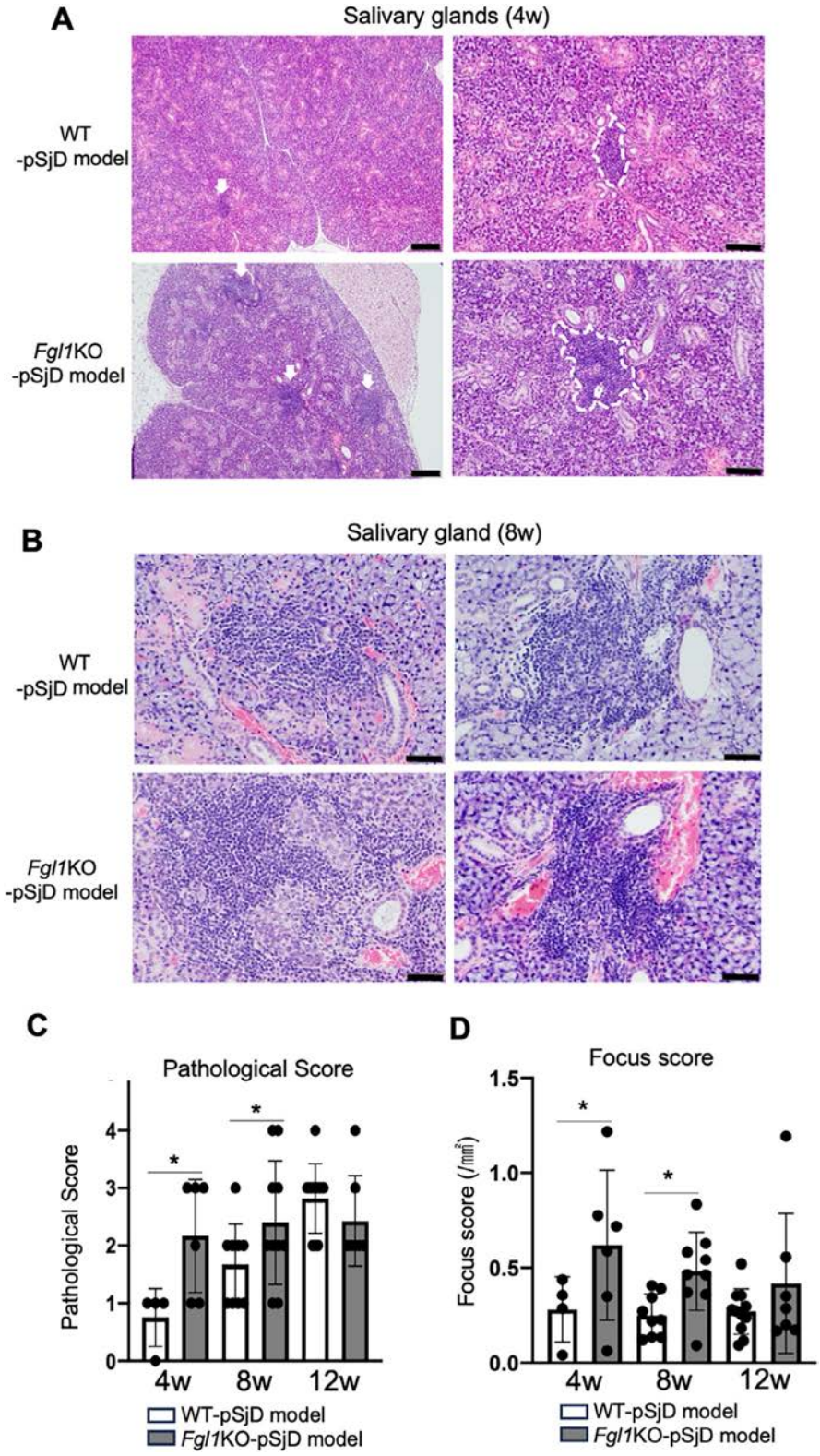

Figure 4. Pathology of the salivary glands (SGs) in an *Fgl1*KO-pSjD model mice. (A) Histopathology of SGs in four-week-old WT- and *Fgl1*KO-pSjD model mice were shown to represent each group. Scale bar: 200 μm (left photos), and 100 μm (right photos). (B) Histopathology of SGs in eight-week-old WT- and *Fgl1*KO-pSjD model mice were shown to represent each group. Scale bar: 50 μm. (C) The pathologic score was evaluated using the SG tissues from eight-week-old WT- and *Fgl1*KO-pSjD model mice. Data are shown as averages ± SDs (n = 5–9). (D) Focus score (/mm^2) was evaluated using the SG tissues from eight-week-old WT- and *Fgl1*KO-pSjD model mice. Data are shown as averages ± SDs (n = 5–9). *$P < 0.05$. *Fgl1*KO, fibrinogen-like protein-1 knockout; pSjD, primary Sjögren disease; WT, wild type.

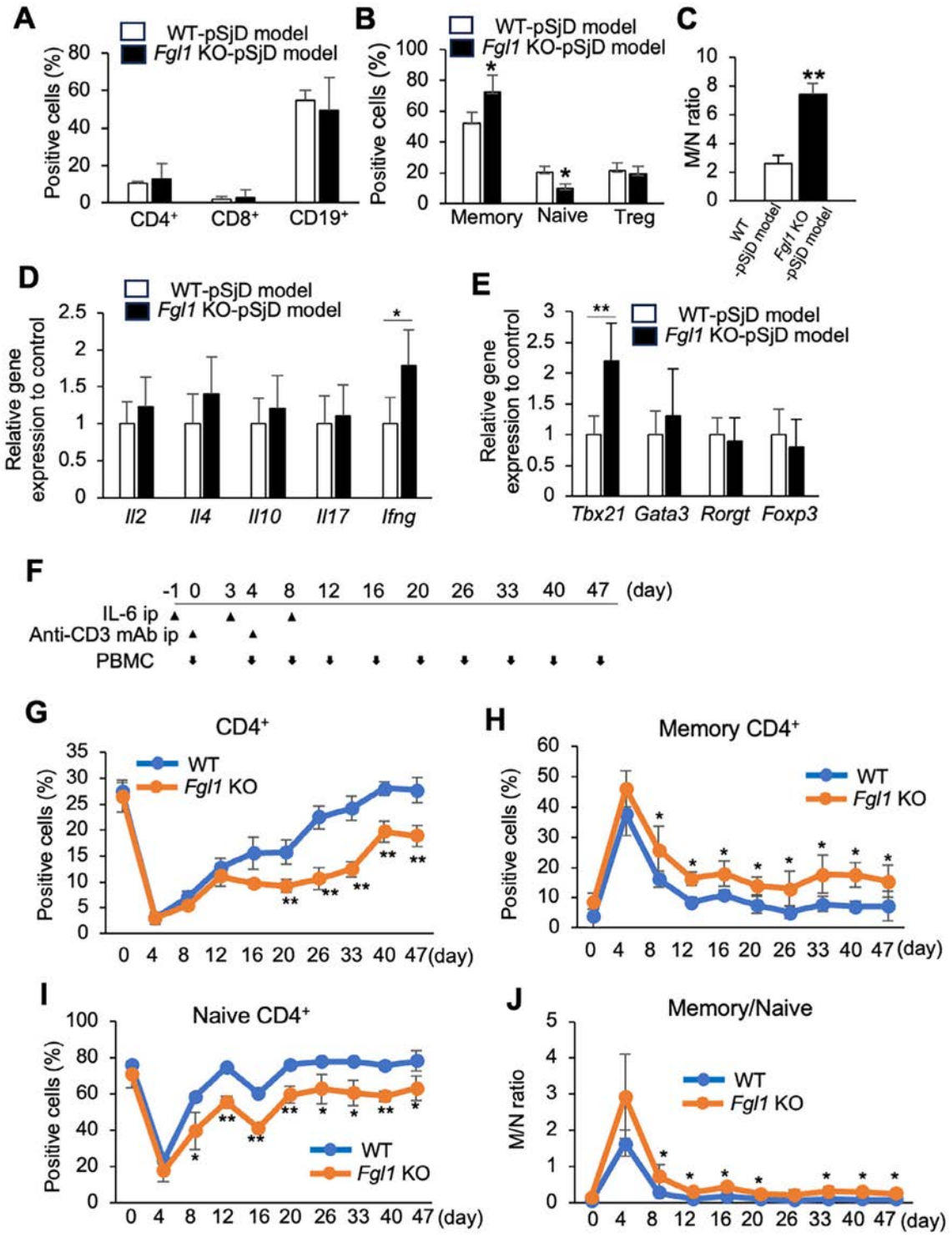

Figure 5. Phenotype and gene expression of T cells in six-week-old female *Fgl1*KO-pSjD model mice. (A–C) The T cell subsets, B cells and M/N were evaluated and data are shown as average ± SD (n = 6). (D) *Il2*, *Il4*, *Il10*, *Il17*, and *Ifng* messenger RNA (mRNA) expression levels of splenic $CD4^+$ cells were determined, and data are shown as average relative expression of ± SD (n = 4). (E) *Tbx21*, *Gata3*, *Rorg*, and *Foxp3* mRNA expression levels are shown as average relative expression of ± SD (n = 4). (F) IL-6 (50 ng/mouse) was intraperitoneally (i.p.) injected three times into eight-week-old female WT and *Fgl1*KO mice (n = 6). Anti-CD3mAb (10 μg/mouse) was i.p. injected twice. PBMCs were collected to check CD4, CD44, and CD62L expressions as indicated in the experimental schedule. (G) The proportion of $CD4^+$ T cells are shown as averages ± SDs. (H) The proportion of memory $CD4^+$ T cells are shown as averages ± SDs. (I) The proportion of naïve $CD4^+$ T cells are shown as averages ± SDs. (J) M/N ratio was evaluated as average ± SD. *$P < 0.05$, **$P < 0.005$. *Fgl1*KO, fibrinogen-like protein-1 knockout; IL-6, interleukin-6; mAb, monoclonal antibody; M/N, memory-to-naïve $CD4^+$ cells; PBMC, peripheral blood mononuclear cell; pSjD, primary Sjögren disease; WT, wild type.

Relationship between FGL-1 and IL-6 in patients with pSjD. To further confirm the clinical significance of FGL-1 in pSjD, we evaluated the serum IL-6 and FGL-1 levels from patients with pSjD using ELISA (Supplementary Table S3). There was no difference in the serum IL-6 levels between controls (n = 10) and patients with pSjD (n = 12) (Figure 6A). The serum FGL-1 levels in patients with pSjD were significantly higher than in controls (Figure 6B). Furthermore, a significant correlation was observed between the IL-6 and FGL-1 levels in patients with pSjD (Figure 6C). An acute inflammation marker related to IL-6, C-reactive protein, did not show any significant changes in either patients or controls (Supplementary Table S3). The findings demonstrate that the interorgan communication via IL-6/FGL-1 between peripheral T cells and the liver contributes to the autoimmune pathogenesis of pSjD.

DISCUSSION

The pSjD model mice used in this study are useful and suitable for in vivo experiments because the onset ratio of pSjD-like lesions is almost 100% at two months old.[20–23] On the other hand, the inflammatory lesions in the salivary and lacrimal glands are observed with aging after three to four months in common SjD model mice, such as nonobese diabetic and MRL/*lpr/lpr* mice, that are considered as secondary SjD models.[28] Therefore, we used this mice model resembling human lesions in pSjD to explore the in vivo role of FGL-1.

FGL-1, also known as hepassocin, is a protein secreted from hepatocyte and contains a fibrinogen-related domain in its C-terminal portion.[24,29] Along with the c-reactive protein, FGL-1 is secreted by the hepatocytes during acute systemic inflammation.[26] FGL-1 is involved in hepatogenesis to promotes hepatocyte proliferation through an extracellular signal–regulated kinase 1/2–dependent autocrine mechanism.[30–32] It also contributes to the pathogenesis of hepatocellular carcinoma, diabetes, obesity, and nonalcoholic fatty liver disease via controlling energy or fatty metabolism.[33–36] Recent reports demonstrated that FGL-1 binds to LAG-3, an immune checkpoint molecule, on T cells to inhibit T cell activation as an immune checkpoint target.[27,37] Moreover, FGL-1 was reported as a novel biomarker for predicting disease activity and prognosis of rheumatoid arthritis.[38] Additionally, the serum FGL-1 levels in patients with SjD were shown to be significantly up-regulated compared with that of controls.[38] This finding coincides with our results using pSjD model mice and patients with pSjD. Based on our results, instead of contributing to chronic pathogenesis, FGL-1 prevents the inhibition of T cell activation during the onset of pSjD. However, because the function of FGL-1 is still unclear, detailed molecular mechanism of T cell regulation via FGL-1/LAG-3 should be further analyzed.

Secretion of FGL-1 from the liver was up-regulated by IL-6 derived from peripheral T cells in pSjD model mice. We confirmed an increase of IL-6$^+$ CD4$^+$ T cells in the SGs, a target organ, and in the spleen of the pSjD model. Although IL-6 has been shown to increase the mRNA and protein levels of FGL-1 in human hepatocytes or hepatocellular carcinoma cells in vitro,[26,30] it is unclear whether IL-6 directly induces FGL-1 expression in the liver in vivo. Our results clearly showed that intraperitoneal injection of IL-6 can up-regulate *FGL-1* mRNA in the liver of normal mice, especially in female mice. As autoimmune diseases, including pSjD, predominantly occur in women,[39,40] sexual dimorphism might be associated with the pathogenesis of autoimmunity. The mechanism of FGL-1 production by hepatocytes is still unclear, and any other factors than IL-6 might stimulate hepatocytes to produce FGL-1 through unknown signaling pathways.

LAG-3, a type 1 transmembrane protein similar to the CD4 molecule, and controls T cell activation to influence autoimmunity,

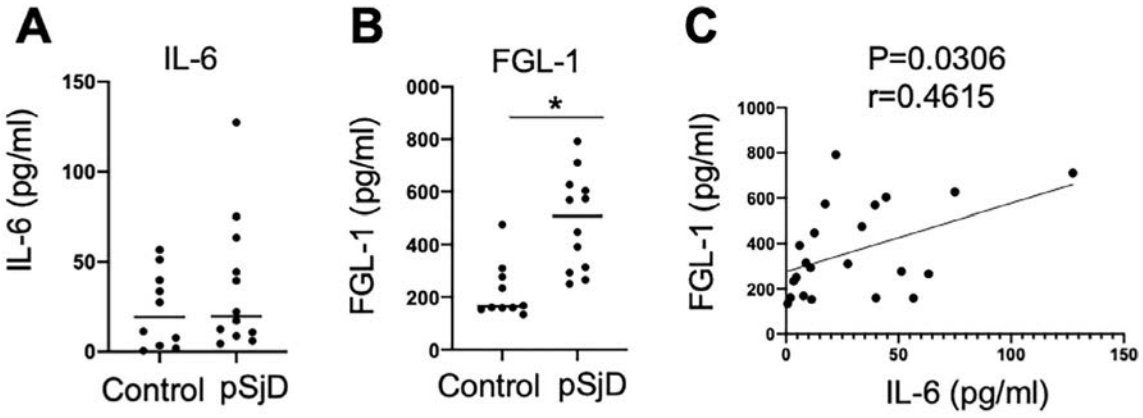

Figure 6. The relationship between IL-6 and FGL-1 in the serum samples of patients with pSjD. (A) IL-6 concentration was measured by enzyme-linked immunosorbent assay (ELISA) using the serum samples of healthy controls (n = 10) and patients with pSjD (n = 12). Data are shown as averages ± SDs of samples. (B) FGL-1 concentration was measured by ELISA using the serum samples of healthy controls (n = 10) and patients with pSjD (n = 12). Data are shown as averages ± SD of samples. *$P < 0.05$. (C) Correlation between IL-6 and FGL-1 in all the serum samples of controls (n = 10) and patients with pSjD (n = 12) was evaluated by a confidence value of 95%. $P = 0.0306$, $r = 0.4615$. FGL-1, fibrinogen-like protein-1; IL-6, interleukin-6; pSjD, primary Sjögren disease.

cancer immunity, and infection in cooperation with other inhibitory co-receptors, such as programmed death 1, an immune checkpoint molecule.[41–45] Although the binding of FGL-1 to LAG-3 on T cells to inhibits T cell activation,[27] a recent report revealed that binding of LAG-3 to a stable peptide major histocompatibility complex class II complex instead of FGL-1 causes T cell suppression to regulate autoimmunity and anticancer immunity.[45] In this study, we found no difference in the autoimmune lesions between WT- and *Fgl1*KO-pSjD model mice at 12 weeks old. However, the onset in *Fgl1*KO-pSjD model mice was earlier than that in WT-pSjD model mice, suggesting that FGL-1 might temporarily regulate T cell activation in pSjD model mice. In addition, an in vivo experiment using the administration of anti-CD3 mAb into *Fgl1*KO mice revealed that FGL-1 may control the balance between naïve and memory $CD4^+$ T cells during homeostatic expansion. Moreover, the expression of LAG-3 was increased on $CD4^+$ T cells in pSjD model mice. The finding suggests that the regulatory mechanisms that suppress autoreactive T cells might be unstable in pSjD model mice. These results indicate that autoreactive T cell activation prevails over the regulatory mechanism of T cells, including LAG-3/FGL-1, during the development of autoimmune lesions in pSjD model mice.

Our first aim was to identify the molecules associated with interorgan communication between the target and other organs in pSjD. We hypothesized that the IL-6 from activated T cells in the target organ or periphery induces FGL-1 secretion in the liver during the onset of pSjD. Further, this FGL-1 might struggle to suppress T cell activation or control naïve and memory homeostasis by binding to LAG-3 on the T cells to delay the onset of autoimmunity in pSjD. However, the regulation of autoreactivity might be irreversible via immune checkpoint molecules.

Negative feedback may work after the regulatory mechanism by FGL-1/LAG-3 axis. It is possible that FGL-1 may play a regulatory role in the onset of autoimmunity in pSjD model mice and patients with pSjD. However, after the duration of onset in autoimmune response, LAG-3 signaling pathway may fail to be active as negative feedback, and then uncontrolled autoimmune response may be developed to form chronic inflammatory lesions in pSjD. Thus, FGL-1 may be a signature of autoreactivity in T cells in pSjD. Several T cell activation and suppression mechanisms have been reported.[46–49] The activation and regulation of autoreactive T cells are so complex that the molecular or cellular pathogenesis of many autoimmune diseases is poorly understood. Our findings show that FGL-1 might mediate interorgan communication during the complicated pathogenesis of pSjD.

In conclusion, we identified FGL-1 as a mediator of interorgan communication between SGs and the liver in pSjD model mice. Further, IL-6 from activated $CD4^+$ T cells up-regulated the production of FGL-1 in the liver. FGL-1 plays a key role in the onset of autoimmunity by suppressing T cell activation in pSjD model mice. It also contributes to the regulation of naïve and memory homeostasis during process of T cell activation (Supplementary Figure 9). Moreover, the serum concentration of FGL-1 is closely related to IL-6 in patients with pSjD. Therefore, FGL-1 can be used as a biomarker for understanding the pathogenesis of pSjD. These results can help develop new therapeutic strategies targeting immune checkpoint molecules, such as LAG-3/FGL-1, in autoimmune diseases, including pSjD.

AUTHOR CONTRIBUTIONS

All authors contributed to at least one of the following manuscript preparation roles: conceptualization AND/OR methodology, software, investigation, formal analysis, data curation, visualization, and validation AND drafting or reviewing/editing the final draft. As corresponding author, Dr Ishimaru confirms that all authors have provided the final approval of the version to be published and takes responsibility for the affirmations regarding article submission (eg, not under consideration by another journal), the integrity of the data presented, and the statements regarding compliance with institutional review board/Declaration of Helsinki requirements.

REFERENCES

1. Thorlacius GE, Björk A, Wahren-Herlenius M. Genetics and epigenetics of primary Sjögren syndrome: implications for future therapies. Nat Rev Rheumatol 2023;19(5):288–306.
2. Fox RI, Fox CM, Gottenberg JE, et al. Treatment of Sjögren's syndrome: current therapy and future directions. Rheumatology (Oxford) 2021;60(5):2066–2074.
3. Nocturne G, Mariette X. Advances in understanding the pathogenesis of primary Sjögren's syndrome. Nat Rev Rheumatol 2013;9(9):544–556.
4. Mæland E, Miyamoto ST, Hammenfors D, et al. Understanding fatigue in Sjögren's syndrome: outcome measures, biomarkers and possible interventions. Front Immunol 2021;12:703079.
5. Vivino FB. Sjögren's syndrome: clinical aspects. Clin Immunol 2017;182:48–54.
6. Fox RI, Fox CM, McCoy SS. Emerging treatment for Sjögren's disease: a review of recent phase II and III trials. Expert Opin Emerg Drugs 2023;28(2):107–120.
7. Seror R, Nocturne G, Mariette X. Current and future therapies for primary Sjögren syndrome. Nat Rev Rheumatol 2021;17(8):475–486.
8. Boris V, Vanessa V. Molecular systems biology approaches to investigate mechanisms of gut-brain communication in neurological diseases. Eur J Neurol 2023;30(11):3622–3632.
9. Martins-Marques T, Girão H. The good, the bad and the ugly: the impact of extracellular vesicles on the cardiovascular system. J Physiol 2023;601(22):4837–4852.
10. Tran VTA, Lee LP, Cho H. Neuroinflammation in neurodegeneration *via* microbial infections. Front Immunol 2022;13:907804.
11. Enaud R, Prevel R, Ciarlo E, et al. The gut-lung axis in health and respiratory diseases: a place for inter-organ and inter-kingdom crosstalks. Front Cell Infect Microbiol 2020;10:9.
12. Zundler S, Günther C, Kremer AE, et al. Gut immune cell trafficking: inter-organ communication and immune-mediated inflammation. Nat Rev Gastroenterol Hepatol 2023;20(1):50–64.
13. Huh JR, Veiga-Fernandes H. Neuroimmune circuits in inter-organ communication. Nat Rev Immunol 2020;20(4):217–228.
14. Priest C, Tontonoz P. Inter-organ cross-talk in metabolic syndrome. Nat Metab 2019;1(12):1177–1188.

15. Nigam SK, Bush KT. Uraemic syndrome of chronic kidney disease: altered remote sensing and signalling. Nat Rev Nephrol 2019;15(5): 301–316.
16. Zhan Q, Zhang J, Lin Y, et al. Pathogenesis and treatment of Sjogren's syndrome: review and update. Front Immunol 2023;14: 1127417.
17. Tian Y, Yang H, Liu N, et al. Advances in pathogenesis of Sjögren's syndrome. J Immunol Res 2021;2021:5928232.
18. Singh N, Cohen PL. The T cell in Sjogren's syndrome: force majeure, not spectateur. J Autoimmun 2012;39(3):229–233.
19. Chiorini JA, Cihakova D, Ouellette CE, et al. Sjögren syndrome: advances in the pathogenesis from animal models. J Autoimmun 2009;33(3–4):190–196.
20. Haneji N, Hamano H, Yanagi K, et al. A new animal model for primary Sjögren's syndrome in NFS/sld mutant mice. J Immunol 1994;153(6): 2769–2777.
21. Ushio A, Arakaki R, Otsuka K, et al. CCL22-producing resident macrophages enhance T cell response in Sjögren's syndrome. Front Immunol 2018;9:2594.
22. Sugiura D, Okazaki IM, Maeda TK, et al. PD-1 agonism by anti-CD80 inhibits T cell activation and alleviates autoimmunity. Nat Immunol 2022;23(3):399–410.
23. Sato-Fukuba M, Arakaki R, Ushio A, et al. $CD4^+$ T-cell-dependent differentiation of $CD23^+$ follicular B cells contributes to the pulmonary pathology in a primary Sjögren's syndrome mouse model. Front Immunol 2023;14:1217492.
24. Yamamoto T, Gotoh M, Sasaki H, et al. Molecular cloning and initial characterization of a novel fibrinogen-related gene, HFREP-1. Biochem Biophys Res Commun 1993;193(2):681–687.
25. Li CY, Cao CZ, Xu WX, et al. Recombinant human hepassocin stimulates proliferation of hepatocytes in vivo and improves survival in rats with fulminant hepatic failure. Gut 2010;59(6):817–826.
26. Liu Z, Ukomadu C. Fibrinogen-like protein 1, a hepatocyte derived protein is an acute phase reactant. Biochem Biophys Res Commun 2008;365(4):729–734.
27. Wang J, Sanmamed MF, Datar I, et al. Fibrinogen-like protein 1 is a major immune inhibitory ligand of LAG-3. Cell 2019;176(1–2):334–347.e312.
28. Gao Y, Chen Y, Zhang Z, et al. Recent advances in mouse models of Sjögren's syndrome. Front Immunol 2020;11:1158.
29. Hara H, Uchida S, Yoshimura H, et al. Isolation and characterization of a novel liver-specific gene, hepassocin, upregulated during liver regeneration. Biochim Biophys Acta 2000;1492(1):31–44.
30. Cao MM, Xu WX, Li CY, et al. Hepassocin regulates cell proliferation of the human hepatic cells L02 and hepatocarcinoma cells through different mechanisms. J Cell Biochem 2011;112(10):2882–2890.
31. Yan J, Yu Y, Wang N, et al. LFIRE-1/HFREP-1, a liver-specific gene, is frequently downregulated and has growth suppressor activity in hepatocellular carcinoma. Oncogene 2004;23(10):1939–1949.
32. Gao M, Yan H, Yin RH, et al. Hepassocin is required for hepatic outgrowth during zebrafish hepatogenesis. Biochem Biophys Res Commun 2015;463(3):466–471.
33. Wu HT, Lu FH, Ou HY, et al. The role of hepassocin in the development of non-alcoholic fatty liver disease. J Hepatol 2013;59(5):1065–1072.
34. Wu HT, Ou HY, Hung HC, et al. A novel hepatokine, HFREP1, plays a crucial role in the development of insulin resistance and type 2 diabetes. Diabetologia 2016;59(8):1732–1742.
35. Wu HT, Chen SC, Fan KC, et al. Targeting fibrinogen-like protein 1 is a novel therapeutic strategy to combat obesity. FASEB J 2020;34(2): 2958–2967.
36. Demchev V, Malana G, Vangala D, et al. Targeted deletion of fibrinogen like protein 1 reveals a novel role in energy substrate utilization. PLoS One 2013;8(3):e58084.
37. Qian W, Zhao M, Wang R, et al. Fibrinogen-like protein 1 (FGL1): the next immune checkpoint target. J Hematol Oncol 2021;14(1):147.
38. Liu S, Guo Y, Lu L, et al. Fibrinogen-like protein 1 is a novel biomarker for predicting disease activity and prognosis of rheumatoid arthritis. Front Immunol 2020;11:579228.
39. Ceribelli A, De Santis M, Selmi C. Sex and autoimmune disease: four mechanisms pointing at women. Mediterr J Rheumatol 2019;30(3): 162–166.
40. Selmi C, Gershwin ME. Sex and autoimmunity: proposed mechanisms of disease onset and severity. Expert Rev Clin Immunol 2019; 15(6):607–615.
41. Bettini M, Szymczak-Workman AL, Forbes K, et al. Cutting edge: accelerated autoimmune diabetes in the absence of LAG-3. J Immunol 2011;187(7):3493–3498.
42. Okazaki T, Okazaki IM, Wang J, et al. PD-1 and LAG-3 inhibitory coreceptors act synergistically to prevent autoimmunity in mice. J Exp Med 2011;208(2):395–407.
43. Woo SR, Turnis ME, Goldberg MV, et al. Immune inhibitory molecules LAG-3 and PD-1 synergistically regulate T-cell function to promote tumoral immune escape. Cancer Res 2012;72(4):917–927.
44. Andrews LP, Yano H, Vignali DAA. Inhibitory receptors and ligands beyond PD-1, PD-L1 and CTLA-4: breakthroughs or backups. Nat Immunol 2019;20(11):1425–1434.
45. Maruhashi T, Okazaki IM, Sugiura D, et al. LAG-3 inhibits the activation of $CD4^+$ T cells that recognize stable pMHCII through its conformation-dependent recognition of pMHCII. Nat Immunol 2018; 19(12):1415–1426.
46. Boyman O, Sprent J. The role of interleukin-2 during homeostasis and activation of the immune system. Nat Rev Immunol 2012;12(3): 180–190.
47. Lucca LE, Dominguez-Villar M. Modulation of regulatory T cell function and stability by co-inhibitory receptors. Nat Rev Immunol 2020; 20(11):680–693.
48. Chapman NM, Boothby MR, Chi H. Metabolic coordination of T cell quiescence and activation. Nat Rev Immunol 2020;20(1):55–70.
49. Hosokawa H, Rothenberg EV. How transcription factors drive choice of the T cell fate. Nat Rev Immunol 2021;21(3):162–176.

Arthritis & Rheumatology
Vol. 77, No. 11, November 2025, pp 1585–1595
DOI 10.1002/art.43237

Hand Swelling and Other Non–Raynaud Phenomenon Symptoms as the Initial Presentation of Systemic Sclerosis: Prevalence and Clinical Associations in Two US Cohorts

Iqtidar Hanif,[1] Shervin Assassi,[1] Maureen D. Mayes,[1] Zsuzsanna H. McMahan,[1] Meng Zhang,[1] Julio Charles,[1] John M. VanBuren,[2] Jessica S. Alvey,[2] Kimia Ghaffari,[2] Elana J. Bernstein,[3] Flavia V. Castelino,[4] Lorinda Chung,[5] Luke Evnin,[6] Tracy M. Frech,[7] Jessica K. Gordon,[8] Faye N. Hant,[9] Laura K. Hummers,[10] Dinesh Khanna,[11] Kimberly S. Lakin,[8] Dorota Lebiedz-Odrobina,[2] Yiming Luo,[3] Ashima Makol,[12] Jerry A. Molitor,[13] Duncan F. Moore,[14] Carrie Richardson,[14] Nora Sandorfi,[15] Ami A. Shah,[10] Ankoor Shah,[16] Victoria K. Shanmugam,[17] Virginia D. Steen,[18] Elizabeth R. Volkmann,[19] Carleigh Zahn,[11] and Brian Skaug[1]

Objective. Raynaud phenomenon (RP) is often the initial clinical manifestation of systemic sclerosis (SSc), but some patients develop other manifestations first. To help elucidate the diversity of SSc presentation in its early stages, we describe the initial clinical manifestations and antinuclear antibody (ANA) profiles of patients in two early SSc cohorts.

Methods. All patient data in the Genetics vs Environment in Scleroderma Outcomes Study (GENISOS) and Collaborative National Quality and Efficacy Registry (CONQUER) cohorts were reviewed. Both studies enrolled patients within five years of the first non-RP symptom.

Results. In GENISOS and CONQUER, respectively, 194 (44.2%) of 439 and 292 (31.1%) of 938 patients had a non-RP initial symptom, most commonly puffy fingers/hands. Black patients had a non-RP symptom before RP more commonly than patients in other race and ethnicity categories. Non-RP first patients were more likely than RP first patients to have diffuse cutaneous involvement and joint contractures at enrollment and had a higher prevalence of RNA polymerase III antibody positivity.

Conclusion. In two large US cohorts, >30% of patients began to manifest SSc with puffy fingers/hands or other symptoms, without the "warning sign" of RP as their initial symptom. These patients presented with more severe skin and musculoskeletal disease on average, highlighting the importance of early recognition. The most common autoantibody associated with this presentation was RNA polymerase III. These results should be considered in efforts to recognize SSc in its earliest stages. Puffy fingers/hands, even in the absence of RP, should prompt consideration of early SSc and testing for ANA and SSc-associated autoantibodies, including RNA polymerase III.

The Collaborative National Quality and Efficacy Registry (CONQUER) consortium was supported by the Scleroderma Research Foundation. Dr Assassi's work was supported by the Department of Defense (DOD; grant W81XWH-22-1-0162) and the National Institute of Arthritis and Musculoskeletal and Skin Diseases (NIAMS), NIH (grant R01-AR-081280). Dr Bernstein's work was supported by the NIAMS, NIH (grant K23-AR-07511); the National Heart, Lung, and Blood Institute, NIH (grant RO1-HL-164758); and the DOD (grant W81XWH-22-1-0163). Dr A. A. Shah's work was supported by the NIAMS, NIH (grant K24-AR-080217). Dr Skaug's work was supported by the NIAMS, NIH (grant K08-AR-081402) and by an Investigator Award from the Rheumatology Research Foundation.

[1]Iqtidar Hanif, MD, MS, Shervin Assassi, MD, MS, Maureen D. Mayes, MD, MPH, Zsuzsanna H. McMahan, MD, MHS, Meng Zhang, MS, Julio Charles, MS, Brian Skaug, MD, PhD: University of Texas Health Science Center at Houston; [2]John M. VanBuren, PhD, Jessica S. Alvey, MS, Kimia Ghaffari, MPH, Dorota Lebiedz-Odrobina, MD, RhMSUS: University of Utah, Salt Lake City; [3]Elana J. Bernstein, MD, MSc, Yiming Luo, MD, MHS: Columbia University Irving Medical Center, New York City, New York; [4]Flavia V. Castelino, MD: Massachusetts General Hospital, Boston; [5]Lorinda Chung, MD, MS: Palo Alto VA Health Care System and Stanford University, Palo Alto, California; [6]Luke Evnin, PhD: Scleroderma Research Foundation, San Francisco, California; [7]Tracy M. Frech, MD, MS: Vanderbilt University Medical Center and Veterans Affairs Medical Center, VA Tennessee Valley Healthcare System, Nashville; [8]Jessica K. Gordon, MD, MSc, Kimberly S. Lakin, MD, MS: Hospital for Special Surgery, New York City, New York; [9]Faye N. Hant, DO: Medical University of South Carolina, Charleston; [10]Laura K. Hummers, MD, MSc, Ami A. Shah, MD, MHS: Johns Hopkins University, Baltimore, Maryland; [11]Dinesh Khanna, MBBS, MSc, Carleigh Zahn, DO: University of Michigan, Ann Arbor; [12]Ashima Makol, MD: Mayo Clinic, Rochester, Minnesota; [13]Jerry A. Molitor, MD, PhD: University of Minnesota, Minneapolis; [14]Duncan F. Moore, MD, RhMSUS, Carrie Richardson, MD, MHS: Northwestern University, Chicago, Illinois; [15]Nora Sandorfi, MD: University of Pennsylvania, Philadelphia; [16]Ankoor Shah, MD, MHS: Duke University, Durham, North Carolina; [17]Victoria K. Shanmugam, MD: The George Washington University, Washington, DC; [18]Virginia D. Steen, MD: Georgetown University Medical Center, Washington, DC; [19]Elizabeth R. Volkmann, MD, MS: University of California, Los Angeles.

INTRODUCTION

Systemic sclerosis (SSc) is a chronic disease characterized by fibrosis of the skin and internal organs, vasculopathy, and dysregulation of the immune system, including production of antinuclear antibodies (ANAs).[1,2] SSc causes morbidity through its progressive effects on multiple organs and has the highest standardized mortality ratio among the major rheumatic diseases.[3] Currently available treatments, though not curative, can have disease-modifying impacts,[4–9] and ongoing research and clinical trials raise the potential for additional treatment options in the future. Given the progressive nature of SSc and an increasing ability to intervene effectively, early diagnosis should be a major priority. However, SSc is a rare and heterogenous disease that is challenging to recognize in its early stages.

Raynaud phenomenon (RP) is one of the hallmark vascular manifestations of SSc, occurring in most patients with SSc and often preceding other clinical manifestations by years. RP has been recognized by SSc experts as a cardinal feature of early SSc[10,11] and was considered a necessary inclusion criterion in two longitudinal studies investigating the early stages of SSc. In these two studies of patients presenting with RP, the investigators showed that abnormal nailfold capillaries, puffy fingers, positivity for ANA, and positivity for SSc-associated specific autoantibodies were each prognostic for eventual progression to definite or classifiable SSc.[12,13] For patients who present to clinicians with RP, these studies provide a valuable evidence base to support identification of those who are likely to be in the early stages of SSc. However, observations from multiple cohorts indicate that non-RP manifestations, particularly puffy fingers/hands, preceded the onset of RP in some patients with SSc.[14–17] In fact, in one of the original descriptions of RNA polymerase III antibody and its strong association with diffuse cutaneous SSc, 4 (8%) of 50 patients with SSc with this antibody had not experienced RP.[18] These observations indicate that RP, if viewed as a means of screening for early SSc, lacks the sensitivity needed to identify some patients when SSc first begins to manifest.

An additional challenge in early SSc diagnosis is the lack of a published consensus on the optimal ANA testing approach to screen patients for SSc. HEp-2 immunofluorescence assay (IFA) is positive in >90% of patients with SSc, with a diversity of staining patterns, including speckled, centromere, or nucleolar depending on the patient's specific autoantibody.[19] Indeed, several specific autoantibodies have been identified in association with SSc, typically mutually exclusive and associated with distinct disease trajectories and complications.[20] Testing for SSc-associated specific autoantibodies is available to US clinicians via commercial laboratories. However, most of these autoantibodies are not included in some of the multiplex autoantibody panels that are often used as ANA screening tools in clinical practice.

To achieve the goal of recognition of SSc at its earliest stages, it is important to understand the full spectrum of presenting manifestations and to use an ANA testing approach with high sensitivity. With this context in mind, we describe the initial clinical manifestations and ANA profiles of two independent US cohorts of patients with early SSc, with a focus on those whose initial manifestation was not RP.

PATIENTS AND METHODS

Patient cohorts. All patients enrolled in the Genetics vs Environment in Scleroderma Outcomes Study (GENISOS) and the Collaborative National Quality and Efficacy Registry (CONQUER) whose baseline visits occurred before March 16, 2024, were examined. GENISOS is a prospective study conducted at University of Texas Health Science Center at Houston (UTHealth Houston), University of Texas Medical Branch Health at Galveston, and UTHealth San Antonio, enrolling from 1998 to present.[21] Inclusion criteria are as follows: (1) age >18 years, (2) satisfaction of the American College of Rheumatology (ACR) 1980 preliminary SSc classification criteria[22] (for those enrolled from 1998 to 2013) or the 2013 ACR/EULAR SSc classification criteria,[23] and (3) disease onset (defined as the first non-RP symptom) within the previous five years. CONQUER is a prospective registry comprising 18 academic SSc specialty centers across the United States in partnership with the Scleroderma Research Foundation, enrolling from 2018 to present.[24] Inclusion criteria are the same as those noted for GENISOS, except that all patients in CONQUER are classified according to the 2013 ACR/EULAR SSc classification criteria.[23] Institutional review board approval was obtained at each study site, and all study participants provided written informed consent.

All patients in both cohorts were analyzed as long as their date of RP onset or the absence of RP before enrollment was recorded. Eleven patients who enrolled in both cohorts were analyzed as part of CONQUER but not GENISOS.

Data collection. Both cohorts collect clinical data during regularly scheduled clinic visits using standardized forms. For this study, clinical data from the baseline visit (the visit during which the patient enrolled in GENISOS or CONQUER) were analyzed. Patient race and ethnicity were self-reported. The dates of onset for RP and non-RP symptoms were recorded based on the clinician's history obtained from the patient. GENISOS and CONQUER use similar criteria items regarding non-RP symptoms

Additional supplementary information cited in this article can be found online in the Supporting Information section (https://acrjournals.onlinelibrary.wiley.com/doi/10.1002/art.43237).

Author disclosures are available at https://onlinelibrary.wiley.com/doi/10.1002/art.43237.

Address correspondence via email to Brian Skaug, MD, PhD, at brian.a.skaug@uth.tmc.edu.

Submitted for publication October 9, 2024; accepted in revised form April 30, 2025.

that can define disease onset, with two notable exceptions: (1) regarding respiratory symptoms, GENISOS requires objective evidence of pulmonary disease to consider "pulmonary" as disease onset, whereas CONQUER accepts dyspnea as a non-RP symptom that can qualify as disease onset, and (2) GENISOS requires objective evidence of synovitis (determined by the clinician) to classify arthritis as disease onset, whereas CONQUER accepts arthralgia or arthritis. GENISOS uses the term "puffy hands," and CONQUER uses the term "hand swelling/puffy hands" to include patients with puffy fingers or diffuse hand swelling—referred to in this article as "puffy fingers/hands."

Patients were considered to have non-RP first if the date of onset of their first non-RP symptom (ie, the symptom used to define SSc onset) preceded the date of RP onset. Patients were considered to have RP first if the date of their first non-RP symptom was after or concurrent with the date of RP onset. Therefore, patients with the same date of onset for RP and their first non-RP symptom were analyzed in the RP first group. Patients who had not experienced RP by the time of enrollment were analyzed in the non-RP first group. Clinical metrics, including the modified Rodnan skin score (mRSS), joint contracture, and tendon friction rubs, were determined based on examination by the clinician-investigators. Patients in both cohorts completed the Scleroderma Health Assessment Questionnaire (SHAQ),[25] which includes the following question: "In the past week how much have Raynaud's attacks interfered with your daily activities?" Patients answer by marking a 0 to 10 scale.

In GENISOS, ANA positivity and pattern were determined by HEp-2 IFA (ANA Test Kit, Antibodies Incorporated) in the laboratory of the UTHealth Houston Division of Rheumatology using serum diluted 1:80. Centromere antibody determination was based on staining pattern.[19] Topoisomerase-I/Scl-70 and RNP antibodies were determined by passive immunodiffusion against calf thymus extract (Inova Diagnostics). RNA polymerase III antibody was determined by enzyme-linked immunosorbent assay (MBL, RG-M7836-D, Nagoya, Japan). Antibodies against PM-Scl, fibrillarin/U3 RNP, Th/To, and Ku were determined for a subset of patients (n = 294) in a previously published study[26]; the remaining patients in GENISOS (n = 145) had missing data for these antibodies. In CONQUER, ANA and specific autoantibody results were obtained from the medical records from testing in commercial laboratories that was done as part of clinical care. Results obtained at the baseline visit or any follow-up visit during patients' participation in CONQUER were examined. Each patient's results were reviewed and adjudicated by CONQUER's data quality committee. Of 938 CONQUER participants, 836 (89.1%) had ANA and/or autoantibody data available for analysis in this study. Missingness for the specific autoantibodies varied, but percentages for autoantibody prevalence were determined based on the total number of patients with any available ANA and/or autoantibody data. Patients who tested positive for ANA with a nucleolar pattern but did not test positive for any specific autoantibody were noted as "isolated nucleolar." Patients who tested positive for ANA with any pattern other than centromere or nucleolar and did not test positive for any specific autoantibody were noted as "ANA only (no subserology)." Patients positive for more than one specific autoantibody were grouped separately as having two subserologies.

Statistical analyses. Differences in clinical manifestations and serologic profiles between non-RP first and RP first groups were evaluated using a two-sided Student's *t*-test for continuous variables, the chi square test or Fisher's exact test for dichotomous variables depending on sample size, and the Wilcoxon rank sum test for ordinal variables. All *P* values were calculated as two-sided and considered statistically significant when less than 0.05. We used multivariable logistic regression to predict diffuse cutaneous involvement using time from first RP symptom to first non-RP symptom as the main effect while controlling for race. Analyses were conducted using GraphPad Prism (version 10.2.3) or SAS software 9.4 (SAS Institute, Inc).

RESULTS

Prevalence of non-RP versus RP initial SSc symptom and patient demographics. In the GENISOS and CONQUER cohorts, 194 (44.2%) of 439 and 292 (31.1%) of 938 patients, respectively, had a non-RP initial manifestation that preceded RP (Table 1). Non-RP first was more common among Black patients than those of other race and ethnicity categories (Table 1 and Supplemental Table 1). Collectively among the two cohorts, nearly half of Black patients (93 of 188) had a non-RP symptom preceding RP. There were no significant differences in age or sex between patients with RP first and those with non-RP first. In GENISOS, current smoking was significantly more prevalent in patients with RP first than those with non-RP first (Table 1). This observation was not replicated in CONQUER, in which the overall prevalence of smoking was lower. In each cohort, disease duration (defined as the time from the first non-RP symptom to enrollment) was similar between RP first and non-RP first groups. The mean time from RP onset to enrollment was greater by several years in patients with RP first compared to those with non-RP first.

Non-RP initial SSc manifestations. Chi square analysis showed that there was a significant difference ($P < 0.0001$) in the distribution of initial non-RP symptoms between cohorts, perhaps reflecting variation in referral patterns and/or patient populations. Nevertheless, in both cohorts, the most common initial manifestation among patients with non-RP first was puffy fingers/hands (40.4% in GENISOS, 52.9% in CONQUER) (Figure 1). Other skin and musculoskeletal symptoms (skin tightening, arthralgia or arthritis, or hypopigmentation or hyperpigmentation) collectively accounted for 32.0% and 20.4% of first

Table 1. Patient demographics and disease onset by first SSc symptom status*

	GENISOS, RP as first symptom			CONQUER, RP as first symptom		
	No (n = 194)	Yes (n = 245)	*P* value	No (n = 292)	Yes (n = 646)	*P* value
Age at baseline visit, mean (SD), y	49.4 (13.1)	48.1 (13.3)	0.32[a]	53.2 (12.8)	51.7 (14.1)	0.11[a]
Female, n (%)	157 (80.9)	205 (83.7)	0.45[b]	231 (79.7)	540 (83.7)	0.13[b]
Race and ethnicity, n (%)			0.18[c]			0.007[c]
Hispanic	47 (24.2)	76 (31.0)	–	33 (11.4)	68 (10.6)	–
Non-Hispanic White	93 (47.9)	119 (48.6)	–	186 (64.1)	457 (71.3)	–
Non-Hispanic Black or African American	45 (23.2)	40 (16.3)	–	48 (16.6)	55 (8.6)	–
Non-Hispanic Asian	7 (3.6)	9 (3.7)	–	19 (6.6)	43 (6.7)	–
Non-Hispanic other	2 (1.0)	1 (0.4)	–	4 (1.4)	18 (2.8)	–
Smoking status current, n (%)	16 (8.3)	45 (19.1)	0.001[b]	9 (3.1)	27 (4.2)	0.43[b]
Disease duration from date of first non-RP symptom to baseline visit, mean (SD), y	2.4 (1.5)	2.5 (1.5)	0.76[a]	2.5 (1.3)	2.5 (1.4)	0.62[a]
Duration from date of first RP symptom to baseline visit, mean (SD), y	1.6 (1.3)	4.8 (5.2)	<0.001[a]	1.8 (1.3)	5.9 (8.0)	<0.001[a]
RP symptom present at time of cohort enrollment, n (%)	168 (86.6)	–	–	247 (84.6)	–	–

* CONQUER, Collaborative National Quality and Efficacy Registry; GENISOS, Genetics vs Environment in Scleroderma Outcomes Study; RP, Raynaud phenomenon; SSc, systemic sclerosis.
[a] *t*-test with unpooled variance estimates.
[b] Chi square test.
[c] Fisher's exact test.

symptoms in GENISOS and CONQUER, respectively. Smaller percentages of patients had reflux, other gastrointestinal symptoms, pulmonary disease or dyspnea, digital ulcers, or carpal tunnel syndrome as their initial SSc symptom.

Disease severity in patients with non-RP versus RP initial symptom. In both cohorts, there was a significantly higher prevalence of diffuse cutaneous involvement among patients whose initial disease manifestation was non-RP compared to RP (Table 2). Consistent with this observation, the mean mRSS was significantly higher in the non-RP first group (Table 2 and Supplemental Figure 1). The relative risk of diffuse cutaneous involvement associated with an initial symptom of puffy fingers/hands compared to RP was 1.41 (95% confidence interval [CI] 1.17–1.66) in GENISOS and 1.26 (95% CI 1.11–1.41) in CONQUER (Supplemental Table 2). Among patients with non-RP initial symptoms, there was no significant difference in the risk of diffuse cutaneous involvement among those with puffy fingers/hands as the initial symptom compared to other non-RP initial symptoms (Supplemental Table 3).

There was also a significantly higher prevalence of joint contractures and tendon friction rubs among patients with non-RP first. Therefore, having a non-RP initial symptom was associated with more severe skin and musculoskeletal disease compared to having RP as the first symptom.

In CONQUER, patients with non-RP first had lower values in the peripheral vascular Medsger severity scale compared to patients with RP first (Supplemental Table 4). Abnormal nailfold capillaries were noted in 78.4% of those with non-RP first and 84.3% of those with RP first. Patients with non-RP first had significantly lower mean University of California, Los Angeles Scleroderma Clinical Trials Consortium gastrointestinal tract version 2 scores. No significant differences were observed in the prevalence of scleroderma renal crisis, forced vital capacity percentage predicted, or estimated right ventricular systolic pressure based on an echocardiogram. Despite the indicators of less severe disease in the peripheral vascular and gastrointestinal domains noted, patients with non-RP first had higher mean values (high being unfavorable) in physician global assessments of overall health, scleroderma activity, and scleroderma damage. These higher values might reflect the greater severity of skin and musculoskeletal disease noted, although other variables could also be involved.

High prevalence of RNA polymerase III antibody in patients with non-RP initial symptom. As expected, close to 95% of patients in both cohorts tested positive for ANA by HEp-2 IFA. The most common ANA staining pattern in both cohorts was speckled. Nucleolar, centromere, and homogenous staining patterns were also observed (data not shown). The most common SSc-associated specific autoantibody in patients with non-RP first was RNA polymerase III (Figure 2). In both cohorts, the prevalence of RNA polymerase III antibody was significantly higher in patients with non-RP first compared to patients with RP first (25.9% vs 14.7% [$P < 0.01$] in GENISOS, 34.7% vs 19.9% [$P < 0.01$] in CONQUER). Anticentromere antibody was significantly less prevalent in patients with non-RP first compared to those with RP first (7.8% vs 16.8% [$P < 0.01$] in GENISOS, 12.6% vs 23.2% [$P < 0.01$] in CONQUER).

As shown in Supplemental Figures 2 and 3, puffy fingers/hands or skin tightening was more commonly the initial SSc symptom among RNA polymerase III antibody–positive patients

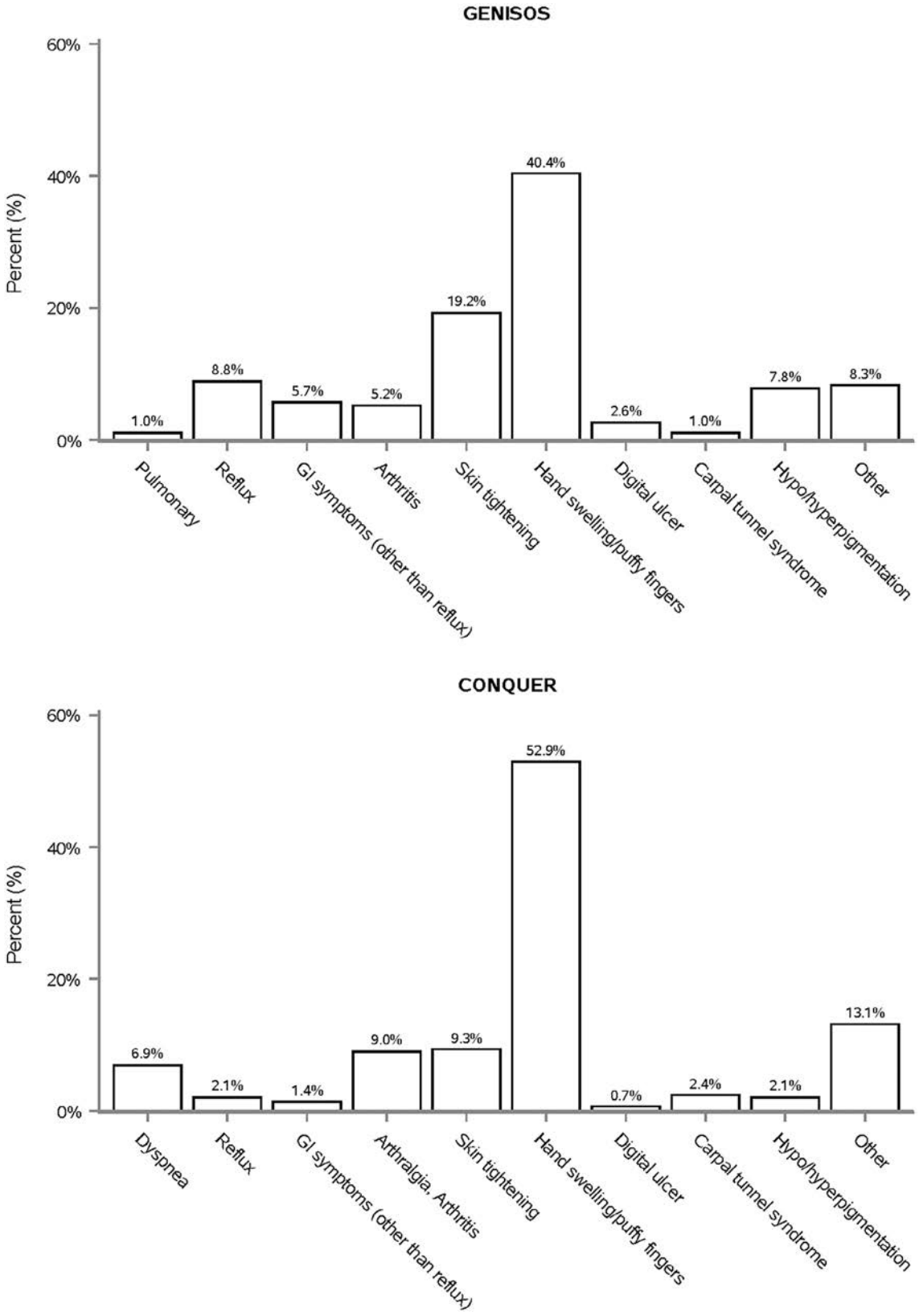

Figure 1. Initial systemic sclerosis symptom among patients whose initial symptom was not Raynaud phenomenon in GENISOS (top) and CONQUER (bottom). CONQUER, Collaborative National Quality and Efficacy Registry; GENISOS, Genetics vs Environment in Scleroderma Outcomes Study; GI, gastrointestinal.

Table 2. Patient baseline characteristics by first SSc symptom status*

	GENISOS, RP as first symptom			CONQUER, RP as first symptom		
	No (n = 194)	Yes (n = 245)	*P* value	No (n = 292)	Yes (n = 646)	*P* value
Diffuse cutaneous, n (%)	140 (72.2)	130 (53.1)	<0.001[a]	204 (69.9)	368 (57.0)	<0.001[a]
mRSS, mean (SD)	19.3 (12.1)	14.0 (10.9)	<0.001[b]	15.1 (11.6)	11.1 (10.2)	<0.001[b]
Joint contracture, n (%)	100 (51.5)	99 (40.4)	0.020[a]	146 (51.2)	252 (40.2)	0.002[a]
Small joint contracture (finger, hand, wrist joint), n (%)	98 (50.5)	98 (40.0)	0.028[a]	139 (48.8)	243 (38.9)	0.005[a]
Tendon friction rubs, n (%)	44 (22.7)	39 (15.9)	0.072[a]	58 (20.7)	53 (8.6)	<0.001[a]

* CONQUER, Collaborative National Quality and Efficacy Registry; GENISOS, Genetics vs Environment in Scleroderma Outcomes Study; mRSS, modified Rodnan skin score; RP, Raynaud phenomenon; SSc, systemic sclerosis.
[a] Chi square test.
[b] *t*-test with unpooled variance estimates.

compared to negative patients and, congruently, in patients with diffuse cutaneous SSc compared to those with limited cutaneous SSc. The same was true for carpal tunnel syndrome (CTS), although CTS was rarely the initial SSc symptom.

Diffuse cutaneous involvement was associated with shorter time interval from first RP to first non-RP symptom. The time interval from first RP to first non-RP symptom was greater on average in patients with limited cutaneous involvement compared to those with diffuse cutaneous involvement (Supplemental Figure 4). In a multivariable logistic regression model, after adjustment for Black race, longer time interval from first RP to first non-RP symptom was associated with significantly lower odds of diffuse cutaneous involvement in both cohorts, albeit with small effect sizes (Supplemental Table 5). These results are consistent with those described by van den Hombergh et al.[14] Although it is not the objective of this study to develop a prognostic model, these results suggest that the RP to non-RP time interval can be considered as a potential prognostic factor in future longitudinal research. We emphasize though that this interval is not applicable to patients who have not experienced RP.

Patients without RP at the time of enrollment. In GENISOS and CONQUER, 26 (5.9%) of 439 and 45 (4.8%) of 938 patients, respectively, had not experienced RP by the time of enrollment (Table 3). This subgroup is noteworthy because these patients could not have been eligible for inclusion in the two aforementioned longitudinal studies on early SSc,[12,13] which required RP as an inclusion criterion. Importantly, the majority of patients reported here had diffuse cutaneous involvement, and a large percentage had joint contractures. Despite the absence of RP, 34 (75.6%) of 45 patients in CONQUER were noted to have abnormal nailfold capillaries at enrollment.

A diversity of ANA results was seen among this subgroup of patients. In GENISOS, the most common ANA profile was "ANA only" (ANA positive with a pattern other than centromere or nucleolar and without positivity for a specific autoantibody), found in six (23.1%) patients. Four (15.4%) patients tested positive for Scl-70, four (15.4%) patients tested positive for RNA polymerase III antibody, and four (15.4%) patients tested positive for ANA in a nucleolar pattern without positivity for a specific autoantibody. In CONQUER, the most common ANA and/or autoantibody result was RNA polymerase III antibody, found in 11 patients (33.3% of those with available ANA and/or autoantibody data).

DISCUSSION

Examining two independent US cohorts, we found that non-RP manifestations preceded RP in >30% of patients with SSc, with puffy fingers/hands being the most common non-RP initial symptom. Our results provide independent validation of prior observations that some patients with SSc, mostly with diffuse cutaneous involvement, manifested puffy fingers/hands before the onset of RP[16] and that a subset of patients developed diffuse cutaneous SSc in the absence of RP.[18] Importantly, non-RP symptoms preceding RP onset was associated with more severe skin disease and a higher prevalence of joint contractures, both of which are major causes of morbidity in SSc. The most common autoantibody associated with non-RP first presentation was RNA polymerase III.

Our observations regarding initial SSc symptoms reinforce the important concept of heterogeneity in the clinical presentation of SSc. Heterogeneity from the outset is perhaps to be expected given the multifaceted disease manifestations and the broad spectrum of disease severity that are well described in patients with classifiable SSc.[1] In addition to RP, which is well characterized as a potential harbinger of future SSc,[12,13] our results highlight additional symptoms that should prompt consideration of early SSc. This diagnostic approach may be of particular importance for identification of early SSc among Black patients, who experienced non-RP symptoms before RP onset more often than patients in other race and ethnicity categories. Although there was variability in initial symptoms between the two cohorts, the most common non-RP initial symptom in both cohorts was puffy fingers/hands. Puffy fingers has been recognized as an alarm feature to raise suspicion for SSc[11] and was an independent risk

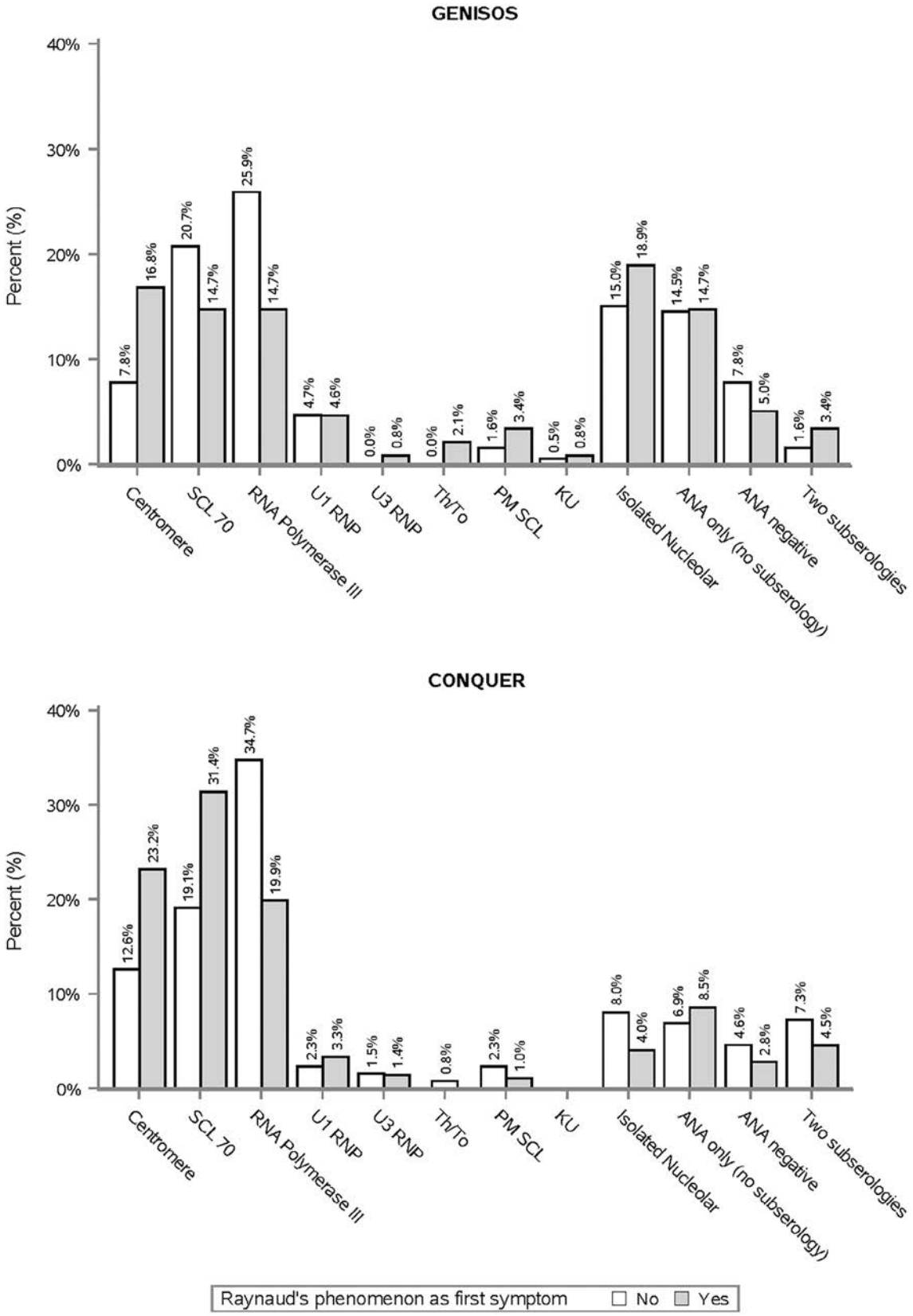

Figure 2. ANA results in GENISOS (top) and CONQUER (bottom) by first systemic sclerosis symptom of Raynaud phenomenon (gray) or a non–Raynaud phenomenon symptom (white). ANA, antinuclear antibody; CONQUER, Collaborative National Quality and Efficacy Registry; GENISOS, Genetics vs Environment in Scleroderma Outcomes Study.

Table 3. Patient demographics and clinical characteristics for patients without RP at time of baseline visit*

	GENISOS (n = 26)	CONQUER (n =45)
Age at baseline visit, mean (SD), y	52.5 (12.39)	57.4 (12.3)
Female, n (%)	23 (88.5)	31 (72.1)
Race and ethnicity, n (%)		
Hispanic	7 (26.9)	5 (11.6)
Non-Hispanic White	13 (50.0)	26 (60.5)
Non-Hispanic Black or African American	5 (19.2)	5 (11.6)
Non-Hispanic Asian	1 (3.8)	4 (9.3)
Non-Hispanic other	0 (0.0)	3 (7.0)
Smoking status current, n (%)	1 (3.8)	1 (2.3)
Disease duration from date of first non-RP symptom to baseline visit, mean (SD), y	2.3 (1.7)	2.0 (1.4)
Diffuse cutaneous, n (%)	22 (84.6)	30 (66.7)
mRSS, mean (SD)	19.6 (12.2)	15.5 (13.5)
Joint contracture, n (%)	11 (42.3)	22 (51.2)
Small joint contracture (finger, hand, wrist joint), n (%)	11 (42.3)	21 (48.8)
Abnormal nailfold capillaries, n (%)	–	34 (75.6)
ANA/autoantibody classification, n (%)		
Centromere	3 (11.5)	7 (21.2)
Scl-70	4 (15.4)	7 (21.2)
RNA polymerase III	4 (15.4)	11 (33.3)
U1 RNP	0 (0.0)	1 (3.0)
U3 RNP	0 (0.0)	0 (0.0)
Th/To	0 (0.0)	0 (0.0)
PM-Scl	0 (0.0)	0 (0.0)
KU	0 (0.0)	0 (0)
Isolated nucleolar	4 (15.4)	1 (3.0)
ANA only (no subserology)	6 (23.1)	2 (6.1)
ANA negative	3 (11.5)	4 (12.1)
Two subserologies	2 (7.7)	0 (0.0)

* Unless otherwise specified, all variables are as recorded at baseline. ANA, antinuclear antibody; CONQUER, Collaborative National Quality and Efficacy Registry; GENISOS, Genetics vs Environment in Scleroderma Outcomes Study; mRSS, modified Rodnan skin score; RP, Raynaud phenomenon.

factor for progression from RP to classifiable SSc in the Very Early Diagnosis of Systemic Sclerosis (VEDOSS) study.[13] Puffy fingers/hands as an initial presenting symptom (ie, in the absence of RP) has not been studied prospectively to our knowledge, but the findings from the PRESS cohort[16] and this study suggest that it ought to prompt further evaluation for SSc even when RP is not present. Puffy fingers/hands can also be a valuable sign to help distinguish SSc from scleroderma mimics, such as eosinophilic fasciitis, which typically spares the fingers.[27]

Considering that the absence of RP might make it more challenging to identify patients in the early stages of SSc, we report two additional examination findings that might have implications for clinical evaluation of these patients. First, we found that tendon friction rubs were more prevalent among patients with non-RP first in this study. Tendon friction rubs are strongly associated with diffuse cutaneous SSc and are a harbinger of future worsening of skin fibrosis.[16,28] Examination for tendon friction rubs could therefore be a valuable tool for identification of patients with early SSc who are likely to progress to diffuse skin involvement. We also found that >75% of those patients who had developed classifiable SSc in the absence of RP had abnormal nailfold capillaries. Abnormal nailfold capillaries are another cardinal vascular feature by which patients with RP can be stratified for their risk of progression to SSc.[12,13] Our observations suggest that the pathophysiology underlying the microvascular damage evident on nailfold capillary examination can occur independently of the peripheral vasoconstriction underlying RP. Nailfold capillary examination may therefore be a valuable tool even in the absence of RP if early SSc is being considered in the differential diagnosis. We acknowledge that the prevalence of these examination findings in our patients before study enrollment cannot be determined and could have been different from what we observed at the time of enrollment. Moreover, we acknowledge that our data on abnormal nailfold capillaries lack the granularity to compare specific patterns between those with and without RP.

The autoantibody results from GENISOS and CONQUER reinforce that ANA testing by HEp-2 IFA can serve as a sensitive screening tool for SSc. Moreover, the majority of patients in both cohorts tested positive for an SSc-associated specific autoantibody. The most common specific autoantibody associated with non-RP first presentation was RNA polymerase III, found in >25% of patients with non-RP initial manifestations in both cohorts. RNA polymerase III antibody is strongly associated with diffuse skin involvement[18,29] and with rapid progression from disease onset to peak skin disease severity.[30,31] Our results imply that the unique disease trajectory associated with RNA

polymerase III antibody extends back to the initial disease onset, in that many of these patients develop a non-RP initial symptom rather than the RP first presentation more typical of SSc overall. This combination of clinical features presents a diagnostic challenge: the patients most likely to develop rapidly progressive skin fibrosis may present without the classic "warning sign" of RP. Recognition of non-RP symptoms as potential harbingers of SSc is particularly important for this patient population because the time window from disease onset to severe skin fibrosis is narrow. With this context in mind, it bears emphasis that RNA polymerase III is not included in several ANA multiplex platforms widely used in US clinical practice as "reflex" testing in response to positive HEp-2 IFA results or performed as standalone "ANA" screens bypassing HEp-2 IFA altogether. Anecdotally, we have observed patients presenting with diffuse cutaneous SSc who were under the impression that they had tested negative for ANA when in fact they had been tested only for antibodies against the small subset of antigens present in commonly used multiplex panels that do not include RNA polymerase III. This issue was previously highlighted in a study showing that only 50% of patients with SSc screened by "multiplex ANA" panels tested positive, compared to >90% of those screened for ANA by HEp-2 IFA.[32] Inability to detect RNA polymerase III and several other SSc-associated autoantibodies is a major limitation of using the common multiplex panels as "ANA" screens when SSc is in the differential diagnosis.

This study has several strengths. Two independent cohorts with enrollment spanning from the late 1990s to present had similar findings. Supporting the generalizability of the results, both cohorts are large and ethnically diverse. Moreover, CONQUER is nationally representative, including 18 SSc specialty centers across the United States. All patients in both cohorts were evaluated at SSc specialty centers by physicians with expertise in SSc.

This study also has limitations. Data on SSc manifestations preceding study enrollment relied on patient report, introducing risks of recall bias and imprecision. There was not a standardized approach across study sites for ascertaining the presence of RP. This issue is counterbalanced by the fact that each clinician-investigator in both cohorts has clinical expertise in SSc and works in an SSc referral center, where obtaining a detailed RP history (presence or absence and the date of onset) is routine standard of care and a requirement for study enrollment. Additionally, patients who were ascertained not to have RP in this study had median values of 0.2 (GENISOS) and 0.0 (CONQUER) on a 0 to 10 scale on the standardized SHAQ question regarding the extent to which RP was affecting their daily activities, in contrast to median values of 1.7 (GENISOS) and 2.0 (CONQUER) among those ascertained to have experienced RP (data not shown). These values from a standardized patient-reported outcome measure support the accuracy of our ascertainment of RP status. The retrospective nature of the study precludes determination of the prevalence of and risk factors for progression from puffy fingers/hands or other symptoms to SSc. Patients in both cohorts had missing data for some of the autoantibodies, particularly those with low prevalence (PM-Scl, Th/To, U3 RNP, Ku). Because the autoantibody results show the percentages of patients who tested positive across the entire cohort (not restricted to those tested for each specific antibody), the presented values may be underestimates. Because the autoantibody determination methods varied across cohorts and, in the case of CONQUER, varied according to the methodologies and reference ranges used by commercial laboratories, relationships between autoantibody titers and initial SSc symptoms could not be determined. The results from both cohorts could be influenced by referral bias, in that many of the patients with SSc seen at academic medical centers are referred by other rheumatologists or independently seek a second opinion. It is possible that these two categories of patients are not fully representative of all patients with early SSc. It is also likely that results from patients with SSc in the US are not fully generalizable to other locations because of a variety of genetic, environmental, and social factors. For example, non-RP symptoms preceding RP onset might be a more common presentation of early SSc in the United States than in Europe because of a proportionately larger Black population and a higher prevalence of RNA polymerase III antibody.

In summary, our results highlight several points important for clinicians who are in a position to evaluate patients in the early stages of SSc, when differential diagnoses and diagnostic testing are being considered: (1) RP is the most common initial SSc symptom, but it is not uncommon for other symptoms to precede the onset of RP by several months. A subset of patients goes on to develop classifiable SSc, including some with diffuse skin involvement, without experiencing RP. (2) There is a diversity of non-RP clinical manifestations that can emerge as the patient's first symptom during the early stages of SSc. The most common is puffy fingers/hands. (3) Patients with non-RP initial manifestations are more likely than RP first patients to progress to diffuse cutaneous disease and joint contracture. Early recognition of these patients before this progression occurs is challenging because of the absence of the "warning sign" of RP and the relatively short time window between symptom onset and progression. But early diagnosis and treatment initiation in this subgroup of patients could be particularly impactful, especially because joint contractures tend to be progressive and irreversible.[33] (4) When early SSc is considered in the differential diagnosis, ANA screening should be performed by HEp-2 IFA owing to its high sensitivity. Positive results should be followed by testing for SSc-associated specific autoantibodies, including RNA polymerase III.

This diagnostic framework could cultivate early recognition, treatment initiation, and specialty referral of patients at risk for rapid progression of skin fibrosis and joint contractures. It could also facilitate research on early SSc pathogenesis and interventions to prevent progression to irreversible damage. Research on early SSc that requires RP for inclusion is susceptible to selection bias, in that some patients likely to develop severe skin

fibrosis (ie, those with non-RP initial manifestations) would not be eligible for research in the earliest stages of their disease. Future research aimed at understanding and/or treating patients in the early stages of SSc should be inclusive of those presenting without RP if other risk features (eg, puffy fingers/hands, abnormal nailfold capillaries, skin tightening, tendon friction rubs, positivity for ANA and SSc-associated specific autoantibodies) are present.

ACKNOWLEDGMENTS

We thank Dr Sam Theodore (UTHealth Houston) for coordination of GENISOS. We thank all of the study coordinators at each of the CONQUER study sites.

AUTHOR CONTRIBUTIONS

All authors contributed to at least one of the following manuscript preparation roles: conceptualization AND/OR methodology, software, investigation, formal analysis, data curation, visualization, and validation AND drafting or reviewing/editing the final draft. As corresponding author, Dr Skaug confirms that all authors have provided the final approval of the version to be published and takes responsibility for the affirmations regarding article submission (eg, not under consideration by another journal), the integrity of the data presented, and the statements regarding compliance with institutional review board/Declaration of Helsinki requirements.

REFERENCES

1. Denton CP, Khanna D. Systemic sclerosis. Lancet 2017;390(10103):1685–1699.
2. Volkmann ER, Andréasson K, Smith V. Systemic sclerosis. Lancet 2023;401(10373):304–318.
3. Nikpour M, Baron M. Mortality in systemic sclerosis: lessons learned from population-based and observational cohort studies. Curr Opin Rheumatol 2014;26(2):131–137.
4. Tashkin DP, Elashoff R, Clements PJ, et al; Scleroderma Lung Study Research Group. Cyclophosphamide versus placebo in scleroderma lung disease. N Engl J Med 2006;354(25):2655–2666.
5. Tashkin DP, Roth MD, Clements PJ, et al. Mycophenolate mofetil versus oral cyclophosphamide in scleroderma-related interstitial lung disease (SLS II): a randomised controlled, double-blind, parallel group trial. Lancet Respir Med 2016;4(9):708–719.
6. Sullivan KM, Goldmuntz EA, Keyes-Elstein L, et al; SCOT Study Investigators. Myeloablative autologous stem-cell transplantation for severe scleroderma. N Engl J Med 2018;378(1):35–47.
7. Distler O, Highland KB, Gahlemann M, et al; SENSCIS Trial Investigators. Nintedanib for systemic sclerosis-associated interstitial lung disease. N Engl J Med 2019;380(26):2518–2528.
8. Khanna D, Lin CJF, Furst DE, et al; focuSSced investigators. Tocilizumab in systemic sclerosis: a randomised, double-blind, placebo-controlled, phase 3 trial. Lancet Respir Med 2020;8(10):963–974.
9. Ebata S, Yoshizaki A, Oba K, et al. Safety and efficacy of rituximab in systemic sclerosis (DESIRES): a double-blind, investigator-initiated, randomised, placebo-controlled trial. Lancet Rheumatol 2021;3(7):e489–e497.
10. LeRoy EC, Medsger TA Jr. Criteria for the classification of early systemic sclerosis. J Rheumatol 2001;28(7):1573–1576.
11. Avouac J, Fransen J, Walker UA, et al; EUSTAR Group. Preliminary criteria for the Very Early Diagnosis of Systemic Sclerosis: results of a Delphi Consensus Study from EULAR Scleroderma Trials and Research Group. Ann Rheum Dis 2011;70(3):476–481.
12. Koenig M, Joyal F, Fritzler MJ, et al. Autoantibodies and microvascular damage are independent predictive factors for the progression of Raynaud's phenomenon to systemic sclerosis: a twenty-year prospective study of 586 patients, with validation of proposed criteria for early systemic sclerosis. Arthritis Rheum 2008;58(12):3902–3912.
13. Bellando-Randone S, Del Galdo F, Lepri G, et al; Very Early Diagnosis of Systemic Sclerosis collaborators. Progression of patients with Raynaud's phenomenon to systemic sclerosis: a five-year analysis of the European Scleroderma Trial and Research group multicentre, longitudinal registry study for Very Early Diagnosis of Systemic Sclerosis (VEDOSS). Lancet Rheumatol 2021;3(12):e834–e843.
14. van den Hombergh WM, Carreira PE, Knaapen-Hans HK, et al. An easy prediction rule for diffuse cutaneous systemic sclerosis using only the timing and type of first symptoms and auto-antibodies: derivation and validation. Rheumatology (Oxford) 2016;55(11):2023–2032.
15. Rubio-Rivas M, Corbella X, Pestaña-Fernández M, et al; RESCLE investigators, Autoimmune Diseases Study Group (GEAS). First clinical symptom as a prognostic factor in systemic sclerosis: results of a retrospective nationwide cohort study. Clin Rheumatol 2018;37(4):999–1009.
16. Jaafar S, Lescoat A, Huang S, et al. Clinical characteristics, visceral involvement, and mortality in at-risk or early diffuse systemic sclerosis: a longitudinal analysis of an observational prospective multicenter US cohort. Arthritis Res Ther 2021;23(1):170.
17. Domsic RT, Gao S, Laffoon M, et al. Defining the optimal disease duration of early diffuse systemic sclerosis for clinical trial design. Rheumatology (Oxford) 2021;60(10):4662–4670.
18. Okano Y, Steen VD, Medsger TA Jr. Autoantibody reactive with RNA polymerase III in systemic sclerosis. Ann Intern Med 1993;119(10):1005–1013.
19. Tan EM, Rodnan GP, Garcia I, et al. Diversity of antinuclear antibodies in progressive systemic sclerosis. Anti-centromere antibody and its relationship to CREST syndrome. Arthritis Rheum 1980;23(6):617–625.
20. Shah S, Denton CP. Scleroderma autoantibodies in guiding monitoring and treatment decisions. Curr Opin Rheumatol 2022;34(6):302–310.
21. Reveille JD, Fischbach M, McNearney T, et al; GENISOS Study Group. Systemic sclerosis in 3 US ethnic groups: a comparison of clinical, sociodemographic, serologic, and immunogenetic determinants. Semin Arthritis Rheum 2001;30(5):332–346.
22. Masi AT; Subcommittee for Scleroderma Criteria of the American Rheumatism Association Diagnostic and Therapeutic Criteria Committee. Preliminary criteria for the classification of systemic sclerosis (scleroderma). Arthritis Rheum 1980;23(5):581–590.
23. van den Hoogen F, Khanna D, Fransen J, et al. 2013 classification criteria for systemic sclerosis: an American College of Rheumatology/-European League Against Rheumatism collaborative initiative. Arthritis Rheum 2013;65(11):2737–2747.
24. Shanmugam VK, Frech TM, Steen VD, et al. Collaborative National Quality and Efficacy Registry (CONQUER) for Scleroderma: outcomes from a multicenter US-based systemic sclerosis registry. Clin Rheumatol 2020;39(1):93–102.
25. Steen VD, Medsger TA Jr. The value of the Health Assessment Questionnaire and special patient-generated scales to demonstrate change in systemic sclerosis patients over time. Arthritis Rheum 1997;40(11):1984–1991.
26. Wodkowski M, Hudson M, Proudman S, et al; Canadian Scleroderma Research Group (CSRG); Australian Scleroderma Interest Group (ASIG); Genetics versus Environment in Scleroderma Outcome Study (GENISOS). Clinical correlates of monospecific anti-PM75 and anti-PM100 antibodies in a tri-nation cohort of 1574 systemic sclerosis subjects. Autoimmunity 2015;48(8):542–551.

27. Nashel J, Steen V. Scleroderma mimics. Curr Rheumatol Rep 2012; 14(1):39–46.
28. Steen VD, Medsger TA Jr. The palpable tendon friction rub: an important physical examination finding in patients with systemic sclerosis. Arthritis Rheum 1997;40(6):1146–1151.
29. Kuwana M, Kaburaki J, Mimori T, et al. Autoantibody reactive with three classes of RNA polymerases in sera from patients with systemic sclerosis. J Clin Invest 1993;91(4):1399–1404.
30. Herrick AL, Peytrignet S, Lunt M, et al. Patterns and predictors of skin score change in early diffuse systemic sclerosis from the European Scleroderma Observational Study. Ann Rheum Dis 2018;77(4): 563–570.
31. Domsic RT, Medsger TA Jr, Gao S, et al. A data-driven approach finds RNA polymerase III antibody and tendon friction rubs as enrichment tools for early diffuse scleroderma trials. Rheumatology (Oxford) 2023;62(4):1543–1551.
32. Shanmugam VK, Swistowski DR, Saddic N, et al. Comparison of indirect immunofluorescence and multiplex antinuclear antibody screening in systemic sclerosis. Clin Rheumatol 2011;30(10): 1363–1368.
33. Buni M, Joseph J, Pedroza C, et al. Predictors of hand contracture in early systemic sclerosis and the effect on function: a prospective study of the GENISOS cohort. J Rheumatol 2019; 46(12):1597–1604.

American College of Rheumatology
Empowering Rheumatology Professionals

Arthritis & Rheumatology
Vol. 77, No. 11, November 2025, pp 1596–1604
DOI 10.1002/art.43254

BRIEF REPORT

Precision Medicine in Pediatric Autoimmunity: Leniolisib Treatment of Childhood-Onset Lupus Nephritis Due to Activated Phosphoinositide 3-Kinase δ Syndrome

Jonathan P. Lim,[1] Mansooreh Ahmadian,[2] Hongyu Du,[2] Christian Rickert,[2] Tusharkanti Ghosh,[2] Fuyong Xing,[2] Angela Minic,[2] Sara A. Johnson,[1] Jason P. Weinman,[1] Nicholas Willard,[1] Clara Lin,[1] Jennifer C. Cooper,[1] Melisha Hanna,[1] Vijaya Knight,[1] Debashis Ghosh,[2] Kimberly R. Jordan,[2] and Elena W. Y. Hsieh[1]

Objective. The objective of this study was to investigate the mechanistic underpinnings and treatment response of lupus nephritis (LN) in activated phosphoinositide 3-kinase δ syndrome type 1 (APDS1) using pathway-specific therapy and advanced spatial proteomics.

Methods. We conducted mechanistic investigation of refractory class V LN in an 18-year-old female patient with genetically confirmed APDS1 (PIK3CD c.3061G>A, p.E1021K mutation). Response to leniolisib, a selective phosphoinositide 3-kinase δ (PI3Kδ) inhibitor, was evaluated through clinical parameters and flow cytometry of peripheral blood lymphocytes. Kidney tissue immune architecture was characterized using multiplexed ion beam imaging by time-of-flight (MIBI-TOF) spectrometry, comparing the APDS1-LN tissue signature with 12 patients with childhood-onset LN and 5 healthy controls.

Results. Following three years of unsuccessful treatment with conventional immunosuppressives, leniolisib treatment normalized hyperactive PI3Kδ signaling, resulting in significant improvements in proteinuria, complement levels, and peripheral edema. Multiplexed Ion Beam Imaging (MIBI)-Time-of-Flight (TOF) revealed a distinct tissue-specific immunopathology with significantly increased proportions of $CD8^+$ T cells (21.6% in APDS1 vs 12.0% in typical LN; $P = 0.0410$) and M1 macrophages (42.0% in APDS1 vs 9.0% in typical LN; $P = 0.1445$) clustering around glomeruli with immune complex deposition. This immune signature aligns with the constitutively active PI3Kδ pathway's effect on lymphocyte exhaustion and inflammatory phenotype.

Conclusion. This investigation advances rheumatology by demonstrating that APDS1-associated LN displays a specific tissue immune signature and responds to targeted inhibition of the causative molecular pathway. Our findings provide mechanistic insights into genetic drivers of autoimmunity and support pathway-specific therapeutic approaches for refractory autoimmune manifestations in primary immunodeficiencies.

INTRODUCTION

Inborn errors of immunity (IEI), also known as primary immunodeficiency disorders, encompass more than 550 clinically, genetically, and molecularly diverse disorders caused by deleterious single-gene variants that affect the development and/or function of the immune system.[1] These conditions can manifest at any age with varying degrees of severity (ie, penetrance and

Drs Ahmadian, Du, Rickert, T. Ghosh, Xing, Johnson, D. Ghosh, and Jordan were supported by the Boettcher Foundation Webb-Waring Biomedical research grant, the Lupus Research Alliance, the Lupus Innovation Award, and the Global Team Science Award. Drs T. Ghosh and D. Ghosh were supported by the Grohne-Stepp Endowed Chair for Cancer Research and the Division of Mathematical Sciences (grant 1914937).

[1]Jonathan P. Lim, DO, Sara A. Johnson, PhD, Jason P. Weinman, MD, Nicholas Willard, DO, Clara Lin, MD, Jennifer C. Cooper, MD, PharmD, Melisha Hanna, MD, Vijaya Knight, MD, PhD, Elena W. Y. Hsieh MD: University of Colorado Anschutz Medical Campus and Children's Hospital of Colorado, Aurora; [2]Mansooreh Ahmadian, PhD, Hongyu Du, MS, Christian Rickert, PhD, Tusharkanti Ghosh, PhD, Fuyong Xing, PhD, Angela Minic, MS, Debashis Ghosh, PhD, Kimberly R. Jordan, PhD: University of Colorado Anschutz Medical Campus, Aurora.

Drs Lim and Ahmadian are co-first authors and contributed equally to this work.

Additional supplementary information cited in this article can be found online in the Supporting Information section (https://acrjournals.onlinelibrary.wiley.com/doi/10.1002/art.43254).

Author disclosures and graphical abstract are available at https://onlinelibrary.wiley.com/doi/10.1002/art.43254.

Address correspondence via email to Elena W. Y. Hsieh, MD, at elena.hsieh@cuanschutz.edu.

Submitted for publication March 3, 2025; accepted in revised form May 8, 2025.

expressivity), though they often present in childhood with increased susceptibility to infections, autoimmunity, autoinflammation, atopy, and malignancy. Patients with IEI are often seen by rheumatologists because they exhibit inflammatory and autoimmune symptoms that mimic more common rheumatologic conditions, such as lupus, arthritis, or recurrent fevers. Early recognition of IEI is critical because targeted therapies may prevent irreversible organ damage and improve quality of life and mortality outcomes.

Among these disorders, activated phosphoinositide 3-kinase δ syndrome (APDS) is a recently recognized condition caused by mutations affecting the phosphoinositide 3-kinase (PI3K) pathway,[2–4] which plays a crucial role in immune cell development and function. APDS presents with a constellation of clinical features, including recurrent respiratory infections, persistent enlargement of lymph nodes, liver and spleen enlargement, chronic viral infections (particularly Epstein-Barr virus), and an elevated risk of developing lymphoma or other lymphoid cancers. Together these clinical features have significant overlap with complications of classic rheumatic diseases, like systemic lupus erythematosus (SLE), which can be associated with lymphoid hyperplasia, splenomegaly, and lymphomas.[5] Several recent publications suggest rheumatic disease as a manifestation of IEI, with sequencing of IEI patient cohorts revealing that monogenic disorders are more commonly diagnosed among patients presenting with immune dysregulation, including organ-specific autoimmunity such as lupus nephritis (LN).[6,7] Identification of the genetic basis and the resultant pathophysiologic disease mechanism of IEI has led to targeted therapeutic approaches, especially in the realm of immune dysregulation pathway-specific therapy. For example, diagnosis of CTLA-4 insufficiency or LRBA deficiency has led to treatment with CTLA-4Ig (abatacept).[6,8] STAT1 or STAT3 gain-of-function-associated immune dysregulation has been successfully treated with JAK inhibitors,[9] whereas selective PI3Kδ inhibitors represent an efficacious therapeutic option in patients with APDS.[10] Therefore, rheumatologists must recognize APDS as a differential in these patients to guide precise management. Historically, management options for patients with APDS were limited to treating symptoms and complications as they arose using antibiotics, Igs, or immunosuppressants without addressing the underlying cause of disease. A significant advancement in targeted therapy has emerged with leniolisib, the first US Food and Drug Administration (FDA)–approved medication specifically designed to inhibit the overactive PI3Kδ pathway responsible for the immune dysregulation in patients with APDS.

PI3Ks are lipid kinases that play important roles in cell growth, function, and survival. There are multiple classes of PI3K (IA, IB, II, and III). Immune signaling relies on class IA PI3K, which is activated by cell surface receptors such as T cell and B cell receptors, toll-like receptors, and CD19.[3] Class IA PI3Ks comprise a p110 catalytic subunit (p110α, p110β, and p110δ) linked to a regulatory subunit (p85, p55, or p50). The p110α and p110β catalytic subunits are ubiquitously expressed, whereas p110δ is primarily expressed in leukocytes. Phosphorylation of phosphatidylinositol 4,5-bisphosphate by class IA PI3K generates phosphatidylinositol 3,4,5-trisphosphate, a second messenger that activates downstream molecules such as protein kinase B and mammalian target of rapamycin.[2–4] APDS occurs in two forms, distinguished by the affected subunit; APDS1 results from heterozygous gain-of-function mutations in the *PIK3CD* gene, encoding the p110δ catalytic subunit, whereas APDS2 stems from heterozygous loss-of-function mutations in the *PIK3R1* gene, encoding the regulatory p85α subunit.[2–4]

Lymphocyte development and function require precise regulation of the PI3Kδ pathway.[3,11–15] Constitutively active PI3Kδ results in persistent lymphocyte activation and eventual exhaustion, leading to abnormal immune cell development and function. Hence, patients with APDS may experience a vast range of symptoms, encompassing microbial susceptibility (eg, sinopulmonary infections, herpesviruses) and immune dysregulation, which can include systemic and organ-specific autoimmunity, autoinflammation and/or hyperinflammation, severe atopy malignancy, and lymphoproliferation.[11,13–17] Lymphadenopathy is primarily driven by B cell proliferation and infiltration of T follicular helper cells expressing programmed cell death protein.[11,14,15,17]

Approximately 40% of patients with APDS develop clinically significant autoimmune complications, spanning hematologic, rheumatologic, gastrointestinal, endocrine, and dermatological disorders. Among these, autoimmune hematologic conditions, specifically autoimmune hemolytic anemia and immune thrombocytopenic purpura, are the most common, occurring in 76.2% of APDS cases.[11,14,15,17] Furthermore, comorbidity of APDS with multiple autoimmune diseases occurs in as many as 6.5% of patients. In contrast, rheumatologic disorders have been documented in only three published reports of five pediatric patients (all <10 years old) who met criteria for SLE.[18–20] Three of these patients, siblings described in a single publication,[19] developed classes III–IV LN. Their treatment adhered to standard protocols (eg, high-dose steroids and cyclophosphamide induction therapy followed by maintenance immunosuppression) and was not changed based on their underlying genetic diagnosis.

Treatment of immune dysregulation in APDS has mainly relied on empirical approaches, with care directed toward individual clinical manifestations in the affected organ(s). Prophylactic antimicrobials and Ig replacement therapy (IgRT) have been used successfully to reduce the number of severe infections and significantly improve quality of life. Hematopoietic stem cell transplantation has been pursued in some cases, but outcomes[21] were variable. Importantly, neither of these treatment strategies target disease pathogenesis–hyperactive PI3Kδ signaling.[11,14,17] Leniolisib, an orally bioavailable small molecule inhibitor selectively engineered to target PI3Kδ,[22] has been recently approved by the FDA for APDS treatment. In a 12-week dose-finding clinical trial of

6 patients[23] and a subsequent 12-week fixed-dose (70 mg) randomized, triple-blinded, placebo-controlled phase 3 trial of 31 patients,[23] leniolisib was shown to be well tolerated, reduce PI3Kδ pathway hyperactivity, partially reconstitute lymphocyte subsets, and decrease lymphoproliferation[23] (as measured by reduced spleen size and lymphadenopathy). As this pathway-specific therapy becomes more widely used for APDS, assessing its therapeutic effectiveness for individual patients will be crucial for optimizing treatment outcomes. Monitoring should include evaluation of specific T and B cell subpopulations and activation markers not only in peripheral blood but also in affected tissue(s), given the organ-specific nature of APDS-driven immune dysregulation.

Here, we report successful treatment of a teenage girl diagnosed with APDS1 complicated by SLE with biopsy-proven LN using pathway-specific and personalized therapy. Notably, her renal disease was recalcitrant to standard-of-care treatments but responded to leniolisib, illustrating the importance of understanding underlying disease mechanisms to guide treatment of autoimmunity. This report further reveals leniolisib's therapeutic effect on APDS-related immune dysregulation, expanding outcome metrics beyond splenomegaly and lymphadenopathy, to demonstrate "normalization" of peripheral blood T and B cell immune phenotypes and tissue in situ immune infiltrates and improved renal function.

MATERIALS AND METHODS

Human research. Archived formalin-fixed paraffin-embedded (FFPE) kidney blocks remaining from clinical diagnostic use from 12 patients with childhood-onset class IV/V LN (cLN; <18 years old) according to the International Society of Nephrology/Renal Pathology Society (ISN/RPS) criteria[24] were identified by pathologists and selected for tissue imaging (including "control LN/Ctrl LN", which is used as a technical control for signal normalization purposes). FFPE blocks from patients who underwent a kidney biopsy and were ruled out for immune-mediated renal disease per histopathology were included as healthy controls (HCs). The patient described clinically in this report was prospectively enrolled and provided consent at Children's Hospital Colorado rheumatology clinics in 2022 and was observed longitudinally with routine clinical care and peripheral blood collection until study completion under an institutional review board–approved protocol for which Dr Hsieh is the principal investigator.

Clinical immune assessment. Clinical immune assessment of peripheral blood mononuclear cells was performed by the Immunopathology and Hematopathology Laboratory at Children's Hospital Colorado perClinical Laboratory Improvement Amendments requirements for flow cytometry–based analyses. Testing included identification of TBNK subsets. Specific antibody details can be found in Supplementary Table S1.

Multiplexed ion beam imaging by time-of-flight spectrometry analysis. The Human Immune Monitoring Shared Resource at the University of Colorado School of Medicine performed multiplexed ion beam imaging by time-of-flight (MIBI-TOF) imaging. FFPE kidney tissue was sectioned onto gold slides (Ionpath, Inc) and stained with a panel of metal isotope prelabeled antibodies (Standard Biotools) and custom-labeled (Standard Biotools conjugation kits per manufacturer's protocol) BSA-free commercially available monoclonal antibodies (Supplementary Table S2). Tissue-mounted slides were prepared and stained per the manufacturer's protocols, essentially as described by Ptacek et al.[25] Details regarding data acquisition are provided in the Supplementary Methods.

MIBI-TOF data analysis. Denoising and artifact removal was done using a preprocessing pipeline.[26] Segmentation was performed using a pretrained deep learning–based whole-cell segmentation method,[27] resulting in the identification of 798,235 cells. Cell boundaries were defined, and detailed cell information, including morphology, two-dimensional coordinates, and marker expression in nuclear, cytoplasmic, or membrane compartments, was extracted. Each matrix row represented a single cell, and columns denoted the average marker expression normalized by cell size. This matrix was subsequently used as input for unsupervised clustering algorithms to identify cell types. We applied K-means clustering with k = 200, first using all markers to distinguish $CD45^+$ leukocytes from $CD45^-$ cells, then using immune-specific markers to cluster immune cells and epithelial markers for the remaining cells.

RESULTS

Leniolisib treatment targets pathway-specific mechanisms in APDS-associated LN. A now 18-year-old female patient presented with a variety of symptoms, including failure to thrive and recurrent sinopulmonary infections, prompting genetic testing, which identified a pathogenic *PIK3CD* mutation consistent with APDS1. Shortly after, she developed edema and proteinuria, leading to an additional diagnosis of LN. At the time of this second diagnosis, management of her APDS was primarily symptomatic, including IgRT to reduce severe infections and various immunosuppressive agents to address her renal disease. It was not until the approval of leniolisib that she was able to transition to a more targeted therapy directed at the underlying immunopathophysiology of her disease, stemming from her specific genetic mutation. Leniolisib, a PI3Kδ inhibitor, induced complete renal response in this patient with APDS complicated by SLE with LN. Following three years of conventional immunosuppressive therapy with limited efficacy, the patient experienced significant

improvement in peripheral edema, proteinuria, hypocomplementemia, and renal function (urine protein/creatinine ratio) after initiating leniolisib, allowing discontinuation of prednisone and rituximab (Figure 1A).

A complete timeline of disease episodes and treatments can be found in Figure 1B. In brief, the patient initially presented with failure to thrive, recurrent sinopulmonary infections, and steroid-dependent respiratory disease from age two years. By age 11 years, she had developed mixed restrictive/obstructive pulmonary disease and diffuse bronchiectasis with moderate bronchial wall thickening (Figure 1C). A serologic evaluation revealed evolving autoimmunity with positive antinuclear antibodies, anti-Smith, SS-A, and RNP antibodies, along with hypocomplementemia, suggesting a lupus-like phenotype. Immunologic assessment at age 12 years showed normal lymphocyte counts and Ig levels but compromised functional responses, including poor proliferation to both mitogens and antigens. Flow cytometry revealed an autoimmune phenotype with skewing toward exhausted CD21lo cells, class-switched memory B cells, plasmablasts, effector memory T cells, and senescent/exhausted CD8 T cell populations (Figure 1D, earlier dates). Markers used to identify specific cell subtypes are shown in Supplementary Table S1 (right and left).

Genetic testing revealed APDS1 with a pathogenic heterozygous *PIK3CD* mutation (c.3061G>A, p.E1021K). Despite supportive management with antimicrobial prophylaxis, IgRT, and pulmonary interventions, her condition progressed. At age 13 years, the patient developed nephrotic syndrome with class V LN confirmed by kidney biopsy (Figure 1E). Her initial kidney biopsy demonstrated extensive intramembranous and subepithelial immune complex deposits (Figure 1E, top); glomerulosclerosis in 20% of glomeruli and mesangial hypercellularity (Figure 1E, middle); "full house" immune complex deposition of IgG, IgM, IgA, C1q, and C3 (IgG is shown, middle); and tubuloreticular inclusions consistent with ISN/RPS class V LN (Figure 1E, bottom). Despite treatment with mycophenolate mofetil (MMF), glucocorticoids, hydroxychloroquine, and tacrolimus, her renal function declined. She underwent a second kidney biopsy approximately two years after the initial LN diagnosis, which still demonstrated significant disease with class V LN, an activity index score of 4, and a chronicity score of 5 (data not shown; Figure 1E). Six cycles of rituximab over 24 months nearly eliminated B cells (with rapid repopulation requiring continuous cycles), reduced CD8 T cell subpopulations, and modestly improved renal function. Yet she remained clinically unstable with ongoing proteinuria, hypocomplementemia, and an elevated erythrocyte sedimentation rate (Figure 1A, earlier dates). Furthermore, this level of significant immunosuppression resulted in recurrent infections, including shingles, which required inpatient treatment with acyclovir and varicella-zoster virus Ig. The patient started treatment with leniolisib after its FDA approval for APDS in 2023 (17 years old). In addition to experiencing improvement in her peripheral edema, proteinuria, and hypocomplementemia, her B and T cell subsets stabilized, and she remained free from complications from an infection and pulmonary disease standpoint (Figure 1D, later dates). She was able to stop further infusions of rituximab without worsening of her renal disease (Figure 1A) and discontinue systemic steroids eight months after initiating leniolisib. She continues to take hydroxychloroquine and MMF for SLE, with plans to potentially taper immunosuppression if her renal response remains stable.

Distinct renal immune signature in APDS-associated LN revealed by spatial proteomics. Childhood-onset SLE is characterized by increased incidence of kidney involvement. As with adult SLE, the failure to achieve clinical remission in LN is associated with long-term kidney damage. This is particularly concerning in children who have the potential to accrue kidney damage over decades.[28] Despite recent treatment advances, less than half of all patients in large clinical trials achieve complete renal response.[29–31] This underscores the need to better understand disease heterogeneity at the tissue level, preserving molecular, cellular, and histopathologic features with single-cell and spatial resolution to enable precision management and to develop additional therapies targeting underlying mechanisms.

To evaluate the tissue-specific immunologic disease process, we applied MIBI to study the patient's second biopsy. MIBI is a state-of-the-art imaging system that allows for analysis of ≥40 protein targets on a single FFPE tissue slice[9,10,15] rather than dissociated tissue. MIBI features up to a 250-nm resolution while maintaining information on tissue morphology and microenvironment.[9] Integration of MIBI data with clinical pathology and immunohistochemistry data provides a renal/immune landscape that enables precise disease classification. Within this framework, we analyzed biopsy samples from our patient with APDS (LN_APDS), 12 patients with class III/IV LN (initial diagnostic renal biopsy before immunosuppression), and five HCs. Notably, we analyzed one patient with LN multiple times across batches (Ctrl LN) to serve as a technical control for signal stability and a biologic control for cell population consistency. Multiple fields of view (FOV) were analyzed from each patient biopsy sample (Supplementary Table S2).

Assessment of the cellular distribution of $CD45^+$ leukocytes versus $CD45^-$ nonleukocyte renal intrinsic cells shows that HC tissue has significantly fewer leukocytic infiltrates (1.4% HC vs 13.2% LN; $P = 0.0001$; Figure 2A and B). Within each compartment, expression of specific cell markers was used to define leukocytic versus nonleukocytic populations (Supplementary Table S3 and Supplementary Methods). Because of the limited panel of markers (40 parameters), some leukocytes (0.3% HC vs 1.3% LN; $P = 0.0074$) and nonleukocytes (25.7% HC vs 5.7% LN; $P = 0.0146$) remained unidentified (Figure 2A and B). The distribution of nonleukocyte renal intrinsic cells was similar between HCs and patients with cLN, including the patient with APDS

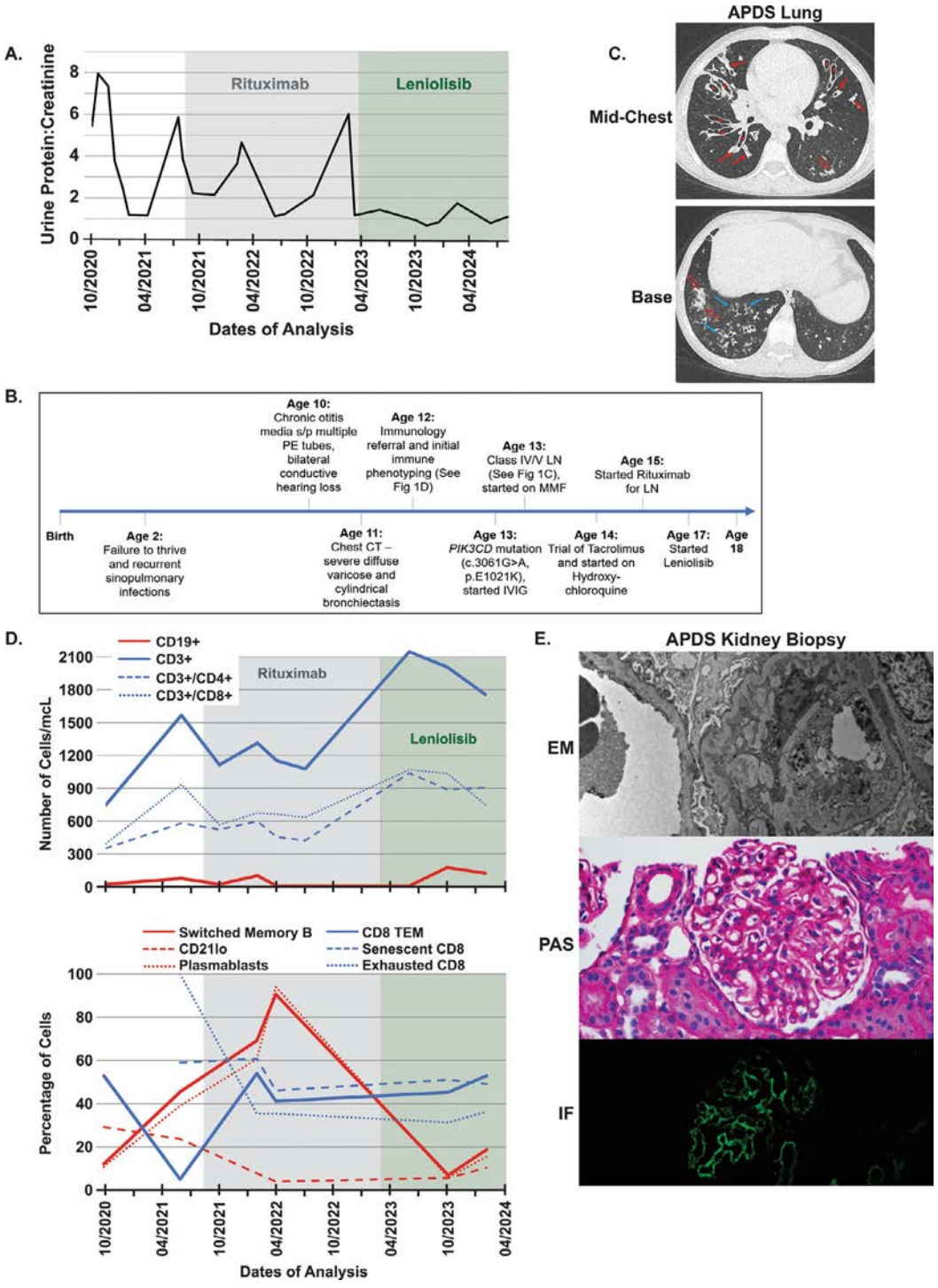

Figure 1. Clinical history and APDS disease pathology in individual tissues: kidney, lungs, and peripheral blood. (A) Renal function testing via urine protein/creatinine ratio before therapy (white) and during rituximab (gray) and leniolisib (green) therapy. (B) Timeline highlighting key events leading to diagnosis and treatment decisions. (C) Axial CT images of the chest at age 11 years. (Top) Mid chest with cylindrical and varicose bronchiectasis (red asterisks) with associated bronchial wall thickening and patchy areas of peripheral mucus plugging (solid red arrows). (Bottom) Lung bases with tree in bud opacites (blue arrows), peripheral mucus plugging, and patchy area of consolidation (open red arrows). (D) Flow cytometric analyses of immune cells in peripheral blood over time before therapy (white) and during rituximab (gray) and leniolisib (green) therapy. (Top) Circulating leukocyte counts. (Bottom) Percentages of immune cell subsets specifically associated with chronic cell activation and autoimmunity. (E) Kidney biopsy images by EM (top), PAS staining (middle), and IF (bottom). APDS, activated phosphoinositide 3-kinase δ syndrome; CT, computed tomography; EM, electron microscopy; IF, immunofluorescence; IVIG, intravenous immunoglobulin; LN, lupus nephritis; MMF, mycophenolate mofetil; PAS, Periodic Acid-Schiff; PE, pressure equalizing; TEM, effector memory T.

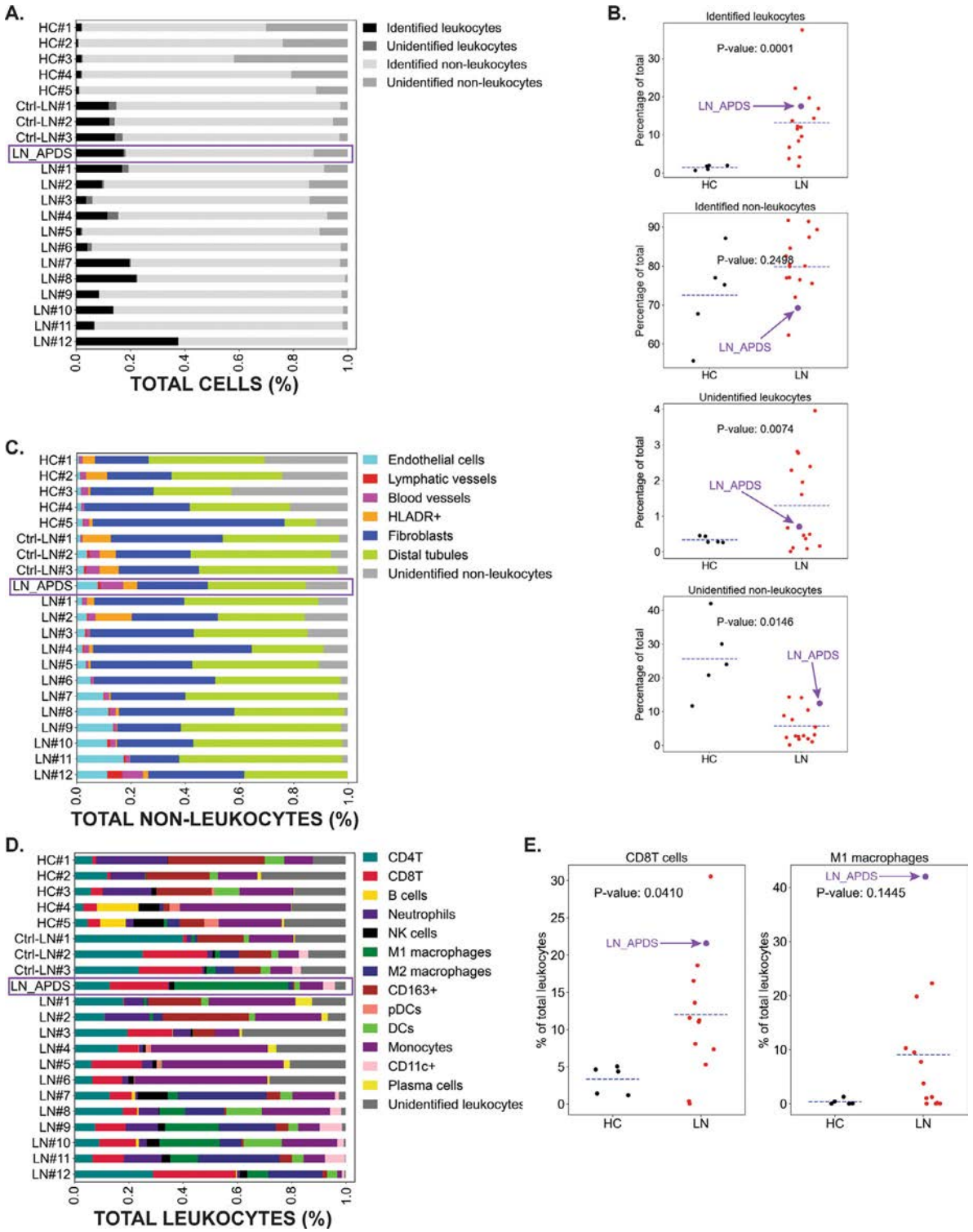

Figure 2. The patient with APDS shows distinct renal-specific cell signature with increased CD8 T cells and M1 macrophages. Forty-parameter MIBI antibody panel applied to FFPE renal biopsies for all patients to classify and quantify cells by type. LN_APDS patient is marked in purple in all panels. (A and B). Percentage of total analyzed cells for entire biopsy sample classified as leukocytes ($CD45^+$) or nonleukocytes ($CD45^-$) for each study participant. Scatter plots compare HCs (black) to patients with LN (red), with means marked by a dotted line, and *P* values are displayed. (C) Bar graph depicting nonleukocytes broken down into specific cell categories. (D) Bar graph depicting leukocytes broken down into specific cell categories. (E) Scatter plots of CD8 T cells (left) and M1 macrophages (right), expressed as the percentage of total leukocytes, comparing HCs (black) to patients with LN (red). Means are marked by dotted lines, and *P* values are displayed. APDS, activated phosphoinositide 3-kinase δ syndrome; DCs, dendritic cells; FFPE, formalin-fixed paraffin-embedded; HC, healthy control; LN, lupus nephritis; MIBI, multiplexed ion beam imaging; NK, natural killer; pDCs, plasmacytoid dendritic cells. Color figure can be viewed in the online issue, which is available at http://onlinelibrary.wiley.com/doi/10.1002/art.43254/abstract.

(Figure 2C). However, within the leukocyte compartment, the patients with cLN, including the patient with APDS, compared to HCs, showed significantly increased proportions of CD8 T cells (3.3% HC vs 12.0% LN; $P = 0.0410$; 21.6% LN_APDS, purple dot, not included in statistical analysis) and M1 macrophages (0.3% HC vs 9.0% LN; $P = 0.1445$; 42.0% LN_APDS, purple dot not included in statistical analysis) (Figure 2D and E). In specific FOV, obvious clusters of CD8 T cells and M1 macrophages (Figure 3A), as well as significant immune complex deposition (Figure 3B), can be observed surrounding glomeruli in the LN_APDS patient. These features are nearly absent in HCs (Figure 3C and D) and are only present in a few patients with LN (Figure 2D, LN 9 and 10; imaging picture not shown). Renal tissue infiltrating CD8 T cells[32,33] and macrophages[34] have been previously associated with disease progression and poorer clinical outcomes in LN. However, examination of this patient's renal biopsy sample reveals that in APDS-driven LN, genetically mediated aberrant T cell lymphoproliferation happens in both the periphery

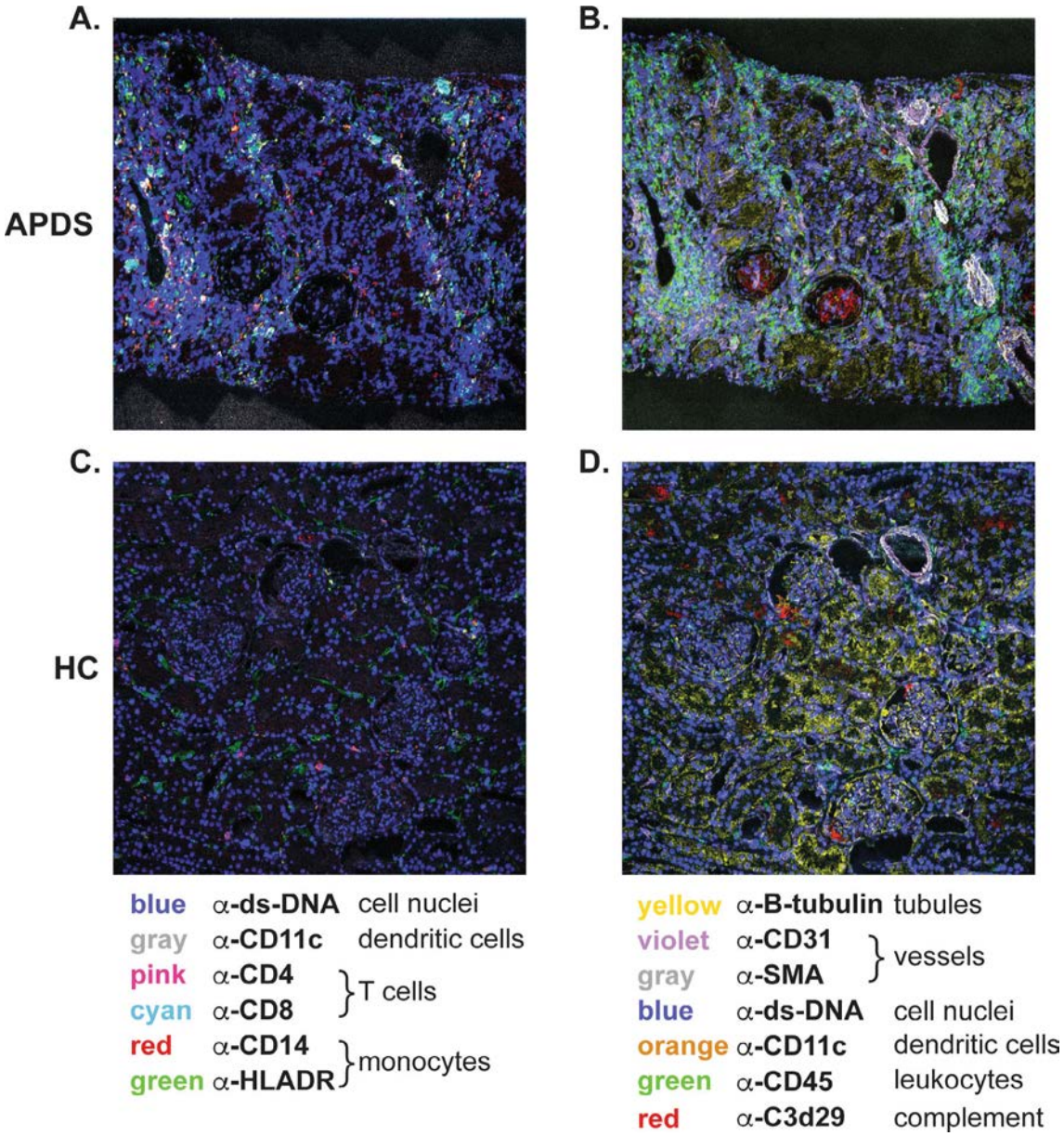

Figure 3. The patient with APDS shows distinct renal-specific spatial organization. MIBI applied to FFPE renal biopsies for all patients to map spatial organization of immune cells relative to kidney architecture. Marker colors are shown at the bottom of each column. (A and B) The biopsy sample from the patient with APDS shows increased immune cellular infiltrates and complement deposition (red) within the glomerular structure and tubulointerstitium. (C and D) Representative biopsy samples of HCs. α, anti; ds-DNA, double-stranded DNA; SMA, smooth muscle actin; APDS, activated phosphoinositide 3-kinase δ syndrome; FFPE, formalin-fixed paraffin-embedded; HC, healthy control; MIBI, multiplexed ion beam imaging. Color figure can be viewed in the online issue, which is available at http://onlinelibrary.wiley.com/doi/10.1002/art.43254/abstract.

and the tissues, as evidenced by the significantly higher CD8 T and M1 frequency in the immunologic infiltrate, despite immunosuppression with cyclophosphamide induction, MMF, prednisone, and rituximab. Notably, the patients with LN were all treatment naive and analyzed at the height of their inflammatory process at the diagnostic biopsy. The increased CD8 T cell effector phenotype and consequent enhanced T cell activity likely drove this immune infiltration and renal disease progression in the patient with APDS. M1 macrophages, which are known to correlate with chronicity scores, were markedly elevated in both diagnostic and follow-up biopsy samples from the patient with APDS.

DISCUSSION

Our patient with APDS1 showed a remarkable response to leniolisib treatment, demonstrating improved kidney function with substantial reduction in both proteinuria and hypocomplementemia, enabling significant reduction of immunosuppression, including complete discontinuation of glucocorticoids and rituximab. Although this report focuses on the impact of leniolisib in relation to the patient's renal disease, this targeted therapy also stabilized her pulmonary health. During treatment, she experienced significantly fewer pulmonary flares, resulting in fewer emergency department/urgent care visits and fewer school absences. Although our findings specifically describe a single patient with APDS-associated LN, they support the growing body of evidence that IEI can underlie more common "classic" rheumatologic disorders and that genetic identification can guide targeted therapeutic decisions and improve disease outcomes. Although both "classic LN" and APDS-driven LN share certain features, such as CD8 T cell and M1 macrophage infiltration into renal tissue, our patient with APDS demonstrated a substantial quantitative difference in M1 macrophage infiltration—approximately four times the relative frequency seen in typical patients with LN and 40 times that of HCs. These observations suggest that heightened PI3K pathway activity might contribute to peripheral and local CD8 T cell proliferation, which in turn affects M1 macrophage recruitment. As shown in Figure 2D and E, other cases of LN also demonstrated increased CD8 T cell and M1 macrophage frequency, suggesting that their proliferation and tissue infiltration may constitute an immunologic driver of renal damage. As such, although most LN cases will not be genetically driven by a hyperactive PI3K pathway, the ability of leniolisib to ameliorate the lymphoproliferation and disease progression in this patient provides a rationale for its potential use in other patients with LN who may also have this elevated CD8 T cell and M1 macrophage phenotype. Future studies will be needed to determine whether leniolisib or other PI3K inhibitors might benefit specific subsets of patients with refractory LN (or other manifestations of SLE) in the absence of APDS. Importantly, this study provides proof of principle that investigation of rare IEI can illuminate the immune mechanisms active in more common rheumatologic disorders, potentially allowing the identification of additional therapeutic targets.

The clinical course of APDS can vary dramatically among patients, reflecting the diverse range of symptoms and complications associated with the disorder. Patients may experience recurrent infections, lymphoproliferation, autoimmunity, or malignancies. The recent approval of leniolisib, a selective PI3Kδ inhibitor, marks a significant advancement in the treatment of APDS, offering patients targeted therapy that addresses the underlying molecular mechanisms driving disease pathogenesis. As such, early identification and intervention are expected to substantially improve the prognosis for many patients with APDS. Clinical trials met both coprimary end points, demonstrating statistically significant reductions in lymph node size and increased numbers of naive B cells as a proportion of total B cells. These improvements correlated with a reduction in clinical pathology. The most common side effects observed in the leniolisib trial were mild gastrointestinal symptoms, transient elevations in liver enzyme levels, and headaches, none of which were observed in our patient.

This brief report highlights the importance of recognizing APDS as a distinct primary immunodeficiency disorder and underscores the vital role of genetic testing in achieving accurate diagnoses. It also offers hope that application of tissue-specific molecular and cellular feature analysis will expand the use of biopsy samples to guide pathway-specific therapy. Early identification will enable more effective management, allow better disease control, and reduce the need for other immunosuppressive therapies, a critical consideration for those with compromised immune systems. This concept is illustrated by the patient's clinical improvement in her immune dysregulation (pulmonary and renal function) and infectious complications (no hospitalizations for infection management). The use of targeted therapies such as leniolisib offers significant promise for improving both the quality of life and long-term prognosis in patients with APDS. Our study is limited by its focus on a single patient with APDS, which constrains the generalizability of our findings. To our knowledge, this is the first reported case of a patient with LN secondary to APDS successfully treated with leniolisib. As genetic testing becomes more common practice, it is essential that clinicians understand the full potential of targeted therapies. Continued research into precision treatments could potentially revolutionize care for individuals with this rare condition.

ACKNOWLEDGMENTS

We would like to thank the patients and their families, the clinical coordinators, the pediatric rheumatology physicians and nurses, the pathologists and histology technicians, and regulatory personnel who helped with the enrollment of study participants and attainment of their kidney biopsy samples. We thank the University of Colorado Human Immune Monitoring Shared Resource for their assistance with the generation of the MIBI data.

AUTHOR CONTRIBUTIONS

All authors contributed to at least one of the following manuscript preparation roles: conceptualization AND/OR methodology, software, investigation, formal analysis, data curation, visualization, and validation

AND drafting or reviewing/editing the final draft. As corresponding author, Dr Hsieh confirms that all authors have provided the final approval of the version to be published and takes responsibility for the affirmations regarding article submission (eg, not under consideration by another journal), the integrity of the data presented, and the statements regarding compliance with institutional review board/Declaration of Helsinki requirements.

REFERENCES

1. Bousfiha AA, Jeddane L, Moundir A, et al. The 2024 update of IUIS phenotypic classification of human inborn errors of immunity. Journal of Human Immunity 2025;1(1):e20250002.
2. Fruman DA, Chiu H, Hopkins BD, et al. The PI3K pathway in human disease. Cell 2017;170(4):605–635.
3. Okkenhaug K. Signaling by the phosphoinositide 3-kinase family in immune cells. Annu Rev Immunol 2013;31:675–704.
4. Okkenhaug K, Vanhaesebroeck B. PI3K in lymphocyte development, differentiation and activation. Nat Rev Immunol 2003;3(4):317–330.
5. Rodolfi S, Della-Torre E, Bongiovanni L, et al. Lymphadenopathy in the rheumatology practice: a pragmatic approach. Rheumatology (Oxford) 2024;63(6):1484–1493.
6. Elsink K, Huibers MMH, Hollink IHIM, et al; Genetics First for Primary Immunodeficiency Disorders Consortium. Implementation of early next-generation sequencing for inborn errors of immunity: a prospective observational cohort study of diagnostic yield and clinical implications in Dutch genome diagnostic centers. Front Immunol 2021;12:780134.
7. Sogkas G, Dubrowinskaja N, Schutz K, et al. Diagnostic yield and therapeutic consequences of targeted next-generation sequencing in sporadic primary immunodeficiency. Int Arch Allergy Immunol 2022;183(3):337–349.
8. Egg D, Rump IC, Mitsuiki N, et al. Therapeutic options for CTLA-4 insufficiency. J Allergy Clin Immunol 2022;149(2):736–746.
9. Forbes LR, Vogel TP, Cooper MA, et al. Jakinibs for the treatment of immune dysregulation in patients with gain-of-function signal transducer and activator of transcription 1 (STAT1) or STAT3 mutations. J Allergy Clin Immunol 2018;142(5):1665–1669.
10. Sogkas G, Adriawan IR, Dubrowinskaja N, et al. Homeostatic and pathogenic roles of PI3Kδ in the human immune system. Adv Immunol 2020;146:109–137.
11. Coulter TI, Chandra A, Bacon CM, et al. Clinical spectrum and features of activated phosphoinositide 3-kinase δ syndrome: a large patient cohort study. J Allergy Clin Immunol 2017;139(2):597–606.e4.
12. Crank MC, Grossman JK, Moir S, et al. Mutations in PIK3CD can cause hyper IgM syndrome (HIGM) associated with increased cancer susceptibility. J Clin Immunol 2014;34(3):272–276.
13. Lucas CL, Kuehn HS, Zhao F, et al. Dominant-activating germline mutations in the gene encoding the PI(3)K catalytic subunit p110δ result in T cell senescence and human immunodeficiency. Nat Immunol 2014;15(1):88–97.
14. Maccari ME, Abolhassani H, Aghamohammadi A, et al. Disease evolution and response to rapamycin in activated phosphoinositide 3-kinase δ syndrome: the European Society for Immunodeficiencies-Activated Phosphoinositide 3-Kinase δ Syndrome Registry. Front Immunol 2018;9:543.
15. Oh J, Garabedian E, Fuleihan R, et al. Clinical manifestations and outcomes of activated phosphoinositide 3-kinase δ syndrome from the USIDNET Cohort. J Allergy Clin Immunol Pract 2021;9(11):4095–4102.
16. Lucas CL, Zhang Y, Venida A, et al. Heterozygous splice mutation in PIK3R1 causes human immunodeficiency with lymphoproliferation due to dominant activation of PI3K. J Exp Med 2014;211(13):2537–2547.
17. Elkaim E, Neven B, Bruneau J, et al. Clinical and immunologic phenotype associated with activated phosphoinositide 3-kinase δ syndrome 2: a cohort study. J Allergy Clin Immunol 2016;138(1):210–218.e9.
18. Li GM, Liu HM, Guan WZ, et al. A mutation in PIK3CD gene causing pediatric systemic lupus erythematosus: a case report. Medicine (Baltimore) 2019;98(18):e15329.
19. Wang Y, Yang Q, Chen X, et al. Phenotypic characterization of patients with activated PI3Kδ syndrome 1 presenting with features of systemic lupus erythematosus. Genes Dis 2020;8(6):907–917.
20. Yin J, Ma J, Xia J, et al. Activated PI3Kδ syndrome 1 mimicking systemic lupus erythematosus and secondary Sjögren's syndrome-like phenotype without recurrent infections: a case report. Front Pediatr 2022;10:1077324.
21. Notarangelo LD. Hematopoietic stem cell transplantation for activated phosphoinositide 3-kinase δ syndrome: who, when, and how? J Allergy Clin Immunol 2019;143(1):91–93.
22. Hoegenauer K, Soldermann N, Zécri F, et al. Discovery of CDZ173 (leniolisib), representing a structurally novel class of PI3K delta-selective inhibitors. ACS Med Chem Lett 2017;8(9):975–980.
23. Rao VK, Webster S, Dalm VASH, et al. Effective "activated PI3Kδ syndrome"-targeted therapy with the PI3Kδ inhibitor leniolisib. Blood 2017;130(21):2307–2316.
24. Hachiya A, Karasawa M, Imaizumi T, et al. The ISN/RPS 2016 classification predicts renal prognosis in patients with first-onset class III/IV lupus nephritis. Sci Rep 2021;11(1):1525.
25. Ptacek J, Locke D, Finck R, et al. Multiplexed ion beam imaging (MIBI) for characterization of the tumor microenvironment across tumor types. Lab Invest 2020;100(8):1111–1123.
26. Ahmadian M, Rickert C, Minic A, et al. A platform-independent framework for phenotyping of multiplex tissue imaging data. PLoS Comput Biol 2023;19(9):e1011432.
27. Greenwald NF, Miller G, Moen E, et al. Whole-cell segmentation of tissue images with human-level performance using large-scale data annotation and deep learning. Nat Biotechnol 2022;40(4):555–565.
28. Kaneko M, Jackson SW. Recent advances in immunotherapies for lupus nephritis. Pediatr Nephrol 2023;38(4):1001–1012.
29. Furie R, Rovin BH, Houssiau F, et al. Two-year, randomized, controlled trial of belimumab in lupus nephritis. N Engl J Med 2020;383(12):1117–1128.
30. Rovin BH, Solomons N, Pendergraft WF III, et al. A randomized, controlled double-blind study comparing the efficacy and safety of dose-ranging voclosporin with placebo in achieving remission in patients with active lupus nephritis. Kidney Int 2019;95(1):219–231.
31. Rovin BH, Teng YKO, Ginzler EM, et al. Efficacy and safety of voclosporin versus placebo for lupus nephritis (AURORA 1): a double-blind, randomised, multicentre, placebo-controlled, phase 3 trial. Lancet 2021;397(10289):2070–2080.
32. Zhang T, Wang M, Zhang J, et al. Association between tubulointerstitial CD8+T cells and renal prognosis in lupus nephritis. Int Immunopharmacol 2021;99:107877.
33. Winchester R, Wiesendanger M, Zhang HZ, et al. Immunologic characteristics of intrarenal T cells: trafficking of expanded CD8+ T cell β-chain clonotypes in progressive lupus nephritis. Arthritis Rheum 2012;64(5):1589–1600.
34. Kwant LE, Vegting Y, Tsang-A-Sjoe MWP, et al. Macrophages in lupus nephritis: exploring a potential new therapeutic avenue. Autoimmun Rev 2022;21(12):103211.

Arthritis & Rheumatology
Vol. 77, No. 11, November 2025, pp 1605

DOI 10.1002/art.43228

Clinical Images: A classic case of linear IgA bullous dermatosis in a child

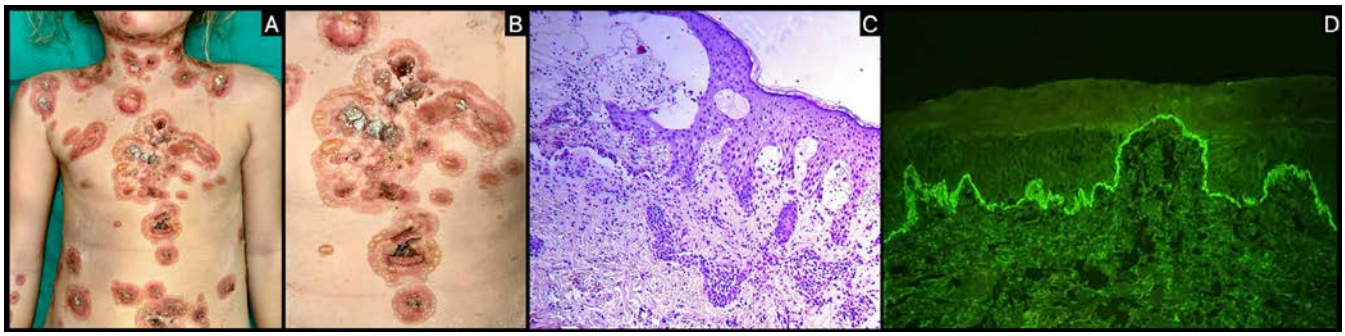

The patient, an eight-year-old girl, presented with a one-week history of intensely pruritic vesiculobullous lesions. Clinical examination revealed tense vesicles, bullae, and urticarial plaques, many arranged in annular patterns with peripheral clustering, reminiscent of a "string of pearls" (A and B). The lesions involved the face, trunk, abdomen, back, and proximal limbs. The patient was otherwise well, afebrile, and without mucosal involvement or systemic symptoms. Histopathology demonstrated a subepidermal blister with a superficial perivascular neutrophilic infiltrate (C). Direct immunofluorescence of perilesional skin revealed linear IgA deposition along the basement membrane zone (D), confirming the diagnosis of linear IgA bullous dermatosis (LABD). LABD is the most common autoimmune blistering disorder in children. It is characterized by IgA deposition at the dermoepidermal junction, targeting antigens such as LAD-1 and LABD97. Although both pediatric and adult forms share similar immunopathologic features, clinical manifestations differ. In children, LABD is typically idiopathic, with onset between ages 2 and 10 years and a predilection for perioral, perineal, and abdominal areas. Mucosal involvement is more common in neonates.[1] The distinctive morphology, including the "string of pearls" appearance, and direct immunofluorescence findings that are highly specific for LABD are key for diagnosis. These features help differentiate LABD from other blistering conditions, such as bullous impetigo, dermatitis herpetiformis, and herpes simplex. Early recognition of LABD is essential to avoid unnecessary investigations and ensure appropriate treatment with immunomodulatory therapies such as dapsone, which is considered first-line treatment.[1,2]

Author disclosures are available at https://onlinelibrary.wiley.com/doi/10.1002/art.43228.

1. Mori F, Saretta F, Liotti L, et al. Linear immunoglobulin A bullous dermatosis in children. Front Pediatr 2022;10:937528.
2. Shin L, Gardner JT II, Dao H Jr. Updates in the diagnosis and management of linear IgA disease: a systematic review. Medicina (Kaunas) 2021;57(8):818.

Eduardo López-Vera, MD
elopez.vera@outlook.es
Jose A. Llamas-Carmona, MD
Dermatology Department
Hospital Regional Universitario de Málaga
Málaga, Spain
Juan S. Rodríguez-Moncada, MD
Pathology Department
Hospital Regional Universitario de Málaga
Málaga, Spain

American College of Rheumatology
Empowering Rheumatology Professionals

Arthritis & Rheumatology
Vol. 77, No. 11, November 2025, pp 1606–1614

LETTER

DOI 10.1002/art.43196

Epitope spreading and systemic sclerosis: comment on the article by Kotani et al

To the Editor:

Epitope spreading (ES) refers to the intramolecular-dependent and intermolecular-independent processes of antibody diversification from a dominant primary antigenic epitope to secondary antigenic epitopes. This phenomenon can occur both within the original antigen at different parts of the antigen and across different antigens, leading to the perpetuation and exacerbation of autoimmunity, including systemic sclerosis (SSc).[1] The recent study published in *Arthritis & Rheumatology* by Kotani et al demonstrates a strong correlation between ES and skin sclerosis severity, suggesting that ES could serve as a novel surrogate marker for SSc management.[2] This investigation identifies intermolecular ES in anti–RNA polymerase III (anti–RNAP III) subunits among anti–RNAP III antibody–positive individuals, showing a strong correlation with the modified Rodnan skin thickness score and the interstitial lung disease (ILD) biomarker surfactant protein D. Although the study is commendable in its scope and depth, several key points merit further discussion to deepen our understanding of this important subject.

First, human RNAP III is a multisubunit enzyme consisting of 17 subunits: 10 conserved core subunits (RPC1, RPC2, RPAC1, RPAC2, RPABC1, RPABC2, RPABC3, RPABC4, RPABC5, and RPC10) and 7 peripheral subunit complexes (an RPC8–RPC9 stalk, RPC3–RPC6–RPC7 heterotrimer, and RPC4–RPC5 heterodimer).[3] Kotani et al have defined synthesis of 17 full-length subunit proteins and 5 truncated forms of RPC1. What are the RNAP III subunits that contribute to ES in SSc? What subunit of the RNAP III complex functions as a major antigen for ES in anti–RNAP III antibody–positive SSc? What are the key amino acids in RNAP III subunits contributing to ES?

Second, RNAP III ES has been observed among other autoimmune conditions, such as systemic lupus erythematosus (SLE).[2] Is anti-RNAP III ES in SSc a disease-specific phenomenon or does a shared mechanism of ES exist across various autoimmune diseases, including SLE, multiple sclerosis (MS), and SSc. RNAP III is a complex of 17 proteins, and antigenic epitope can span over multiple subunits. It is possible that antigenic epitopes become buried within the complex when the antigenic mixture contains more subunits, potentially resulting in 70% anti–RNAP III antibody positivity with a mixture of eight antigens. In contrast, when the antigenic mixture consists of five antigens, the epitopes are more exposed and accessible to anti–RNAP III antibodies, yielding 90% positivity.

Third, what is the coorelation between ES and molecular mimicry? Does molecular mimicry contribute to ES?[4] Does molecular mimicry contribute to ES in SSc and SSc with ILD? I believe molecular mimicry can act as an initial trigger for autoimmune disorder. For example, Epstein-Barr virus infection potentially triggers onset and exacerbation of MS.[5] The immune system first targets a pathogen, and because of structural similarities between the pathogen and self-antigens, it attacks additional self-antigens, resulting in exacerbation of autoimmunity through ES.

It has been proposed that in SSc, ES occurs via both independent and dependent pathways. Independent ES is triggered by increased autoantigen exposure due to tissue damage from chronic inflammation, leading antigen-presenting cells to present self-antigens to T helper cells.[1,2,5] This is more common in early-stage SSc, particularly when localized to the skin (scleroderma). The dependent mechanism of ES, involving T helper and B cell activation through antigen processing and presentation, is more likely in SSc with ILD, in which systemic involvement and widespread immune activation occur.[1,2,5,6] What is the authors' perspective on the dependent and independent mechanisms in the context of anti–RNAP III antibody positivity and the involvement of RNAP III complex subunits?

In summary, Kotani et al have demonstrated a correlation between anti–RNAP III antibody positivity and disease severity at the interface of ES across RNAP III complex subunits. The developed assay can be refined to assess the coordinated involvement of core and peripheral RNAP III subunits. However, exploring the roles of molecular mimicry, direct versus indirect ES, anti–RNAP III antibody disease specificity, and ES stratification in ILD could provide a foundation for more effective SSc management.

Author disclosures are available at https://onlinelibrary.wiley.com/doi/10.1002/art.43196.

Ranjeet Singh Mahla, PhD
rmahla@fredhutch.org
Fred Hutchinson Cancer Center, Seattle, Washington
Kennedy Institute of Rheumatology, University of Oxford, Oxford, United Kingdom

1. Cornaby C, Gibbons L, Mayhew V, et al. B cell epitope spreading: mechanisms and contribution to autoimmune diseases. Immunol Lett 2015;163(1):56–68.
2. Kotani H, Matsuda KM, Yamaguchi K, et al. Diversity and epitope spreading of anti-RNA polymerase III antibodies in systemic sclerosis:

a potential biomarker for skin and lung involvement. Arthritis Rheumatol 2025;77(1):67–79.

3. Wang Q, Lei M, Wu J. A structural perspective of human RNA polymerase III. RNA Biol 2022;19(1):246–255.
4. Fehringer M, Vogl T. Molecular mimicry in the pathogenesis of autoimmune rheumatic diseases. J Transl Autoimmun 2025;10:100269.
5. Bjornevik K, Münz C, Cohen JI, et al. Epstein-Barr virus as a leading cause of multiple sclerosis: mechanisms and implications. Nat Rev Neurol 2023;19(3):160–171.
6. Fahlquist-Hagert C, Wittenborn TR, Terczyńska-Dyla E, et al. Antigen presentation by B cells enables epitope spreading across an MHC barrier. Nat Commun 2023;14(1):6941.

DOI 10.1002/art.43198

Secular trends in biologic prescribing for psoriasis and psoriatic arthritis, 2014–2024

To the Editor:

Psoriatic arthritis (PsA) is a chronic inflammatory arthritis that affects roughly one in every four patients with psoriasis.[1] Multiple biologic disease-modifying antirheumatic drugs (bDMARDs) have received regulatory approval for the treatment of psoriasis and PsA, including tumor necrosis factor inhibitors (TNFi) and therapies targeting interleukin-12/23 (IL-12/23i), IL-17, and IL-23. Neither the 2021 Group for Research and Assessment of Psoriasis and Psoriatic Arthritis (GRAPPA) nor the EULAR guidelines for PsA and psoriasis favor one bDMARD class over another, instead suggesting an approach targeted to disease domains and comorbidities.[2,3] Whether physicians prescribe one class over another and how such prescribing patterns have changed over time is unknown.

We conducted an observational study using the US-based electronic based health records database TriNetX to evaluate secular trends in bDMARD prescribing. In brief, patients were included if they had ≥2 *International Classification of Diseases, Ninth Revision, Clinical Modification* or *International Classification of Diseases, Tenth Revision, Clinical Modification* or PsA codes for psoriasis that were separated by >30 days and <365 days and were new users (one-year lookback period) of a biologic agent that had been approved by the US Food and Drug Administration for psoriasis or PsA (infliximab, adalimumab, etanercept, golimumab, certolizumab pegol, guselkumab, risankizumab, tildrakizumab, ustekinumab, secukinumab, ixekizumab, brodalumab, or bimekizumab). Exclusion criteria included missing demographic data (age or sex), age <18 years or >85 years, <1 year of follow-up time before the index date, receiving a prescription for more than one biologic class within 28 days of the index date, or an index date before January 1, 2014, or after December 6, 2024, when the data set was requested.

We identified 32,758 patients (mean age at diagnosis 51.5 years; 56.6% female) who initiated biologic therapies for psoriasis or PsA (Table 1). Patients had a mean disease duration of 3.9 years before starting a biologic agent. TNFi were the most commonly prescribed initial therapy (59.2%), followed by IL-17i (15.9%), IL-23i (14.1%), and IL-12/23i (10.8%). In the overall cohort, TNFi initiation decreased from 86.2% in 2014 to 38.6% in 2024, and IL-12/23i use declined from 13.6% in 2014 to 5.0% in 2024 (Supplementary Table 1). Conversely, IL-17i and IL-23i prescribing increased from 0.2% in 2014 to 19.9% in 2024 and 0.1% in 2014 to 36.5% in 2024, respectively. Similar trends were noted in analyses stratified by disease, although the shift from TNFi to IL-23i was more pronounced among patients with psoriasis as opposed to those who also had PsA (Figure 1, Supplementary Tables 2 and 3).

This study highlights secular trends in prescribing patterns of bDMARDs for patients with psoriasis and PsA since 2014. TNFi remain the most common initial bDMARD for PsA, but IL-23i have become the most commonly prescribed bDMARD for patients with isolated psoriasis. This likely reflects the superior efficacy of IL-23i for skin clearance, favorable safety profiles, and convenient dosing schedules as compared to other biologics.[4] The plateau in

Table 1. Demographic and clinical characteristics of included patients*

Characteristic	Patients (N = 33,012)
Age at diagnosis, mean (SD)	51.5 (14.4)
Sex, n (%)	–
Male	14,340 (43.4)
Female	18,672 (56.6)
Race and ethnicity, n (%)	–
White	24,133 (73.1)
Black or African American	1,802 (5.5)
Hispanic or Latino	2,247 (6.8)
Asian	1,441 (4.4)
Other/NA	944 (2.9)
Psoriatic arthritis at baseline, n (%)	–
No	22,323 (67.6)
Yes	10,689 (32.4)
Years with psoriasis or psoriatic arthritis, mean (SD)	3.9 (5.4)
Admissions during previous year, mean (SD)	0.3 (1.5)
Charlson Comorbidity Index, n (%)	0.6 (1.2)
Comorbidities at diagnosis, n (%)	–
Obesity	5,432 (16.5)
Diabetes	4,963 (15.0)
Chronic obstructive pulmonary disease	3,974 (12.0)
Smoking	1,059 (3.2)
CKD-3	557 (1.7)

* CKD-3, chronic kidney disease Stage 3; NA, not applicable.

a potential biomarker for skin and lung involvement. Arthritis Rheumatol 2025;77(1):67–79.

3. Wang Q, Lei M, Wu J. A structural perspective of human RNA polymerase III. RNA Biol 2022;19(1):246–255.
4. Fehringer M, Vogl T. Molecular mimicry in the pathogenesis of autoimmune rheumatic diseases. J Transl Autoimmun 2025;10:100269.
5. Bjornevik K, Münz C, Cohen JI, et al. Epstein-Barr virus as a leading cause of multiple sclerosis: mechanisms and implications. Nat Rev Neurol 2023;19(3):160–171.
6. Fahlquist-Hagert C, Wittenborn TR, Terczyńska-Dyla E, et al. Antigen presentation by B cells enables epitope spreading across an MHC barrier. Nat Commun 2023;14(1):6941.

DOI 10.1002/art.43198

Secular trends in biologic prescribing for psoriasis and psoriatic arthritis, 2014–2024

To the Editor:

Psoriatic arthritis (PsA) is a chronic inflammatory arthritis that affects roughly one in every four patients with psoriasis.[1] Multiple biologic disease-modifying antirheumatic drugs (bDMARDs) have received regulatory approval for the treatment of psoriasis and PsA, including tumor necrosis factor inhibitors (TNFi) and therapies targeting interleukin-12/23 (IL-12/23i), IL-17, and IL-23. Neither the 2021 Group for Research and Assessment of Psoriasis and Psoriatic Arthritis (GRAPPA) nor the EULAR guidelines for PsA and psoriasis favor one bDMARD class over another, instead suggesting an approach targeted to disease domains and comorbidities.[2,3] Whether physicians prescribe one class over another and how such prescribing patterns have changed over time is unknown.

We conducted an observational study using the US-based electronic based health records database TriNetX to evaluate secular trends in bDMARD prescribing. In brief, patients were included if they had ≥2 *International Classification of Diseases, Ninth Revision, Clinical Modification* or *International Classification of Diseases, Tenth Revision, Clinical Modification* or PsA codes for psoriasis that were separated by >30 days and <365 days and were new users (one-year lookback period) of a biologic agent that had been approved by the US Food and Drug Administration for psoriasis or PsA (infliximab, adalimumab, etanercept, golimumab, certolizumab pegol, guselkumab, risankizumab, tildrakizumab, ustekinumab, secukinumab, ixekizumab, brodalumab, or bimekizumab). Exclusion criteria included missing demographic data (age or sex), age <18 years or >85 years, <1 year of follow-up time before the index date, receiving a prescription for more than one biologic class within 28 days of the index date, or an index date before January 1, 2014, or after December 6, 2024, when the data set was requested.

We identified 32,758 patients (mean age at diagnosis 51.5 years; 56.6% female) who initiated biologic therapies for psoriasis or PsA (Table 1). Patients had a mean disease duration of 3.9 years before starting a biologic agent. TNFi were the most commonly prescribed initial therapy (59.2%), followed by IL-17i (15.9%), IL-23i (14.1%), and IL-12/23i (10.8%). In the overall cohort, TNFi initiation decreased from 86.2% in 2014 to 38.6% in 2024, and IL-12/23i use declined from 13.6% in 2014 to 5.0% in 2024 (Supplementary Table 1). Conversely, IL-17i and IL-23i prescribing increased from 0.2% in 2014 to 19.9% in 2024 and 0.1% in 2014 to 36.5% in 2024, respectively. Similar trends were noted in analyses stratified by disease, although the shift from TNFi to IL-23i was more pronounced among patients with psoriasis as opposed to those who also had PsA (Figure 1, Supplementary Tables 2 and 3).

This study highlights secular trends in prescribing patterns of bDMARDs for patients with psoriasis and PsA since 2014. TNFi remain the most common initial bDMARD for PsA, but IL-23i have become the most commonly prescribed bDMARD for patients with isolated psoriasis. This likely reflects the superior efficacy of IL-23i for skin clearance, favorable safety profiles, and convenient dosing schedules as compared to other biologics.[4] The plateau in

Table 1. Demographic and clinical characteristics of included patients*

Characteristic	Patients (N = 33,012)
Age at diagnosis, mean (SD)	51.5 (14.4)
Sex, n (%)	–
Male	14,340 (43.4)
Female	18,672 (56.6)
Race and ethnicity, n (%)	–
White	24,133 (73.1)
Black or African American	1,802 (5.5)
Hispanic or Latino	2,247 (6.8)
Asian	1,441 (4.4)
Other/NA	944 (2.9)
Psoriatic arthritis at baseline, n (%)	–
No	22,323 (67.6)
Yes	10,689 (32.4)
Years with psoriasis or psoriatic arthritis, mean (SD)	3.9 (5.4)
Admissions during previous year, mean (SD)	0.3 (1.5)
Charlson Comorbidity Index, n (%)	0.6 (1.2)
Comorbidities at diagnosis, n (%)	–
Obesity	5,432 (16.5)
Diabetes	4,963 (15.0)
Chronic obstructive pulmonary disease	3,974 (12.0)
Smoking	1,059 (3.2)
CKD-3	557 (1.7)

* CKD-3, chronic kidney disease Stage 3; NA, not applicable.

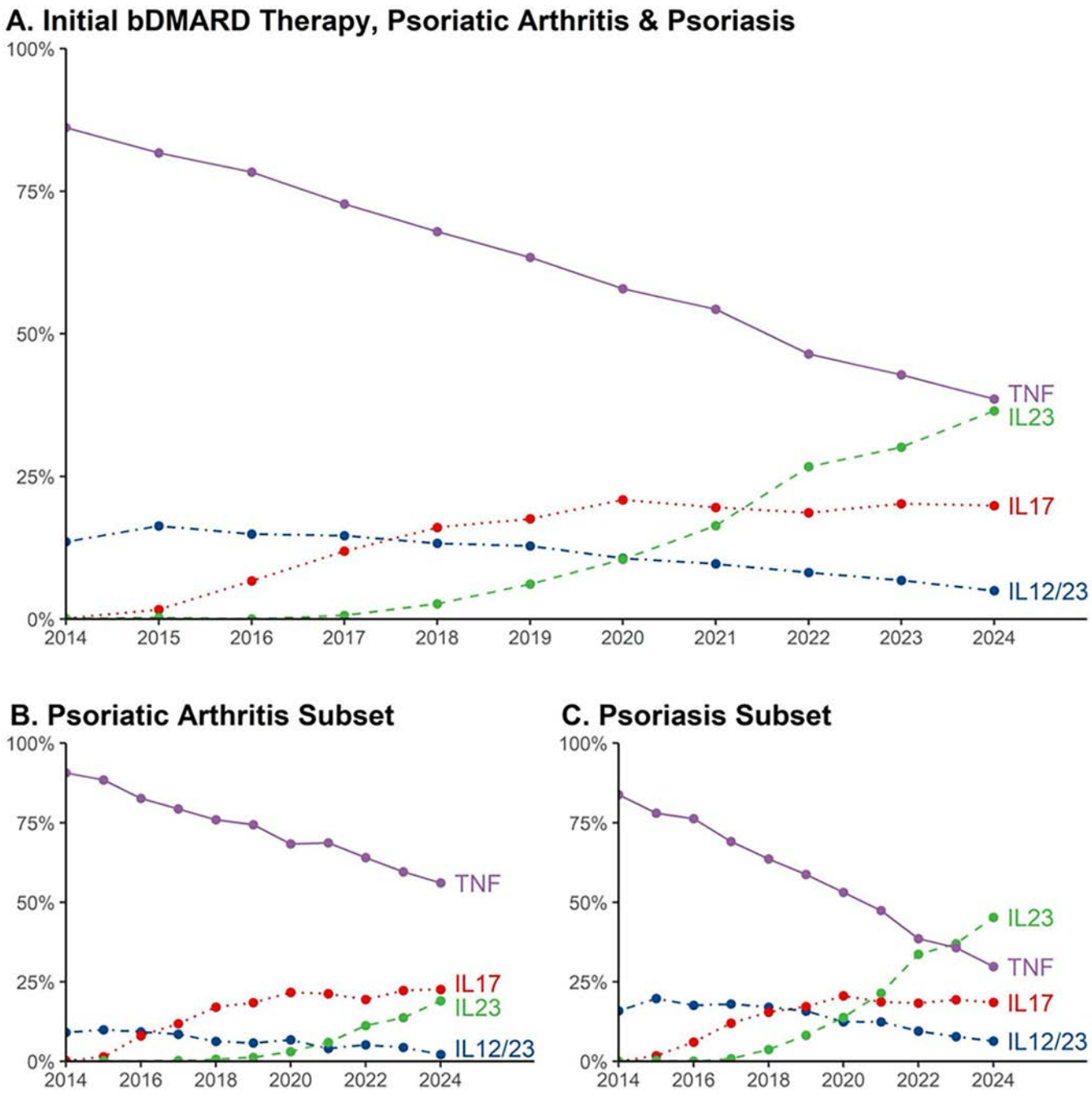

Figure 1. First biologic therapy for psoriasis or psoriatic arthritis, stratified by biologic class: (A) Combined data for patients with psoriatic arthritis or psoriasis, n = 33,012; (B) Subset of patients with psoriatic arthritis, n = 10,689; (C) Subset of patients with psoriasis, n = 22,323. *Incomplete data for 2024. TNF, tumor necrosis factor; IL-12/23, interleukin-12/23. Color figure can be viewed in the online issue, which is available at http://onlinelibrary.wiley.com/doi/10.1002/art.43198/abstract.

IL-17i use is notable but does not account for the advent of newer, more potent IL-17i, such as bimekizumab. Although current EULAR and GRAPPA guidelines do not favor one class of bDMARD therapy over others, these trends demonstrate how evolving clinical evidence and real-world experience are shaping treatment practices and decisions. As the therapeutic landscape evolves, efforts should be made to understand the comparative safety and efficacy of initial bDMARD therapies for psoriasis and PsA.

Dr Liew's work was supported by the National Institute of Arthritis and Musculoskeletal and Skin Diseases, NIH (grant K23-AR-082938); the Rheumatology Research Foundation (Investigator Award); and the Spondyloarthritis Research and Treatment Network (SPARTAN seed grant). Data will be made available upon reasonable request.

Author disclosures are available at https://onlinelibrary.wiley.com/doi/10.1002/art.43198.

Mahum Mirza, DO
Mike Putman, MD
Shikha Singla, MD
ssingla@mcw.edu
Medical College of Wisconsin, Milwaukee
Jean W. Liew, MD
Boston University Chobanian and Avedisian School of Medicine Boston, Massachusetts

1. Gladman DD, Antoni C, Mease P, et al. Psoriatic arthritis: epidemiology, clinical features, course, and outcome. Ann Rheum Dis 2005;64 Suppl 2(Suppl 2):ii14–ii17.
2. Soriano ER, Coates LC, Kavanaugh A. GRAPPA 2021 treatment recommendations for psoriatic arthritis. J Rheumatol 2023;50(suppl 2):31–32.
3. Gossec L, Kerschbaumer A, Ferreira RJO, et al. EULAR recommendations for the management of psoriatic arthritis with pharmacological therapies: 2023 update. Ann Rheum Dis 2024;83(6):706–719.
4. Blauvelt A, Papp KA, Griffiths CE, et al. Efficacy and safety of guselkumab, an anti-interleukin-23 monoclonal antibody, compared with adalimumab for the continuous treatment of patients with moderate to severe psoriasis: results from the phase III, double-blinded, placebo- and active comparator-controlled VOYAGE 1 trial. J Am Acad Dermatol 2017;76(3):405–417.

DOI 10.1002/art.43203

Methodological limitations and cross-population validation needs in plasma proteomic studies of osteoarthritis risk: comment on the article by Kang et al

To the Editor:

We read with great interest the study by Kang et al[1] entitled "Plasma Proteomic Profiles Predict Individual Future Osteoarthritis Risk," which explored the possibility of predicting the risk of osteoarthritis (OA) through plasma proteomic profiles, but the study's issues need further discussion. First, the study relies on patients' self-reported data and *International Classification of Diseases, Tenth Revision* diagnostic codes, which may introduce biased results. For example, the diagnosis of OA in the UK Biobank is mainly based on doctor records, and early asymptomatic OA may be missed.[2] This can confuse individuals who have not yet shown symptoms with those who have been diagnosed, affecting the accuracy of protein markers.

Second, the study only analyzed blood samples at a certain point in time and cannot determine whether these proteins actually cause OA. Although abnormal levels of collagen type IX alpha 1 chain (COL9A1) and cartilage acidic protein 1(CRTAC1) proteins were found 10 years before the diagnosis of OA, this association may be influenced by other unmeasured factors, such as lifestyle habits or genetic background.[3]

Third, the predictive power of the model has only been verified within the study. Although the five-year prediction accuracy is approximately 73%, it has not been validated in other populations (such as people from racial and ethnic minority groups) and may not be widely applicable. In addition, 92.8% of the participants in the UK Biobank were White, and the results may not be applicable to other races.

Fourth, the study did not clarify how these proteins lead to OA. Although COL9A1 and CRTAC1 are associated with joint cartilage repair, there is a lack of experimental evidence to prove that they directly cause OA, and they may only be accompanying phenomena of the disease.

Fifth, the study included "pain" as one of the predictive factors, but pain is usually a late-stage symptom of OA, which may make the model better at predicting patients who have already experienced symptoms, rather than truly achieving early warning. In addition, the study did not include imaging examination data (such as magnetic resonance imaging [MRI]), precluding assessment of joint structural damage severity.

Finally, the study focuses on the predictive effect over 5 to 10 years, but OA is a long-term disease.[4] The accuracy of predictions over 10 years has decreased to 71%, indicating that the model has limited effectiveness in long-term prediction and requires longer data support. Although the study offers novel insights into OA early detection, these limitations highlight the need to validate the clinical utility of these biomarkers via long-term follow-up, objective imaging (eg, MRI), and cross-population validation.

Drs Wang and Xing contributed equally to this work.

Author disclosures are available at https://onlinelibrary.wiley.com/doi/10.1002/art.43203.

Qing Wang, MD
2064798131@qq.com
Shuxing Xing, MD, PhD
Chengdu Fifth People's Hospital Chengdu, Sichuan, China

1. Kang Z, Zhang J, Liu W, et al. Plasma proteomic profiles predict individual future osteoarthritis risk. Arthritis Rheumatol 2025;77(8):981–995.
2. Ramazanian T, Fu S, Sohn S, et al. Prediction models for knee osteoarthritis: review of current models and future directions. Arch Bone Jt Surg 2023;11(1):1–11.
3. Appleyard T, Thomas MJ, Antcliff D, et al. Prediction models to estimate the future risk of osteoarthritis in the general population: a systematic review. Arthritis Care Res (Hoboken) 2023;75(7):1481–1493.
4. Kloppenburg M, Namane M, Cicuttini F. Osteoarthritis. Lancet 2025;405(10472):71–85.

DOI 10.1002/art.43204

Reply

To the Editor:

We appreciate the thoughtful comments by Drs Wang and Xing regarding our study.[1] Their insights underscore important methodologic and translational considerations in osteoarthritis (OA) biomarker research. In this article, we address each concern systematically.

Regarding the validity of OA diagnoses in our study, we acknowledge that reliance on clinician-reported data and *International Classification of Diseases, Tenth Revision* codes may miss subclinical cases. To mitigate this limitation, we used a multisource approach combining hospital records, primary care data, and mortality registries within the UK Biobank (UKB). This methodology aligns with established practices in large-scale epidemiologic studies and enhances diagnostic specificity.[2–4] Although asymptomatic early OA remains a challenge, the predictive power of protein biomarkers up to 10 years before diagnosis suggests their sensitivity to preclinical biologic changes. Future studies incorporating imaging data (eg, magnetic resonance imaging) could further refine case definitions, although such detailed assessment remains rare in population cohorts.

On the question of causality and confounding factors, we emphasize that our observational design inherently limits causal claims. To control for confounders, our Cox models rigorously adjusted for demographics, lifestyle factors, and comorbidities. Collagen type IX alpha 1 chain (COL9A1) and cartilage acidic protein 1 (CRTAC1) remained strongly associated with OA risk after adjustment (hazard ratios 1.54 and 1.65, respectively). These findings align with previous work by Nielsen et al,[5] who also identified these two proteins as prognostic biomarkers for OA progression. Longitudinal studies with repeated proteomic measurements and detailed assessment of lifestyle and genetic factors are needed to further confirm the temporal relationship and causal nature of these associations.

We fully agree with Drs Wang and Xing's concern about the limited racial diversity in the UKB cohort, in which most participants identified as White. External validation in multiethnic cohorts is critical to assess broader applicability. We encourage replication in diverse populations to assess generalizability.

Although our study identifies associations between proteins and OA risk, mechanistic pathways require further investigation. COL9A1 and CRTAC1 are implicated in cartilage integrity and repair processes,[6,7] but their direct role in OA pathogenesis needs experimental confirmation. We view our findings as a foundation for future mechanistic studies.

Pain was included in our model to reflect OA's clinical heterogeneity, but sensitivity analyses excluding pain variables demonstrated minimal impact on predictive accuracy (area under the curve decline <2%). This indicates the independent value of proteomic biomarkers in early risk stratification. We acknowledge the UKB's lack of structural imaging data and emphasize that integrating biomarkers with imaging data in future models could better distinguish presymptomatic from symptomatic OA.

Finally, the modest decline in predictive accuracy over 10 years (73–71%) aligns with biomarker trajectory patterns observed in chronic diseases. Although longer follow-up would strengthen our findings, the 5- to 10-year predictive window remains clinically actionable for lifestyle or therapeutic interventions.[8]

In conclusion, we agree that clinical translation of OA biomarkers demands mechanistic validation, diverse cohort validation, and integration with imaging. Our study serves as a foundational step toward these goals. We thank Drs. Wang and Xing for their constructive critique and welcome collaborative efforts to advance OA risk prediction and prevention.

Zijian Kang, MD
Shanghai Sixth People's Hospital Affiliated to Shanghai Jiao Tong University School of Medicine
Shanghai, China
Qiang Tong, MD, PhD
Shanghai Sixth People's Hospital Affiliated to Shanghai Jiao Tong University School of Medicine
Shanghai, China
Queen Mary Hospital, University of Hong Kong
Hong Kong, China
Sheng-Ming Dai, MD, PhD
shengmingdai@163.com
Shanghai Sixth People's Hospital Affiliated to Shanghai Jiao Tong University School of Medicine
Shanghai, China

1. Kang Z, Zhang J, Liu W, et al. Plasma proteomic profiles predict individual future osteoarthritis risk. Arthritis Rheumatol 2025;77(8):981–995.
2. Deng YT, You J, He Y, et al. Atlas of the plasma proteome in health and disease in 53,026 adults. Cell 2025;188(1):253–271.e7.
3. He H, Wang Y, Hunter D, et al. Association of walking with incident knee osteoarthritis: a prospective cohort study using data from the UK Biobank. Ann Rheum Dis 2025;84(4):632–642.
4. Kang Z, Zhang J, Zhu C, et al. Impaired pulmonary function increases the risk of gout: evidence from a large cohort study in the UK Biobank. BMC Med 2024;22(1):606.
5. Nielsen RL, Monfeuga T, Kitchen RR, et al. Data-driven identification of predictive risk biomarkers for subgroups of osteoarthritis using interpretable machine learning. Nat Commun 2024;15(1):2817.
6. Imagawa K, de Andrés MC, Hashimoto K, et al. Association of reduced type IX collagen gene expression in human osteoarthritic chondrocytes with epigenetic silencing by DNA hypermethylation. Arthritis Rheumatol 2014;66(11):3040–3051.
7. Styrkarsdottir U, Lund SH, Saevarsdottir S, et al. The CRTAC1 protein in plasma is associated with osteoarthritis and predicts progression to

joint replacement: a large-scale proteomics scan in Iceland. Arthritis Rheumatol 2021;73(11):2025–2034.

8. Mahmoudian A, Lohmander LS, Mobasheri A, et al. Early-stage symptomatic osteoarthritis of the knee - time for action. Nat Rev Rheumatol 2021;17(10):621–632.

DOI 10.1002/art.43205

Beyond the numbers: recognizing disease severity and hidden influences in physical therapy for knee osteoarthritis: comment on the article by Neogi et al

To the Editor:

We read with great interest the recently published article titled "Association of physical therapy care with use of intra-articular injections in people with knee osteoarthritis: a real-world cohort study" by Neogi et al.[1] The authors provided a thorough analysis of how the timing, dose, and modality of physical therapy (PT) may influence subsequent intra-articular injection (IAI) usage in patients newly diagnosed with knee osteoarthritis (OA). Although this study offers valuable insights into the role of early and sufficiently frequent PT, we would like to share a few constructive perspectives that may further enrich the discussion.

First, patients' disease severity can have far-reaching implications for treatment decisions and outcomes. For instance, those presenting with milder, earlier-stage OA may be more amenable to—and more motivated for—PT, leading to better symptom management and delayed recourse to IAIs.[2] In contrast, individuals with advanced OA or comorbid conditions (eg, diabetes, cardiovascular disease, or severe obesity) might experience greater functional limitations or more intense pain, limiting their ability to participate fully in PT.[3] This could in turn raise the likelihood of requiring IAIs down the line. Although the study under discussion stratifies by prior injection experience, it remains possible that underlying severity variations are influencing both early PT usage and future injection risk.

Second, although the authors account for several measured covariates, other factors—such as patients' pain tolerance, prior exercise habits, or social support—are difficult to capture accurately via claims data. These unmeasured factors could result in residual confounding, especially if they intersect with treatment adherence, therapy initiation, or clinical follow-up patterns. For example, an older adult living alone without transportation might struggle to attend frequent PT sessions. Meanwhile, an active individual with robust social support might find it easier to begin PT sooner and continue regularly, thereby lowering the chance of subsequent IAIs. The article's mention of E-values suggests the authors recognize the possibility of confounding, yet a targeted look at key personal and psychosocial variables could refine our understanding of why some individuals do not initiate PT early or attend multiple visits.

Finally, prospective collection of standardized functional severity measures (eg, Western Ontario and McMaster Universities Osteoarthritis Index scores, objective physical function tests) and patient-reported outcomes could deepen our insight into how disease progression interacts with PT engagement and injection needs. If future studies integrate validated severity scales into claims-based research, investigators can more effectively tease out whether early PT confers benefit across all severity levels or if it is primarily those with mild or moderate OA who show meaningful reduction in IAI use.

Overall, the research team has contributed important evidence on the impact of PT timing and dose in knee OA. I am grateful for the authors' efforts and look forward to further investigations that continue to refine our grasp of how best to optimize care for people living with knee OA.

Author disclosures are available at https://onlinelibrary.wiley.com/doi/10.1002/art.43205.

Yadi Li, MD
yadili9232@gmail.com
Department of Traditional Chinese Medicine, Deyang People's Hospital,
Deyang, China

1. Neogi T, Dubreuil M, Peloquin C, et al. Association of physical therapy care with use of intra-articular injections in people with knee osteoarthritis: a real-world cohort study. Arthritis Rheumatol 2025;77(8):1006–1014.
2. MacKay C, Hawker GA, Jaglal SB. Qualitative study exploring the factors influencing physical therapy management of early knee osteoarthritis in Canada. BMJ Open 2018;8(11):e023457.
3. Zambon S, Siviero P, Denkinger M, et al; Eposa Research Group. Role of osteoarthritis, comorbidity, and pain in determining functional limitations in older populations: European project on osteoarthritis. Arthritis Care Res (Hoboken) 2016;68(6):801–810.

DOI 10.1002/art.43202

Reply

To the Editor:

We would like to thank Dr Li for their constructive feedback. Our article directly addresses many of the concerns identified by Dr Li, including possible influences of disease severity, referral patterns, challenges with access, patient preferences, unmeasured socioeconomic factors, etc.[1] However, we appreciate the opportunity to provide a more detailed response.

We agree that disease severity could influence health-seeking behaviors in people with knee osteoarthritis (OA). However, our cohort was people with incident knee OA, meaning that people with advanced OA were not likely to be included because they would have had prior OA diagnoses. However, there can still

be variability in severity even among people newly diagnosed with knee OA, which could influence their health-seeking behaviors. Although claims data do not directly provide any information on symptom severity, we adjusted for prescription nonsteroidal anti-inflammatory drug use as a proxy for symptom severity and stratified by prior use of intra-articular therapies, which may also reflect more severe symptoms. Regarding the comment about comorbidities influencing the results, we adjusted for relevant comorbidities available in our analyses.

We also acknowledge that unmeasured confounders, some of which were identified by Dr Li, such as pain tolerance, prior exercise habits, and social support, could influence the results. As Dr Li noted, these factors are not captured in a claims data set. However, we did anticipate some of these potential confounders and attempted to account for them using information that was available, such as type of insurance, race, and geographic location as a proxy for socioeconomic status. We adjusted for health care use, which may in part address the ability to access health care services as well. Also, as Dr Li noted, we recognized the potential for unmeasured confounding and therefore reported E-values, which reflect the minimum strength of association needed between an unmeasured confounder and both the exposure and the outcome to nullify the observed effect estimate. Our E-values indicated that large residual confounding would need to be present to nullify our results. Therefore, given our robust confounder adjustments, although possible, it is quite unlikely that the residual confounding due to the factors identified by Dr Li would be large enough to influence our results, and thus the interpretations, substantially.

We agree with Dr Li's final comment that information on OA-specific outcomes could further clarify the role of physical therapy for people with knee OA in future studies.

Author disclosures are available at https://onlinelibrary.wiley.com/doi/10.1002/art.43202.

Tuhina Neogi, MD, PhD
Maureen Dubreuil, MD
Christine Peloquin, MPH
Lee Marinko, PT, ScD
James Camarinos, PT
David T. Felson, MD
Deepak Kumar, PT, PhD
kumard@bu.edu
Boston University
Boston, MA

1. Neogi T, Dubreuil M, Peloquin C, et al. Association of physical therapy care with use of intra-articular injections in people with knee osteoarthritis: a real-world cohort study. Arthritis Rheumatol 2025;77(8):1006–1014.

DOI 10.1002/art.43201

Targeting long noncoding RNA H19 in subchondral bone osteocytes for alleviating cartilage degradation in osteoarthritis; comment on the article by Wang et al

To the Editor:

We read with great interest the recent study by Wang et al investigating the role of the osteocyte-specific long noncoding RNA H19 in modulating subchondral bone remodeling and cartilage degeneration in osteoarthritis (OA). The study provides important insights, in particular demonstrating that suppression of H19 by targeted nanoparticle-based antisense oligonucleotides (ASOs) effectively ameliorates OA progression in animal models by reducing subchondral bone sclerosis and associated cartilage erosion.[1] However, several critical issues require further clarification and detailed investigation before definitive clinical implications can be confidently stated.

First, although the study convincingly identifies the phosphatidylinositol 3-kinase (PI3K)/Akt/glycogen synthase kinase 3 (GSK3) pathway as a downstream mediator of H19 function, it remains unclear whether this signaling axis fully accounts for the observed therapeutic outcomes. OA is a highly heterogeneous disease involving complex crosstalk between multiple cell types and signaling cascades within joint tissues. Although the study demonstrates modulation of this specific pathway, additional mechanisms, including canonical Wnt/β-catenin signaling, transforming growth factor β signaling, and NF-κB–related inflammation, may also contribute to or synergize with H19-mediated effects. Future studies integrating multiomics approaches or using more comprehensive systems biology analyses may help to delineate whether the H19/PI3K/Akt axis acts independently or synergistically with other critical OA-related pathways.

Second, although the current research used mouse models and demonstrated efficacy in vivo, translating these findings into clinical practice raises questions regarding the applicability of conditional H19 knockout and nanoparticle-based ASO delivery in humans. The subchondral bone microarchitecture and mechanotransduction responses in human OA joints are much more complex than in mouse models. Furthermore, the therapeutic success of magnetic field-guided nanoparticle-based ASO delivery in rodents may face significant challenges in clinical translation, such as achieving precise targeting in the anatomically complex and dynamic mechanical environment of human knee joints. Further investigations should prioritize bridging this translational gap by performing in-depth analyses of human OA tissues, focusing on the spatiotemporal expression patterns of H19 and downstream mechanotransduction targets and

validating delivery systems in larger animal models or ex vivo human joint models.

Third, a major limitation not fully addressed by the study is the discrepancy observed in the mechanistic influence of H19 on cyclooxygenase 2 (Ptgs2) expression between animal models and human OA samples. Although the authors effectively demonstrated positive regulation of Ptgs2 by H19 in preclinical experiments, this correlation was not reflected in clinical samples. Such divergence may be due to inherent differences between experimental OA induction models and the multifactorial, slowly progressive nature of human OA. In addition, the relatively small sample size in the clinical validation phase and the lack of stratification by OA severity and anatomic compartment involvement may further dilute significant associations. Thus, future research with larger well-defined patient cohorts is needed to clarify the true clinical relevance of H19-mediated mechanotransduction pathways.

In addition, the study proposed an innovative magnetic-responsive nanoparticle-based ASO delivery system, which showed considerable success in mouse models. However, the translation of this method into clinical treatment raises practical and safety considerations. The clinical efficacy of magnetic field–directed drug delivery is highly dependent on magnetic field strength, duration, and patient compliance, which may vary significantly in real-world clinical scenarios. In addition, the specificity of the magnetic targeting approach may be compromised by the anatomic complexity of OA joints, raising concerns about unintended off-target effects or inadequate therapeutic concentrations in deeply located lesions. These critical considerations highlight the need for comprehensive biomechanical and pharmacokinetic evaluations to optimize magnetic targeting parameters and assess potential long-term adverse effects before clinical application.

Finally, the molecular mechanism underlying the interaction between H19 and epigenetic regulators, particularly EZH2, deserves further investigation. The present study suggests a possible H19-mediated regulation of osteocyte mechanotransduction through PI3K/AKT/GSK3 and protein phosphatase 2A pathways. However, the precise molecular interactions between H19 and EZH2 or other histone modifications in the context of subchondral bone remodeling remain largely unexplored. Given the established importance of epigenetic alterations in OA pathology, elucidation of these complex regulatory mechanisms may open new therapeutic avenues specifically targeting epigenetic modulators in OA treatment. Comprehensive epigenetic profiling in subchondral bone osteocytes under conditions of mechanical stress may further elucidate the role of H19 in epigenetic regulation of mechanotransduction.

In conclusion, although the study significantly advances our understanding of the role of osteocyte-derived H19 in OA subchondral bone remodeling and highlights an innovative therapeutic strategy, these promising results should be viewed in the context of several important limitations. Further mechanistic exploration, rigorous clinical validation, and optimization of translational strategies will be critical to ultimately establish H19-targeted therapies as viable clinical options for the treatment of OA.

Author disclosures are available at https://onlinelibrary.wiley.com/doi/10.1002/art.43201.

Suqi Wu, MD
Guangyin Yu, MD
Yankui Leng, PhD, MD
13967440045@163.com
Department of Cardiology, Department of Orthopedics, Jinhua Hospital of Traditional Chinese Medicine, Zhejiang, China

1. Wang R, Mehrjou B, Dehghan-Banian D, et al. Targeting long noncoding RNA H19 in subchondral bone osteocytes and the alleviation of cartilage degradation in osteoarthritis. Arthritis Rheumatol 2025;77(3):283–297.

DOI 10.1002/art.43230

Reply

To the Editor:

We thank the authors of the letter for their thoughtful and detailed commentary on our recent publication.[1] We appreciate the opportunity to respond to the concerns raised and to clarify the scope and implications of our study.

We acknowledge that pathways such as Wnt/β-catenin, transforming growth factor β, and NF-κB may also play roles in osteoarthritis (OA) pathogenesis, potentially interacting with H19-mediated effects. Investigating the broader interplay between the H19 pathway and other signaling networks through multiomics and systems biology approaches is an exciting future direction. Such explorations, although beyond the scope of our current work, are critical next steps to fully elucidate H19's contributions to OA.

We recognize the valid concern regarding the differences between mouse models and human OA, particularly in replicating the mechanical complexity of human subchondral bone remodeling. Our study aimed to provide proof of concept for H19-targeted therapy in a controlled murine setting, and we view translation to human applications as a future research priority rather than a resolved outcome of this work. We also thank Wu and colleagues for noting the discrepancy in cyclooxygenase 2 (Ptgs2) and H19 correlation between human OA samples and our preclinical models. We further concur that larger stratified human cohorts are needed to examine the spatiotemporal expression of H19 and related genes. Further validation of the therapeutic outcome of antisense oligonucleotide (ASO) delivery

validating delivery systems in larger animal models or ex vivo human joint models.

Third, a major limitation not fully addressed by the study is the discrepancy observed in the mechanistic influence of H19 on cyclooxygenase 2 (Ptgs2) expression between animal models and human OA samples. Although the authors effectively demonstrated positive regulation of Ptgs2 by H19 in preclinical experiments, this correlation was not reflected in clinical samples. Such divergence may be due to inherent differences between experimental OA induction models and the multifactorial, slowly progressive nature of human OA. In addition, the relatively small sample size in the clinical validation phase and the lack of stratification by OA severity and anatomic compartment involvement may further dilute significant associations. Thus, future research with larger well-defined patient cohorts is needed to clarify the true clinical relevance of H19-mediated mechanotransduction pathways.

In addition, the study proposed an innovative magnetic-responsive nanoparticle-based ASO delivery system, which showed considerable success in mouse models. However, the translation of this method into clinical treatment raises practical and safety considerations. The clinical efficacy of magnetic field–directed drug delivery is highly dependent on magnetic field strength, duration, and patient compliance, which may vary significantly in real-world clinical scenarios. In addition, the specificity of the magnetic targeting approach may be compromised by the anatomic complexity of OA joints, raising concerns about unintended off-target effects or inadequate therapeutic concentrations in deeply located lesions. These critical considerations highlight the need for comprehensive biomechanical and pharmacokinetic evaluations to optimize magnetic targeting parameters and assess potential long-term adverse effects before clinical application.

Finally, the molecular mechanism underlying the interaction between H19 and epigenetic regulators, particularly EZH2, deserves further investigation. The present study suggests a possible H19-mediated regulation of osteocyte mechanotransduction through PI3K/AKT/GSK3 and protein phosphatase 2A pathways. However, the precise molecular interactions between H19 and EZH2 or other histone modifications in the context of subchondral bone remodeling remain largely unexplored. Given the established importance of epigenetic alterations in OA pathology, elucidation of these complex regulatory mechanisms may open new therapeutic avenues specifically targeting epigenetic modulators in OA treatment. Comprehensive epigenetic profiling in subchondral bone osteocytes under conditions of mechanical stress may further elucidate the role of H19 in epigenetic regulation of mechanotransduction.

In conclusion, although the study significantly advances our understanding of the role of osteocyte-derived H19 in OA subchondral bone remodeling and highlights an innovative therapeutic strategy, these promising results should be viewed in the context of several important limitations. Further mechanistic exploration, rigorous clinical validation, and optimization of translational strategies will be critical to ultimately establish H19-targeted therapies as viable clinical options for the treatment of OA.

Author disclosures are available at https://onlinelibrary.wiley.com/doi/10.1002/art.43201.

Suqi Wu, MD
Guangyin Yu, MD
Yankui Leng, PhD, MD
13967440045@163.com
Department of Cardiology, Department of Orthopedics, Jinhua Hospital of Traditional Chinese Medicine, Zhejiang, China

1. Wang R, Mehrjou B, Dehghan-Banian D, et al. Targeting long noncoding RNA H19 in subchondral bone osteocytes and the alleviation of cartilage degradation in osteoarthritis. Arthritis Rheumatol 2025;77(3):283–297.

DOI 10.1002/art.43230

Reply

To the Editor:

We thank the authors of the letter for their thoughtful and detailed commentary on our recent publication.[1] We appreciate the opportunity to respond to the concerns raised and to clarify the scope and implications of our study.

We acknowledge that pathways such as Wnt/β-catenin, transforming growth factor β, and NF-κB may also play roles in osteoarthritis (OA) pathogenesis, potentially interacting with H19-mediated effects. Investigating the broader interplay between the H19 pathway and other signaling networks through multiomics and systems biology approaches is an exciting future direction. Such explorations, although beyond the scope of our current work, are critical next steps to fully elucidate H19's contributions to OA.

We recognize the valid concern regarding the differences between mouse models and human OA, particularly in replicating the mechanical complexity of human subchondral bone remodeling. Our study aimed to provide proof of concept for H19-targeted therapy in a controlled murine setting, and we view translation to human applications as a future research priority rather than a resolved outcome of this work. We also thank Wu and colleagues for noting the discrepancy in cyclooxygenase 2 (Ptgs2) and H19 correlation between human OA samples and our preclinical models. We further concur that larger stratified human cohorts are needed to examine the spatiotemporal expression of H19 and related genes. Further validation of the therapeutic outcome of antisense oligonucleotide (ASO) delivery

targeting H19 with a larger animal model of OA is a compelling next step, though it will require collaborative efforts and additional resources.

We appreciate the concerns raised regarding the clinical feasibility of our nanoparticle-based ASO delivery system. Although our study demonstrates effective targeting in mice, we recognize that the human knee joint anatomy and biomechanical forces present additional translational barriers. As outlined in our discussion,[1] it is warranted to evaluate the long-term efficacy and safety of the magnetic metal–organic framework approach while optimizing delivery to account for joint geometry and patient comfort alongside magnetic field strength. We also agree that the relationship between H19 and EZH2 in osteocyte mechanotransduction deserves deeper investigation. Our data suggest EZH2 may negatively regulate protein phosphatase 2A (PP2A) transcription, impacting H19-mediated PP2A expression in osteocytes. More detailed mechanistic studies are needed to clarify this interaction and its role in osteocyte function and OA development.

In conclusion, we sincerely appreciate the constructive critiques, which align with our ongoing efforts to refine mechanistic insights and enhance translational potential.

Author disclosures are available at https://onlinelibrary.wiley.com/doi/10.1002/art.43230.

Rongliang Wang, PhD
Department of Orthopaedics and Traumatology, Faculty of Medicine, The Chinese University of Hong Kong, Hong Kong, China; Li Ka Shing Institute of Health Sciences, The Chinese University of Hong Kong, Hong Kong, China; SH Ho Scoliosis Research Laboratory, Joint Scoliosis Research Center of the Chinese University of Hong Kong and Nanjing University, The Chinese University of Hong Kong, Hong Kong, China; and State Key Laboratory of Pharmaceutical Biotechnology, Division of Sports Medicine and Adult Reconstructive Surgery, Nanjing Drum Tower Hospital, The Affiliated Hospital of Nanjing University Medical School Nanjing, China
Wayne Yuk Wai Lee, PhD
waynelee@cuhk.edu.hk
Department of Orthopaedics and Traumatology, Faculty of Medicine, The Chinese University of Hong Kong, Hong Kong, China; Li Ka Shing Institute of Health Sciences, The Chinese University of Hong Kong, Hong Kong, China; SH Ho Scoliosis Research Laboratory, Joint Scoliosis Research Center of the Chinese University of Hong Kong and Nanjing University, The Chinese University of Hong Kong, Hong Kong, China; Center for Neuromusculoskeletal Restorative Medicine, InnoHK Centres, Hong Kong Science Park, Hong Kong, China Hong Kong, China

1. Wang R, Mehrjou B, Dehghan-Banian D, et al. Targeting long noncoding RNA H19 in subchondral bone osteocytes and the alleviation of cartilage degradation in osteoarthritis. Arthritis Rheumatol 2025;77(3): 283–297.